

# **XTAP** (eXpandable Transient Analysis Program)

Ver. 2.41

---

Test Cases of XTAP

# eXpandable Transient Analysis Program

XTAP Ver. 2.41

Test Cases of XTAP

# Test Cases of XTAP

## 1. Basic Test Cases

EDU-01-A	PU Calculation - 1 .....	1
EDU-01-B	PU Calculation - 2 .....	5
EDU-01-C	PU Calculation - 3 .....	9
EDU-01-D	PU Calculation - 4 .....	13
EDU-01-E	PU Calculation - 5 .....	18
EDU-02	Calculation of Three-Phase Circuit PQVI.....	22
EDU-03	Comparison with Y Method, which is an Effective Value Analysis Method- Load P Attached .....	26
EDU-04	Comparison with Y Method, which is an Effective Value Analysis Method – Change in Impedance Z .....	30

## 2. Power Electronics and Control System

PE-01	Simulation of Three-phase PWM Inverter Circuit .....	34
DLL-01	Basic Operations using DLL Control Block Components .....	41

## 3. HVDC, FACTS

HVDC-01	Separately Excited HVDC Model .....	45
HVDC-02	Self-Excited HVDC Model .....	55
HVDC-03	Self-Excited HVDC Model (Half Bridge MMC).....	63
HVDC-04	Self-Excited HVDC Model (Full Bridge MMC).....	71
FACTS-01	Simulation Start of STATCOM.....	78
FACTS-02	STATCOM Model.....	83
FACTS-03	Separately Excited SVC Model.....	91

## 4. Power Quality Analysis

PQ-01	Simulation of Flicker Suppression Using Separately Excited SVC .....	96
PQ-02-A	Calculation of Excitation Inrush Current under Pressurization of Customer	

Transformer.....	101
------------------	-----

## 5. Protection Relay

RELAY-01	Distance Relay Modeling .....	108
RELAY-02	Coordinated Study of the Fault Current Interrupting Arcing Horn and Transmission Line Protection Relay .....	117

## 6. Machine

MAC-01-A	Synchronous Generator (Single-Line 3 LG-O Fault and Constant Excitation Occurring in a Single-Machine Infinite Bus System) .....	129
MAC-01-B	Synchronous Generator (Single-Line 3 LG-O Fault Occurring in a Single- Machine Infinite Bus System with AVR) .....	140
MAC-01-C	Synchronous Generator (Torsional Torque Simulation) .....	144
MAC-01-D	Synchronous Generator (Considering Magnetic Saturation) (Single-Line 3 LG-O Fault Occurring in a Single-Machine Infinite Bus System with AVR Control) .....	150
MAC-02	3 LG-O Simulation of Induction Motor .....	154

## 7. Power System Analysis

PS-01-A	Simulation of the WEST 10 System of the Institute of Electrical Engineers of Japan .....	159
PS-02-A	Simulation of EAST 10-Machine Power System of the Institute of Electrical Engineers of Japan (IEEJ).....	165

## 8. Circuit Breaker

CB-01	Current Breaking Simulation of 66-Kv Fault Current Interrupting Arcing Horn .....	170
CB-02	Analysis of Terminal Short-Circuit Breaker and Capacitive Current Switching in 154-Kv System .....	177

## 9. Switching Surge

SLD-01	Flashover Analysis of 6.6-kV Distribution Line.....	187
SLD-02	Lightning Surge Aspects Occurring in Secondary Side of a Pole-mounted Transformer During Lightning Strike on a Distribution Line.....	197
SLS-01	Lightning Surge Calculation of 500-kVAir-insulated Substation .....	205
SSW-01	Switching Surge Calculation of a 500-Kv Vertically Arranged Double-Circuit Transmission Line.....	213
SSW-02	Switching surge Analysis of a 275-kV System.....	221
SSW-03	Analysis of Input Surge Owing to Block Energization during Large-scale System Restoration .....	238
SSW-04	Comparison of the Ground-fault Surge Analysis of a 500-kV Power Transmission Line with the Actual Measurements .....	247
SSWD-01	Ground-fault Surge Propagation Analysis of a 6.6-kV Power Distribution Line .....	261
STL-01	Simulation of Surge Propagation of a 500-kV Horizontally-arranged Single Circuit Transmission Line.....	272
STL-02	Simulation of Surge Propagation in a 500-kV Vertically Arranged Double-circuit Transmission Line.....	279
STL-03	Flashover Calculation using Arcing Horn Flashover Model for Short-tail Waves (Detailed Model, AC Superimposition not Possible).....	287
STL-04	Flashover Calculation Using Arcing Horn Flashover Model (Simplified Model, AC Superimposition Possible) for Short Tail Waves.....	297

## 10. Photovoltaic Systems

PV-01	Simulation of Single-phase Inverter Circuit for Solar Power Generation .....	304
PV-02-A	Simulation of a system fault using a basic transient analysis model of PCS for utility-scale solar power station (Switching model).....	309
PV-02-B	Simulation of a system fault using a basic transient analysis model of PCS for utility-scale solar power station (average value model).....	317

Examples of XTAP		No.	EDU-01-A
Example Name	PU Calculation - 1		
Field	Basic calculation (power systems)		
Literature	Japan Electric Association, NEC Technical Standards Committee: "Grid interconnection code JEAC 9701-2006," p. 196, 4th edition of issue dated June 30, 2006		
Overview	<p>In the Y method, which is effectively applied to a value analysis, the system calculation is conducted in the PU system. In the present example, the checking method using the PU system through an instantaneous value analysis is shown. The ultimate aim is the target learning regarding the relationship of five cases, EDU-01-A to 01-E, and the parasitic-/system-based PU using actual examples.</p> <p>The following system is the specific target of this study.</p> <p>Power - impedance - transformer - impedance - 3 LG fault</p> <ul style="list-style-type: none"> <li>• In the PU system, the capacity and voltage are specified. Although the current can be calculated from the relationship between the two, the specific lesson learned here is that this is a short circuit current (when <math>Z = 1 \text{ pu}</math>).</li> </ul> <p>Short-circuit current: Power - impedance - 3LG current at the time of the fault!</p> <p>Through this, we also learned that the PU is extremely useful for a system check.</p>		

## Analysis Circuit and Conditions

Figure 1 shows the analysis circuit.

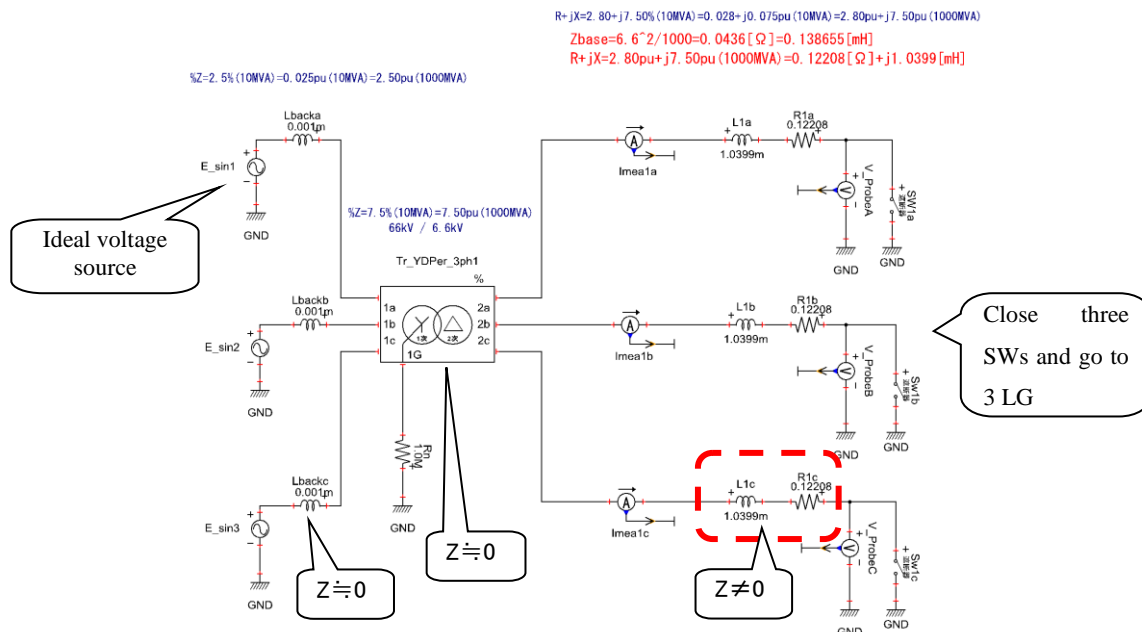


Figure 1 Analysis circuit

[System voltage]

Upper system: Line voltage of 66 [kV]. Distribution system: Line voltage of 6.6 [kV]

Standard  $Z = V^2 [kV] / S [MVA]$

[Calculation of R and L]

$Z_{base} = 6.6^2 / 1000 = 0.0436 [\Omega] = 0.138655 [mH]$ . This value of Z corresponds to 1 pu

- ① In the literature, this is written as  $R + jX = 2.80 + j7.50\%$  (10 MVA).
- ② This becomes  $R + jX = 2.80 + j7.50\%$  (10 MVA) =  $0.028 + j0.075$  pu (10 MVA) =  $2.80$  pu +  $j7.50$  pu (1000 MVA).

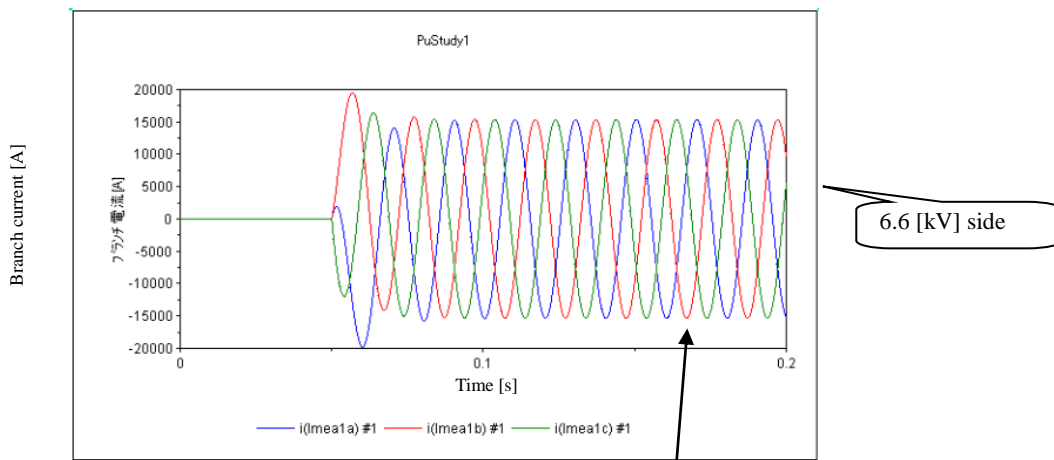
Here, a 1000 MVA base is generally used in the trunk transmission system. The line impedance of the 6.6-kV system becomes a large value when we consider the trunk transmission system (※). This image is important. A system fault on the 6.6-kV side becomes distant when viewed from the trunk transmission system. This is in line with the image. If this image is viewed with the impedance (pu) specifically, it becomes the image of ※.

- ③  $R + jX = 2.80$  pu +  $j7.50$  pu (1000 MVA) =  $0.12208 [\Omega] + j1.0399 [mH]$  These are the input data.

$$2.80\text{pu} \times 0.0436 [\Omega]$$

$$7.50\text{pu} \times 0.138655 [mH]$$

## Analysis Results



Three-phase current waveform [A]

Because  $I = V / Z$ , the short-circuit current at 3 LG is calculated using  $I = 1 \text{ [pu]} / Z \text{ [pu]}$ .

Here,  $Z[\text{pu}] = R + jX = 2.80 + j7.50 \text{ [pu]} (1000 \text{ MVA}) \rightarrow |Z| = 8.0 \text{ [pu]}$

At the time of 3 LG, the short circuit current  $I = V/Z = 1 \text{ [pu]} / 8 \text{ [pu]} = 0.125 \text{ [pu]}$  (1000 MVA, 6.6 kV)

The current of 1 [pu] of the 1000 MVA based on the 6.6-kV side is

$$I = S/V = \{(1000 * 10^6)/3\} / \{6600/\sqrt{3}\} = 87477.31 \text{ [rms, A]} = 123711.6 \text{ [peak, A]},$$

because  $S = V * I$  from the relationship  $I = S / V$

The short circuit current is calculated as  $I = 0.125 \text{ [pu]} = 15463.95 \text{ [peak, A]}$ .

It was checked whether the line constant was set in accordance with the assumptions.

→ PU is very useful for a system check

End

Change log		
Date	Example file version	Content changes
2014/11/19	2.0	Modified for XTAP Version 2.00
2013/10/02	1.3	Example name change to EDU-01-A from EDU-01 consequent to the addition of the pu calculation example
2012/07/19	1.2	Modified for XTAP Version 1.20
2011/10/18	1.1	Modified for XTAP Version 1.11 Voltage probe and current probe that had been used for the use of control output changed for the use of XPLT output
2010/09/02	1.0	First edition created (for XTAP Version 1.10)

Examples of XTAP		No.	EDU-01-B
Example Name	PU Calculation - 2		
Field	Basic calculation (power systems)		
Literature	Japan Electric Association, NEC Technical Standards Committee: “Grid interconnection code JEAC 9701-2006,” p. 196, 4th edition of issue dated June 30, 2006		
Overview	<p>In the Y method, which is effectively used in a value analysis, the system calculation is conducted in the PU system. In the present example, the checking method using the PU system through an instantaneous value analysis is shown. The ultimate aim is the target learning regarding the relationship of five cases of EDU-01-A to 01-E and parasitic-/system-based PU using actual examples.</p> <p>The following system is the specific target of this study.</p> <p>Power - impedance - transformer - impedance - 3 LG fault</p> <ul style="list-style-type: none"> <li>• The present example focuses on transformers.</li> </ul>		

# Analysis Circuit and Conditions

Figure 1 shows the analysis circuit.

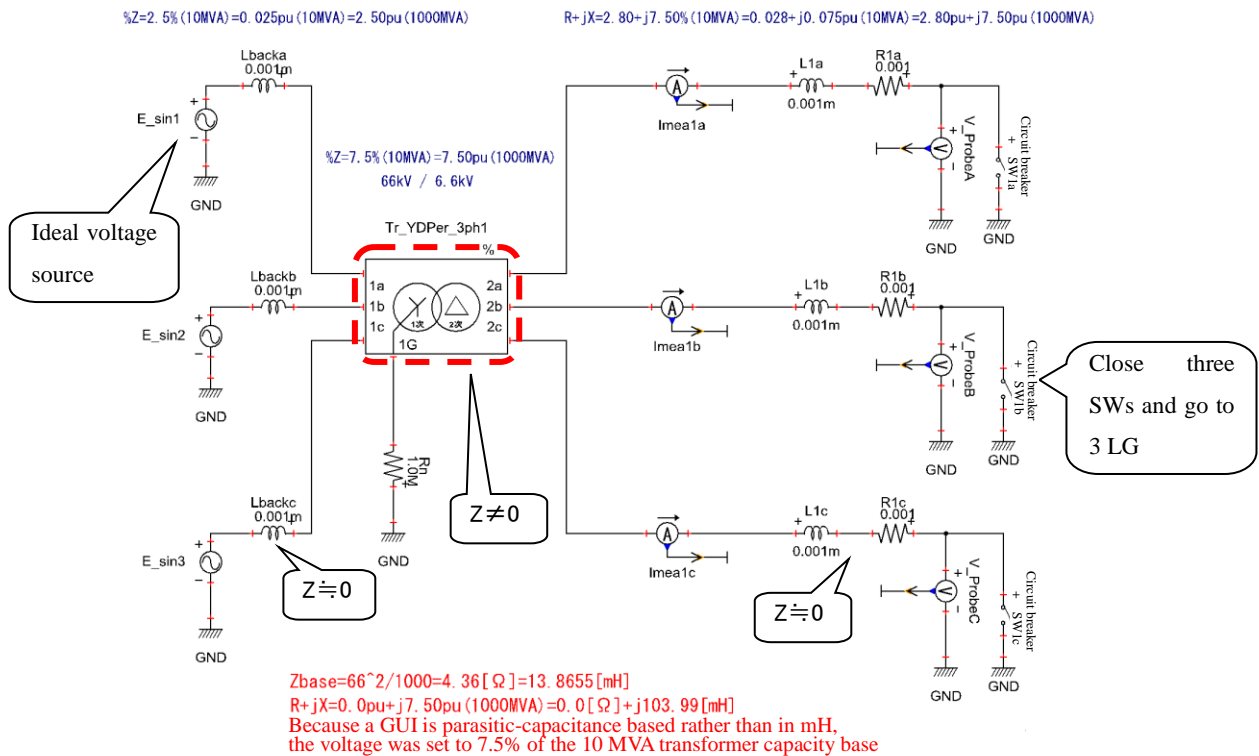


Figure 1 Analysis circuit

[System voltage]

Upper system: Line voltage of 66 [kV]. Distribution system: Line voltage of 6.6 [kV]

Standard  $Z = V^2 [kV] / S [MVA]$

[Calculation of transformer leakage Z: Considering 66-kV primary side]

$Z_{base} = 66^2/1000 = 4.36 [\Omega] = 13.8655 [mH]$  This Z value corresponds to 1 pu

- ① In the literature, this is written as % Z = 7.5% (10 MVA).
- ② Because a GUI is parasitic-capacitance based rather than in mH, the voltage was set to 7.5% of the 10 MVA transformer capacity base

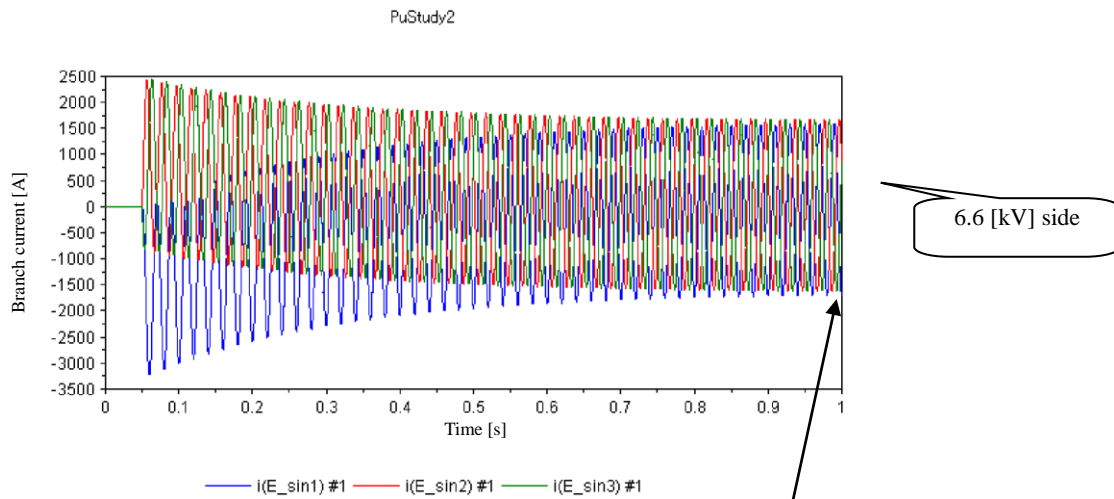
Since %Z = 7.5% (10 MVA) = 7.50 pu (1000 MVA),

$R + jX = 0.0pu + j7.50 pu (1000 MVA) = 0.0 [\Omega] + j103.99 [mH]$

7.50pu × 13.8655 [mH]

The same analysis result is obtained even if the leakage Z of the transformer is set to the minimum value (for example, 0.0001%) and the Lback is set to 103.99 mH.

## Analysis Results



Three-phase current waveform [A]

The system voltage is 1 [pu] of the line voltage 66 [kV]. Here, only the 66-kV side of the transformer is set up.

Because  $I = V/Z$ , the short-circuit current at the time of 3 LG is calculated using  $I = 1 \text{ [pu]} / Z \text{ [pu]}$ .

Here,  $Z \text{ [pu]} = R + jX = 0.0 + j7.50 \text{ [pu]} \text{ (1000 MVA)} \rightarrow |Z| = 7.5 \text{ [pu]}$

Short-circuit current at 3 LG  $I = V/Z = 1 \text{ [pu]} / 7.5 \text{ [pu]} = 0.133 \text{ [pu]} \text{ (1000 MVA, 66 kV)}$

The current of 1 [pu] of the 1000 MVA base on the 66 kV side is

$$I = S/V = \{ (1000 * 10^6)/3 \} / \{ 66000/\sqrt{3} \} = 8747.731 \text{ [rms, A]} = 12371.16 \text{ [peak, A]},$$

because  $S = V * I$  from the relationship  $I = S / V$ .

The short circuit current is calculated as  $I = 0.133 \text{ [pu]} = 1645.36 \text{ [peak, A]}$ .

It was checked whether the line constant was set in accordance with the assumptions.

→ PU is very useful for a system check.

End

Change log		
Date	Example file version	Content changes
2014/11/19	2.0	Modified for XTAP Version 2.00
2013/10/02	1.3	Example name change to EDU - 01 - B from EDU - 02 consequent to the addition of the pu calculation example
2012/07/19	1.2	Modified for XTAP Version 1.20
2011/10/18	1.1	Modified for XTAP Version 1.11 Voltage probe and current probe that had been used for the application of the control output was changed for the use of the XPLT output
2010/09/02	1.0	First edition created (for XTAP Version 1.10)

Examples of XTAP		No.	EDU-01-C
Example Name	PU calculation - 3		
Field	Basic calculation (power systems)		
Literature	Japan Electric Association, NEC Technical Standards Committee: “Grid interconnection code JEAC 9701-2006,” p. 196, 4th edition of issue dated June 30, 2006		
Overview	<p>In the Y method, which is an effective value analysis method, the system calculation is conducted in the PU system. In the present example, the checking method using the PU system through an instantaneous value analysis is shown. The ultimate aim is the target learning regarding the relationship of the five cases of EDU-01-A to 01-E and the parasitic-/system-based PU using actual examples.</p> <p>The following system is the specific target of the study.</p> <p>Power - impedance - transformer - impedance - 3 LG fault</p> <ul style="list-style-type: none"> <li>• In the PU, the capacitance and voltage are specified. Although the current can be calculated from the relationship between the two, the specific lesson learned here is that this is a short-circuit current (when <math>Z = 1</math> pu).</li> </ul> <p>Short-circuit current: Power - impedance - 3LG current at the time of the fault!</p> <p>What we would like to prove through this example is that “the short-circuit current does not change with the pu.” The advantage of a PU is that it can be used uniformly irrespective of changes in the voltage class, and this fact has been widely acknowledged in several publications. In other words, the base <math>Z</math> [<math>\Omega</math>] changes with a change in voltage class, and hence the ampere of the short circuit current changes; however, it remains the same in the PU, which is the greatest merit of the PU system. That is, the short-circuit current [pu] does not depend on the voltage class in the PU system, and it is therefore very convenient to measure the strength (<math>1/X</math>) of the line!</p>		

# Analysis Circuit and Conditions

Figure 1 shows the analysis circuit.

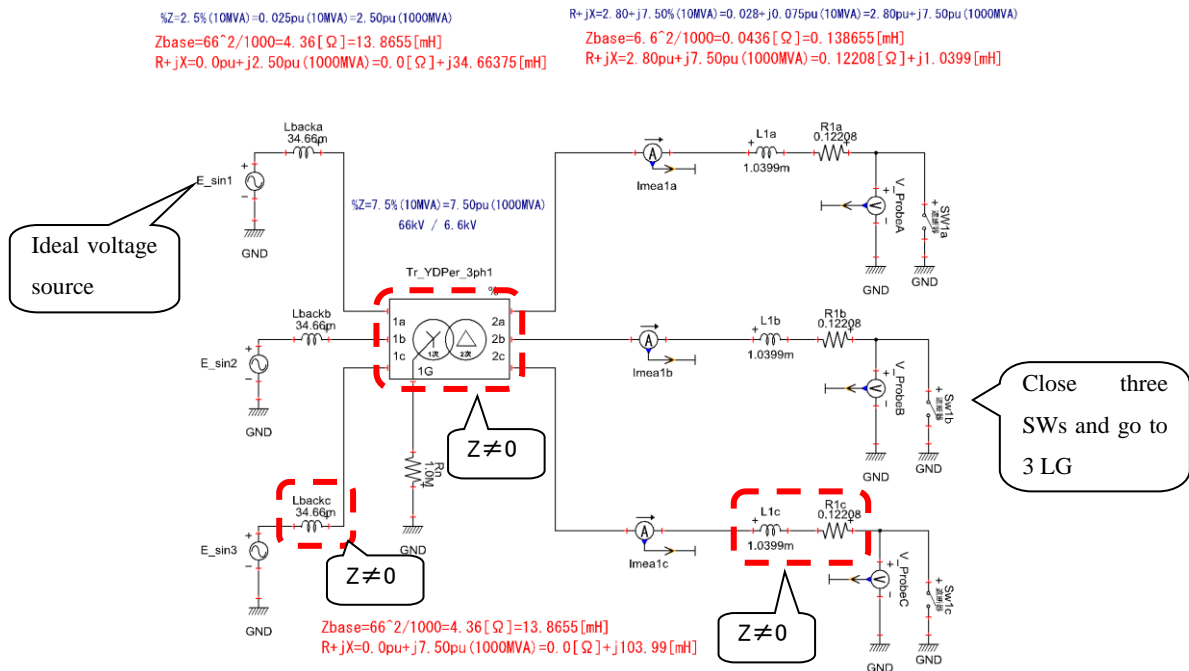


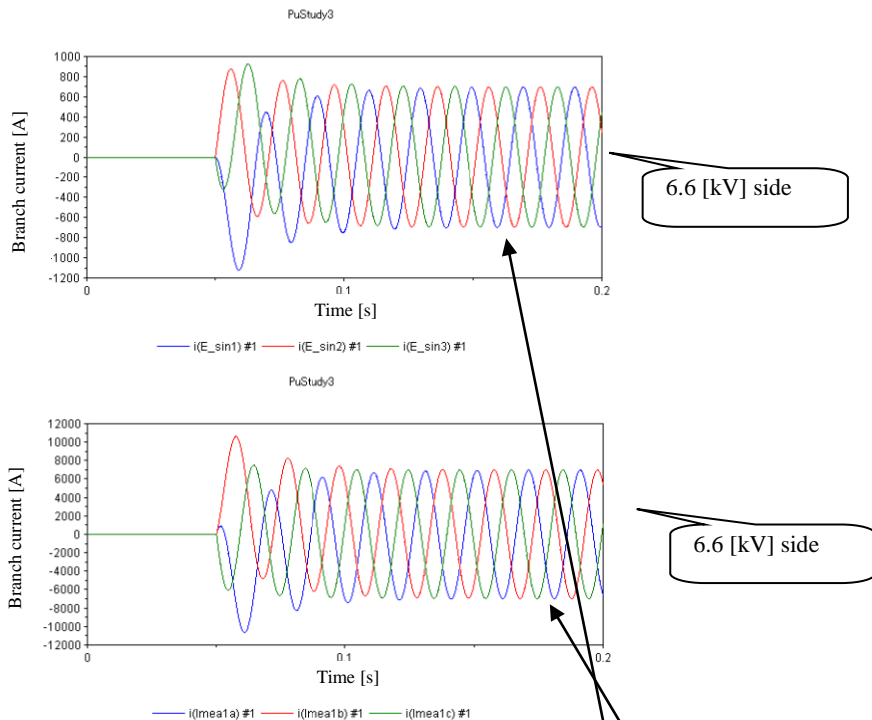
Figure 1 Analysis circuit

[System voltage]

Upper system: Line voltage of 66 [kV].      Distribution system: Line voltage of 6.6 [kV]

Standard  $Z = V^2 [kV] / S [MVA]$

## Analysis Results



Three-phase current waveform [A]

Because  $I = V / Z$ , the short-circuit current at 3 LG is calculated using  $I = 1 \text{ [pu]} / Z \text{ [pu]}$ .

Here,  $Z[\text{pu}] = (0 + j2.5) + (0.0 + j7.5) + (2.80 + j7.50) \text{ [pu]} (1000 \text{ MVA}) = 2.80 + j17.50 \rightarrow |Z| = 17.72[\text{pu}]$

At the time of 3 LG, the short circuit current  $I = V/Z = 1[\text{pu}] / 17.72 \text{ [pu]} = 0.0564 \text{ [pu]} (1000 \text{ MVA}, 66 \text{ kV})$

The current of 1 [pu] of the 1000 MVA base on the 66 kV side is

$$I = S/V = \{ (1000 * 10^6) / 3 \} / \{ 66000/\text{sqrt}(3) \} = 8747.731 \text{ [rms, A]} = 12371.16 \text{ [peak, A]}$$

because  $S = V * I$  from the relationship  $I = S / V$

The short-circuit current is calculated as  $I = 0.0564 \text{ [pu]} = 697.73 \text{ [peak, A]}$

In contrast, the current of 1 [pu] based on 1000 MVA on the 6.6 kV side is

$$I = S/V = \{ (1000 * 10^6) / 3 \} / \{ 6600 / \text{sqrt}(3) \} = 87477.31 \text{ [rms, A]} = 123711.6 \text{ [peak, A]}$$

since  $S = V * I$  from the relationship  $I = S / V$ .

The short-circuit current on the 6.6-kV low-voltage side is calculated as  $I = 0.0564 \text{ [pu]} = 6977.3 \text{ [peak, A]}$ .

Moreover, the voltage class comes into view when converting the value of the secondary side to the primary side (MKS system).

This appears when converting the value of the primary side to the secondary side.

In the analysis of the PU system, the voltage class becomes irrelevant on both the primary and secondary sides, and the effective and instantaneous value analyses are the same. Consequently, **the relaxed responses of the fundamental waves in the results of the effective and instantaneous value analyses**

Calculate on your own and try to understand the PU system

Parasitic base must be converted to the system

**must coincide.** If this does not occur, then either the modeling or the PU system is considered to be flawed.

End

Change log		
Date	Example file version	Content changes
2014/11/19	2.0	Modified for XTAP Version 2.00
2013/10/02	1.3	Example name changed to EDU- 01-C from EDU-03 consequent to the addition of the pu calculation example
2012/07/19	1.2	Modified for XTAP Version 1.20
2011/10/18	1.1	Modified for XTAP Version 1.11 Voltage and current probes used for the change in control output for use of XPLT output
2010/09/02	1.0	First edition created (for XTAP Version 1.10)

Examples of XTAP		No.	EDU-01-D
Example Name	PU Calculation - 4		
Field	Basic calculation (power systems)		
Literature	Japan Electric Association, NEC Technical Standards Committee: “Grid interconnection code JEAC 9701-2006,” p. 196, 4th edition of issue dated June 30, 2006		
Overview	<p>Regarding the PU, (a) the conversion of the secondary side impedance to the primary side (when the voltage classes are different) and (b) the parasitic capacitance and system bases (when the standard capacities are different) have been dealt with in detail in various publications. The aim of this example is to learn (a) above using actual examples.</p> <p>The following systems are the specific targets of the present study.</p> <p>Power - impedance - transformer - impedance - 3 LG fault</p> <p>• It is mentioned at the end of EDU-01-C that the “voltage class” comes into view when converting the <math>\circ</math> side to the <math>\Delta</math> side. The correct expression is <b>converting the amount in the MKS system of the <math>\circ</math> side to that of the <math>\Delta</math> side</b>. The important aspect here is that, having conducted the study using an equivalent circuit of the transformer, <u>the term <math>a^2 * L</math> is used when converting the series circuit L on the secondary side to the primary side. When converting the parallel circuit M on the secondary side to the primary side, the term <math>a^2 * M</math> is used.</u> However, this has nothing to do with the pu system.</p>		

## Analysis Circuit and Conditions

Figure 1 shows the analysis circuit.

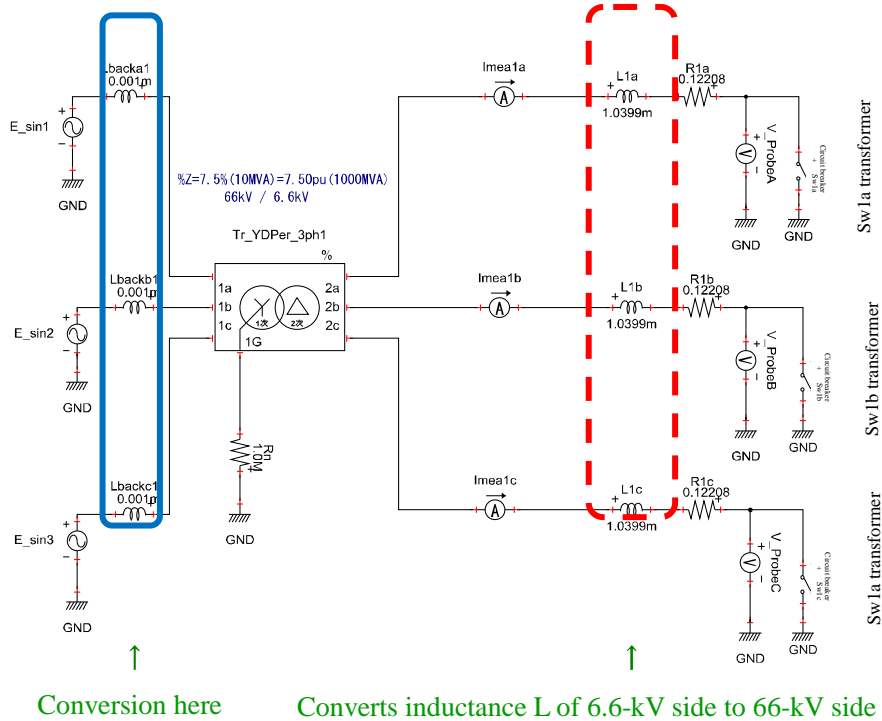


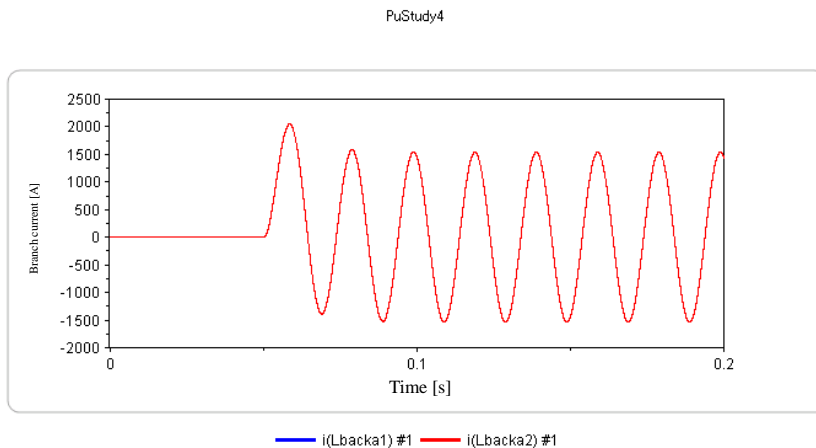
Figure 1 Analysis circuit

Figure (a) shows the inductance L on the 6.6-kV side surrounded by the dotted line.

Figure (b) shows a circuit in which the inductance L is converted into the 66-kV side.

In Figures (a) and (b), the currents passing through the inductance L surrounded by the solid line are compared. Because only the inductance L is converted, the waveforms are the same.

## Analysis Results



The graph was plotted by superimposing the current of phase A on the 66-kV side. This indicates that the conversion was carried out satisfactorily. The method of conversion is as follows.

The inductance at 6.6 and 66 kV increases 10- or 1/10-fold. Because the inductance is  $a^2 \cdot L$ , as in the case of a transformer conversion, it should be increased 100-fold.

$$L \text{ on the 6.6-kV side} = 1.0399 \text{ [mH]}$$

$$L \text{ on the 66-kV side} = 103.99 \text{ [mH]}$$

⇒ It has been ascertained that the **amount on the  $\circ$  side in the MKS system has been converted to that of the  $\Delta$  side**. There is no reference to the pu.

The discussion regarding the pu is as follows.

Let us look at an expression such as “Let the leakage reactance of the transformer be 10%.” Regardless of whether X is placed on the primary or secondary side,  $X = 0.10$  pu. This occurs because the expression essentially means “there is a 10% voltage drop when a rated current flows through the transformer.”

Instead, suppose there is a specification stating that the leakage reactance is 10% at the transformer parasitic capacitance base (10 MVA). Suppose we try to convert X using this as the data of the analysis program of the system base, namely, 1000 MVA. It was previously stated in the example of EDU-01-A that “ $R + jX = 0.028 + j 0.075$  pu (10 MVA) = 2.80 pu + j 7.50 pu (1000 MVA).” It was also mentioned that “the line impedance of the 6.6-kV system becomes a large value when we consider the trunk transmission system.” Taking this into consideration, we have  $X = 10\%$  (10 MVA) = 0.1 pu (10 MVA) = 10 pu (1000 MVA) (※).

We will now give a summary of the parasitic and system bases in the impedance of the device. The generator rear X is parasitic-capacitance based and is set to 1.8 pu, for example. When connecting the synchronous generator to the power system, it is converted to the system base and to the system itself (see the figure below). As an image, the large-capacitance generator strengthens the system. Although this has the same value as the parasitic-capacitance based pu value, it means that, as the capacitance increases, X

becomes smaller when converted into the system. This is the same as an image with improved stability. It is sufficient to consider the fact that, “even if the pu value that is based on the parasitic capacitance is the same, the impedance when converted into the system becomes larger as the capacitance becomes smaller,” and remembering the formula is not quite essential.

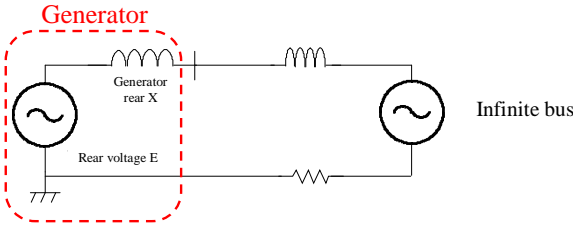


Figure Connection of synchronous generator to the power system

End

Change log		
Date	Example file version	Content changes
2014/11/19	2.0	Modified for XTAP Version 2.00
2014/07/29	1.0	First edition created (for XTAP Version 1.21)

Examples of XTAP		No.	EDU-01-E
Example Name	PU Calculation - 5		
Field	Basic calculation (power systems)		
Literature	Japan Electric Association, NEC Technical Standards Committee: “Grid interconnection code JEAC 9701-2006,” p. 196, 4th edition of issue dated June 30, 2006		
Overview	<p>Regarding the PU, (a) the conversion of the secondary side impedance to the primary side (when the voltage classes are different) and (b) the parasitic capacity and system bases (when the standard capacities are different) have been dealt with in detail in previous publications. The aim of this example is to learn (b) above using actual examples.</p> <p>The following system is the specific target of the study.</p> <p>Power - impedance - transformer - impedance - connecting the load</p> <ul style="list-style-type: none"> <li>• The target circuit is a EDU-01-C circuit connected with a load without a system fault.</li> <li>• The impedance is described in EDU-01-B. The difference between the system and parasitic bases will be described through a graphical representation of the active/reactive power P-Q and current I in the pu system. It is assumed that the example of a “PQVI calculation of a three-phase circuit” has been implemented.</li> </ul>		

## Analysis Circuit and Conditions

Figure 1 shows the analysis circuit.

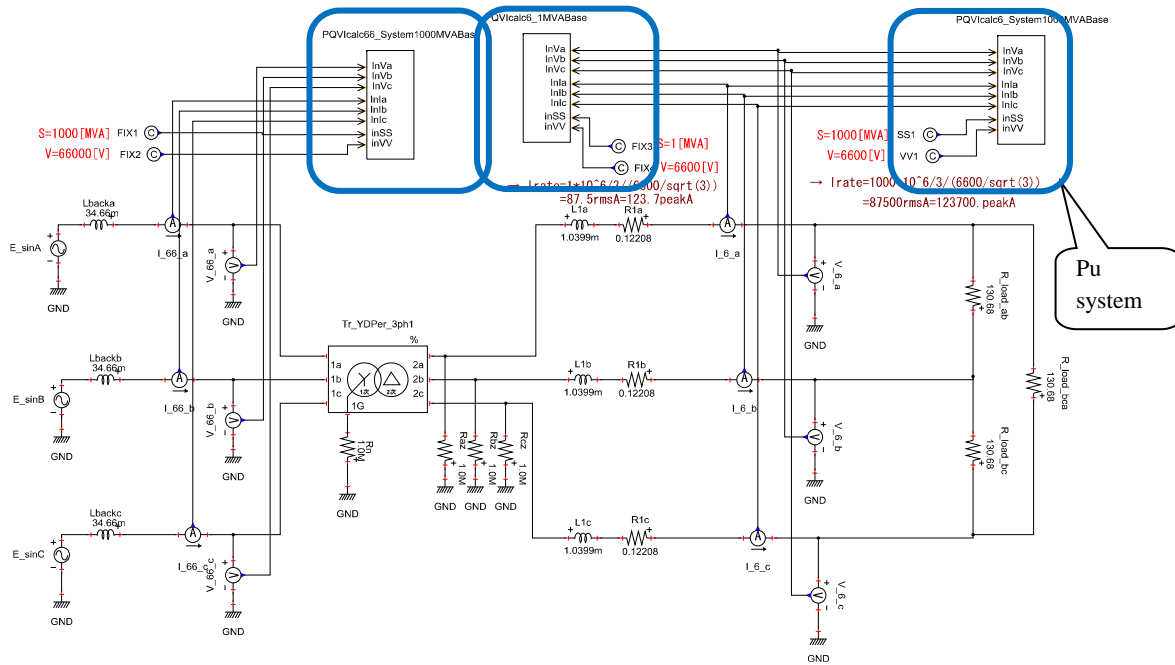
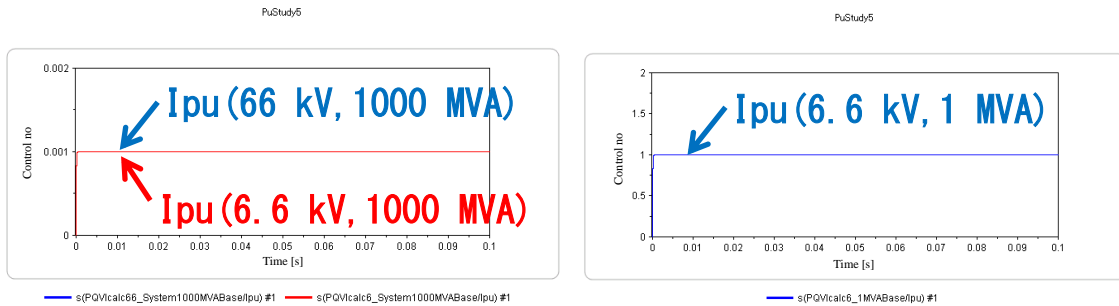


Figure 1 Analysis circuit

A resistive load of 1 MW is attached to the 6.6-kV system. The boxed area is subjected to the pu system. The analysis is conducted under a steady state, and the difference between the system base and the parasitic base is explained through the creation of a graphical representation of the active/reactive power P-Q and current I in the pu system.

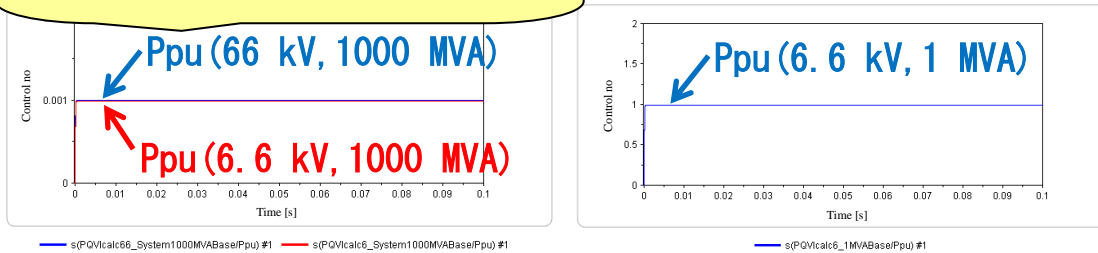
## Analysis Results

If the system base is the same,  $I_{pu}$  remains the same regardless of the change in voltage class, which is the advantage of the pu.



Because the load is 1 MW, this is naturally because the load is 1 MW, this is naturally 1.0 pu in the 1 MVA basis. Here,  $V = 1$  pu. 0.001 pu in the 1000 MVA base.

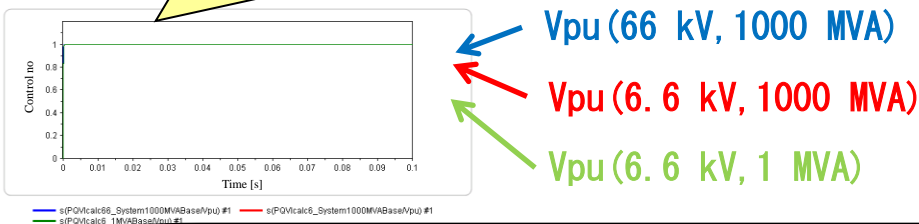
If the system base is the same,  $P_{pu}$  remains the same regardless of the change in voltage class.



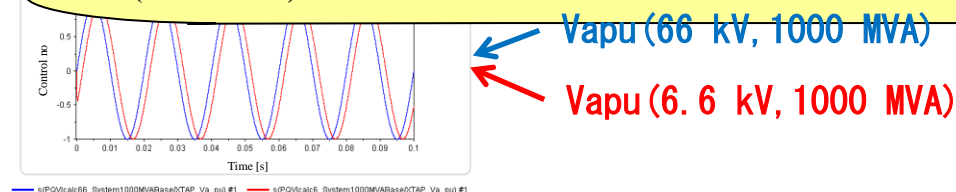
The same meaning is implied.

The same meaning is implied.

When the voltage is converted into the pu, despite the change in voltage class, all the values are 1 pu in the case of the rated voltage, regardless of the change in the system base.



It can be seen that even in the pu system, the difference in the A phase voltage occurs when an active power flows in the transmission line of the inductance owing to the relationship  $P = (V_1 * V_2 / X) * \sin \delta$ .



End

Change log		
Date	Example file version	Content changes
2014/11/19	2.0	Modified for XTAP Version 2.00
2012/11/15	1.0	First edition created (for XTAP Version 1.21)

Examples of XTAP		No.	EDU-02
Example Name	Calculation of Three-Phase Circuit PQVI		
Field	Basic calculation (power systems)		
Literature	Kenzi, Noda, Takenaka: "Development of Instantaneous Value Simulation Method for Induction Motors for Transient Phenomena Analysis," CRIEP Report R 08022, June 2009		
Overview	<p>It is a well-known fact that a PQ calculation is conducted using a VI bar in the Y method, which is effectively applied to a value analysis. In this example, an actual example of a PQVI calculation using the instantaneous value of the voltage/current of the three phases is shown. In particular, we show the calculation method in both the volt ampere system and the pu system. The goal is also to become familiar with a dq conversion (not actual, please refer to the study above) by demonstrating the calculation method using a <math>\alpha\beta</math> conversion.</p> <p>The following calculation is demonstrated.</p> <p>1 . Units [V], [A], [W], [var]</p> <p>(1) Three-phase voltage <math>\cdot</math> current <math>\rightarrow</math> PQ calculation Variable names: PP31 and QQ31</p> <p>(2) Calculation using the 90° lag information mentioned above Variable names: PP 32 and QQ 32</p> <p>(3) abc coordinates <math>\rightarrow</math> calculation of <math>\alpha\beta</math> coordinates of voltage and current Variable names: LAGVal, LAGVbe, LAGIal, and LagIbe</p> <p>(4) Three-phase voltage <math>\cdot</math> current <math>\rightarrow</math> VI calculation Variable names: LAGVsimp and LAGIsimp</p> <p>(5) abc coordinates <math>\rightarrow</math> calculation of <math>\alpha\beta</math> coordinates of voltage and current <math>\rightarrow</math> PQ calculation Variable names: PP and QQ</p> <p>2 . Units [pu]</p> <p>(1) 1. pu system of (3) and (4): VsimPU, IsimPU, ValPU, VbePU, IalPU, and IbePU</p> <p>(2) Calculation using amount of voltage in pu and the current mentioned above Variable names: PPPU and QQPU</p>		

# Analysis Circuit and Conditions

Figure 1 shows the analysis circuit.

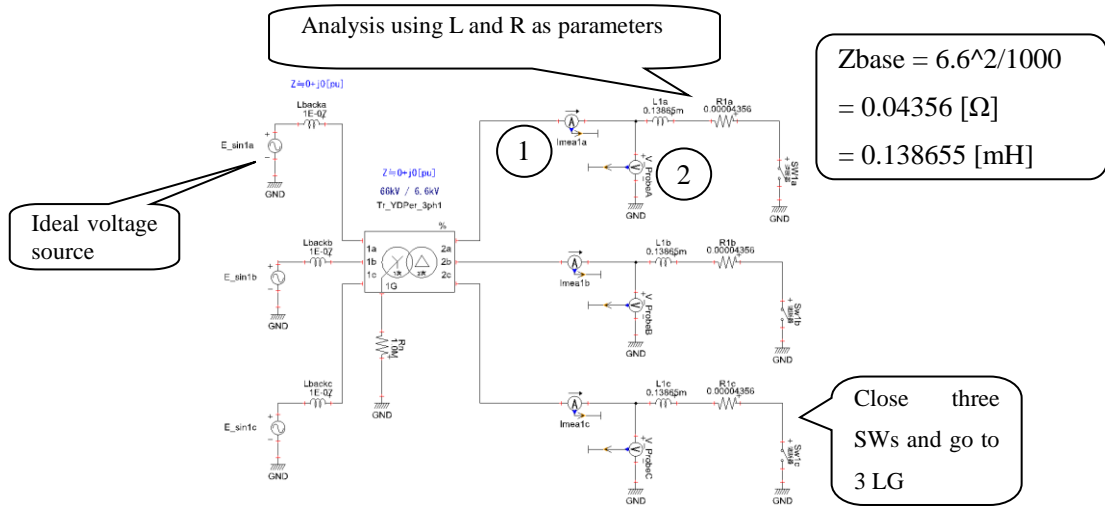
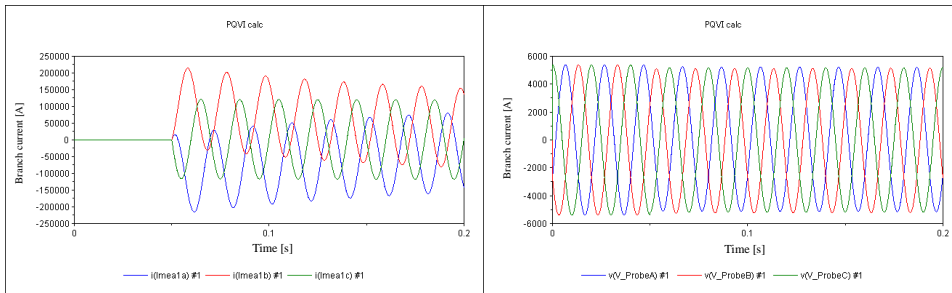


Figure 1 Analysis circuit

- Case1:  $L = 0.138655 \text{ [mH]} = 1.0 \text{ pu}$      $R = 0.00004356 \text{ [}\Omega\text{]} = 0.001 \text{ pu}$  (Figure 1)
- Case2:  $L = 0.138655 \text{ [}\mu\text{H]} = 0.001 \text{ pu}$      $R = 0.00004356 \text{ [k}\Omega\text{]} = 1.0 \text{ pu}$

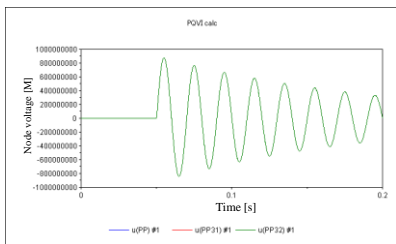
## Analysis result

- Case 1

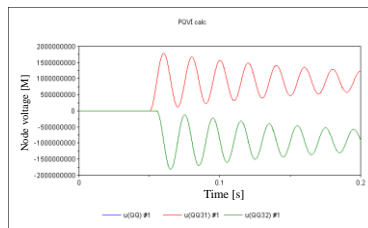


1

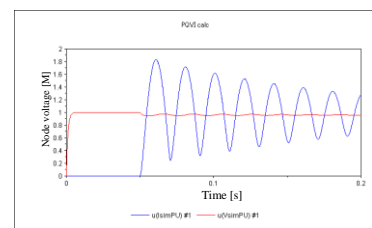
2



P[W] waveform



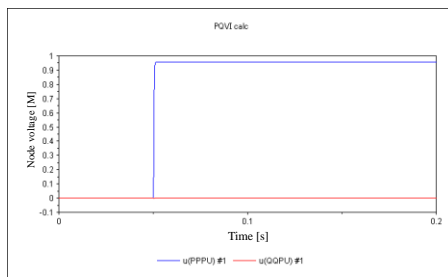
Q[var] waveform



V[pu] and I[pu] waveforms

A DC component is superimposed on the current using 3 LG (①). The voltage is slightly lower owing to the voltage drop of Tr (②). Active power P and reactive power Q fluctuate at 50 Hz owing to the influence of the DC current. During the fault period, because load L is connected in parallel to the voltage source, only Q is 1 pu, and P becomes zero following the attenuation of the DC component current (because the value of load L is set to 1 pu in the Z-base, namely,  $Q = 1$  pu). Because the green waveform of Q alone is calculated using the information of a  $90^\circ$  lag, the waveform is shifted by  $90^\circ$  (shown as a negative quantity for easier understanding).

• Case 2



PQ waveform [pu]

During the fault period, because the load R is connected in parallel to the voltage source, P alone is 1 pu, and Q is zero. Because the only load on the circuit is R, the DC component is quickly attenuated and the PQ waveform does not oscillate with the system frequency. Here, although the circuit load R is 1 pu, P does not become exactly 1 pu because of the voltage drop owing to transformer leakage Z (although very small) and because R is slightly larger owing to the ON resistance of the circuit breaker.

A noteworthy point here is that displaying the pu makes for a clearer understanding, and is recommended because the validity of the analysis result (namely, whether it matches the actual results) can also be easily checked.

End

Change log		
Date	Example file version	Content changes
2014/11/19	2.0	Modified for XTAP Version 2.00
2013/10/02	1.3	Example name change to EDU-02 from EDU-04 consequent to the addition of the pu calculation example
2012/07/19	1.2	Modified for XTAP Version 1.20
2011/10/18	1.1	Modified for XTAP Version 1.11
2010/09/02	1.0	First edition created (for XTAP Version 1.10)

Examples of XTAP		No.	EDU-03
Example Name	Comparison with Y Method, which is an Effective Value Analysis Method - Load P Attached		
Field	Basic calculation (power systems)		
References	None		
Overview	<p>In this example, a comparison of XTAP with the Y method, which is effectively applied to a value analysis, is conducted using a simple circuit. The aim is to understand through an analysis the difference in voltage phase owing to an exchange of P. This holds for both the generator and load.</p>		

# Analysis Circuit and Conditions

Figure 1 shows the analysis circuit.

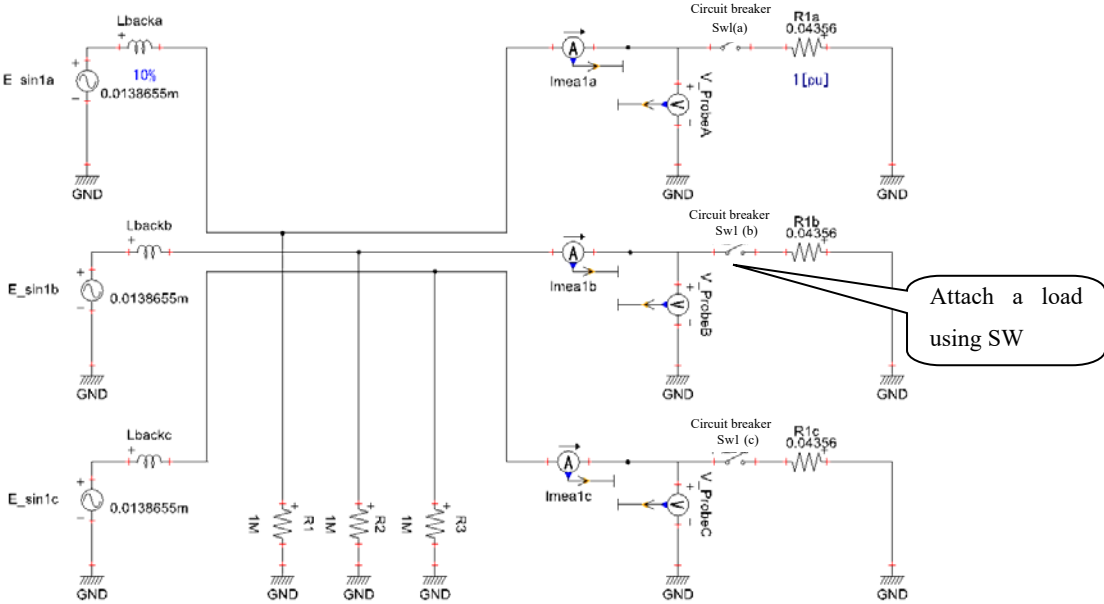
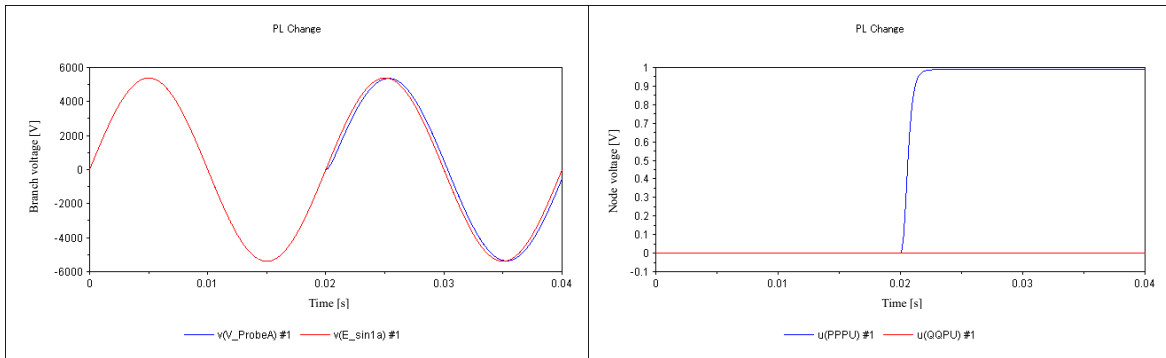


Figure 1 Analysis circuit

A load is normally floated from the zero-phase circuit using a Y - Δ transformer. For the sake of simplicity, in this example the load is attached using SW.

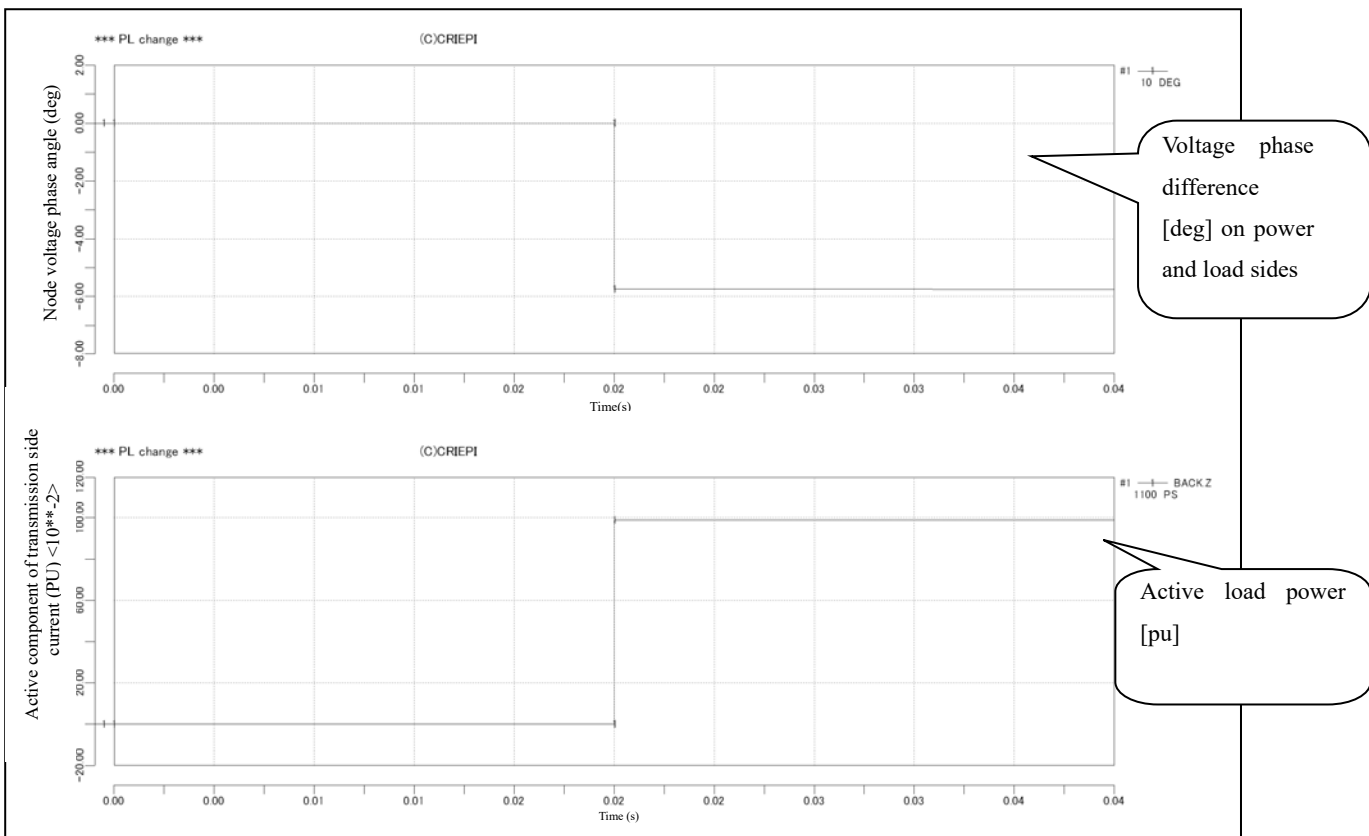
## Analysis Results



Phase A voltage [V] on the power and load sides

PQ [pu] of load

## Y Method Analysis Results



It can be seen that the load generates a phase difference in the voltage on the power supply and load sides. The change in the active power is clean owing to the resistive load.

End

Change log		
Date	Example file version	Content changes
2014/11/19	2.0	Modified for XTAP Version 2.00
2013/10/02	1.3	Example name changed to EDU-03 from EDU-05 consequent to the addition of the pu calculation example
2012/07/19	1.2	Modified for XTAP Version 1.20
2011/10/18	1.1	Modified for XTAP Version 1.11
2010/09/02	1.0	First edition created (for XTAP Version 1.10)

Examples of XTAP		No.	EDU-04
Example Name	Comparison with Y Method, which is an Effective Value Analysis Method – Change in Impedance Z		
Field	Basic calculation (power systems)		
Literature	None		
Overview	<p>In this example, a comparison of XTAP with the Y method, which is effectively applied to a value analysis, is conducted using a simple circuit. The circuit conditions are as follows and only the impedance is changed. The voltages at both ends remain unchanged (<math>V_1</math>, <math>V_2</math>, and <math>\delta</math> do not change).</p> <p>Power supply - impedance - change component <math>\Delta Z</math> - power supply</p> <p>The basic equation of the power transmission is <math>P = V_1 * V_2 / X * \sin \delta</math>. It can be seen from this equation that the active power varies with a change in X. Here, X is a series element with respect to the power system. Through this example, it was verified that in series elements, P varies with a change in X.</p>		

# Analysis Circuit and Conditions

Figure 1 shows the analysis circuit.

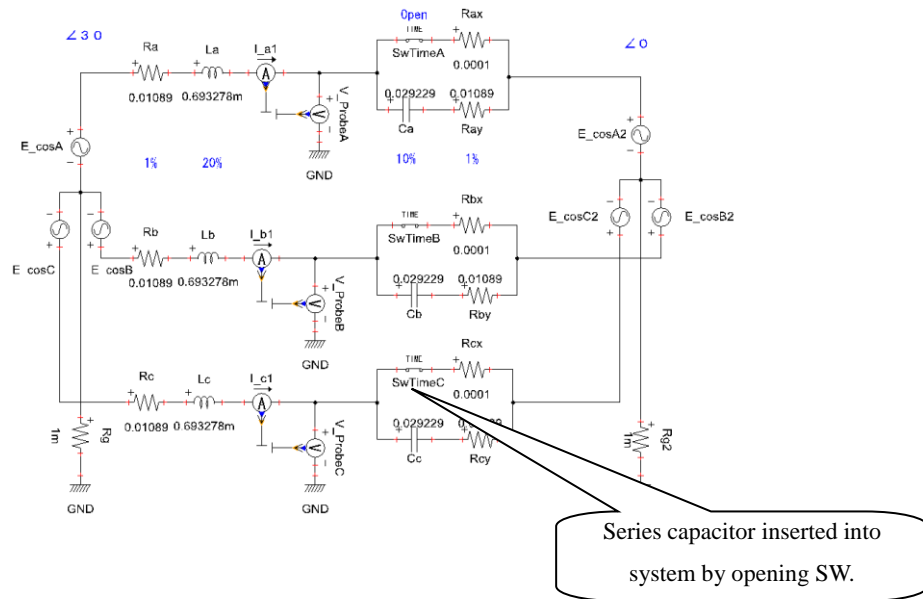
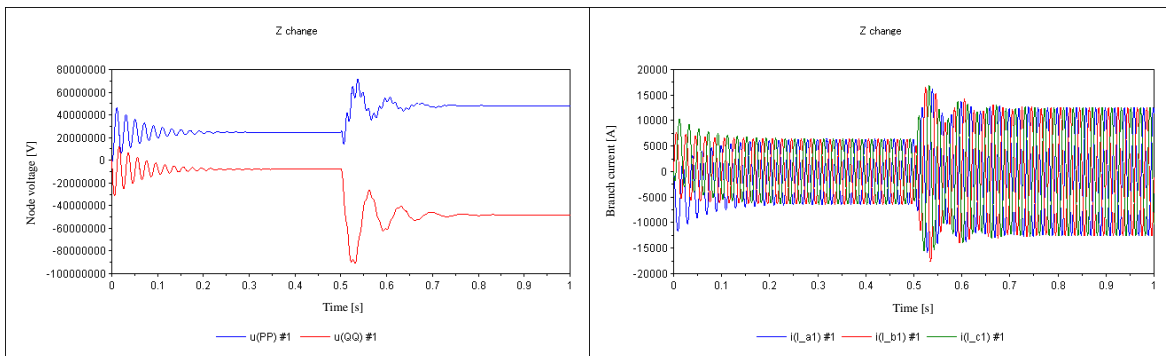


Figure 1 Analysis circuit

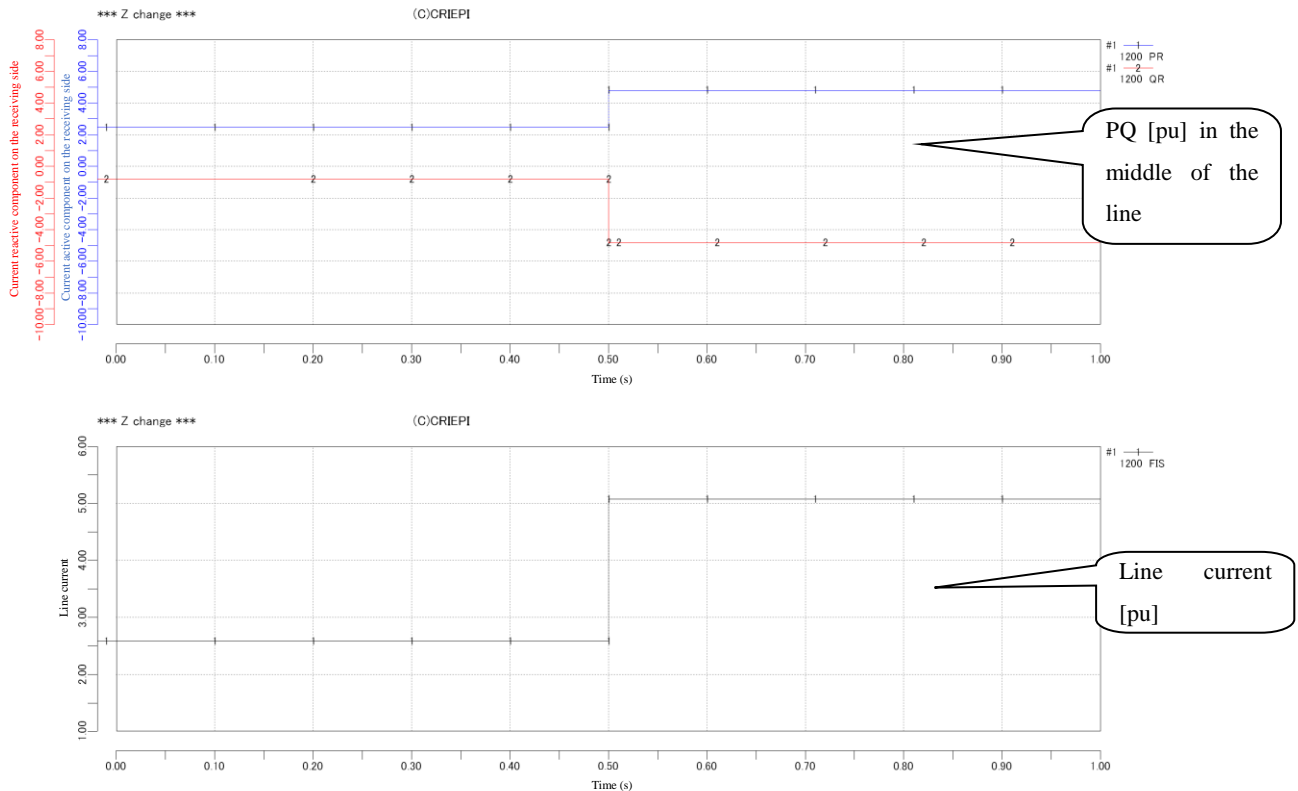
# Analysis Results



P[W], Q[Var] in the middle of the line

Three-phase current [A] in the middle of the line

## Y Method Analysis Result



Because the impedance between the power supplies is small, as seen from the relationship  $P = V_1 * V_2 * \sin \delta / X$ ,  $P$  becomes larger after the capacitor is inserted. Further, because  $P$  is doubled without a change in voltage, the active current doubles. It should be noted that the waveform for the instantaneous value is the combination of the active and reactive components of the current. It was ascertained that the response of the fundamental wave can be understood from the effective value analysis results, and in the instantaneous value analysis, an analysis of the power systems including high-frequency components can be conducted.

Because  $D = \sqrt{\{(R / 2 L) 2 - 1 / (LC)\}} \rightarrow D = \{2 * 0.01890 / (2 * 0.000693)\} 2 - 1 / (0.000693 * 0.0292)$  from the equation of applied sinusoidal voltage to the series circuit  $R - L - C$ , we have  $D = -48696$ .  $\rightarrow \omega = 2 \pi f = \sqrt{48696}$ , from which we have  $f = 35.12$  [Hz]  $\rightarrow T = 0.0284$  [s]. This is the fluctuating frequency component of the current, and in terms of PQ, commercial frequencies of  $50 \text{ Hz} \pm 35 =$  approximately 15 and 85 Hz are obtained. The XTAP analysis results show that the 15 and 85 Hz components were superimposed on the vibration of PQ.

End

Change log		
Date	Example file version	Content changes
2014/11/19	2.0	Modified for XTAP Version 2.00
2013/10/02	1.3	Example name changed to EDU-04 from EDU-06 consequent to the addition of the pu calculation example
2012/07/19	1.2	Modified for XTAP Version 1.20
2011/10/18	1.1	Modified for XTAP Version 1.11
2010/09/02	1.0	First edition created (for XTAP Version 1.10)

<b>XTAP Example Collection</b>		<b>No.</b>	PE-01
<b>Example Name</b>	Simulation of Three-phase PWM Inverter Circuit		
<b>Field</b>	Power electronics		
<b>References</b>	Technical Report No. 761, "Simulation Technology of Power Electronics System," the Institute of Electrical Engineers of Japan		
<b>Outline</b>	<p>In the "Power Electronic System Simulation Technology Cooperative Study Group" set up by the Industrial Application Division of the Institute of Electrical Engineers, several benchmark circuits were created with the purpose of evaluating various analytical programs. In "Benchmark I," the first benchmark circuit, a three-phase PWM inverter circuit is applied as a typical power electronic circuit, and its example is presented herein.</p> <p>This example inverter converts a direct current into a three-phase alternating current of 100 Hz. By combining the control blocks, a PWM pattern corresponding to the three-phase alternating current is generated, by which the six switches constituting the three-phase bridge are switched on and off to convert the direct current into an alternating current. The above switches and reflux diodes are simulated using simplified characteristics based on the ON and OFF resistances.</p>		

## Analysis Circuit and Conditions

Figure 1 shows the analysis circuit

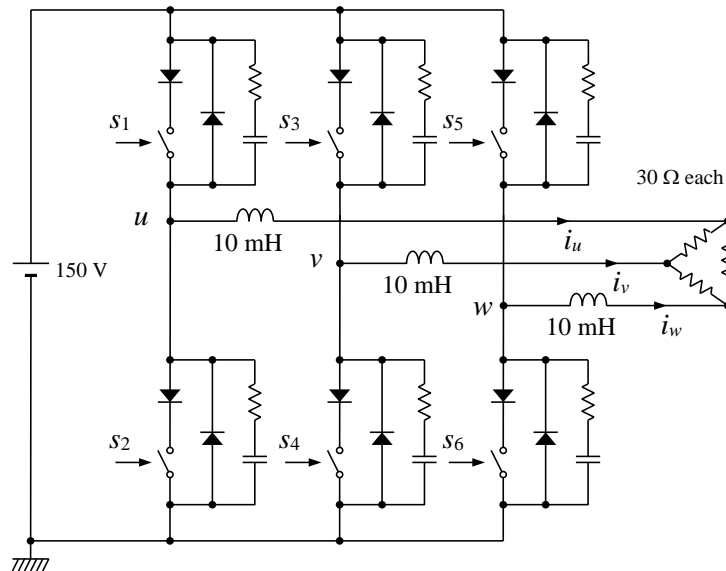


Figure 1 Analysis circuit

### [Circuit Operation]

Apply a 150-V DC voltage generated by the DC voltage source on the left side of Figure 1 to the three-phase bridge. By switching the six switches of the three-phase bridge,  $S_1, S_2, \dots, S_6$ , ON and OFF according to the PWM pattern corresponding to a three-phase alternating current, the applied DC voltage is converted into a three-phase alternating current consisting of  $u, v$ , and  $w$  phases. However, the PWM pattern corresponding to the three-phase alternating current is generated using a separate control system. The above three-phase voltage is applied to the load through a 10-mH reactor, which is a higher harmonic filter. The load is a delta connection of three resistors of  $30 \Omega$ .

### [Generation of PWM Pattern]

A PWM pattern is generated using a triangle wave comparison method. As an example, we determine the PWM pattern to generate a sinusoidal wave of the  $u$ -phase in Figure 2. The  $u$ -phase sinusoidal wave, which is the command value, is superimposed and plotted on a triangular wave of amplitude 1, called the carrier. Because the amplitude of the  $u$ -phase sinusoidal wave is 0.8, the degree of modulation at this time is said to be 0.8. When the sinusoidal wave is smaller than the triangular wave, a zero is output, and when the sinusoidal wave is larger than the triangular wave, the output is 1. This is the PWM pattern for the  $u$ -phase sinusoidal wave. The PWM pattern remains zero for a lengthy time at locations where the command value is small, and remains 1 for a lengthy time where the command value is large. In Figure 2, to avoid complications, the waveform is drawn by lowering the carrier frequency. However, because the carrier frequency is set much higher than the frequency of the sine wave, the PWM pattern changes more frequently, and the command value can be faithfully reproduced based on a time change of time ratio (duty ratio) 1.

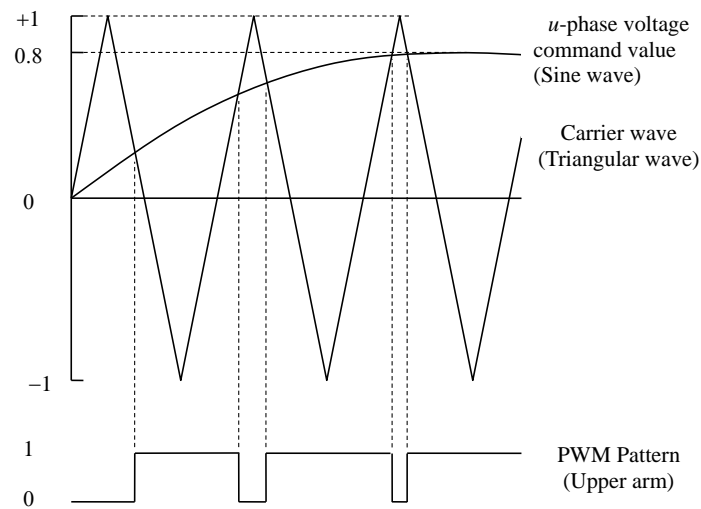


Figure 2 Triangular wave comparison method

Switch  $S_1$  of the upper arm of the leg corresponding to the  $u$ -phase of the three-phase bridge turns ON when the PWM pattern is 1, and is turned OFF when it is zero (note that one switch is called an arm, and upper and lower arms combine to form a leg). In contrast, switch  $S_2$  of the lower arm of the  $u$ -phase leg turns ON when the PWM pattern is zero, and turns OFF when it is 1. However, to prevent the upper and lower arms of the same phase turning on at the same time and short-circuiting the DC power supply, the turn-on timing is delayed by only a small time-delay  $T_d$  between the switches in both arms, and the turn-off timing is advanced by  $T_d$ , which is called the dead time.

In this example, the parameters related to PWM pattern generation are set as follows:

- Carrier frequency: 5 kHz
- Frequency of the sine wave: 100 Hz
- Degree of modulation: 0.8
- Dead time: 5  $\mu$ s

#### [Switching Element, Reflux Diode, and Snubber Circuit]

In an actual PWM inverter, MOSFETs and IGBTs are used as the switching elements. However, in this example, for the sake of simplicity, we conduct a simulation using simplified characteristics such as an ON-resistance of 10 m $\Omega$  and an OFF-resistance of 1 M $\Omega$ . These characteristics are realized by connecting an ideal switch (ON-resistance of zero, OFF-resistance of  $\infty$ ) in-series using a diode with an ON-resistance of 10 m $\Omega$  and an OFF-resistance 1 M $\Omega$ .

In the inverter circuit, the diode is connected anti-parallel to the switching element. This is called a reflux diode. A reflux diode prevents the occurrence of an overvoltage by blocking the inductive load current. This refluxing diode is also simulated using an ON-resistance of 10 m $\Omega$  and an OFF-resistance of 1 M $\Omega$ , as described above.

Normally, a protection circuit is provided to prevent the destruction of the switching element from an overvoltage or overcurrent during the operation of the switching element. This protection circuit is called a snubber circuit. In this example, a CR snubber, which is a series circuit of a capacitor and a resistor, is used. The capacitor value is set to 0.05  $\mu\text{F}$ , and the resistor value is set to 300  $\Omega$ .

[Analysis Conditions]

The analysis conditions are as follows.

- Calculation time step            1  $\mu\text{s}$
- Calculation start time           0 ms
- Calculation end time            40 ms
- Display start time               20 ms
- Display end time                 40 ms

[Example of XTAP Input]

An instance of creating this example using XTAP is shown in Figure 3.

Example Name: Simulation of three-phase PWM inverter circuit

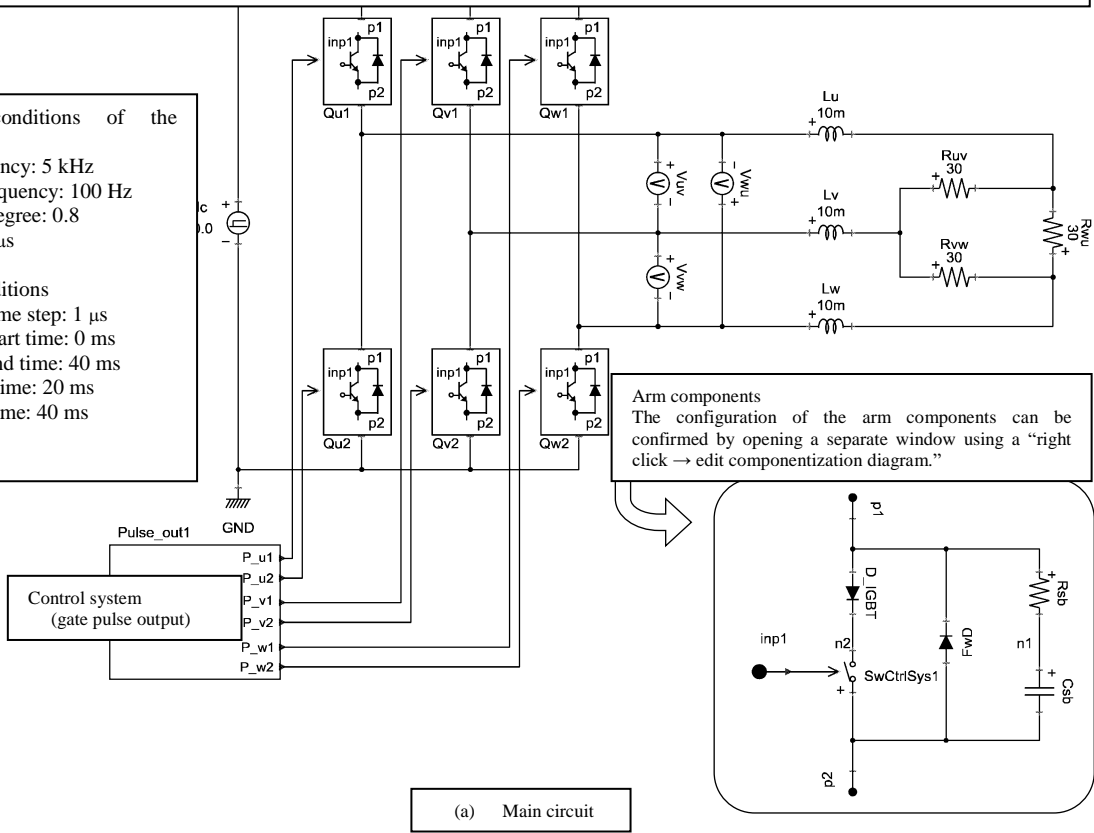
No.: PE-01

This is a three-phase PWM inverter circuit of benchmark test 1 created through the "Joint Research Committee on Simulation Technology of Power Electronics Systems" of the Institute of Electrical Engineers.

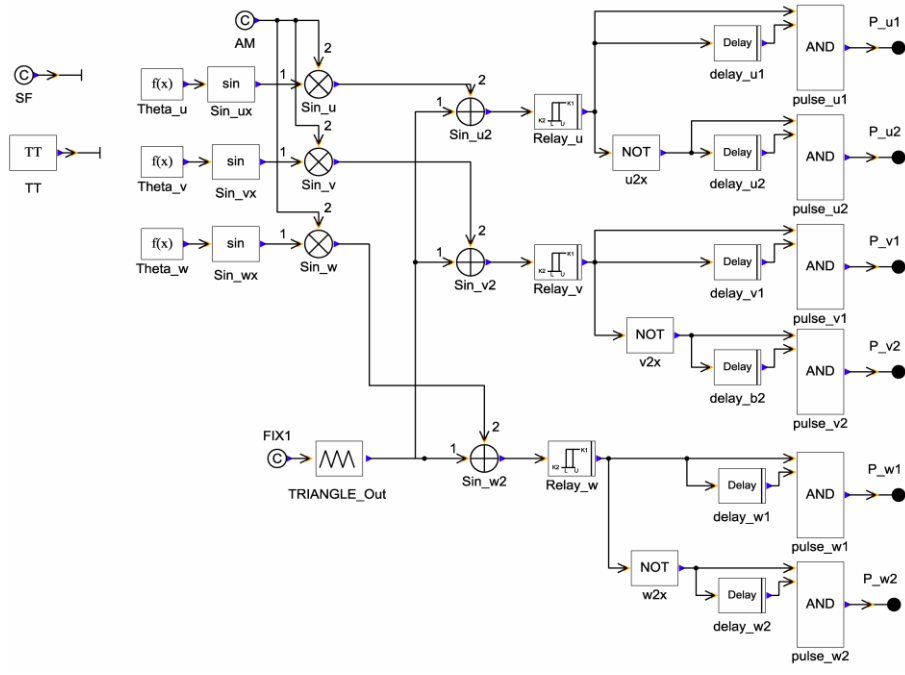
In this circuit, using the componentization function, the arms are componentized and used as upper and lower arms of the phases u, v, and w.

Operating conditions of the inverter  
 Carrier frequency: 5 kHz  
 Sine wave frequency: 100 Hz  
 Modulation degree: 0.8  
 Dead time: 5  $\mu$ s

Analysis conditions  
 Calculation time step: 1  $\mu$ s  
 Calculation start time: 0 ms  
 Calculation end time: 40 ms  
 Display start time: 20 ms  
 Display end time: 40 ms



(a) Main circuit

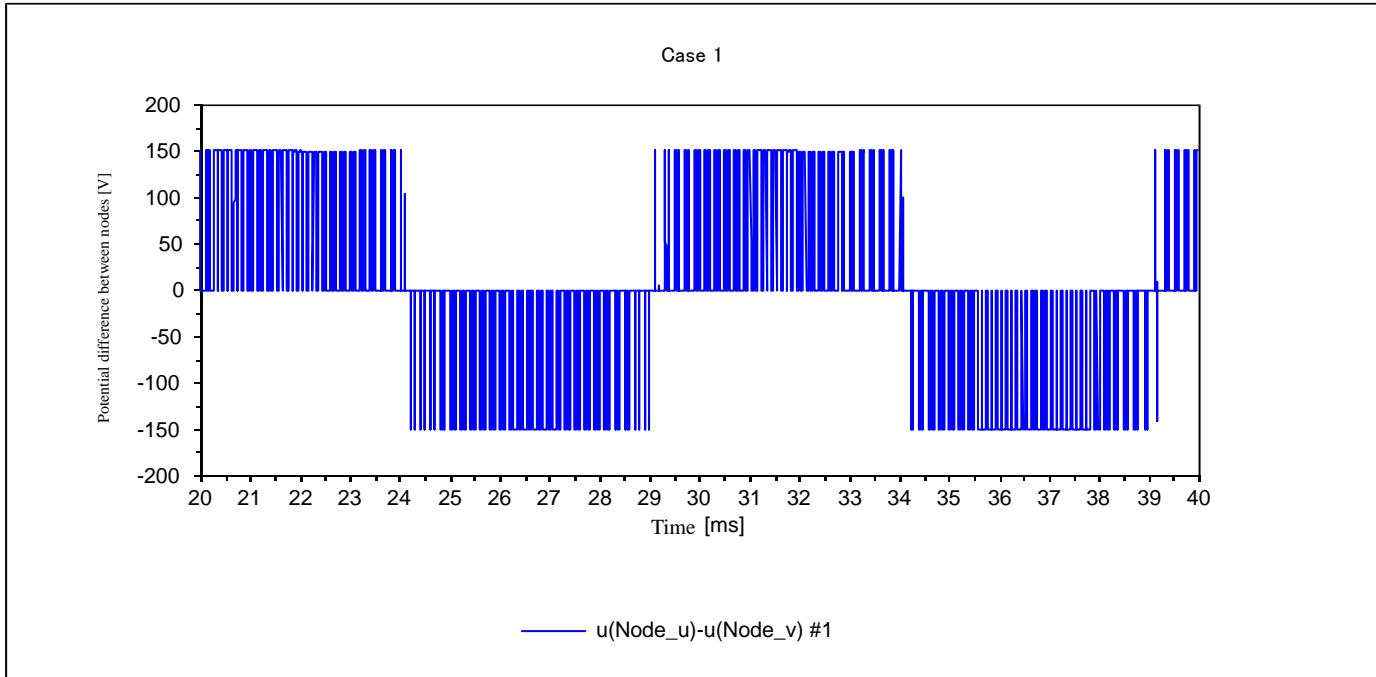


(b) Control system

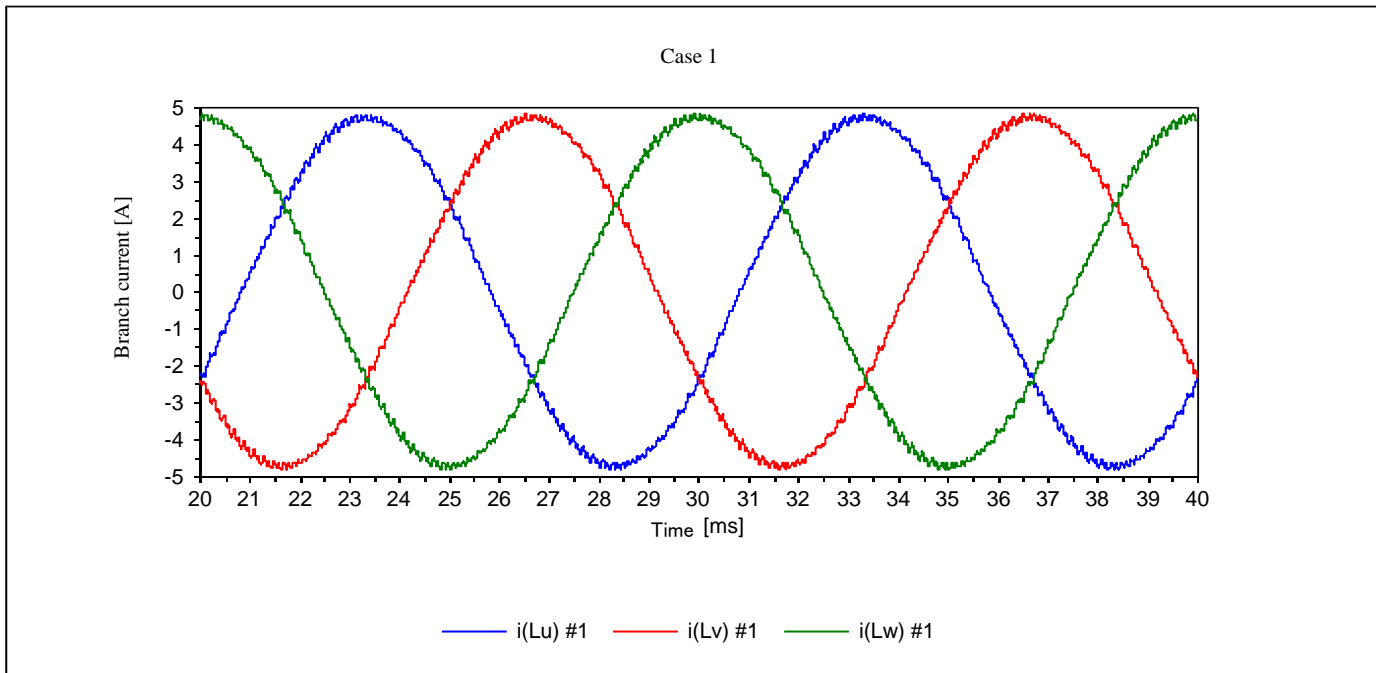
Figure 3 Example of XTAP input

## Analysis Results

The results of executing this example using XTAP are shown in Figure 4. Based on the results of the simulation, it can be confirmed that a direct current is converted into an alternating current of 100 Hz using an inverter and supplied to the load.



(a) Line-to-line voltage between  $u$  and  $v$



(b) Load current

Figure 4 Analysis results

END

Revision History		
Date	Example file Version	Content changes
2014/11/19	2.0	Update for XTAP Version 2.00
2012/07/19	1.3	Update for XTAP Version 1.20
2011/10/18	1.2	Because the parameter inside the delay block [delay_v2] in the control system block is a numerical value (5e-6), it was changed to a variable (Td).
2011/02/14	1.1	Update for XTAP Version 1.11
2010/09/02	1.0	Creation of the first edition (for XTAP Version 1.10)

Examples of XTAP		No.	DLL-01
Example Name	Basic Operations using DLL Control Block Components		
Field	—		
Literature	—		
Overview	<p>This is an example verifying the basic use of the DLL control block components. The DLL control block part is a control component used for the control logic, and was originally described by users in C language or FORTRAN as a control block in XTAP. The control logic is provided in a dynamic link library (DLL). The DLL control block component receives input signals (a maximum of ten signals) at the time of the initial calculation and at the time of the dynamic characteristic calculation (calculation of each time step), and the result of the operation defined in the DLL is output as an output signal (a maximum of ten signals). In addition to the input signal, five types of constants, P1 through P5, may also be specified (given as parameters at the time the analysis is executed). For details such as the method used to create the DLL programs, please refer to the Appendix “How to use DLL control block parts” of the manual.</p>		

## Analysis Circuit and Conditions

Figure 1 shows the control block diagram. A DLL control block component is created as shown in Fig. 1, which executes an operation that integrates input 1 to output 1, and the sum of  $P1 \times \text{input 1}$  and  $P2 \times \text{input 2}$  to output 2. The constants  $P1$  and  $P2$  are assumed to be given as parameters during the program execution.

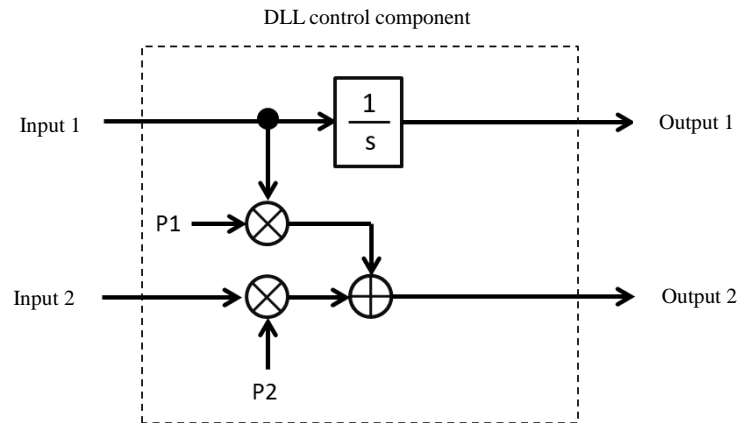


Figure 1 Control block diagram

[XTAP input]

Because this example has two inputs and two outputs, the third to the tenth input and output terminals are not used. Therefore, a dummy input value is connected to the input side, and a termination output terminal is connected to the output side. Further, because the output signal of the DLL control block component is not directly recorded, a gain constant of 1 is applied, as shown in the figure below.

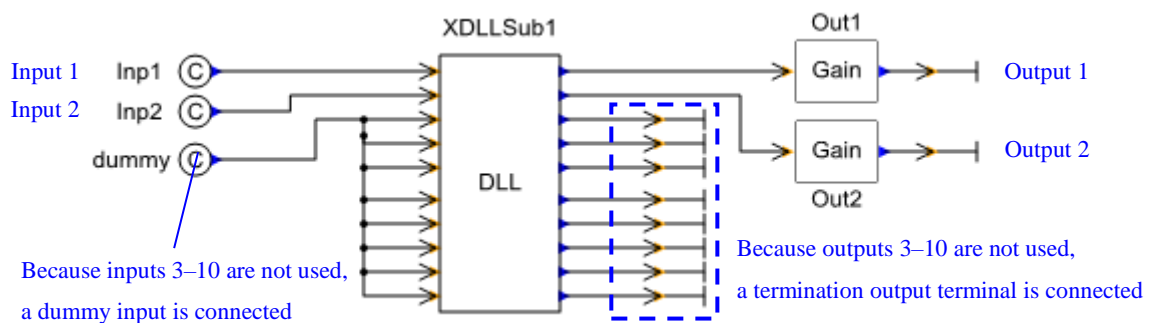


Figure 2 XTAP input

## Analysis Results

The results of executing this example using XTAP are shown in Figure 3. The following values were set in the current calculation example: input 1 = 1.0, input 2 = 2.0, P1 = 0.1, and P2 = 0.2. The simulation results are in agreement with the following numerical values, which can be analytically obtained from the block diagram of Figure 1.

$$(\text{Out1}) = \int_0^t 1.0 dt' = t$$

$$(\text{Out2}) = 1.0 \times 0.1 + 2.0 \times 0.2 = 0.5$$

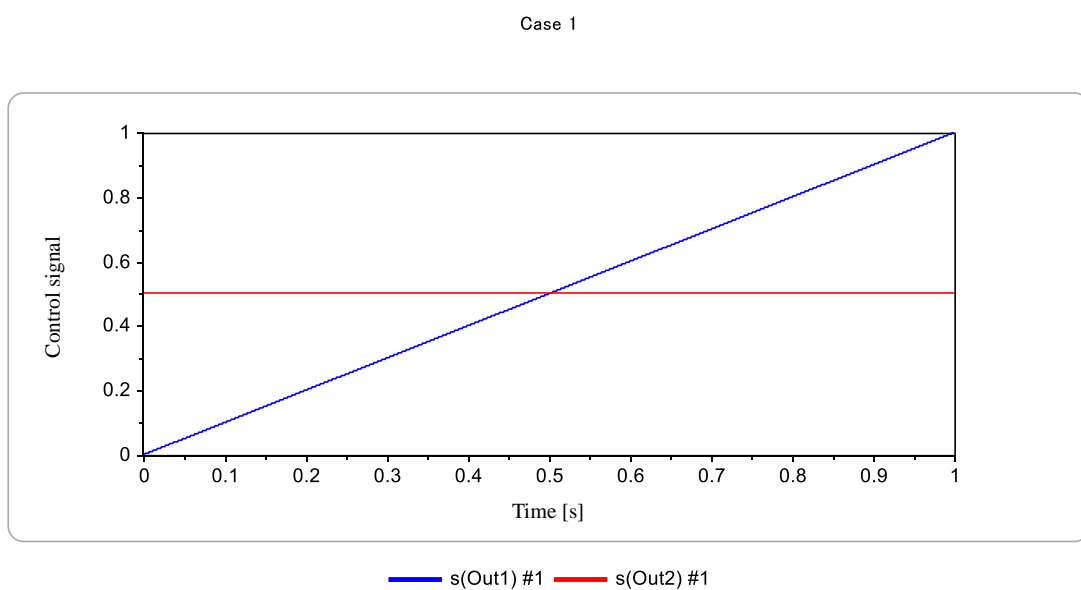


Figure 3 Analysis results

End

Change log		
Date	Example file version	Content changes
2014/11/18	2.0	First edition created (for XTAP Ver. 2.00)

Examples of XTAP		No.	HVDC-01
Name of Example	Separately Excited HVDC Model		
Field	Power electronics		
Literature	“DC Power Transmission Engineering,” Tokyo Denki University Press, written and edited by Takahiko Machida		
Overview	<p>Because this model has basic control and protection systems, it can be applied to other simulations by copying it and changing the rated value.</p> <p>Separately excited converters are currently used for various applications such as a DC power transmission, frequency conversion, and BTB. In this example, the simulation waveforms of the startup of the converter and the AC three-phase ground fault at a frequency conversion station are shown. This may also be used for a DC transmission by adding a DC line to this example.</p> <p>The circuit of the converter consists of two six-phase Gretz wires connected in-series in two stages. Because 11<sup>th</sup>- and 13<sup>th</sup>-order harmonics and their multiples are generated in the system, to remove them, an AC filter is connected between the converter and system. Further, phase-modifying equipment is connected to compensate for the reactive power, which is consumed by a separately excited converter during operation.</p>		

# Introduction · Using the Model

Refer to the table at the end for the parameters required to use the separately excited HVDC model. Further, change “MASTER\_Start” in “HVDC 1/MASTER” when changing the activation time of the separately excited HVDC, and change “Pdorder” in “HVDC1/MASTER” when changing the active power output.

## Analysis Circuit and Conditions

Figure 1 shows the analysis circuit created using XTAP, and Figure 2 shows a schematic diagram of the separately excited HVDC model.

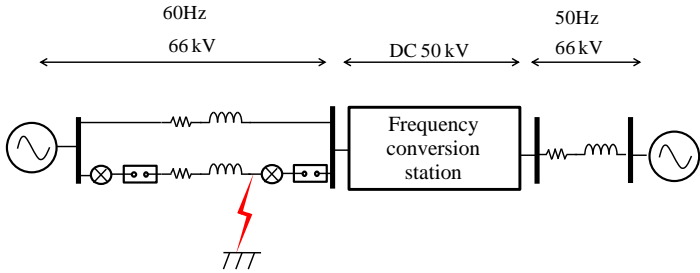


Figure 1 Analysis circuit

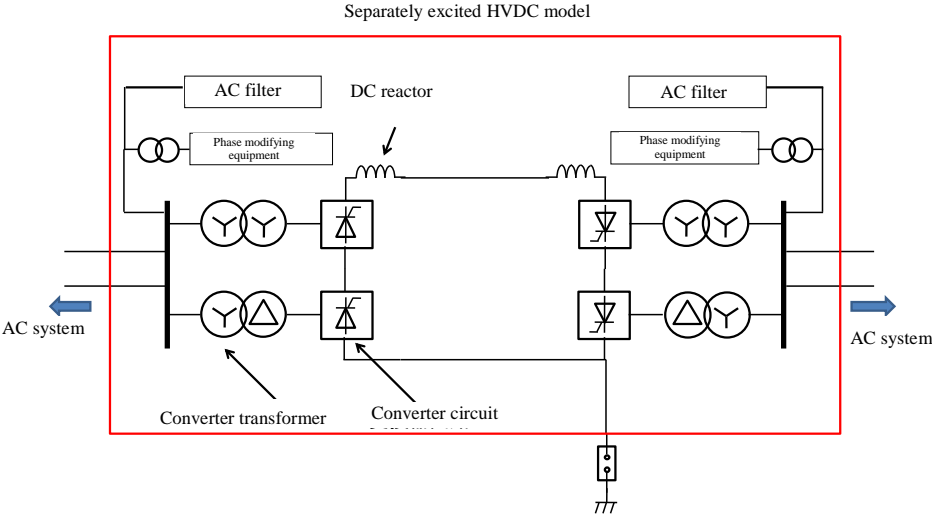


Figure 2 Schematic diagram of model

The main circuit conditions of the converter are as follows:  
 Rated capacity of 50 MW, rated DC voltage of 50 kV, and rated DC current of 1000 A  
 Converter transformer rated voltage of 66/22 kV

## Analysis Results

Figure 3 shows the voltage and current measurement points.

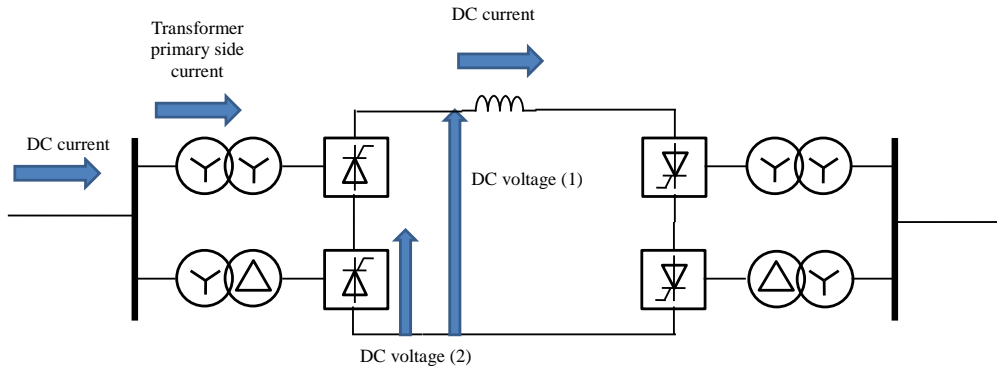


Figure 3 Voltage and current measurement points

Figures 4 and 5 show the DC current and DC voltage waveforms at the startup of the converter. After completion of the startup, both the current and voltage are rated values, and a startup is normally performed.

Case 1

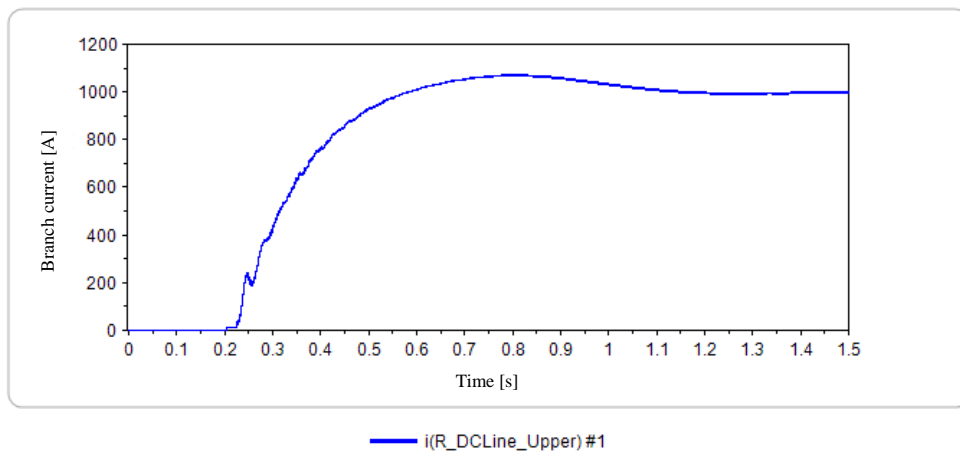


Figure 4 DC current waveform at startup

Case 1

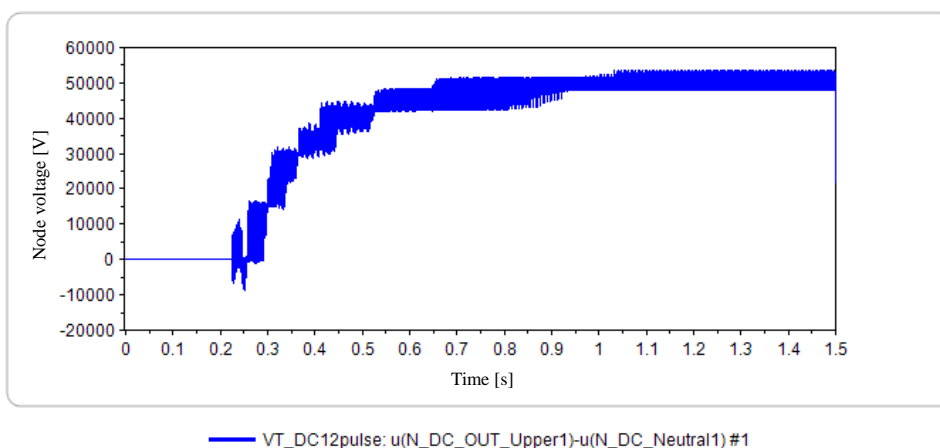


Figure 5 DC voltage waveform at startup (DC voltage ①)

Figure 6 shows the current flowing on the primary side of the transformer, and Figure 7 shows the current flowing in the system. The current flowing through the transformer is close to a square wave, and the direct current has a chopped waveform. This current, which contains large amounts of harmonics, passes through the AC filter where the harmonics are eliminated and the current becomes a sinewave.

Case 1

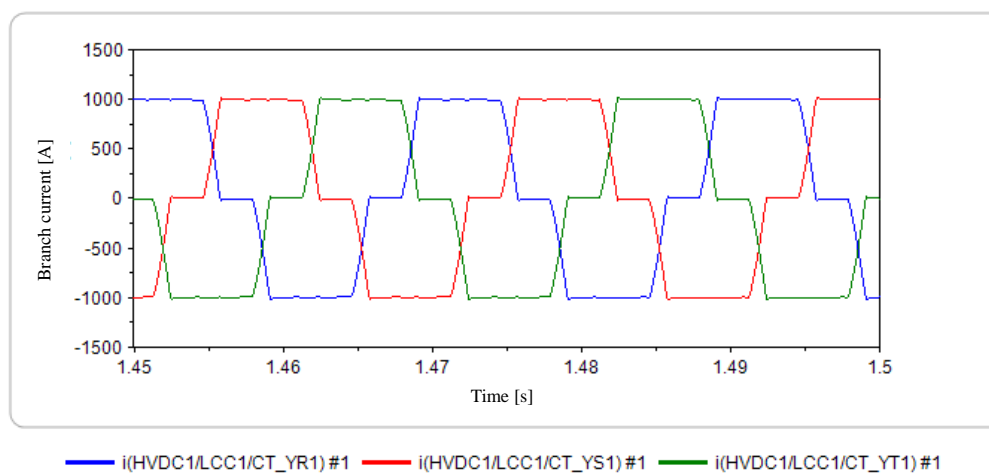


Figure 6 Transformer primary side current

Case 1

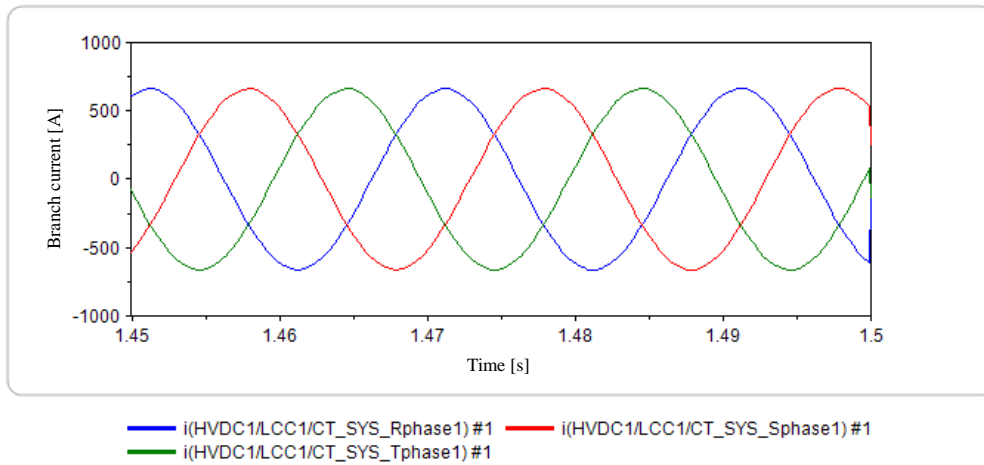


Figure 7 Current flowing through the system

Figure 8 shows the waveform of the control angle  $\alpha$  at the time of the converter startup. From the figure, the control angle on the 60-Hz side is approximately  $20^\circ$  during a steady state, which is less than  $90^\circ$ , indicating that the converter operates as a forward converter.

Case 1

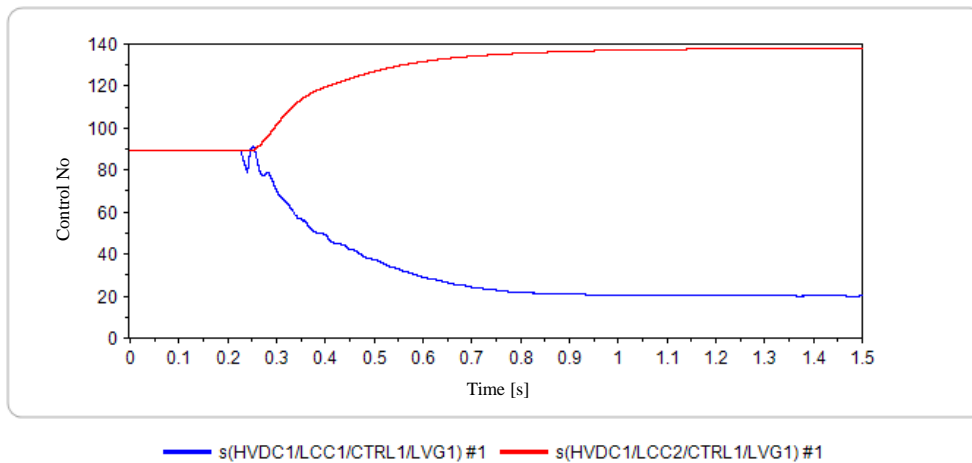


Figure 8 Control angle  $\alpha$  Red line, 50-Hz side; blue line, 60-Hz side

The DC current waveform at the time of the three-phase ground fault on the AC side is shown in Figure 9, the DC voltage waveform is shown in Figure 10, and the control angle is shown in Figure 11. When the system detects a drop in AC voltage, the protection operation of the gate shift (GS)  $\rightarrow$  gate block (GB)  $\rightarrow$  restart (RST) is carried out. Because the GS angle is set to  $100^\circ$  in this simulation, the control angle of the

converter becomes larger than  $100^\circ$  during the gate shift period (in this instance,  $100^\circ$ ). Owing to the action of the GS, the DC current becomes zero, and the converter stops temporarily but restarts after the AC fault has been eliminated and the AC voltage has recovered, and both the voltage and current of the converter are operated again in accordance with the command value.

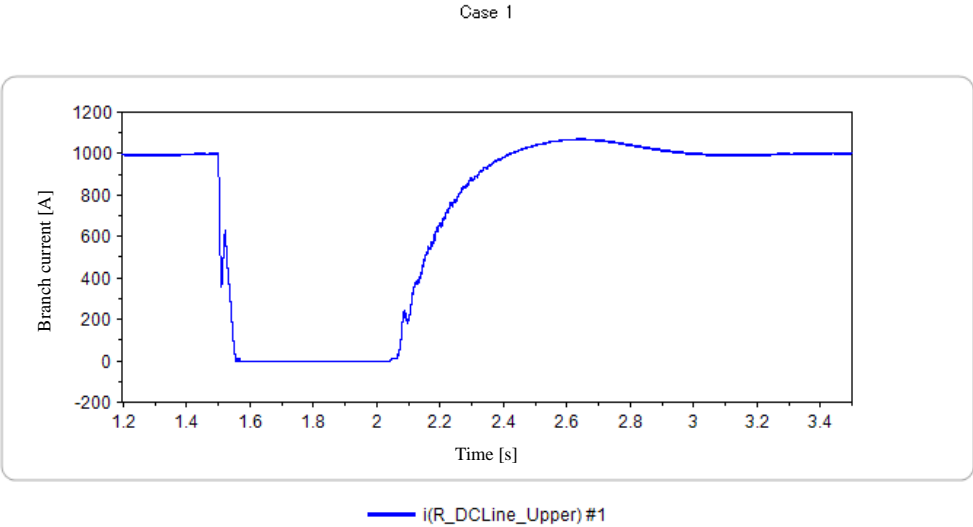


Figure 9 Waveform of DC current

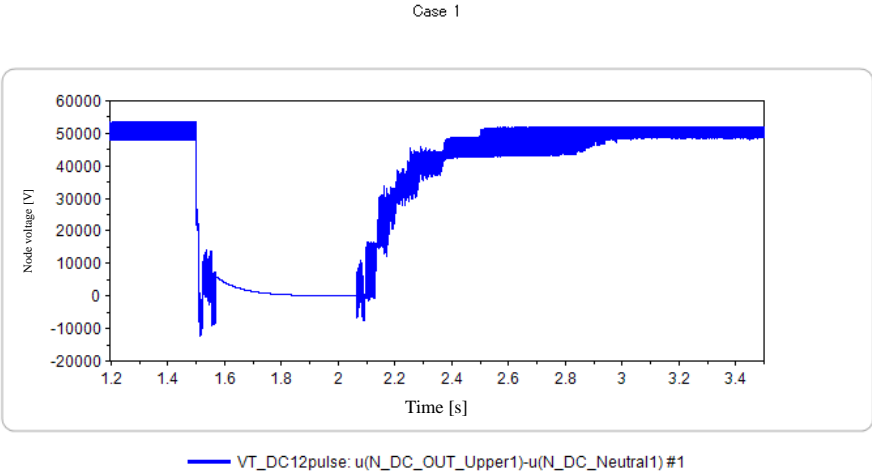


Figure 10 Waveform of DC voltage

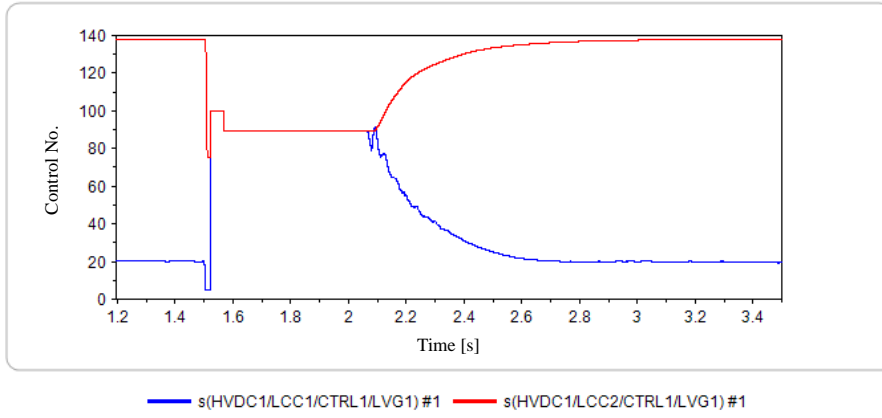


Figure 11 Control angle  $\alpha$  Red line, 50-Hz side; blue line, 60-Hz side

The parameters of the model and their respective descriptions are shown below. Note that in the settings of terminal 2, the variable names are the same as those of terminal 1 except that the 1 at the end is replaced with 2, and hence the details have been omitted here.

Name	Unit	Item
Rate_P	W	Rated power
Rate_Vdc	V	Rated DC voltage
IdcMin	p.u.	Minimum value of DC current
CurrentLimit	p.u.	Maximum current command value at current limit
ReverseTime	s	Power flow reversal speed
ReversePeriod	s	Time taken to widen the control angle limiter for power flow reversal
LimitOpenDelay	s	Time from BPP cancellation for startup to opening of control angle limiter
PulseWidth	deg	Ignition pulse width
SSRelayOffTime	s	Relay dead time of at the start of simulation
APR_K	-	APR gain
APR_T1	s	First-order lag time constant for APR
APR_T2	s	First-order lead time constant for APR
Limit_APR	-	APR limiter (upper limiter, lower limiter)
SystemFrequency1	Hz	System frequency
Rate_S_Trans1	VA	Capacitance of converter transformer (total of Y – Y and Y – D)
L_DCKpu1	H	Standard value of DC reactor inductance (cathode side)
L_DCApu1	H	Standard value of DC reactor inductance (anode side)
R_DCKpu1	$\Omega$	Standard value of resistance of DC reactor (cathode side)
R_DCApu1	$\Omega$	Standard value of resistance of DC reactor (anode side)
Rate_V1_Itol1	Vrms	Effective value of primary side line voltage of transformer (1)
Rate_V2_Itol1	Vrms	Effective value of primary side line voltage of transformer (2)
Trans_Rpu1	p.u.	Resistance of converter transformer
Trans_Lpu1	p.u.	Inductance of converter transformer
IdcBiasDeg1	deg	Current bias (approximate value of control angle during REC operation)
VdcBiasDeg1	deg	Voltage bias (approximate value of control angle during INV operation)
Vdc_Order_Lag1	s	First-order lag time constant when DC voltage command is changed
Idc_Order_Lag1	s	First-order lag time constant when DC current command is changed
IdcMesLag1	s	First-order lag time constant for DC current measurement
VdcMesLag1	s	First-order lag time constant for DC voltage measurement
ACR_K1	-	ACR gain
ACR_T11	s	First-order lag time constant for ACR
ACR_T21	s	First-order lead time constant for ACR
AVR_K1	-	AVR gain
AVR_T11	s	First-order lag time constant for AVR
AVR_T21	s	First-order lead time constant for ACR
GammaZeroDeg1	deg	Margin angle setting
StartDegree1	deg	Start angle
Start_TConst1	s	First-order lag time constant of current rise at startup
AlimitInvU1	deg	Upper limit of control angle (during INV operation)
AlimitRecU1	deg	Lower limit of control angle (during REC operation)
AlimitInvL1	deg	Lower limit of control angle (during INV operation)
AlimitRecL1	deg	Control angle lower limit (during REC operation)
LimitOpenTimeU1	s	First-order lag time constant at change of upper limit of control angle
LimitOpenTimeL1	s	First-order lag time constant at change of lower limit of control angle

VAMP_LAG1	s	First-order lag time constant for AC voltage measurement
FREQ_LAG1	s	First-order lag time constant for frequency detection
K_CFI	-	Gain of commutation failure detection relay (the smaller the value, the higher the sensitivity)
K_DCFRD1	-	Gain of DC fault detection relay (the smaller the value, the higher the sensitivity)
T_DCFRD1	s	First-order lag time constant of DC fault detection relay
Threshold_UV1	p.u.	AC undervoltage relay threshold
Threshold_OV2	p.u.	AC overvoltage relay threshold
Threshold_OF1	p.u.	Frequency rising relay threshold
Threshold_UF1	p.u.	Frequency drop relay threshold
RecoveryTime1	s	Lag from fault relay cancellation to actual cancellation of protection operation
GSTime1	s	GS execution time (time from start of GS to GB)
BPPTime1	s	BPP execution time (time from start of BPP to GB)
GBTime1	s	GB execution time (time from start of GB to CBT)
GSDegree1	deg	GS angle
BFDegree1	deg	Beta advance angle
BF_IncLag1	s	First-order lag time constant at the time of canceling beta advance
BF_DecLag1	s	First-order lag time constant when carrying out beta advance earlier
BFTime1	s	Beta advance period
Rate_V_PM1	Vrms	Rated voltage of transformer for phase modifier
R_Trans_GND1	$\Omega$	Ground resistance of converter transformer (per unit)
Threshold_PM11	p.u.	Shunt reactor 1 on-off threshold
Threshold_PM21	p.u.	Shunt reactor 2 on-off threshold
Threshold_PM31	p.u.	Stacon 1 on-off threshold
Threshold_PM41	p.u.	Stacon 2 on-off threshold
Threshold_PM51	p.u.	Stacon 3 on-off threshold
Threshold_PM61	p.u.	Stacon 4 on-off threshold
Hysteresis_PM1	p.u.	Hysteresis amount of on/off phase adjustment
Spu_Tr_PM1	p.u.	Rated capacity of transformer for phase modifier (denominator is the rated active power of converter)
Lpu_Tr_PM1	p.u.	Inductance of transformer for phase modifier (denominator is the rated active power of converter)
S_Shant_pu1	p.u.	Capacity per shunt reactor (denominator is the rated active power of converter)
S_SC_pu1	p.u.	Capacity per stacon (denominator is the rated active power of converter)
R_Filter_GND1	$\Omega$	Ground resistance of AC filter (per filter)
F_5_pu1	p.u.	Resonance order of fifth-order filter
Q_51	-	Sharpness order of fifth-order filter
S_5_pu1	p.u.	Fundamental wave capacity of fifth-order filter (denominator is the rated active power of converter)
F_11_pu1	p.u.	Resonance order of 11 <sup>th</sup> -order filter
Q_111	-	Sharpness order of 11 <sup>th</sup> -order filter
S_11_pu1	p.u.	Fundamental wave capacity of 11 <sup>th</sup> -order filter (denominator is the rated active power of converter)
F_13_pu1	p.u.	Resonance order of 13 <sup>th</sup> -order filter
Q_131	-	Sharpness order of 13 <sup>th</sup> -order filter
S_13_pu1	p.u.	Fundamental wave capacity of 13 <sup>th</sup> -order filter (denominator is the rated active power of converter)
F_HP_pu1	p.u.	Resonance order of higher-order filters
Q_HP1	-	Sharpness order of higher-order filters
S_HP_pu1	p.u.	Fundamental wave capacity of higher-order filters (denominator is the rated active power of converter)
Rsnubber_pu1	-	R setting of RC snubber
Csnubber_pu1	-	C setting of RC snubber
Rpressure_pu1	-	Voltage divider resistor setting
Lanode_pu1	-	Anode reactor setting
DeionTime1	s	Thyristor deionization time (see Tdeion section of Thy in the manual)

Change log		
Date	Example file version	Content changes
2018/6/29	2.1	Icons of changed parts
2014/11/19	2.0	Modified for XTAP Version 2.00 Modified three-phase voltage source model (the infinite bus generator component was changed to COS wave voltage source)
2013/04/15	1.3	Changes consequent to modifications in model diagram and parameter input format. Added initialization function.
2012/08/29	1.2	Change consequent to modification of the separately excited HVDC model Addition of waveform of 3-phase ground fault on AC side
2012/07/19	1.1	Modified for XTAP Version 1.20
2010/10/18	1.0	First edition created (for XTAP Version 1.11)

Examples of XTAP		No.	HVDC-02
Name of Example	Self-Excited HVDC Model		
Field	Power electronics		
Literature	“DC Power Transmission Engineering,” Tokyo Denki University Press, written and edited by Takahiko Machida		
Overview	<p>Because this model has basic control and protection systems, it can be applied to other simulations by copying it and changing the rated value.</p> <p>This example simulates a DC power transmission system circuit using a self-excited converter. In this example, a two-level converter that was also used in the STATCOM example is connected back-to-back across a DC line, thereby constituting a DC power transmission system. When compared with the separately excited converter, the self-excited converter has the following advantages: ① There is no need for phase adjustment equipment because the converter is capable of outputting reactive power by itself. ② It can also be applied to relatively weak lines with a small short-circuit capacity. In this example, the simulated waveforms at the time of the converter activation, power flow reversal, and DC main line ground fault are shown.</p> <p>Incidentally, if the DC line of this example is ignored, it will have a back-to-back (BTB) configuration and can be used for frequency-conversion purposes.</p>		

## Introduction/Model Use

Refer to the table at the end for the parameters required to use the separately excited HVDC model. Further, “Pdorder” is changed in “HVDC/MASTER” when changing the active power output of the self-exciting HVDC.

## Analysis Circuit and Conditions

Figure 1 shows the analysis circuit, and Figure 2 shows a schematic diagram of the model.

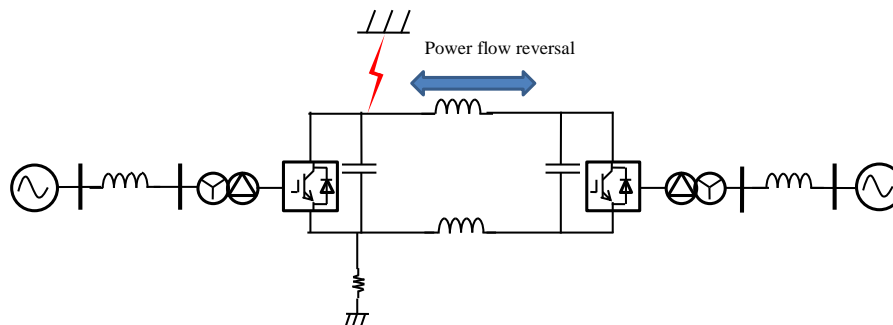


Figure 1 Analysis circuit

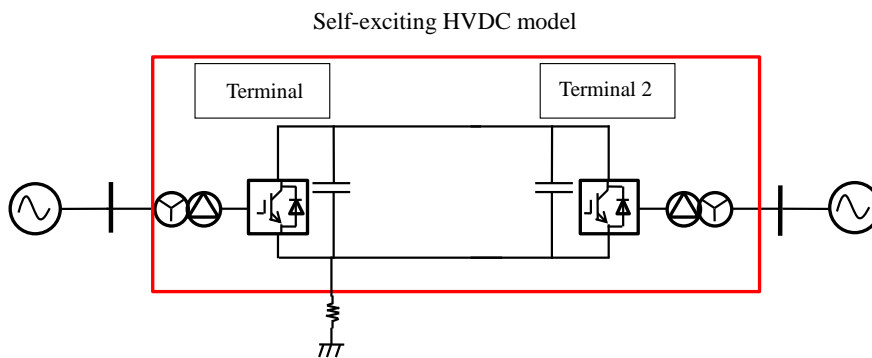


Figure 2 Schematic diagram of model

- Rated equipment capacity = 50 MW (55.9 MVA), primary side rated voltage = 66 kV, secondary side rated voltage = 56 kV, DC voltage = 125 kV.
- The DC power transmission system is linked with the 66-kV system using the impedance of the simulated short-circuit capacity of the system.
- Here, example simulations of the ① startup, ② power flow reversal, and ③ DC main line ground fault are carried out. The converter begins activation at a simulation time of  $t = 0.25$  s. At  $t = 0.25$  s, the control system is activated, and power is transmitted from terminal 1 to terminal 2. The power command value is changed at  $t = 0.5$  s and a power flow reversal begins. The ground fault is eliminated by the circuit

breaker at  $t = 0.8$  s.

### Analysis Results

Refer to the STATCOM model example of FACTS-02 for operation of the converter at startup. Figures 3 and 4 show the voltage and current of the DC circuit during a power flow reversal. Figures 5 and 6 show the active and reactive power output from terminals 1 and 2, respectively, at the time of a power flow reversal. Because the reactive power control of each terminal during this simulation continuously controls the voltage of the AC side (ACAVR), the reactive power is controlled such that the terminal voltage of the converter approaches 1.0 pu.

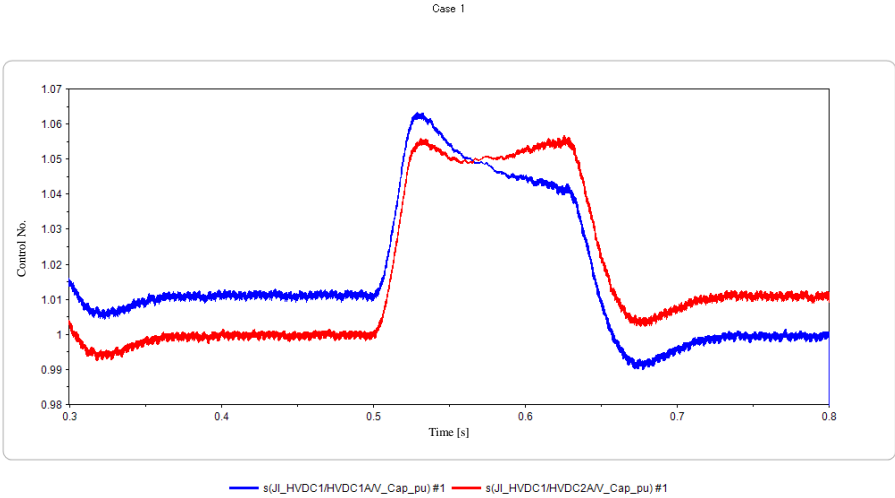


Figure 3 DC voltage [pu] Blue line, terminal 1; red line, terminal 2 (the reference voltage is 125 kV)

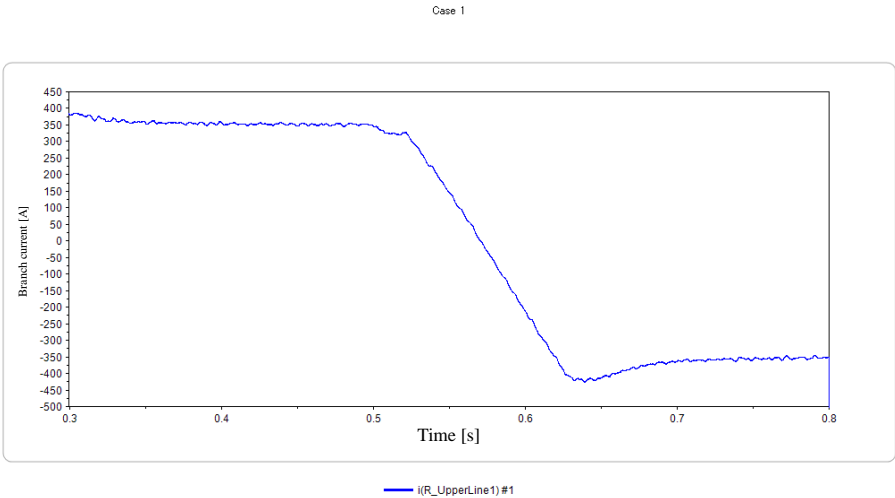


Figure 4 Direct current [A]

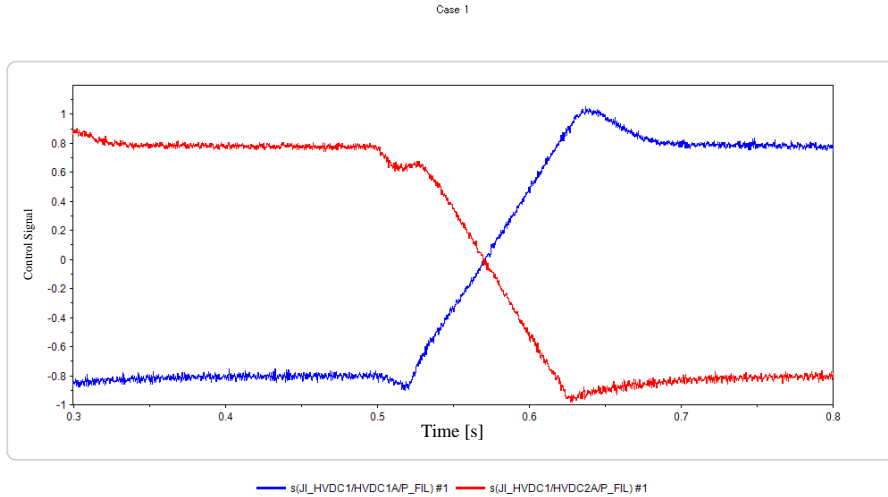


Figure 5 Active power [pu] Blue line, terminal 1; red line, terminal 2 the (reference capacitance is 55.9 MVA)

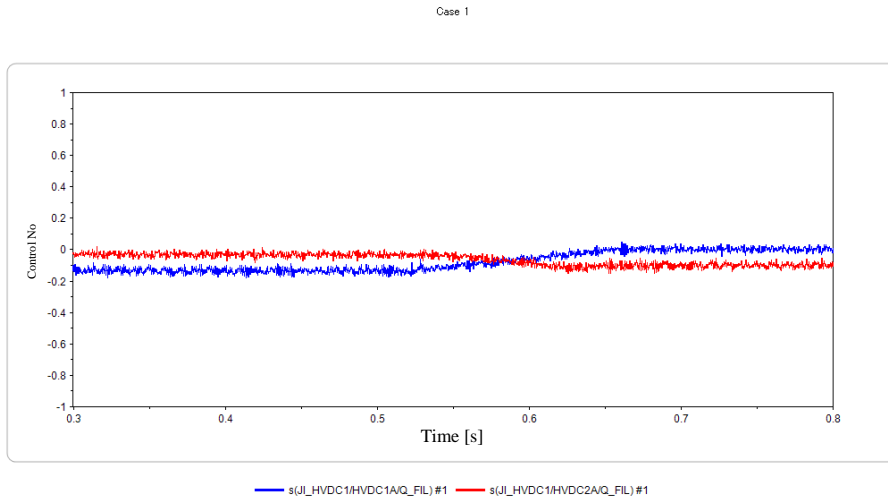


Figure 6 Reactive power [pu] Blue line, terminal 1; red line, terminal 2 (the reference capacitance is 55.9 MVA)

At  $t = 0.5$  s, the power command value switches from 45 MW (0.8 pu) to -45 MW (-0.8 pu), and the power flow reversal begins. The rectifier side applies active power control and determines the power to be sent to the other systems, whereas the inverter side applies DC voltage control and determines the DC voltage. Owing to the voltage drop that occurs from the resistance of the DC line when sending power from terminal 1 to terminal 2, the DC voltage of terminal 2 is 1.0 pu in keeping with the command value (1.0 pu). However, the DC voltage of terminal 1 is higher than the command value. In contrast, when the power flow is reversed, the DC voltage of terminal 1 follows the command value, and the voltage of terminal 2 is higher than the command value.

Figure 7 shows the DC voltage, and Figure 8 shows the system side output current at the time of a DC fault. Because the occurrence of a DC fault at  $t = 0.8$  s amounts to a short circuit of the energy storage capacitor, the DC voltage becomes zero. Further, once the system detects a DC fault, the converter applies a gate block (GB)  $\rightarrow$  circuit breaker release operation, and therefore, despite a large current being output

from the converter during the fault, the output current of the system side becomes zero after the circuit breaker is opened.

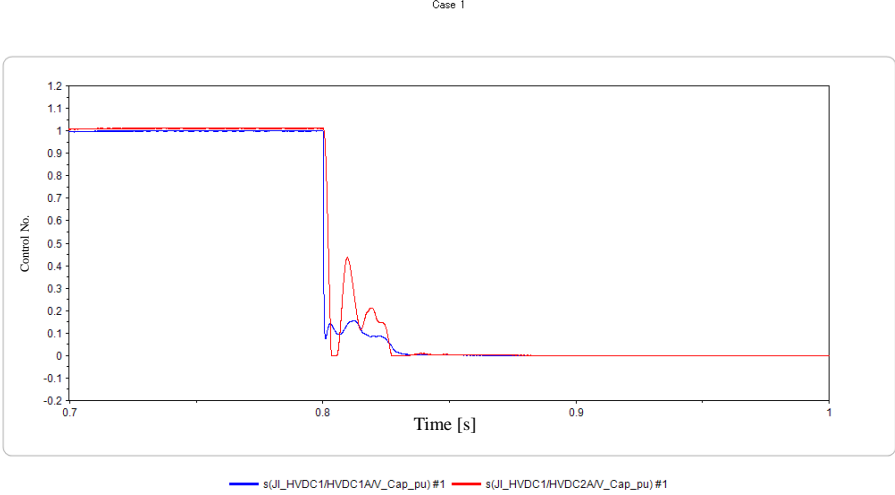


Figure 7 DC voltage [pu] Blue line, terminal 1; red line, terminal 2 (the reference voltage is 125 kV)

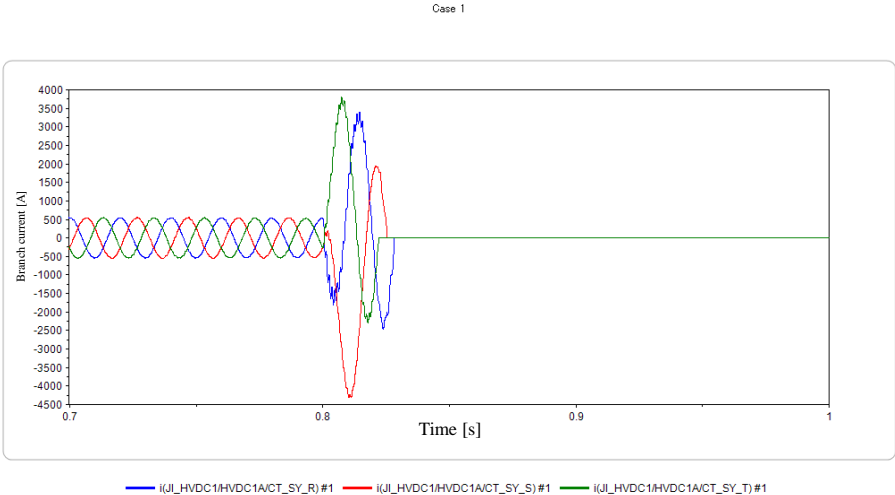


Figure 8 System side output current [A]

The parameters of the model and their respective descriptions are shown below. Note that, in the settings of terminal 2, the variable names are the same as those of terminal 1 except that the 1 at the end is replaced with 2, and hence the details have been omitted here.

	Name	Unit	Item
Common constants	Rate_P	W	Rated active power
	Rate_Vdc	V	Rated DC voltage
	SSRelayOffTime	s	Relay dead time at start of simulation
	SystemFrequency1	Hz	System frequency
	Rate_S1	VA	Rated capacity
	Rate_V1_lto11	V	Effective value of transformer primary side line voltage
	Rate_V2_lto11	V	Effective value of transformer secondary side line voltage
	PWMPulseNumber	-	Number of PWM pulses (per cycle)
	R_TransGND1	$\Omega$	Ground resistance of converter transformer
	H1	s	Electrostatic constant
	Flag_ACAVR1	-	ACAVR flag (1 = used, 0 = not used), Select Flag_AQR
	Flag_AQR1	-	AQR flag (1 = used, 0 = not used), Select Flag_ACAVR
	Vac_order1	p.u.	AC voltage command value (ACAVR command value)
	Q_order1	p.u.	Reactive power command value (AQR command value)
	PWMPhase1	deg	Phase angle of PWM carrier
	R_connect_pu1	p.u.	Converter transformer resistance
	L_connect_pu1	p.u.	Converter transformer inductance
	Spu_filter11	p.u.	Fundamental wave capacity of higher-order filter 1 (denominator is rated capacity of converter)
	Q_filter11	-	Sharpness of higher-order filter 1
	Spu_filter21	p.u.	Fundamental wave capacity of higher-order filter 2 (denominator is rated capacity of converter)
	Q_filter21	-	Sharpness of higher-order filter 2
	Gain_ACR1	-	ACR gain
	T_ACR1	s	ACR time constant
	Gain_APR1	-	APR gain
	T_APR1	s	APR time constant
	Lag_APR1	s	First-order lag time constant for APR
	Gain_DCAVR1	-	DCAVR gain
	T_DCAVR1	s	DCAVR time constant
	Gain_AQR1	-	AQR gain
	T_AQR1	s	AQR time constant
	Gain_ACAVR1	-	ACAVR gain
	T_ACAVR1	s	ACAVR time constant
	Vmag1	-	Voltage margin
	Pmag1	-	Power margin
	Lag_Margin1	s	First-order lag time constant at margin switching (switching speed)
	IinvLimit1	p.u.	Maximum current of converter (denominator is the converter rating)
	K_DCFRD1	-	Gain of DC fault detection relay (the smaller the value, the higher the sensitivity)
T_DCFRD1	s	First-order lag time constant of DC fault detection relay	
Threshold_OC1	p.u.	Overcurrent relay threshold	
Threshold_DCOV1	p.u.	DC overvoltage relay threshold	
Threshold_DCUV1	p.u.	DC undervoltage relay threshold	
Threshold_OV1	p.u.	AC overvoltage relay threshold	

Threshold_UV1	p.u.	AC undervoltage relay threshold
Threshold_OF1	p.u.	Frequency rise relay threshold
Threshold_UF1	p.u.	Frequency drop relay threshold
VAMP_LAG1	s	First-order lag time constant for AC voltage detection
FREQ_LAG1	s	First-order lag time constant for frequency detection
RecoveryTime1	-	Lag from fault relay cancellation to actual cancellation of protection operation
GBTime1	s	GB implementation time
NoDetectPeriod1	s	Partial relay dead time at startup
CalculationTime1	s	Control cycle
DeadTime1	s	Dead time
Flag_DirectSample1	-	Voltage, current amount direct detection flag (selected from among three types)
Flag_AverageSample1	-	Detection flag using moving average of voltage and current amount (selected from among three)
Flag_PeakTopSample1	-	Peak top detection flag of voltage and current amount (selected from among three types)
ChargeCircuitCloseTime1	s	Start time of charging (if starting from a transient state, assign a large negative value)
ChargeTime1	s	Charge time
Control_StartDelay1	s	Time from end of charge to start of control system operation

End

Change log		
Date	Example file version	Content changes
2018/6/29	2.2	Icons of parts changed
2018/1/26	2.1	Modified the creation logic of HOLD signal
2014/11/19	2.0	Modified for XTAP Version 2.00
2014/07/22	1.4	Deletion of snubber capacitor of converter arm and correction of certain mathematical formulas
2013/04/15	1.3	Changes consequent to modifications of model diagram and parameter input format
2012/08/29	1.2	Change consequent to modification of the self-exciting HVDC model Addition of waveform of direct current main line ground fault
2012/07/19	1.1	Modified for XTAP Version 1.20
2010/10/18	1.0	First edition created (for XTAP Version 1.11)

Examples of XTAP		No.	HVDC-03
<b>Example Name</b>	Self-Excited HVDC Model (Half Bridge MMC)		
<b>Field</b>	Power electronics		
<b>Literature</b>	<p>(1) “DC Power Transmission Engineering,” Tokyo Denki University Press, written and edited by Takahiko Machida</p> <p>(2) T. Kikuma, K. Takenaka, M. Takasaki, “Control Protection Method of DC Power Transmission System with Modular Multi-Level Converter Using Full Bridge Cell: Proposal of a Control Method that can Control Fault Current During DC Fault,” Central Research Institute of Electric Power Industry Research Report R11021, (2012).</p> <p>(3) T. Kikuma et al., “Control Method of Double Y-connection Modular Multi-level Converter,” Journal of the Institute of Electrical Engineers of Japan D, Vol. 133, No. 9, pp. 917-927 (2013).</p>		
<b>Overview</b>	<p>Because this model has basic control and protection systems, it can be applied to other simulations by copying it and changing the rated value.</p> <p>This example simulates the circuit of a DC power transmission system using a modular multilevel converter (MMC). It has the same configuration as the self-excited HVDC (HVDC-02) example, except that the converter circuit is replaced by an MMC circuit. In this example, the simulated waveforms at the time of a DC main line ground fault and power flow reversal of the converter are shown.</p> <p>Several MMC models have been created as examples.</p>		

## Simple Explanation of MMC

A brief explanation of an MMC is given below. For a more detailed explanation, please see the references. A converter composed of identical cells (modules) connected in multiple stages is called an MMC. There are cells that use half bridge cells and those that use full bridge (single phase inverter) cells. The present example deals with a half bridge MMC model. The problem with an MMC is that, as the number of cells increases, the number of elements in the circuit becomes enormous, leading to significant calculation costs. To contend with this problem, an average model made by averaging the switching operations has been used in certain cases. This example deals with two types of models:

- ① Half bridge MMC averaging model (HVDC-03A)
- ② Half bridge MMC detailed model (HVDC-03B)

In the absence of any specific reason to use the detailed model, the use of the average model is recommended because it is much faster. The applied control, which is a combination of the controls used in the references, is used as the control in an MMC.

### Introduction/Model Use

Refer to the table at the end for the parameters required to use the MMC model. When changing the active power output of the MMC, “Porder” in “MASTER\_VSC 1,” which is located one level below the highest level of the hierarchy, is changed.

### Analysis Circuit and Conditions

Figure 1 shows the analysis circuit.

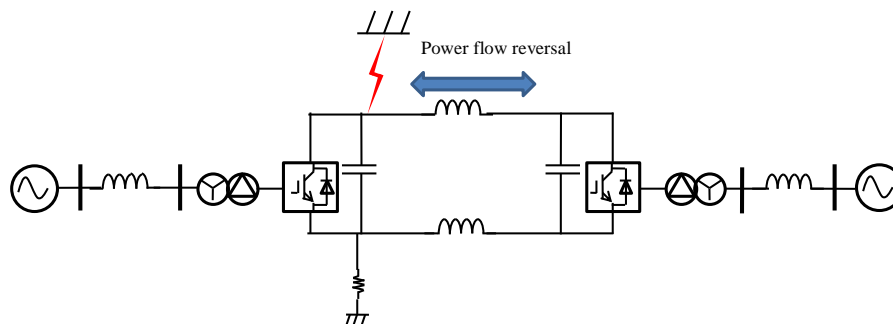


Figure 1 Analysis circuit

- Rated equipment capacity = 50 MW (55.9 MVA), primary side rated voltage = 66 kV, secondary side rated voltage = 56 kV, DC voltage = 125 kV.
- The DC power transmission system is linked with the 66-kV system through the impedance of the simulated short-circuit capacity of the system.
- In this, example simulations of ① a power flow reversal and ② a DC main line ground fault are

carried out. At a simulation time of  $t = 0.5$  s, the power command value changes, and a power flow reversal begins. A ground fault occurs at  $t = 0.8$  s, which is subsequently removed by the circuit breaker.

### Analysis Results

Figures 2 and 3 show the DC capacitor voltage and direct current at the time of a power flow reversal. Figures 4 and 5 show the active and reactive power outputs from terminals and terminal 2 at the time of a power flow reversal, respectively. Because the reactive power control of each terminal during this simulation continuously controls the voltage of the AC side (ACAVR), the reactive power is controlled such that the terminal voltage of the converter approaches 1.0 pu.

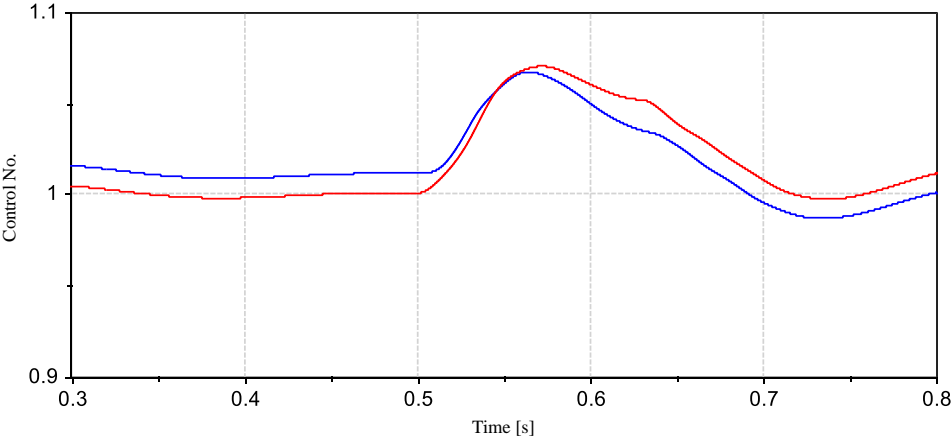


Figure 2 DC capacitor voltage (average value of all cells) [pu] (the reference voltage is 125 kV).

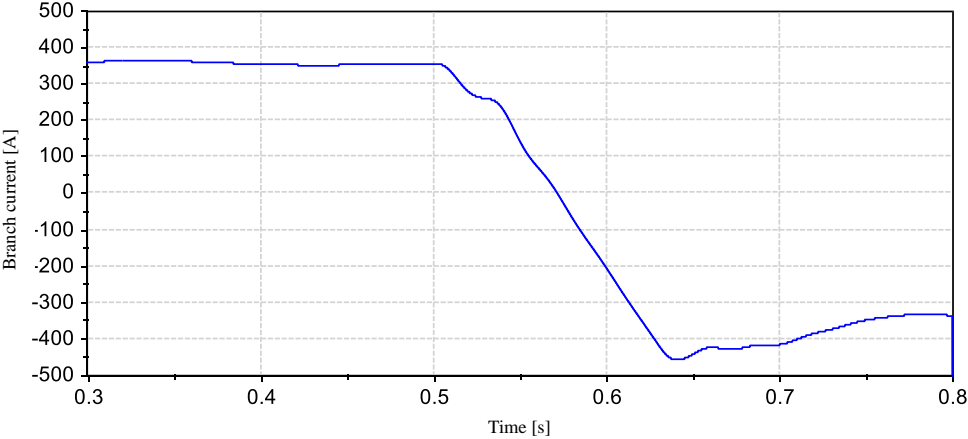


Figure 3 Direct current [A]

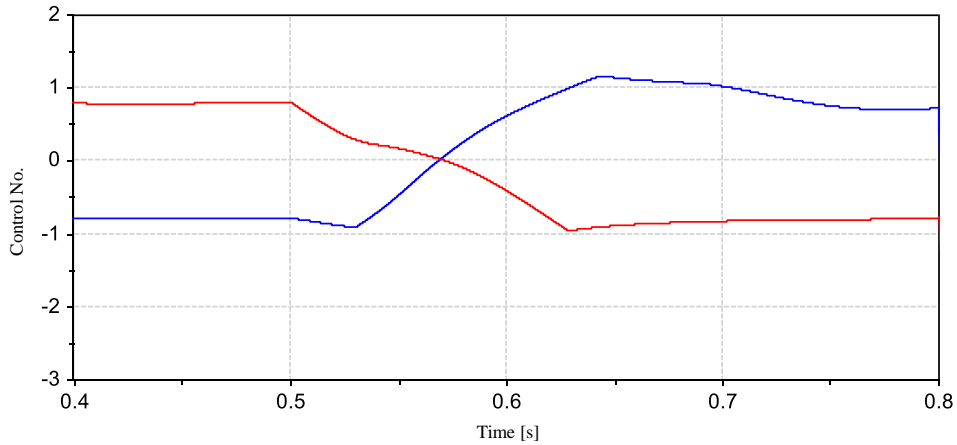


Figure 4 Active power [pu] Blue line, terminal 1; red line, terminal 2 (the reference capacity is 55.9 MVA).

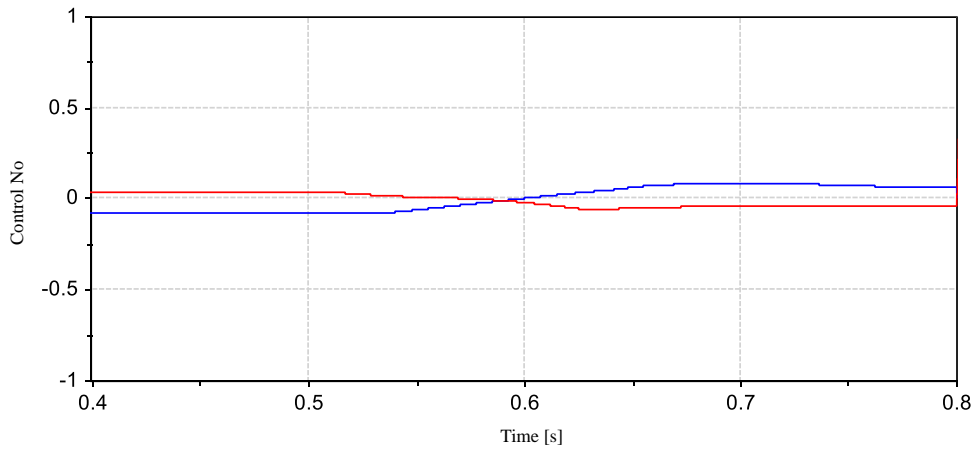


Figure 5 Reactive power [pu]: blue line, terminal 1; Red line, terminal 2 (the reference capacity is 55.9).

At  $t = 0.5$  s, the power command value switches from 45 MW (0.8 pu) to -45 MW (-0.8 pu), and the power flow reversal begins. The rectifier side controls the active power and determines the power to be sent to the other system, whereas the inverter side determines and controls the DC voltage.

Figure 6 shows the DC voltage, and Figure 7 shows the system side output current at the time of a DC fault. A direct current fault occurs at  $t = 0.8$  s. Further, once the system detects a DC fault, the converter performs a gate block (GB)  $\rightarrow$  circuit breaker release operation, and therefore, despite a large current being output from the converter during the fault, the output current of the system side becomes zero after the circuit breaker is opened.

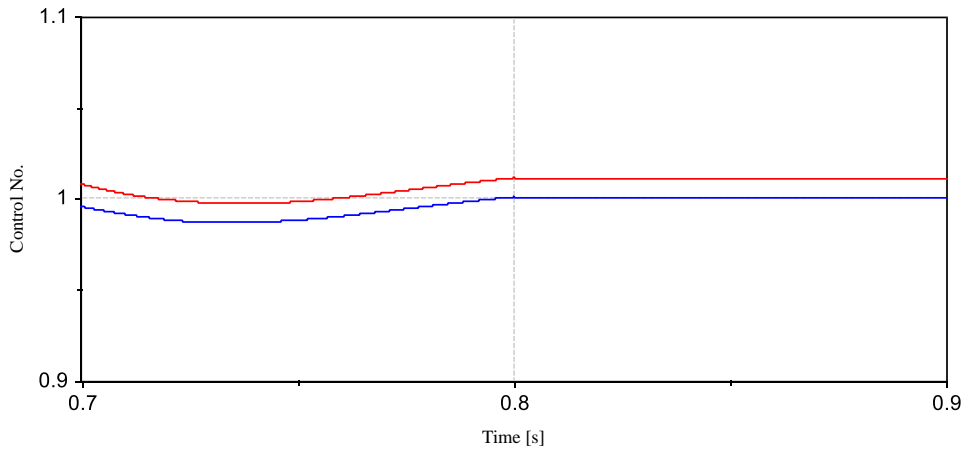


Figure 6. DC voltage [pu]: blue line, terminal 1; red line, terminal 2 (the reference voltage is 125 kV, and is the average value of the capacitor voltages of 6 arms)

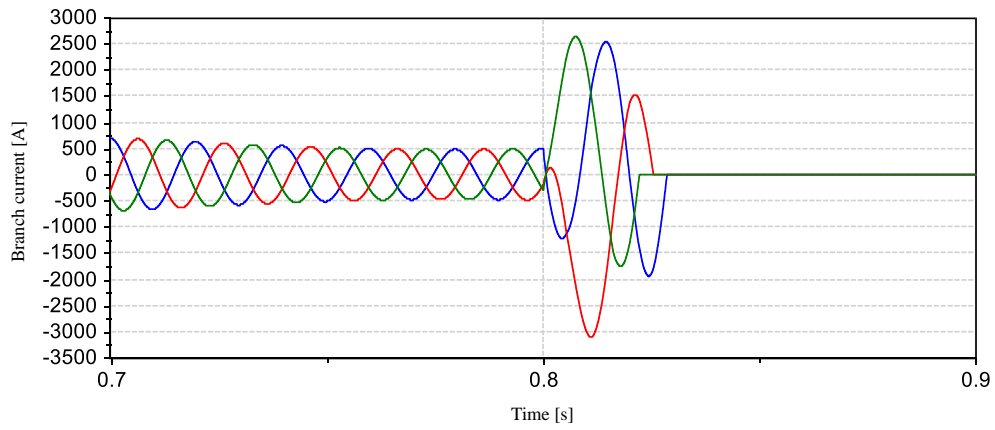


Figure 7 System side output current [A]

The parameters of the model and their respective descriptions are shown below. Note that in the settings of terminal 2, the variable names are the same as those of terminal 1 except that the 1 at the end is replaced with 2, and hence these details have been omitted here.

	Name	Unit	Item
Common constants	Rate_P	W	Rated active power
	Rate_Vdc	V	Rated DC voltage
	SSRelayOffTime	s	Relay dead time at start of simulation
	FlagInitialize	-	Initialization flag (used to start the simulation from a steady state) Input 1 to start from steady state
	V_ThirdOrder	p.u.	Third harmonic injection amount for the modulation rate reduction
	CellNumPerArm	-	Number of stages per arm of MMC cell (in the averaging model, always enter 1)
	SystemFrequency1	Hz	System frequency
	Rate_S1	VA	Rated capacity
	Rate_V1_ltol1	V	Effective value of transformer primary side line voltage
	Rate_V2_ltol1	V	Effective value of transformer secondary side line voltage
	PWMPulseNumber	-	Number of PWM pulses (per cycle)
	R_TransGND1	Ω	Ground resistance of converter transformer
	H1	s	Electrostatic constant
	Flag_ACAVR1	-	ACAVR flag (1 = used, 0 = not used), Select Flag_AQR
	Flag_AQR1	-	AQR flag (1 = used, 0 = not used), Select Flag_ACAVR
	Vac_order1	p.u.	AC voltage command value (ACAVR command value)
	Q_order1	p.u.	Reactive power command value (AQR command value)
	PWMPHase1	deg	Phase angle of PWM carrier
	R_connect_pu1	p.u.	Converter transformer resistance
	L_connect_pu1	p.u.	Converter transformer inductance
	L_Arm_pu1	p.u.	Arm reactor inductance
	L_DCK_pu1	p.u.	Inductance of DC reactor (for upper line) Inductance value = $L\_DCK\_pu1 \times \text{rated DC voltage}^2 / \text{rated active power}$
	L_DCA_pu1	p.u.	Inductance of DC reactor (for lower line)
	Gain_ACR1	-	ACR gain
	T_ACR1	s	ACR time constant
	Gain_APR1	-	APR gain
	T_APR1	s	APR time constant
	Lag_APR1	s	First-order lag time constant for APR
	Gain_DCAVR1	-	DCAVR gain
	T_DCAVR1	s	DCAVR time constant
	Gain_AQR1	-	AQR gain
	T_AQR1	s	AQR time constant
	Gain_ACAVR1	-	ACAVR gain
	T_ACAVR1	s	ACAVR time constant
	Vmag1	p.u.	Voltage margin
	Pmag1	p.u.	Power margin

Lag_Margin1	s	First-order lag time constant at margin switching (switching speed)
IinvLimit1	p.u.	Maximum current of converter (denominator is the converter rating)
K_DCFRD1	-	Gain of DC fault detection relay (the smaller the value, the higher the sensitivity)
T_DCFRD1	s	First-order lag time constant of DC fault detection relay
Threshold_DCOC1	p.u.	DC overcurrent relay threshold
Threshold_OC1	p.u.	Overcurrent relay threshold
Threshold_DCOV1	p.u.	DC overvoltage relay threshold
Threshold_DCUV1	p.u.	DC undervoltage relay threshold
Threshold_OV1	p.u.	AC overvoltage relay threshold
Threshold_UV1	p.u.	AC undervoltage relay threshold
Threshold_OF1	p.u.	Frequency rise relay threshold
Threshold_UF1	p.u.	Frequency drop relay threshold
VAMP_LAG1	s	First-order lag time constant for AC voltage detection
FREQ_LAG1	s	First-order lag time constant for frequency detection
RecoveryTime1	-	Lag from fault relay cancellation to actual cancellation of protection operation
GBTime1	s	GB implementation time
NoDetectPeriod1	s	Partial relay dead time at startup
CalculationTime1	s	Control cycle
DeadTime1	s	Dead time
Flag_DirectSample1	-	Voltage, current amount direct detection flag (selected from among three types)
Flag_AverageSample1	-	Detection flag using moving average of voltage and current amount (selected from among three types)
Flag_PeakTopSample1	-	Peak top detection flag of voltage and current amount (selected from among three types)
ChargeCircuitCloseTime1	s	Start time of charging (if starting from a transient state, assign a large negative value)
ChargeTime1	s	Charge time
Control_StartDelay1	s	Time from end of charge to start of control system operation
ManualCL_Time1	s	Time of starting current limit (current zero control) (used to simulate converter protection)
ManualGB_Time1	s	Time of starting gate block (used to simulate converter protection)
ManuaCBT_Time1	s	Time of starting circuit breaker release (used to simulate converter protection)

End

Change log		
Date	Example file version	Content changes
2018/06/21	1.0	First edition created

Examples of XTAP		No.	HVDC-04
<b>Example Name</b>	Self-Excited HVDC Model (Full Bridge MMC)		
<b>Field</b>	Power electronics		
<b>Literature</b>	<p>(1) “DC Power Transmission Engineering,” Tokyo Denki University Press, written and edited by Takahiko Machida</p> <p>(2) T. Kikuma, K. Takenaka, M. Takasaki, “Control Protection Method of DC Power Transmission System with Modular Multi-Level Converter Using Full Bridge Cell: Proposal of a Control Method that can Control Fault Current During DC Fault,” Central Research Institute of Electric Power Industry Research Report R11021, (2012).</p> <p>(3) T. Kikuma, “Control Protection Method of DC Power Transmission System with Modular Multi Level Converter Using Full Bridge Cell - Part 2: Development of Operation Continuous Control and High-Speed Starting Method at AC Voltage Rise,” Central Research Institute of Electric Power Industry Research Report R14016, (2015).</p> <p>(4) T. Kikuma et al., “Control Method of Double Y-connection Modular Multi-level Converter,” Journal of the Institute of Electrical Engineers of Japan D, Vol. 133, No. 9, pp. 917-927 (2013).</p> <p>(5) T. Kikuma et al., “Control Protection Method of Self-Excited DC Power Transmission System capable of Suppressing DC Fault Current,” Journal of the Institute of Electrical Engineers of Japan, Vol. 133, No. 5. pp. 449-456 (2013).</p>		
<b>Overview</b>	<p>Because this model has basic control and protection systems, it can be applied to other simulations by copying it and changing the rated value.</p> <p>This example simulates the circuit of a DC power transmission system using a modular multilevel converter (full bridge MMC). This has the same configuration as that of HVDC-03 (self-excited HVDC model, half bridge MMC), except that the cells of the MMC are replaced with full bridge cells. For a basic description of the model, refer to HVDC-03. In this example, the simulated waveforms at the time of a power flow reversal and a DC main line ground fault are shown.</p>		

## Introduction/Model Use

Refer to the table at the end for the parameters required to use the MMC model. When changing the active power output of the MMC, “Porder” in “MASTER\_VSC 1,” which is located one level below the highest level of the hierarchy, is changed. This example deals with two types of models:

- ② a full bridge MMC averaging model (HVDC-04A), and
- ② a full bridge MMC detailed model (HVDC-04B).

In the absence of any specific reason to use the detailed model, the use of the average model is recommended because it is much faster.

## Analysis Circuit and Conditions

Figure 1 shows the analysis circuit.

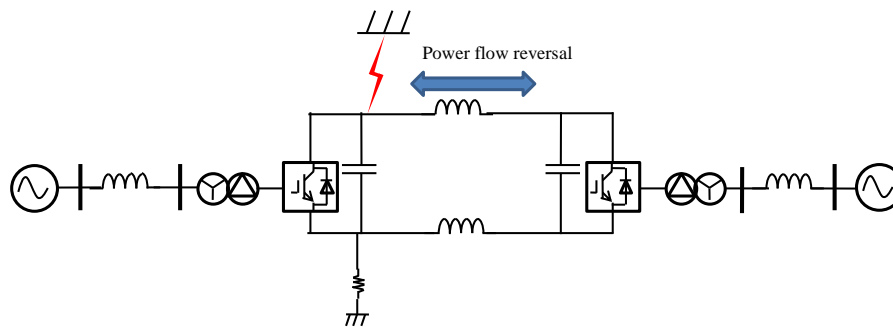


Figure 1 Analysis circuit

- Rated equipment capacity = 50 MW (55.9 MVA), primary side rated voltage = 66 kV, secondary side rated voltage = 56 kV, DC voltage = 125 kV.
- The DC power transmission system is linked with the 66-kV system through the impedance of the simulated short-circuit capacity of the system.
- In this example, simulations of ① a power flow reversal and ② a DC main line ground fault are carried out. At a simulation time of  $t = 0.5$  s, the power command value changes and a power flow reversal begins. A ground fault occurs at  $t = 0.8$  s, after which, the fault removal and restart are carried out through a converter operation.

## Analysis Results

Figures 2 and 3 show the DC capacitor voltage and direct current at the time of a power flow reversal. Figures 4 and 5 show the active and reactive power outputs from terminals 1 and 2 at the time of a power flow reversal, respectively. Because the reactive power control of each terminal in this simulation continuously controls the voltage of the AC side (ACAVR), the reactive power is controlled such that the terminal voltage of the converter approaches 1.0 pu.

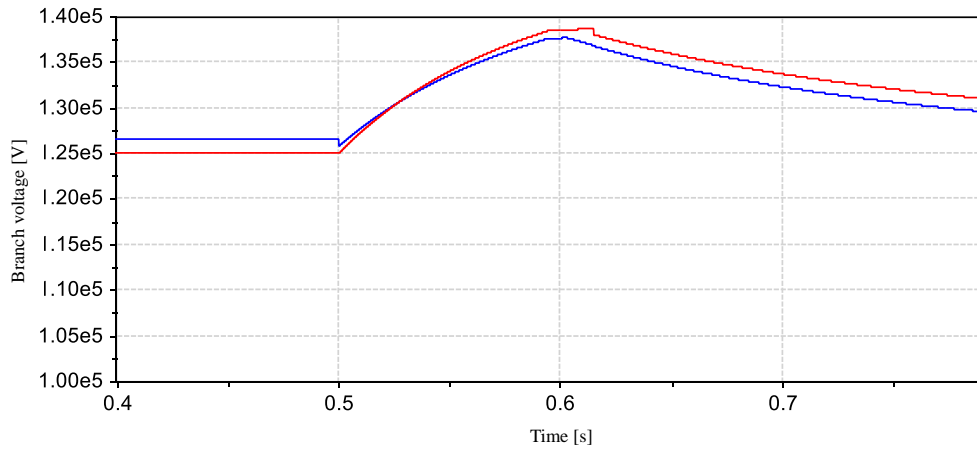


Figure 2 DC voltage [pu]: blue line, terminal 1; red line, terminal 2 (reference voltage of 125 kV)

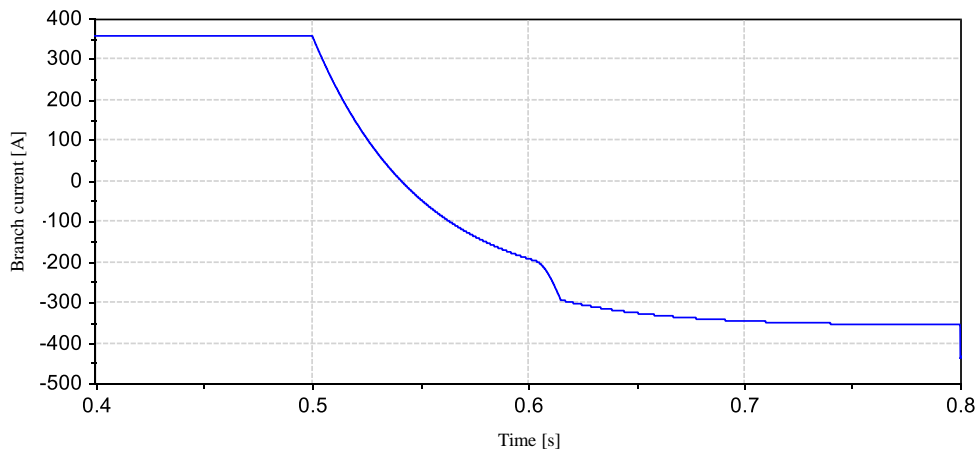


Figure 3 Direct current [A]

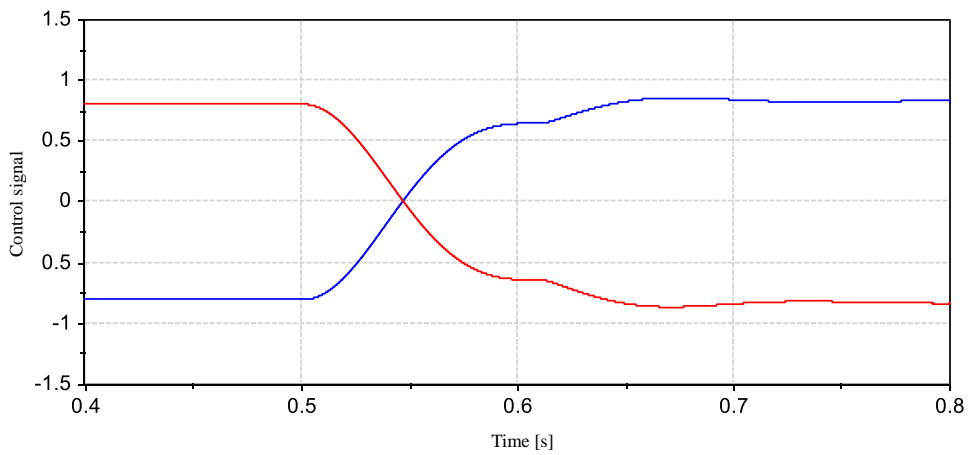


Figure 4 Active power [pu]: blue line, terminal 1; red line, terminal 2 (reference capacity of 55.9 MVA)

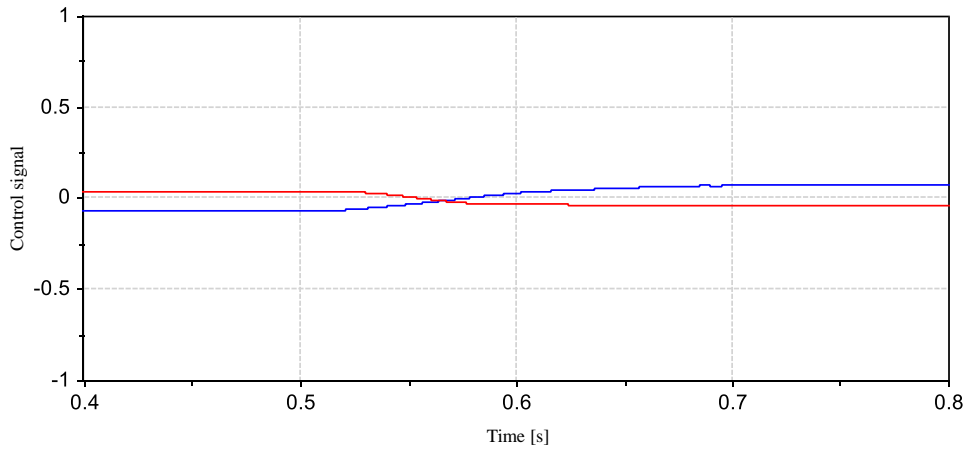


Figure 5 Reactive power [pu]: blue line, terminal 1; red line, terminal 2 (reference capacity of 55.9)

At  $t = 0.5$  s, the power command value switches from 45 MW (0.8 pu) to -45 MW (-0.8 pu), and the power flow reversal begins. The rectifier controls the DC current and determines the power to be sent to another system, whereas the inverter side determines and controls the DC voltage.

Figures 6 and 7 show the DC voltage and current, respectively, at the time of a DC fault. When a direct current fault occurs at  $t = 0.8$  s, the power transmission is temporarily stopped and is restarted based on the function of the converter. For details of the full bridge MMC during a DC fault, see the references.

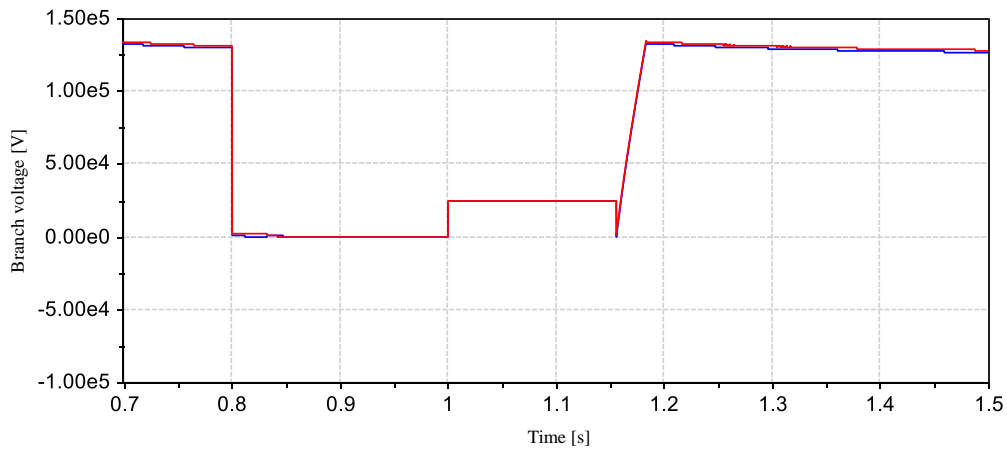


Figure 6 DC voltage [V]: blue line, terminal 1; red line, terminal 2 (reference voltage of 125 kV)

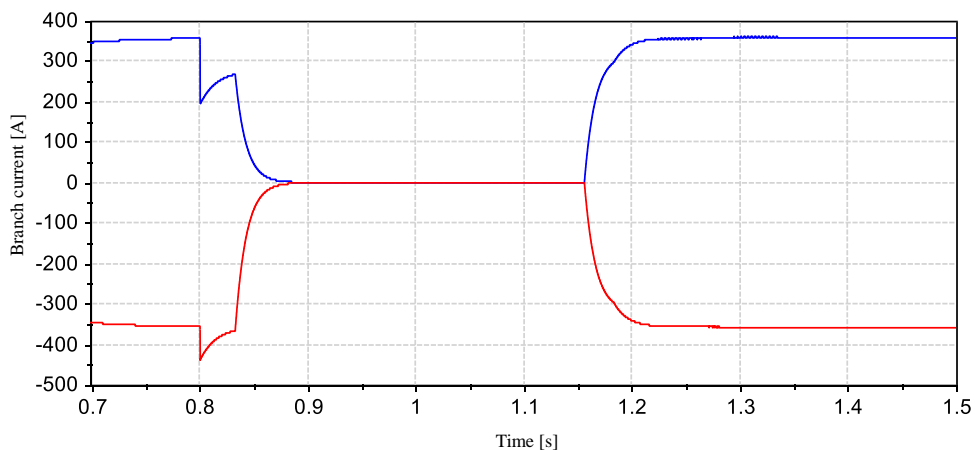


Figure 7 Direct current [A]

The parameters of the model and their respective descriptions are shown below. Note that in the settings of terminal 2, the variable names are the same as those of terminal 1 except that the 1 at the end is replaced with 2, and hence these details have been omitted here.

	Name	Un	Item
Common constants	Rate_P	W	Rated active power
	Rate_Vdc	V	Rated DC voltage
	SSRelayOffTime	s	Relay dead time at start of simulation
	FlagInitialize	-	Initialization flag (used to start simulation from steady state) Input 1 to start from steady state
	V_ThirdOrder	pu	Third harmonic injection amount for the modulation rate reduction
	CellNumPerArm	-	Number of stages per arm of MMC cell (in the averaging model, always enter 1)
	SystemFrequency	Hz	System frequency
	Rate_S1	V	Rated capacity
	Rate_V1_tol1	V	Effective value of transformer primary side line voltage
	Rate_V2_tol1	V	Effective value of transformer secondary side line voltage
	PWMPulseNumbe	-	Number of PWM pulses (per cycle)
	R_TransGND1	$\Omega$	Ground resistance of converter transformer
	H1	s	Electrostatic constant
	Flag_ACAVR1	-	ACAVR flag (1 = used, 0 = not used), select Flag_AQR
	Flag_AQR1	-	AQR flag (1 = used, 0 = not used), select Flag_ACAVR
	Vac_order1	p.u	AC voltage command value (ACAVR command value)
	Q_order1	p.u	Reactive power command value (AQR command value)
	PWMPhase1	de	Phase angle of PWM carrier
	R_connect_pu1	p.u	Converter transformer resistance
	L_connect_pu1	p.u	Converter transformer inductance
	L_Arm_pu1	p.u	Arm reactor inductance
	L_DCK_pu1	p.u	Inductance of DC reactor (for upper line) Inductance value = $L\_DCK\_pu1 \times \text{rated DC voltage}^2 / \text{rated active power}$
	L_DCA_pu1	p.u	Inductance of DC reactor (for lower line)
	Gain_ACR1	-	ACR gain
	T_ACR1	s	ACR time constant
	Gain_APR1	-	APR gain
	T_APR1	s	APR time constant
	Lag_APR1	s	First-order lag time constant for APR
	Gain_DCAVR1	-	DCAVR gain
	T_DCAVR1	s	DCAVR time constant
	Gain_AQR1	-	AQR gain
	T_AQR1	s	AQR time constant
	Gain_ACAVR1	-	ACAVR gain
	T_ACAVR1	s	ACAVR time constant
	Lag_Margin1	s	First-order lag time constant at margin switching (switching speed)
	IinvLimit1	p.u	Maximum current of converter (denominator is the converter rating)
	K_DCFRD1	-	Gain of DC fault detection relay (the smaller the value, the more the sensitivity)

T_DCFRD1	s	First-order lag time constant of DC fault detection relay
Threshold_DCOC	p.u	DC overcurrent relay threshold
Threshold_OC1	p.u	Overcurrent relay threshold
Threshold_DCOV	p.u	DC overvoltage relay threshold
Threshold_DCUV	p.u	DC undercurrent relay threshold
Threshold_OV1	p.u	AC overvoltage relay threshold
Threshold_UV1	p.u	AC undervoltage relay threshold
Threshold_OF1	p.u	Frequency rise relay threshold
Threshold_UF1	p.u	Frequency drop relay threshold
VAMP_LAG1	s	First-order lag time constant for AC voltage detection
FREQ_LAG1	s	First-order lag time constant for frequency detection
RecoveryTime1	-	Lag from fault relay cancellation to actual cancellation of protection operation
GBTime1	s	GB implementation time
NoDetectPeriod1	s	Partial relay dead time at startup
CalculationTime1	s	Control cycle
DeadTime1	s	Dead time
Flag_DirectSampl	-	Voltage, current amount direct detection flag (selected from among three types)
Flag_AverageSam	-	Detection flag using the moving average of voltage and current amount (selected from among three types)
Flag_PeakTopSa	-	Peak top detection flag of voltage and current amount (selected from among three types)
ChargeCircuitClos	s	Start time of charging (if starting from a transient state, assign a large negative value)
ChargeTime1	s	Charge time
Control_StartDela	s	Time from end of charge to start of control system operation
ManualCL_Time1	s	Time of starting current limit (current zero control) (used to simulate converter protection)
ManualGB_Time	s	Time of starting gate block (used to simulate converter protection)
ManualCBT_Time	s	Time of starting circuit breaker release (used to simulate converter protection)
DCRecoveryTime	s	Delay from DC fault detection relay release until actual cancellation of protection operation
DCCLTime1		DC current zero restoration execution time at the time of DC fault (time from detection of DC fault to GB)
Threshold_UVVD		Lowering of DC voltage when AC voltage becomes lower than threshold value
DCVmag1		DC voltage margin
DCAmag1		DC current margin
OVmag1		AC overvoltage margin (margin for lowering of DC voltage for continuous operation during rise of AC voltage)

End

Change log		
Date	Example file version	Content changes
2018/06/21	1.0	First edition created

Examples of XTAP		No.	FACTS-01
Example Name	Simulation Start of STATCOM		
Field	Basic calculation (power systems)		
Literature	None		
Overview	<p>In this example, a calculation of the start simulation of STATCOM is carried out. STATCOM, the subject of this study, is the most basic two-level converter. Dismissing with the details, the design of the converter should cope with a DC voltage fluctuation of <math>\pm 20\%</math>. Normally, the converter charges the DC capacitor of the converter from the outside with an initial charging device, and activates it by interlocking with the power system from the state of a DC voltage of 1 pu. In this example, the DC capacitor was charged using the diode of the self-excited converter and was then set as the activating sequence. This start of the simulation is expected to enhance the understanding of the converter control.</p> <p>Vector control based on the dq rotating coordinate system widely used in STATCOM for power systems was adopted as the converter control. The PWM method was used for the pulse generation, which actually applies the switching. In this example, the conversion factors of the vector and PWM controls are multiplied by the rated modulation factor, which may be found to be useful because such an example has not been specifically discussed in textbooks or other studies. Further, the maximum value of the vector control output (<math>V_{dref}</math> and <math>V_{qref}</math> in the example) is determined from the maximum modulation rate. This aspect also needs to be studied because there are very few examples available. Regarding the control, the aim is to deepen our understanding through this example because the actual converter design (equipment specifications determined based on the requirements of the power system) and control are closely related.</p>		

# Analysis Circuit and Conditions

Figure 1 shows the analysis circuit.

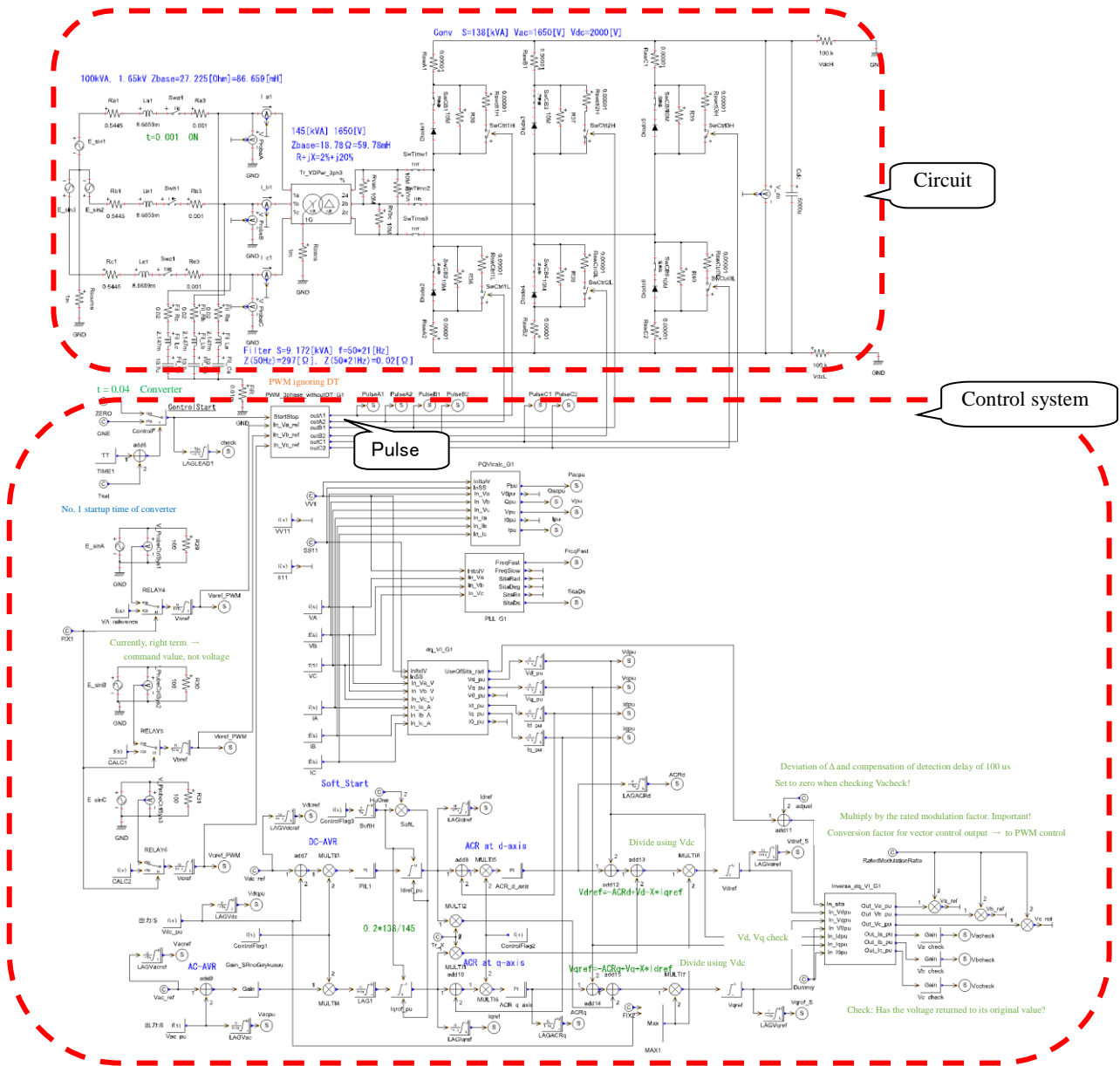


Figure 1 Analysis circuit

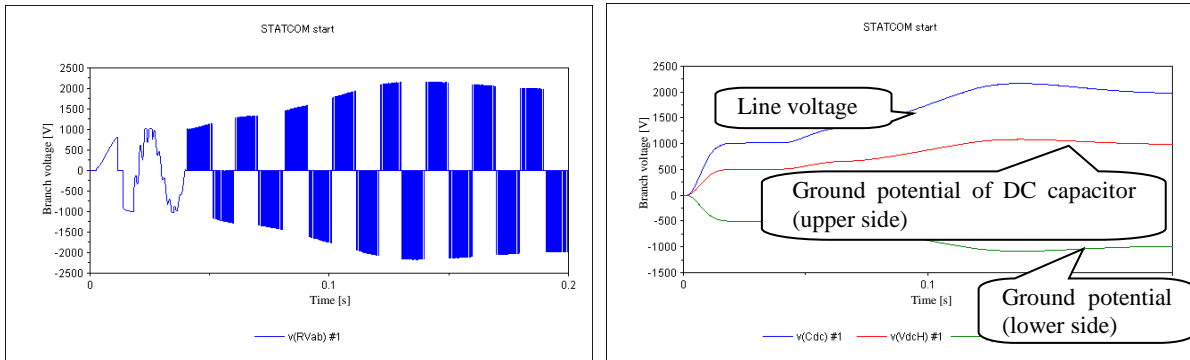
## [Basic conditions]

Power system: 100 kVA, 1.65-kV Zbase = 27.225 [Ohm] = 86.659 [mH]

Converter transformer: 145 [kVA] 1650 [V] R + jX = 2% + j20%

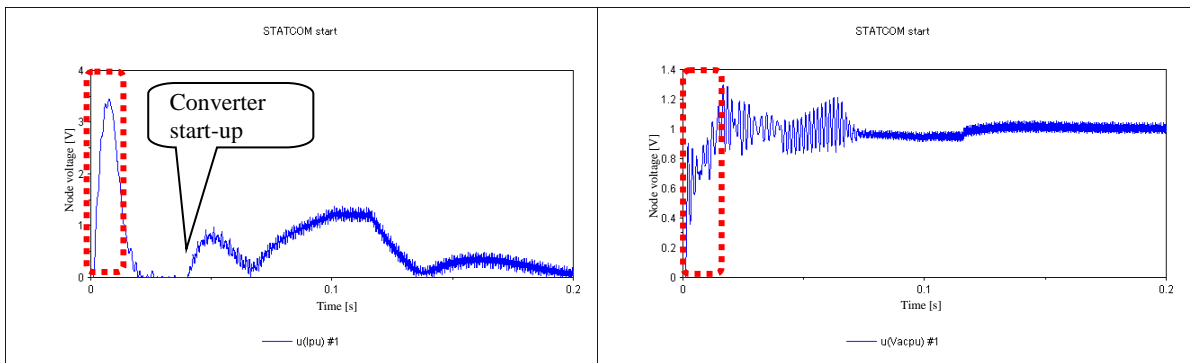
Converter: S = 138 [kVA] Vac = 1650 [V] Vdc = 2000 [V]

## Analysis Results



Converter transformer ab line voltage [V] on secondary side    Line voltage of DC circuit and ground potential [V]

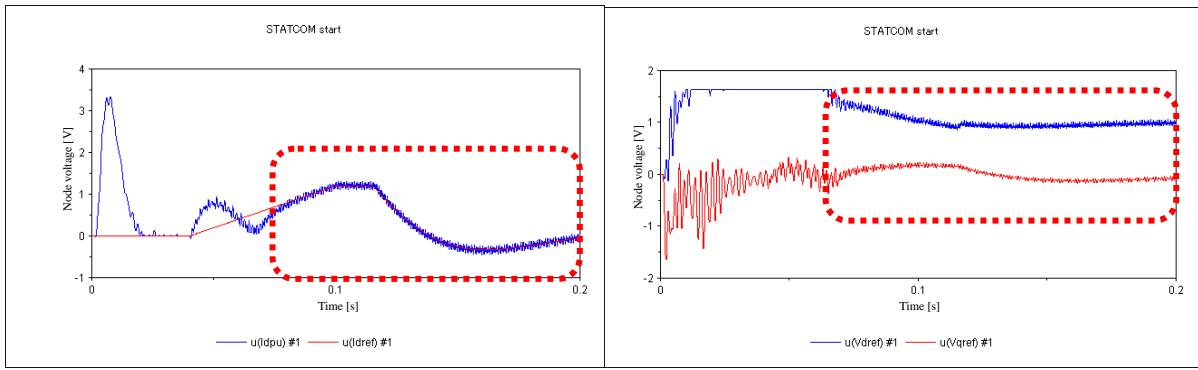
○ A direct current line voltage is selected, and an AC voltage source is created on the secondary side of the converter transformer. Exchange of active/reactive power takes place owing to the phase difference and potential difference between the voltages of this voltage source and the power system. Because the DC circuit side is not grounded, the potential as seen from the ground at both ends of the DC capacitor is  $\pm V_{dc}/2$ . If grounded with a low resistance, the potential of the capacitor (upper side) is  $V_{dc}$ , and the potential of the capacitor (lower side) becomes zero.



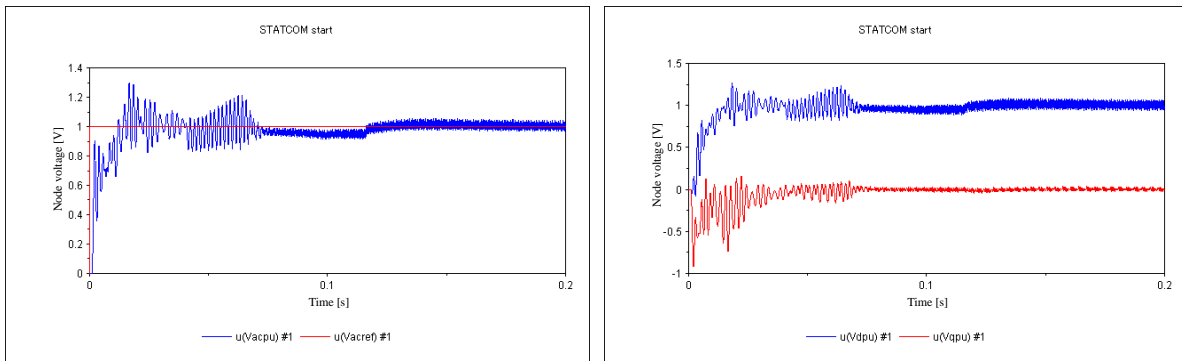
Primary side current [pu] of converter transformer

Primary voltage [pu] of converter transformer

○ When AC - CB is closed, the DC capacitor is charged from the system through the diode. The AC voltage is reduced to approximately 0.7 pu. Because the leakage impedance of the converter transformer is approximately 20%, a current flow of  $\Delta I = \Delta V/Z = 0.7/0.2 = 3.5$  pu is created.



○ The active current command ( $I_{dref}$ ) and active current ( $I_d$ ) are tracked within the range enclosed in red. At this time, the vector control outputs ( $V_{dref}$ ,  $V_{qref}$ ) also operate within the limiter range. Because the converter is assumed to be able to cope with a DC voltage fluctuation of  $\pm 20\%$ , as part of the device specifications, the trackability is ensured when  $V_{dc}$  falls within this range. Thus, it is clear that such matters are not determined solely through converter control, and that the control is closely related to the design of the converter (equipment specifications determined based on the requirements of the power system).



○ The AC voltage command ( $V_{acref}$ ) and AC voltage ( $V_{ac}$ ) have been tracked reasonably well. Because the control circuit is a first-order lag circuit, a steady-state deviation cannot be avoided. The figure on the right shows the waveform as indicated in dq rotation coordinates. In addition,  $V_d = 1$  pu and  $V_q = 0$  pu are achieved under a steady state. Vector control is a theory based on the fact that the control system of the dq axis current is independent, and PQ is not really independent. Through the moment-to-moment tracking of the dq axis when  $V_q = 0$  using PLL, PQ becomes independent as seen from the relationship  $P = V_d * I_d + V_q * I_q = V_d * I_d$ .

A simulation analysis was carried out under severe system conditions such as an extremely large voltage

drop when AC - CB is applied. The ability to judge an analysis result can only come from knowing the fundamentals of electrical circuits and control engineering, and it is therefore important to study the basics.

End

Change log		
Date	Example file version	Content changes
2014/11/19	2.0	Modified for XTAP Version 2.00
2012/07/19	1.2	Modified for XTAP Version 1.20
2011/10/18	1.1	Modified for XTAP Version 1.11
2010/09/02	1.0	First edition created (for XTAP Version 1.10)

Examples of XTAP		No.	FACTS-02
Name of Example	STATCOM Model		
Field	Power electronics		
Literature	None		
Overview	<p>Because this model has basic control and protection systems, it can be applied to other simulations by copying and changing the rated value.</p> <p>In this example, the STATCOM circuit is simulated. STATCOM is a type of equipment that controls the reactive power using a self-exciting semiconductor device. Because it is able to control the reactive power continuously at a high speed, it can respond faster to sudden changes in the system voltage.</p> <p>The characteristics of STATCOM dealt with in this example are described below.</p> <ul style="list-style-type: none"> <li>• The circuit system of the converter is a basic two-level converter.</li> <li>• Performs a reactive power constant control (AQR) operation that outputs a constant reactive power irrespective of the magnitude of the system voltage.</li> <li>• A resistance charging system is employed, which charges the device at the time of the startup through a resistor.</li> <li>• A switching pulse applied to the gate of the semiconductor device is created using the PWM control.</li> </ul>		

## Analysis Circuit and Conditions

Figure 1 shows the analysis circuit.

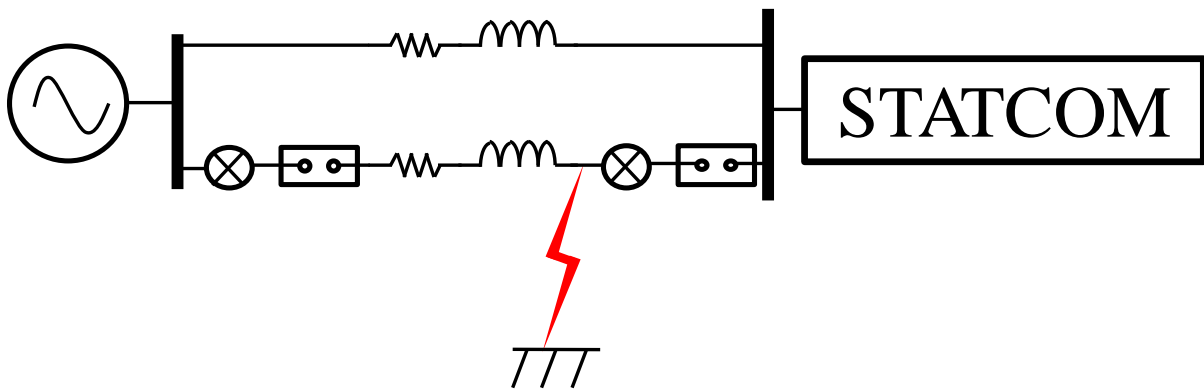


Figure 1 Analysis circuit

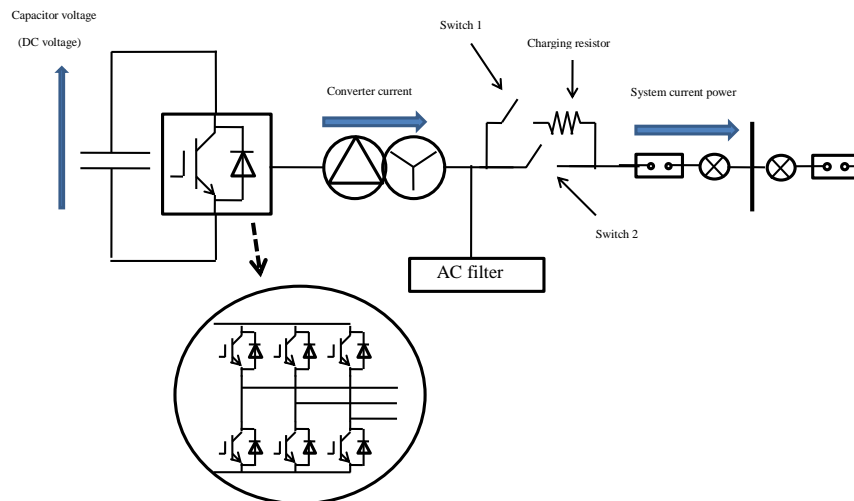


Figure 2 Schematic diagram of model

- Rated equipment capacity = 10 MVA, primary side rated voltage = 66 kV, secondary side rated voltage = 5.6 kV, rated DC voltage = 12.5 kV
- STATCOM is linked with the system (66 kV) through the impedance of the simulated short-circuit capacity of the system.
- A three-wire ground fault occurs at a simulation time of  $t = 0.5$  s, which is removed by the circuit breaker at  $t = 0.6$  s.

## Analysis Results

We first show the waveform at the start of STATCOM. Figure 3 shows the capacitor voltage of STATCOM, Figure 4 shows the reactive power output by STATCOM, and Figure 5 shows the current flowing from the converter to the system.

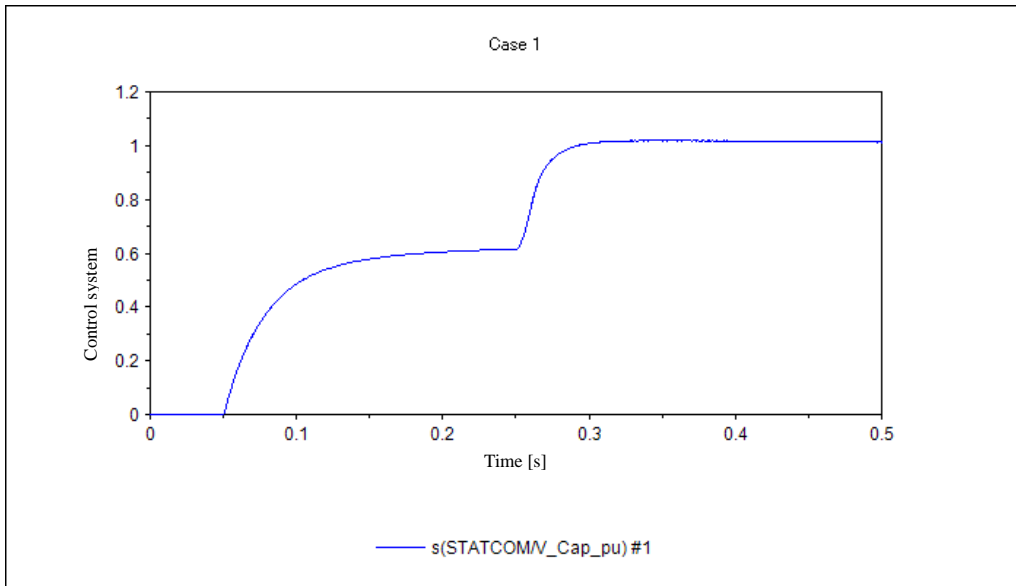


Figure 3 Capacitor voltage for energy storage [pu]

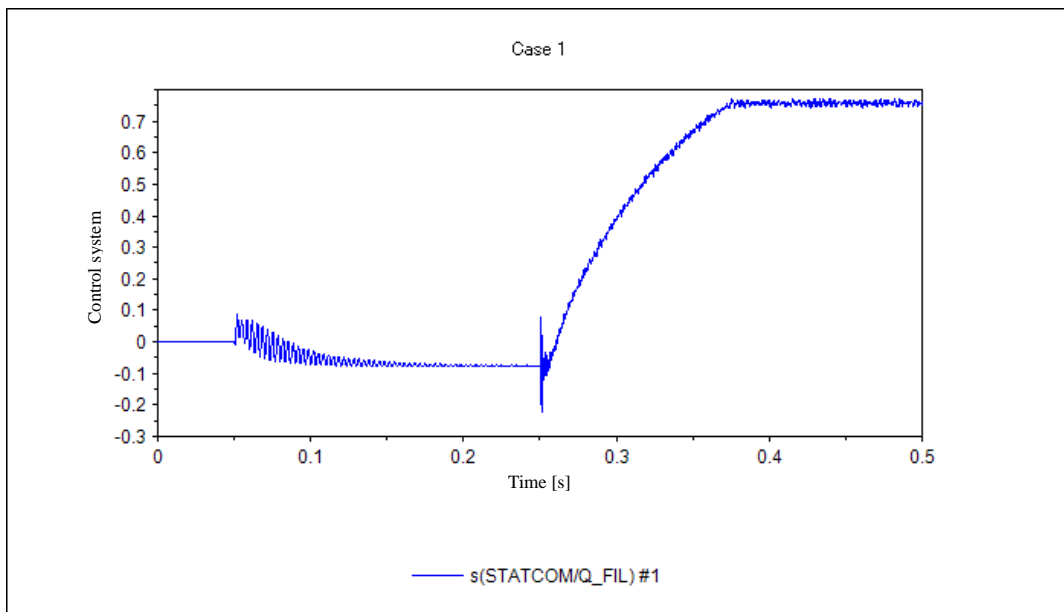


Figure 4 Reactive power output by STATCOM [pu]

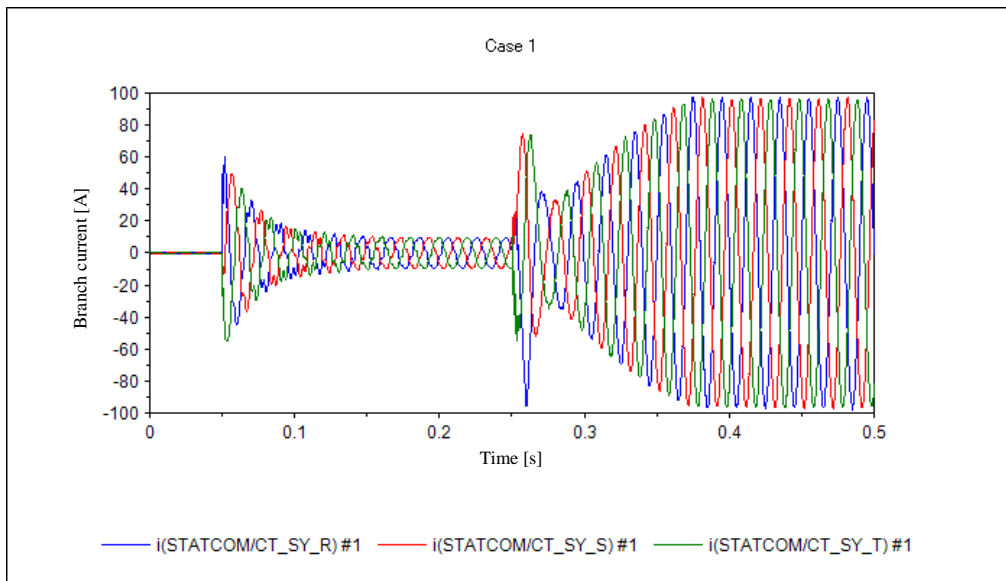


Figure 5 System side output current [A]

Switch 1 is closed at  $t = 0.05$  s and STATCOM becomes linked with the system through the charging resistor, and the DC capacitor for energy storage is charged to approximately 0.6 pu. Switch 2 is then closed at  $t = 0.25$  s, and at the same time at which STATCOM and the system become directly linked, the control system starts to operate. When the control system starts operating, the voltage of the capacitor becomes 1.0 pu, and the reactive power output of STATCOM conforms to the command value (here, 0.8 pu). A steady-state deviation occurs because the reactive power control of STATCOM uses a first-order lag control, and hence the command value and actual reactive power output of STATCOM differ slightly.

Figures 6 and 7 show the converter current and system side output current under a steady state. Because STATCOM applies PWM control, the converter current has a waveform that includes a large amount of harmonics derived from the PWM modulated wave. Because these harmonics are removed using an AC filter connected between the converter and system, the current flowing through the system is a sinusoidal wave.

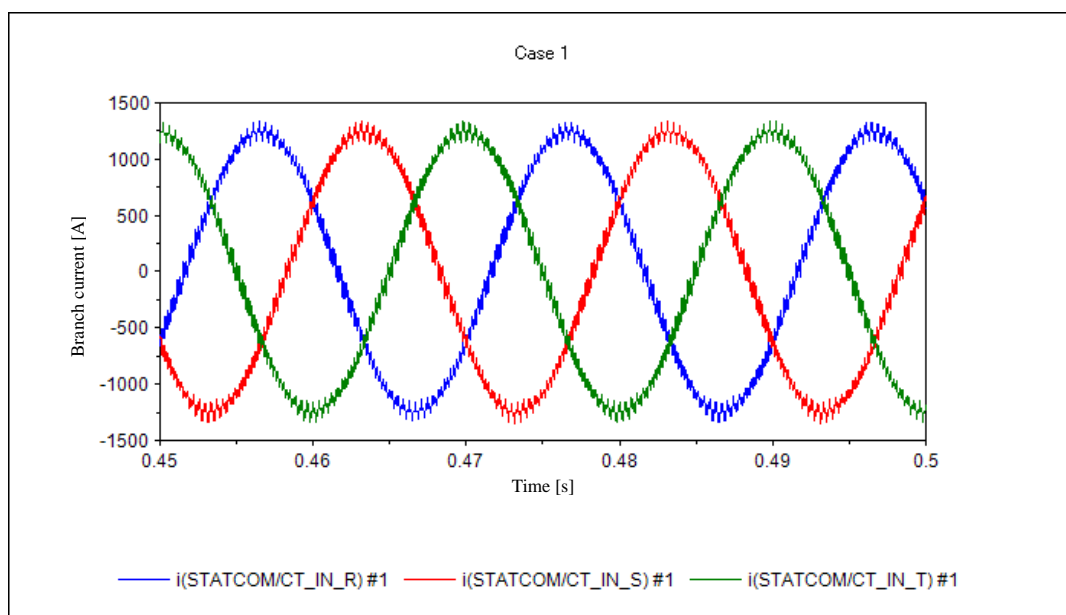


Figure 6 Enlarged view of converter current

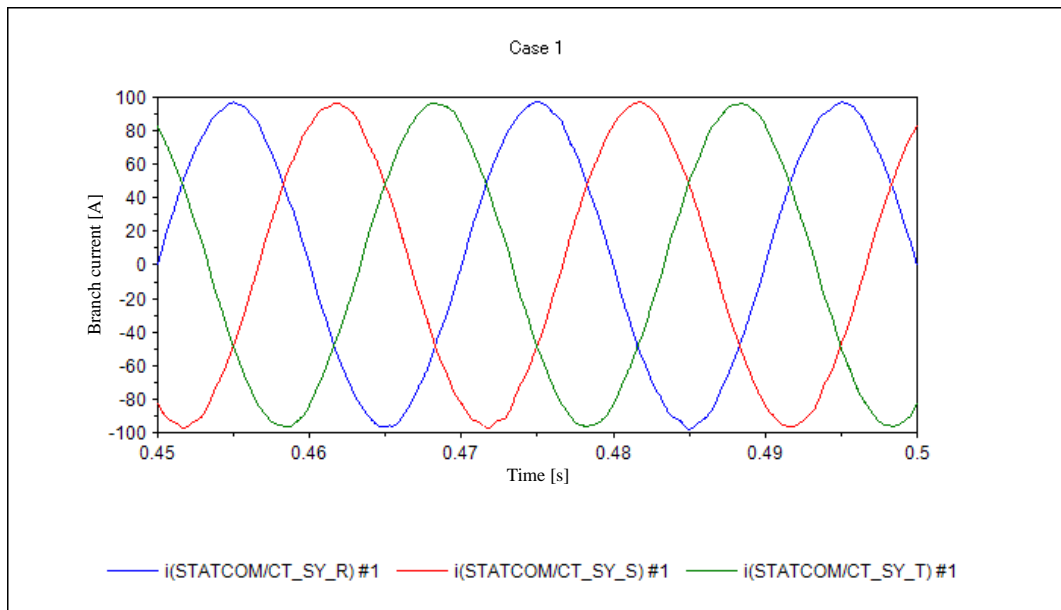


Figure 7 Enlarged view of system side output current

The system voltage at the time of a three-phase ground fault is shown in Figure 8, and the converter current is shown in Figure 9. In this simulation, when there is a drop in the system voltage, STATCOM restarts the operation after a gate block (GB). As can be seen from Figure 8, because the converter is stopped after the GB, the converter current reaches zero. When the fault is removed and the system voltage recovers, the converter automatically restarts.

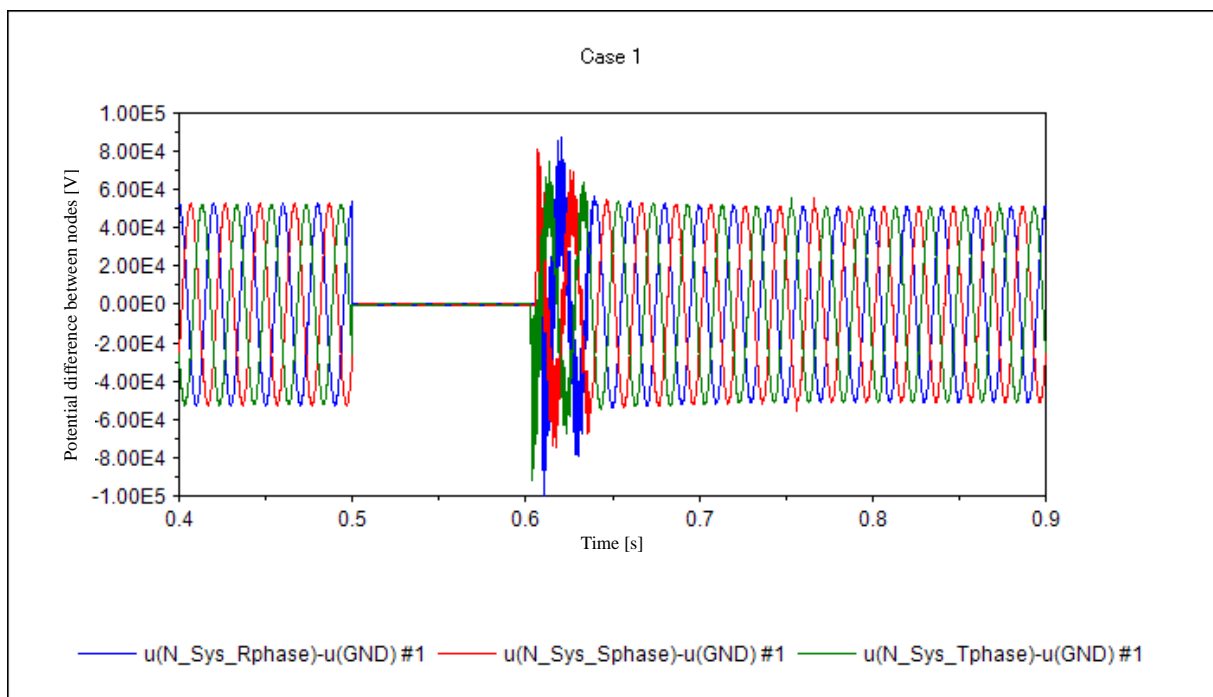


Figure 8 System voltage

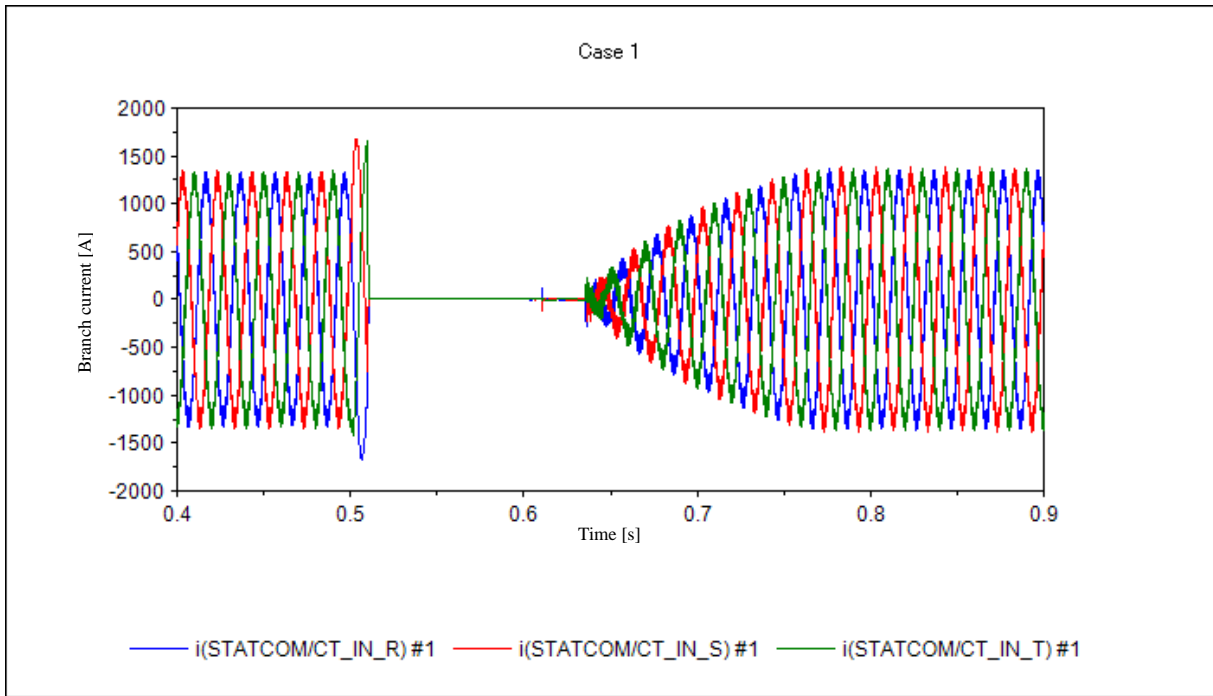


Figure 9 System side output current

The parameters of the model and their description are shown on the next page.

Name	Unit	Item
SystemFrequency	Hz	System frequency
Rate_S	VA	Rated capacity
Rate_V1_ltol	V	Effective value of transformer primary side line voltage
Rate_V2_ltol	V	Effective value of transformer secondary side line voltage
Rate_Vdc	V	Rated DC voltage
PWMPulseNumber	-	Number of PWM pulses (per cycle)
R_TransGND	$\Omega$	Ground resistance of converter transformer
H	s	Electrostatic constant
Flag_ACAVR	-	ACA VR flag (1 = used, 0 = not used). Select Flag_AOR
Flag_AOR	-	AOR flag (1 = used, 0 = not used). Select Flag_ACAVR
Vdc_order	p.u.	DC voltage command value (DCAVR command value)
Vac_order	p.u.	AC voltage command value (ACA VR command value)
O_order	p.u.	Reactive power command value (AOR command value)
PWMPhase	deg	Phase angle of PWM carrier
R_connect_pu	p.u.	Converter transformer resistance
L_connect_pu	p.u.	Converter transformer inductance
Spu_filter1	p.u.	Fundamental wave capacity of the higher-order filter 1 (denominator is rated capacity of converter)
O_filter1	-	Sharpness of higher-order filter 1
Spu_filter2	p.u.	Fundamental wave capacity of higher-order filter 2 (denominator is rated capacity of converter)
O_filter2	-	Sharpness of higher-order filter 2
Gain_ACR	-	ACR gain
T_ACR	s	ACR time constant
Gain_DCAVR	-	DCAVR gain
T_DCAVR	s	DCAVR time constant
Gain_AOR	-	AOR gain
T_AOR	s	AOR time constant
Gain_ACAVR	-	ACA VR gain
T_ACAVR	s	ACA VR time constant
IinvLimit	p.u.	Maximum current of converter (denominator is the converter rating)
Threshold_OC	p.u.	Overcurrent relay threshold
Threshold_DCOV	p.u.	DC overvoltage relay threshold
Threshold_DCUV	p.u.	DC undervoltage relay threshold
Threshold_OV	p.u.	AC overvoltage relay threshold
Threshold_UV	p.u.	AC undervoltage relay threshold
Threshold_OF	p.u.	Frequency rise relay threshold
Threshold_UF	p.u.	Frequency drop relay threshold
VAMP_LAG	s	First-order lag time constant for AC voltage detection
FREQ_LAG	s	First-order lag time constant for frequency detection
RecoveryTime	-	Lag from fault relay cancellation to actual cancellation of protection operation
GBTime	s	GB implementation time
NoDetectPeriod	s	Partial relay dead time at startup
SSRelayOffTime	s	Relay dead time at the start of the simulation
CalculationTime	s	Control cycle
DeadTime	s	Dead time
Flag_DirectSample	-	Voltage, current amount direct detection flag (selected from among three types)
Flag_AverageSample	-	Detection flag using moving average of voltage and current amount (selected from among three types)
Flag_PeakTopSample	-	Peak top detection flag of voltage and current amount (selected from among three types)
ChargeCircuitCloseTime	s	STATCOM start time = start time of charging (If starting from the transient state, assign a large negative value)
ChargeTime	s	Charge time
Control_StartDelay	s	Time from the end of the charge to the start of the control system operation

End

Change log		
Date	Example file version	Content changes
2018/6/29	2.2	Icons of parts changed Ground terminal of transformer added
2018/1/26	2.1	Modified the creation logic of HOLD signal
2014/11/19	2.0	Modified for XTAP Version 2.00
2013/04/15	1.3	Changes consequent to modifications in model diagram and parameter input format
2012/08/29	1.2	Changes consequent to modification of STATCOM model
2012/07/19	1.1	Modified for XTAP Version 1.20
2011/10/18	1.0	First edition created (for XTAP Version 1.11)

Example FACTS-03.doc XTAP collection		No.	FACTS-03
Example Name	Separately Excited SVC Model		
Field	Power electronics		
Literature	Technical Report of the Institute of Electrical Engineers of Japan, Electricity and Energy Department, Power & Energy Department Stationary Equipment Technical Committee, “Energy Saving Technology of Static Reactive Power Compensator” (2004).		
Overview	<p>Because this model has basic control and protection systems, it can be applied to other simulations by copying it and changing the rated value.</p> <p>A separately excited SVC (hereinafter referred to as an SVC) is a device that compensates the reactive power through a control using thyristors. Because a type of SVC that combines a thyristor controlled reactor (TCR) and AC filter (as well as a stacon) is currently the mainstream type used in Japan, the TCR configuration is used here. A TCR is a device that controls the reactive power by continuously controlling the current flowing through a reactor using a thyristor. Here, if the control angle is <math>\alpha</math>, the fundamental wave component flowing in the reactor changes continuously with the change in <math>\alpha</math>. The reactive power is controlled by utilizing this property.</p> <p>Because the current waveform output from the TCR contains large amounts of harmonics, an AC filter is installed such that the harmonic current does not flow out to the grid. Moreover, by installing an AC filter and a stacon, it is possible to supply reactive power in addition to consuming it. The TCR part is connected to the AC filter and the stacon through a delta-delta connection transformer. Most of the harmonics generated in the TCR section are absorbed by the fifth- and seventh-order filters and stacon. To avoid an inrushing current and suppress the harmonic resonance in the stacon, 6% (or 13%) reactors are inserted in-series. If necessary, the SVC may be connected to the system through another transformer, but this feature is not included in the present model.</p>		

## Analysis Circuit and Conditions

Figure 1 shows the analysis circuit created using XTAP, and Figure 2 shows a schematic diagram of the model.

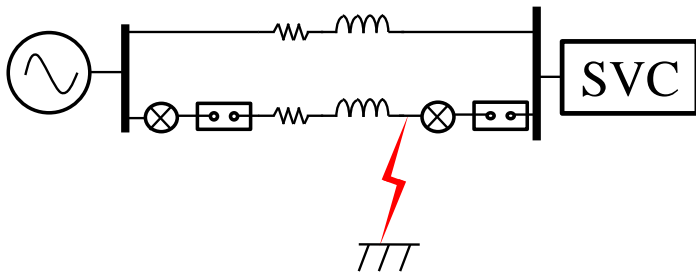
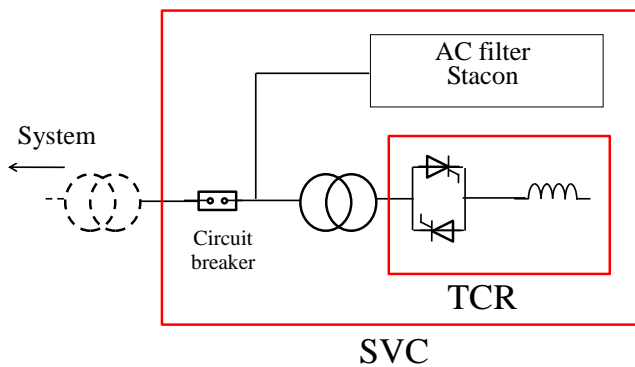
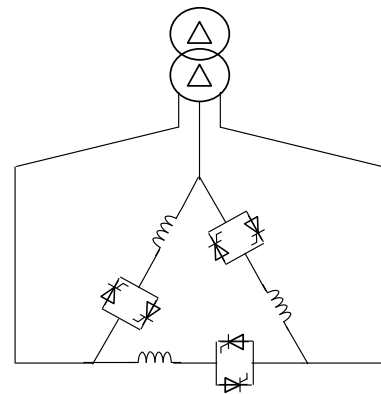


Figure 1 Analysis circuit



(a) Overall view of SVC



(b) TCR circuit diagram

Figure 2 Schematic diagram of the model

- The main ratings are as follows: rated capacity of 100 to -100 MW, and rated voltage of 275/20 kV.
- The SVC is linked with the system (275 kV) through the simulated impedance of the short-circuit capacity of the system.
- A three-wire ground fault occurs at a simulation time of  $t = 0.5$  s, which is removed by the circuit breaker at  $t = 0.6$  s.

## Analysis Results

Figure 3 shows the voltage and current measurement points.

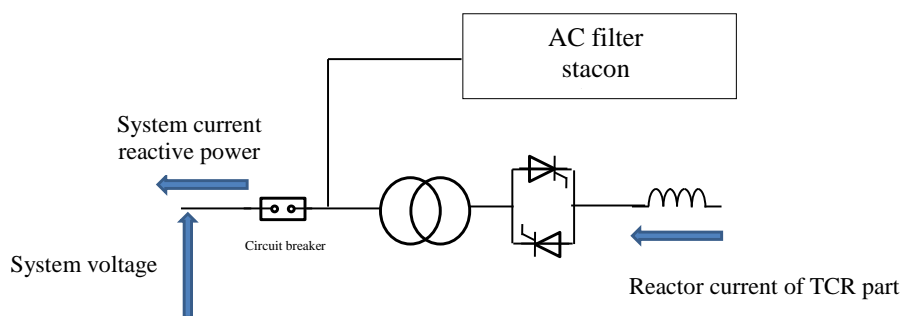


Figure 3 Voltage and current measurement points

Figure 4 shows the voltage and current waveforms during a steady state. The harmonic component of the current output from the TCR is absorbed by the AC filter, and a sinusoidal current is output to the system.

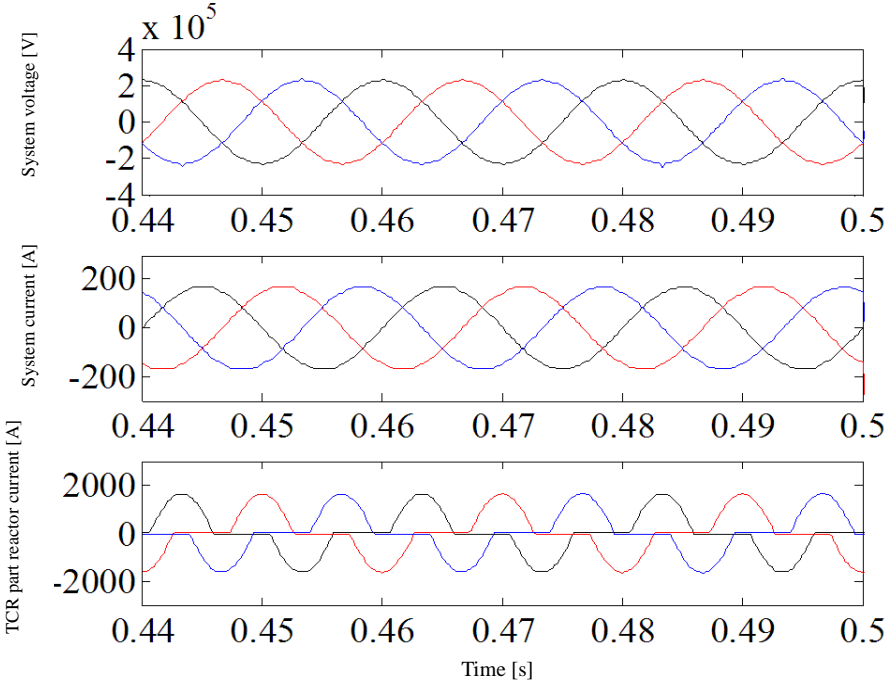


Figure 4 Voltage and current waveforms during a steady state

Figure 5 shows the waveforms from the occurrence of the three-wire ground fault to the point of returning to a steady state after removal of the fault. During this simulation, because the system is controlled to hold down the output from the SVC to zero during the fault period, the reactive power output by the SVC becomes zero immediately after the elimination of the fault, and rises thereafter.

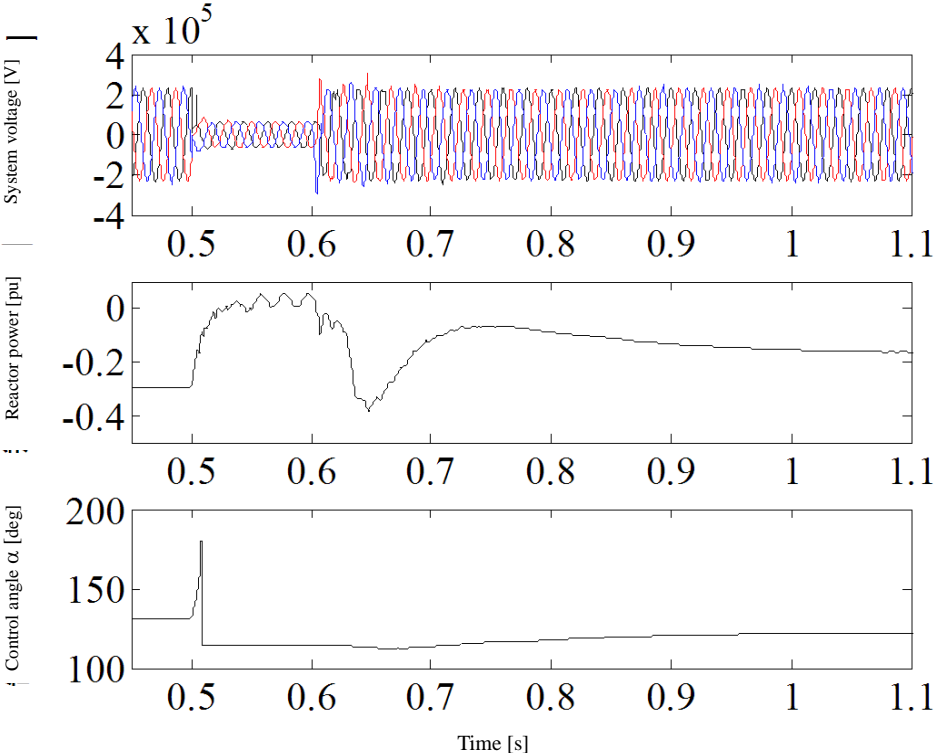


Figure 5 Waveform of each part at the time of three-wire ground fault

The parameters of the model and their descriptions are shown below.

Name	Unit	Item
SystemFrequency	Hz	System frequency
Rate_V1_ltol	Vrms	Effective value of transformer primary side line voltage
Rate_V2_ltol	Vrms	Effective value of transformer secondary side line voltage
Rate_S_TCR	VA	TCR capacity
Rate_SC	VA	Total capacity of stacon and harmonic filter
F_5_pu	p.u.	Resonance order of fifth-order filter
Q5	-	Sharpness of fifth-order filter
S5_pu	p.u.	Ratio of fifth-order filter (denominator is Rate_SC)
F_7_pu	p.u.	Resonance order of seventh-order filter
Q7	-	Sharpness of seventh-order filter
S7_pu	p.u.	Ratio of seventh-order filter (denominator is Rate_SC)
R_GND	$\Omega$	Earth resistance
TCR_Rpu	p.u.	Element resistance of TCR
Trans_Rpu	p.u.	Resistance of TCR transformer
Trans_Lpu	p.u.	Inductance component of TCR transformer
Flag_AQR	-	Reactive power control (AQR) flag (1 or 0)
Q_order	p.u.	Command value of AQR (denominator is Rate_S_TCR)
Gain_AQR	-	AQR gain
T_AQR	s	Time constant of AQR
Flag_ACAVR	-	AC voltage control flag (ACAVR) (1 or 0)
Vac_order	p.u.	Command value of ACAVR
Gain_ACAVR	-	ACAVR gain
T_ACAVR	s	Time constant of ACAVR
Alpha_min	deg	Minimum value of control angle
Alpha_max	deg	Maximum value of control angle
Control_Start	s	Control system start time
SSRelayOffTime	s	Relay dead time at start of the simulation
CalculationTime	s	Control cycle
VAMP_LAG	s	Time constant of first-order lag for AC voltage detection
VAMP_AVE	cycle	Number of cycles of moving average of AC voltage measurement
FREQ_LAG	s	Time constant of first-order lag for frequency detection
Limit_linv	p.u.	Maximum value of current
CurrentShift	p.u.	Current command value at current shift execution
T_LimitOpen	s	Time constant of limiter opening for cancelling current shift
Threshold_OC	p.u.	OC relay threshold
Threshold_OV	p.u.	OV relay threshold
Threshold_UV	p.u.	UV relay threshold
Threshold_OF	p.u.	OF relay threshold
Threshold_UF	p.u.	UF relay threshold
RecoveryTime	s	Lag from fault relay cancellation to actual cancellation of protection operation
GBTime	s	GB implementation time (time from start of GB up to CBT)
DeionTime	s	Thyristor deionization time (see Tdeion section of Thy in the manual)

End

Change log		
Date	Example file version	Content changes
2018/6/29	2.1	Icons of parts changed
2014/11/19	2.0	Modified for XTAP Version 2.00
2013/04/15	1.1	Changes consequent to modifications in model diagram and parameter input format
2012/08/29	1.0	First edition created (for XTAP Version 1.2)

Examples of XTAP		No.	PQ-01
<b>Example Name</b>	Simulation of Flicker Suppression Using Separately Excited SVC		
<b>Field</b>	Basic calculation (power systems)		
<b>Literature</b>	N. Tibaki, K. Takenaka, K. Yukihiro, K. Huuchi, N. Hatano, Y. Takeuchi, T. Ishikawa, "Development of a control scheme for separately excited SVC for suppressing flicker," CRIEP Report R 0 6010, May 2007		
<b>Overview</b>	<p>In this example, the calculation of flicker suppression simulation using a separately excited SVC is carried out.</p> <p>The aim of this example is to learn the simulation of a separately excited converter using a thyristor element. The target of the study is the simulation of the conventional control of SVC suppression of the flicker using a simulated input.</p> <p>The ignition of the frequency conversion stations and HVDC is usually conducted using three-phase batch control. The main difference in the case of flicker suppression is that an ignition is achieved using three-phase individual control because the reverse phase component is also subject to compensation. A conventional control system is designed with a view to detecting the reactive power of the flicker and canceling it.</p> <p>Details of the equipment constants and other factors are provided in the references.</p>		

# Analysis Circuit and Conditions

Figure 1 shows the analysis circuit.

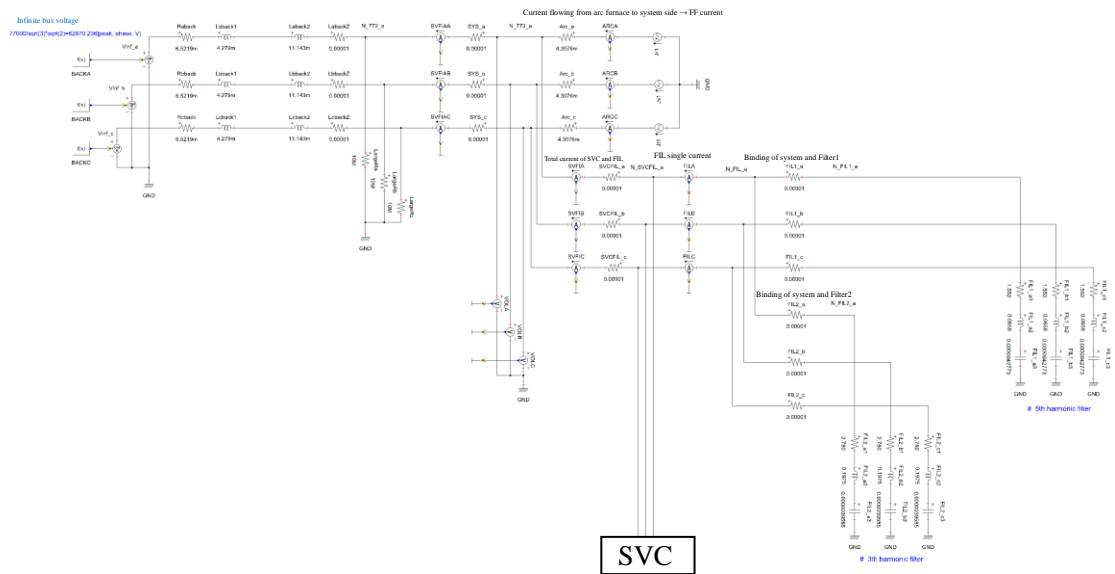


Figure 1 Analysis circuit

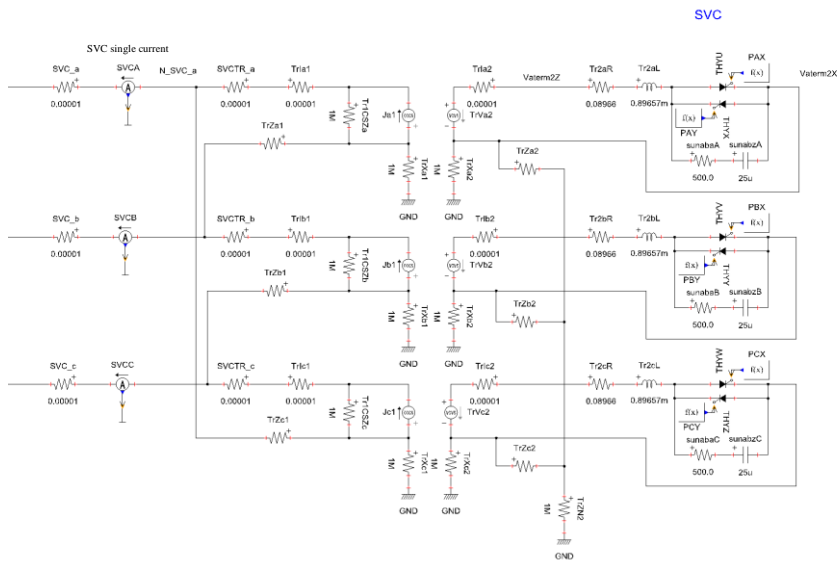
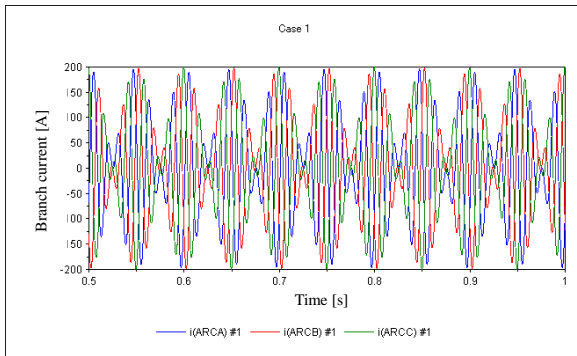
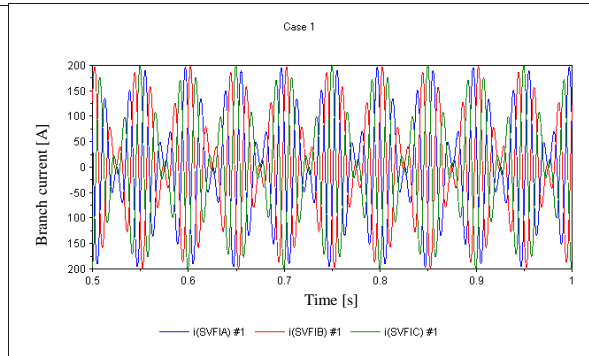


Figure 2 SVC Circuit configuration (TCR)

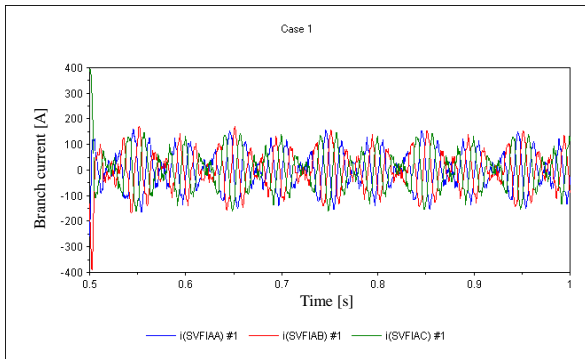
# Analysis Results



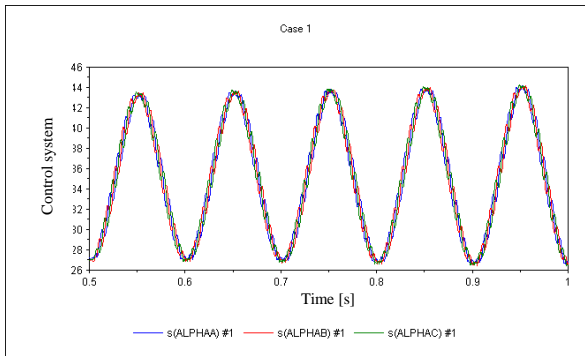
Arc furnace current [A]



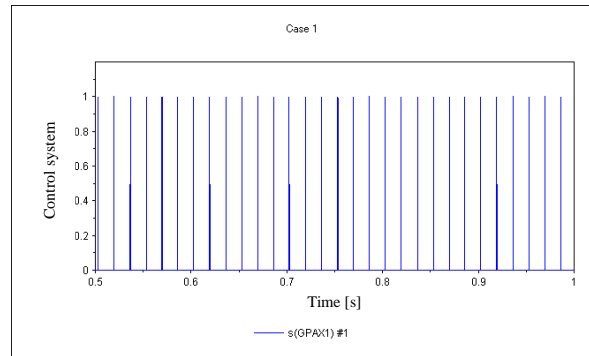
SVC + filter current [A]



Current flowing in the upper system [A]



Control angle  $\alpha$  [deg]



Pulse to A-phase upper element

The arc furnace current and voltage are detected, from which the instantaneous reactive power is determined. The SVC acts in such a manner to cancel this. In actuality, because the TCR can only be controlled by L, to operate the variation of  $\pm Q$ , the arc furnace  $\Delta Q$  is compensated by synthesizing the fundamental wave C of the harmonic filter.

A basic operation of the control is canceling with a feedforward, and hence the gain must be less than 1. Even if the control effect increases, it operates to amplify the disturbances, should they occur unexpectedly, and it is therefore necessary to set the gain to less than 1.

By compensating the arc furnace current with the combined current of the SVC + filter, it can be confirmed that the current flowing to the upper system is smaller.

The control angle  $\alpha$  is seen to move corresponding to the Q variation of the arc furnace. Switching is conducted twice during every cycle using the upper and lower thyristors. The compensable frequency band is smaller when compared with a self-excited converter, but this is not to say that a flicker can be compensated by a separately excited SVC.

End

Change log		
Date	Example file version	Content changes
2014/11/19	2.0	Modified for XTAP Version 2.00
2014/02/25	1.3	The method of simulating the current flowing from the arc furnace to the system side changed from a mathematical waveform of the voltage source to a combination of the Cos wave current source
2012/07/19	1.2	Modified for XTAP Version 1.20
2011/10/18	1.1	Modified for XTAP Version 1.11
2010/08/3	1.0	First edition created (for XTAP Version 1.10)

Examples of XTAP		No.	PQ-02-A
Example Name	Calculation of Excitation Inrush Current under Pressurization of Customer Transformer		
Field	Power quality analysis, excitation inrush current calculation		
Literature	<p>The data of the transformer of the present example were prepared by referring to the following paper.</p> <p>[1] K. Tokunaga, "Inrush Current Analysis of Two-Winding Power Transformer based on Equipment Constants Estimated using Winding Shape Design Procedure," Journal of the Institute of Electrical Engineers of Japan, Vol. 128, No. 9, pp. 1075-1081, 2008.</p>		
Overview	<p>When the transformer is pressurized, the magnetic flux of the iron core is saturated owing to the transient phenomenon during pressurization, and the excessive current flows over many cycles. This is known as the excitation inrush current. From the viewpoint of power quality, a voltage reduction from an excessive current flowing from the upper system becomes a problem, and from the viewpoint of protecting the transformer, the windings are displaced by the electromagnetic force, which generates an overcurrent flowing through the windings, leading to a concern that the insulator force may decrease.</p> <p>In this example, an exciting inrush current calculation is conducted when pressurizing a customer transformer with a 66-kV reception (high power reception). This is a basic example without considering the initial magnetic flux (residual magnetic flux).</p>		

## Analysis Circuit and Conditions

Figure 1 shows a single line connection diagram of the analysis circuit.

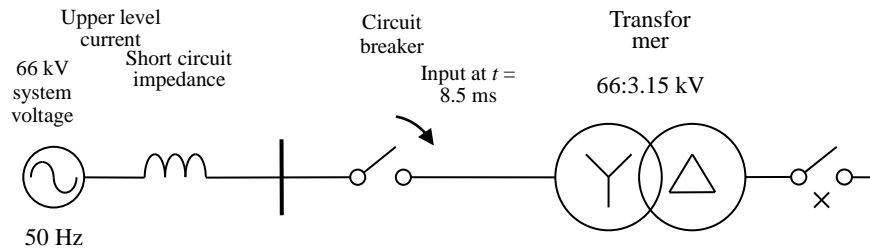


Figure 1 Single line connection diagram of analysis circuit

### [Circuit Operation]

The relationship between the voltage  $v$  applied to the transformer and the magnetic flux  $\phi$  generated in the transformer core is given by

$$v = \frac{d\phi}{dt} \Rightarrow \phi = \int_0^t v(\tau) d\tau$$

Therefore, the average value of the vibration of the magnetic flux does not become zero unless the voltage phase at the time of application is  $90^\circ$ . In particular, when the voltage phase at the time of application is close to  $0^\circ$ , the magnetic flux vibrates at the rated amplitude around the rated peak value.

The maximum magnetic flux reaches approximately 2 pu. Owing to this excessive magnetic flux, the operating point on the current-flux curve (the  $i - \phi$  curve) of the iron core enters the saturation region, resulting in an excessive current flow, which is called an excitation inrush current.

In the circuit in Figure 1, the initial phase of phase a of the system voltage is set to  $0^\circ$  and the circuit breaker is switched on at time of  $t = 8.5$  ms. In other words, the initial phase is not  $90^\circ$  in any of the phases a, b, or c, and hence an excitation inrush current is generated.

### [Simulation of the 66-kV System]

The 66-kV system is simulated using a voltage source generating 66 kV and the short-circuit impedance of the upper system. The value of the short-circuit impedance is investigated in the following document:

“Current Status and the Corresponding Technology of Power Quality in the Distribution System,”  
Electric Technology Research Association, Vol. 60, No. 2, March 2005.

Over 210 bus bars were examined in this document, and the average value of the short-circuit impedance observed from the 6.6 kV bus was found to be  $j0.0353 \Omega$ , and hence this value was adopted for a short circuit. When this value is converted into the value of each phase on the 66-kV side, it becomes 6.49 mH.

[Transformer Simulation]

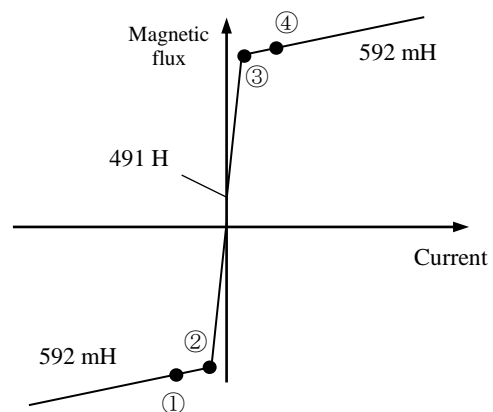
To calculate the inrush current with high accuracy, it is necessary to consider the shape and build of the iron core and winding of the transformer. However, with regard to the excitation impedance portion of the basic equivalent circuit of the transformer (simulating the turn ratio with an ideal transformer, taking into account the winding resistance and leakage inductance excitation impedance), there is also a simpler method for expressing the saturation of the iron core by simulating the excitation inductance with a nonlinear inductance, which is the method adopted in this example.

Because the analyzed transformer has a Y - Δ connection, the XTAP three-phase two-turn transformer component “Y - D (leakage mH/external excitation)” has been used. This is a component in which three sets of basic equivalent circuits of the transformer excluding the excitation impedance are connected in a Y - Δ configuration and the excitation impedance can be connected from the outside. The parameter values are as follows:

- Primary side line voltage = 66 kV
- Secondary side line voltage = 3.15 kV
- Primary side leakage impedance winding resistance = 6.68 Ω      Leakage inductance = 337 mH
- Secondary side leakage impedance winding resistance = 0.04 Ω      Leakage inductance = 16.1 mH
- The capacitance-to-ground value is set in accordance with the fault value

The excitation impedance is described next. The excitation impedance in each phase is a parallel connection of the excitation resistance of 319 kΩ and a nonlinear inductance having the following characteristics. At up to 1.2-times the rated magnetic flux, the nonlinear inductance is 491 H. When this value is exceeded, it reaches the saturation level of the polygonal line of 592 mH (air-core inductance), which is specified by the next current-flux curve ( $i - \phi$  curve).

	Current [A]	Magnetic flux [Wb]
①	-1.0	-206.1
②	-0.4192	-205.8
③	0.4192	205.8
④	1.0	206.1



In XTAP, when specifying the nonlinear characteristics of the parts based on polygonal lines, the characteristics outside the specified range are calculated through a linear extrapolation.

#### [Analysis Conditions]

The analysis conditions are as follows.

- Calculation step time: 0.1 ms
- Calculation end time: 200 ms
- Display start time: 0 ms
- Display end time: 200 ms

#### [Example of XTAP Input]

Figure 2 shows an illustration of executing this example in XTAP

### Analysis Results

The results when executing this example using XTAP are shown in Figure 2. The results appear to be in good agreement with the actual measurement results shown in the literature, except for certain differences from not having considered the initial magnetic flux (residual magnetic flux). For the sake of reference, the b-phase flux waveform (obtained by integrating the b-phase voltage using XPLT) is shown in Figure 3(c). The average value of the vibration of the magnetic flux does not become zero owing to the voltage phase at the time of charging.

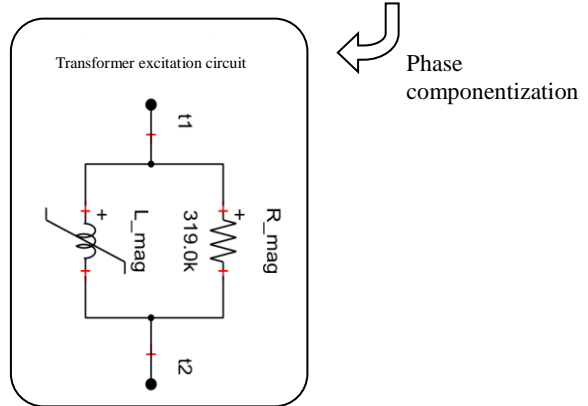
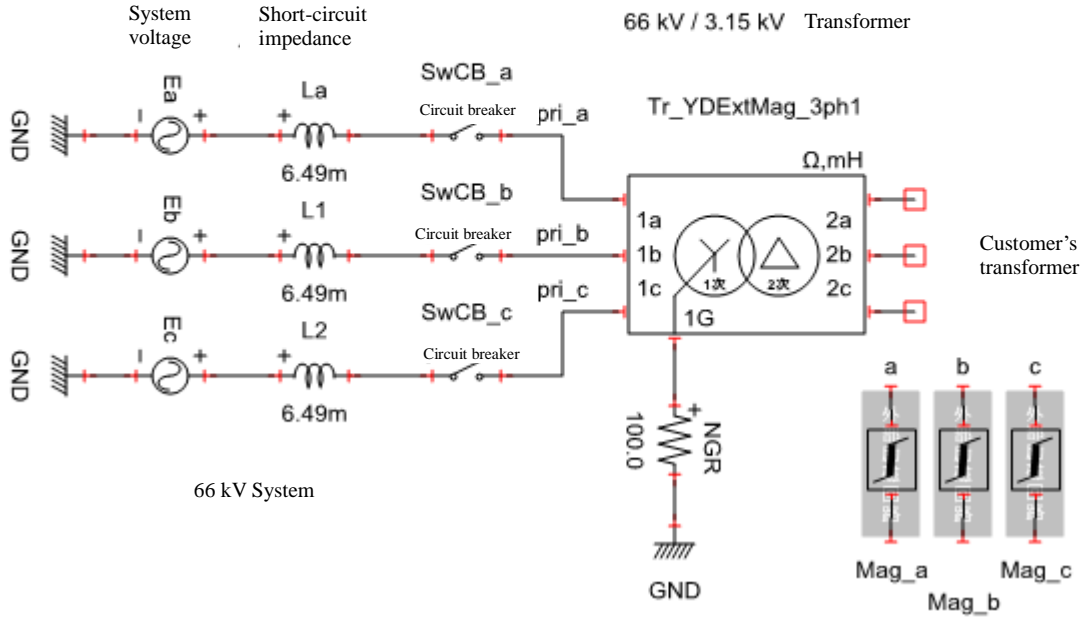
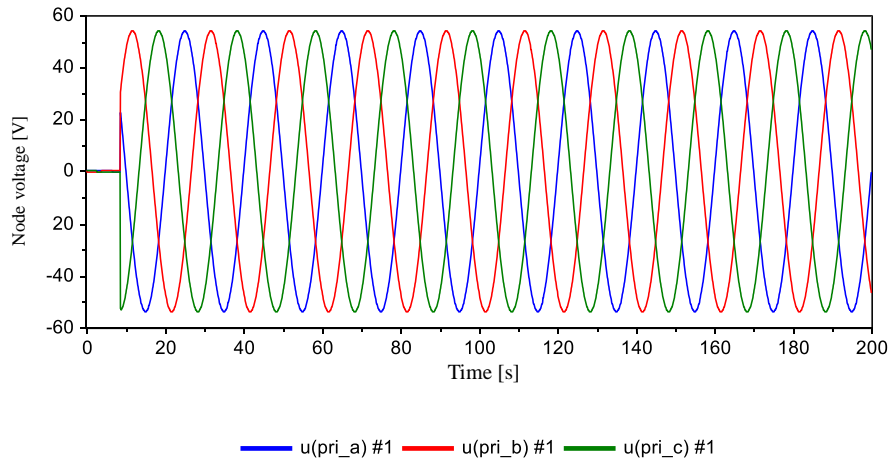
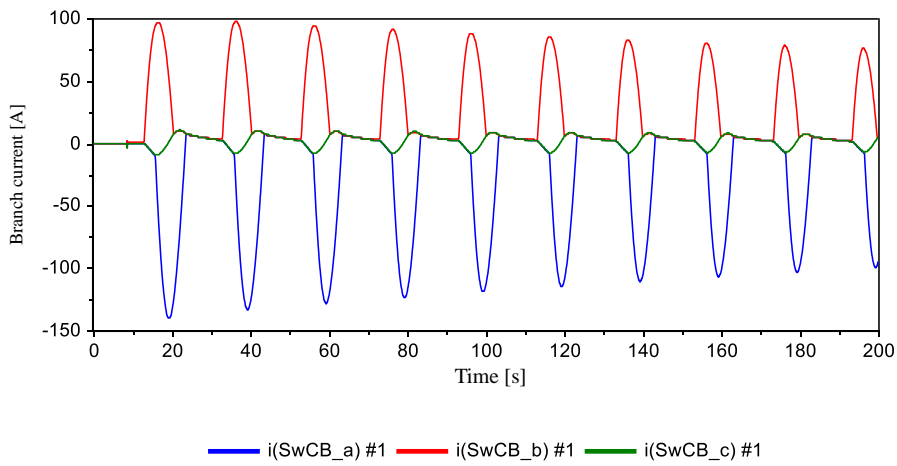


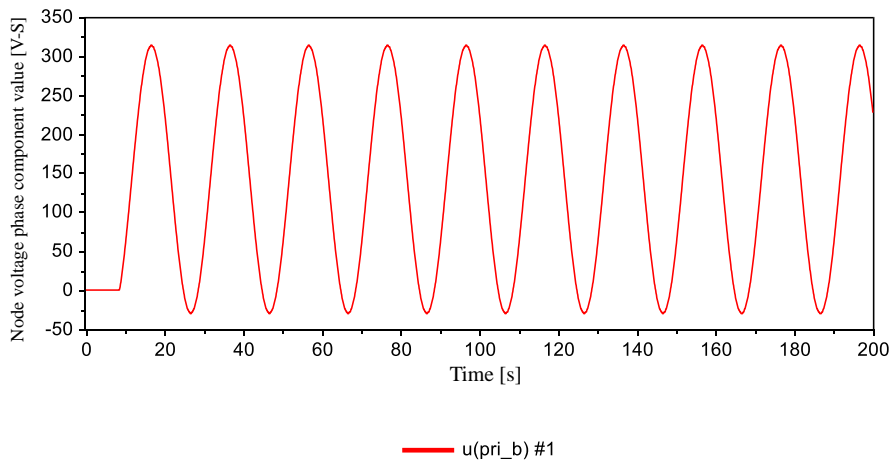
Figure 2 Example of XTAP input



(a) Primary side voltage of transformer



(b) Excitation inrush current



(c) b-phase magnetic flux waveform

Figure 3 Analysis result

End

Change log		
Date	Example file Version	Content changes
2017/12/14	2.1	Change of example file name from PQ-02 to PQ-02-A
2014/11/19	2.0	Modified for XTAP Version 2.00
2013/05/10	1.3	Change in graph of the b-phase magnetic flux waveform in Figure 3(c) for analysis results consequent to the modification of the integral calculation of XPLT
2012/07/19	1.2	Modified for XTAP Version 1.20
2011/10/18	1.1	Modified for XTAP Version 1.11
2010/09/02	1.0	First edition created (for XTAP Version 1.10)

Examples of XTAP		No.	RELAY-01
Example Name	Distance Relay Modeling		
Field	Power system protection		
References	Y. Ohoura, "Protection relay system engineering," the Institute of Electrical Engineers of Japan		
Overview	<p>In the field of protection relays, studies on the settings and co-operative judgments are usually conducted through an effective value analysis. However, in complicated faults involving nonlinear phenomena such as a CT saturation, or in the relay response analysis of faults in complex systems such as congested systems, an instantaneous value analysis has been found to be more useful.</p> <p>To conduct a relay response analysis using XTAP, it is necessary to create a relay model for an instantaneous value analysis. In this example, we introduce a widely used distance relay modeling method.</p>		

## 1. Application History of Protection Relays

Table 1 shows the protection relay system that is commonly used for protecting a transmission line of 66 kV or more, and for protecting the bus. The PCM current differential relay method is generally used as the main protection for the transmission line, and the distance relay method is used as backup protection.

Table 1 Protection relay system

Protection purpose		Direct grounding system	Resistive grounding system
Transmission line protection	Main protection	PCM current differential relay system	PCM current differential relay system Line selection relay system (Parallel 2 wire)
	Backup protection	Distance relay system	Distance relay system
Bus bar protection (double bus configuration)		Current differential relay system (collective) + current differential relay system (divided) Current differential relay system (collective) + current differential relay system (divided)	

## 2. Distinction between Effective and Instantaneous Value Analyses

In the analysis of protection relays, it is important to distinguish between an effective value analysis, which applies a transient stability analysis of the entire system, and an instantaneous value analysis, in which the voltage and current waveforms of a part of the system are analyzed and a simulation is carried out. An effective value analysis is useful when analyzing large-scale systems and in settings with many parameters to consider or in cooperative examinations. However, it is unsuitable for the simulation of complex faults involving a phase dependency and nonlinear phenomena. An instantaneous value analysis permits the relay response analysis of complex faults with nonlinear phenomena such as a CT saturation, and the analysis of faults in complex systems such as congested systems. However, it is unsuitable for an analysis involving large-scale systems or multiple parameters.

## 3. Distance Relay

Distance relays are widely used as back-up protection of transmission lines of over 66 kV (in the case of resistive grounding, however, a ground fault direction relay or a ground fault over voltage relay is used as the ground fault protection).

A typical example of a distance relay is described

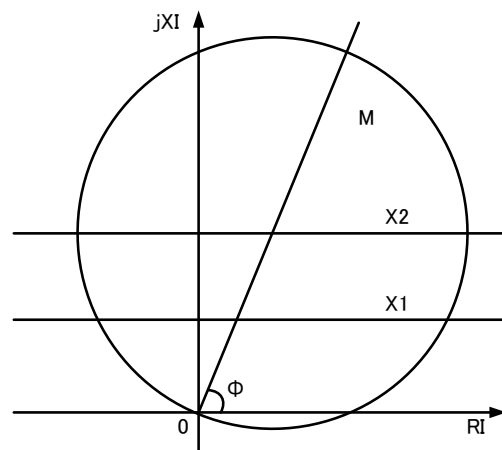


Figure 1 Conceptual diagram of distance relay

with reference to Figure 1. Distance relays have large Mho and reactance characteristics, in which the mho characteristic functions as a direction element and the reactance characteristic functions as a section selection element. The distance relay can detect a fault only through its own voltage and current input and is characterized based on features such as a relatively reliable selection of the fault section and an easy time coordination owing to the timed cutoff at each step according to the protection section.

## 4. Relay Modeling

### 4.1 Modeling Method

There are two main methods of relay modeling. The first is a method of directly computing a vector-type principle formula using the inner product or phase shift (direct operation) (often indicated by a vector-type principle formula). The second is a method of computing using sampling data in the same way as the actual machine (sampling operation). In the case of a sampling operation, it is essential to accurately know the relay algorithm, without which the data modeling cannot be conducted. In the case of a direct operation, modeling can be conducted if the vector type principle formula is known. The features of both methods are shown in Table 2.

The modeling method of a direct operation is introduced in the present example because it is relatively easy and can be carried out without resorting to relay algorithms or constants of the analog filter.

Table 2 Comparison of direct operation and sampling operation

	Direct operation	Sampling operation
Operation method	<ul style="list-style-type: none"> <li>Method of directly calculating inner product of vector type principle formula and amplitude.</li> </ul>	<ul style="list-style-type: none"> <li>Computing method using sampling values in the same way as actual relays</li> </ul>
Features	<ul style="list-style-type: none"> <li>Can be constructed based on the principle formula (the principle formula is common regardless of the algorithm applied)</li> <li>Separately set when considering operation time</li> </ul>	<ul style="list-style-type: none"> <li>Simulate actual relay</li> <li>Operating time characteristics similar to actual relays</li> <li>All information from analog filter to relay algorithm is essential</li> <li>Diverse filter compositions and relay algorithms</li> </ul>

## 4.2 Modeling Example of Basic Relay Operation

The modeling of most protection relays can be achieved by combining three basic relay operations, as shown below. An example of the modeling of each relay operation is shown.

- Phase shift operation (PSHIFT)

This operation is implemented using a delay component. An advancement can be achieved by reversing the delay through a curve fitting method (using the property in which the input waveform is a sinusoidal wave). For instance, a forward current of  $75^\circ$  can be achieved by delaying the current by  $105^\circ$  and reversing it (multiplying by -1).

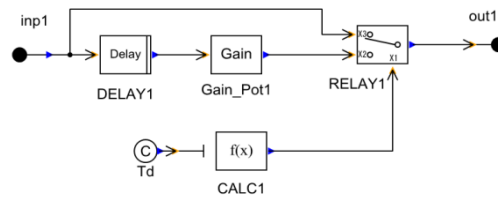


Figure 2 Phase shift operation

- Amplitude calculation

The amplitude is calculated using the moving average. Increasing the data window length generates a calculation delay to the same extent.

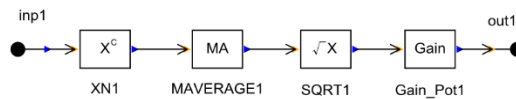


Figure 3 Amplitude calculation

- Phase difference calculation (inner product)

Each vector is decomposed into its components (x and y components), and the inner product is calculated.

$$x \cdot y = x_1y_1 + x_2y_2$$

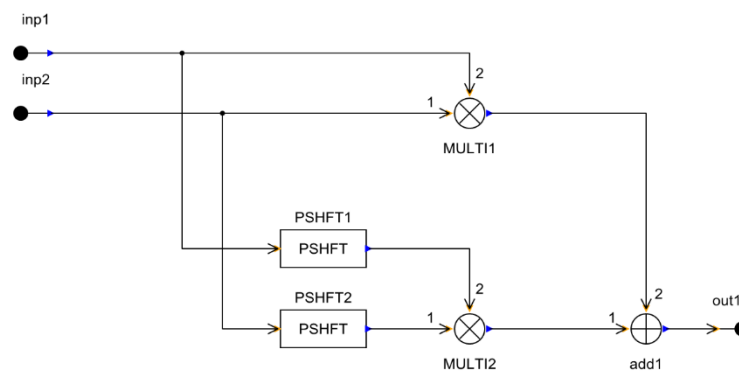


Figure 4 Phase difference calculation

### 4.3 Example of Distance Relay Modeling

The modeling of the relay shown below is obtained by combining the relay calculations described above.

- Mho relay principle for short-circuit protection

$$(Z_S \dot{I}_{ab} \exp(j\phi) - \dot{V}_{ab}) \cdot \dot{V}_{ab} > 0$$

$$Z_S \dot{I}_{ab} \exp(j\phi) \cdot \dot{V}_{ab} - \dot{V}_{ab} \cdot \dot{V}_{ab} > 0 \quad (\text{Note that } \cdot \text{ indicates the inner product})$$

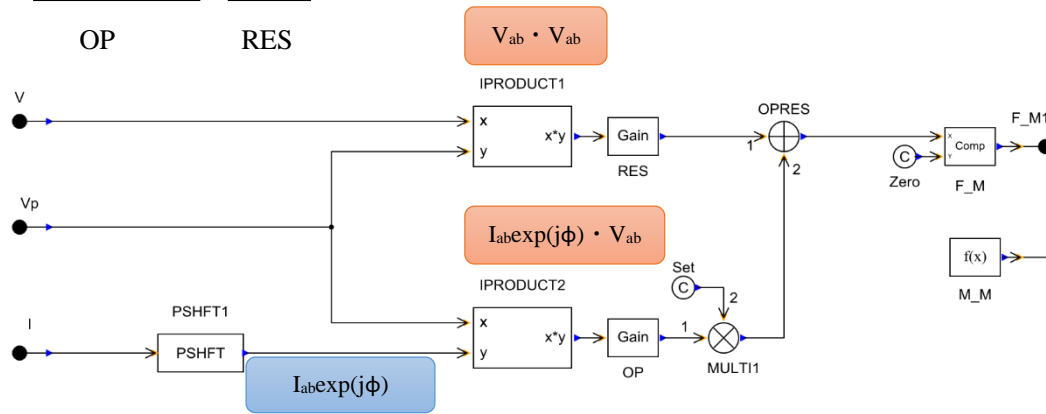


Figure 5 Modeling of Mho elements

- Reactance relay principle for short-circuit protection

$$(Z_S \dot{I}_{ab} \exp(j\phi) - \dot{V}_{ab}) \cdot \dot{I}_{ab} \exp(j\phi) > 0$$

$$Z_S \dot{I}_{ab} \exp(j\phi) \cdot \dot{I}_{ab} \exp(j\phi) - \dot{V}_{ab} \cdot \dot{I}_{ab} \exp(j\phi) > 0$$

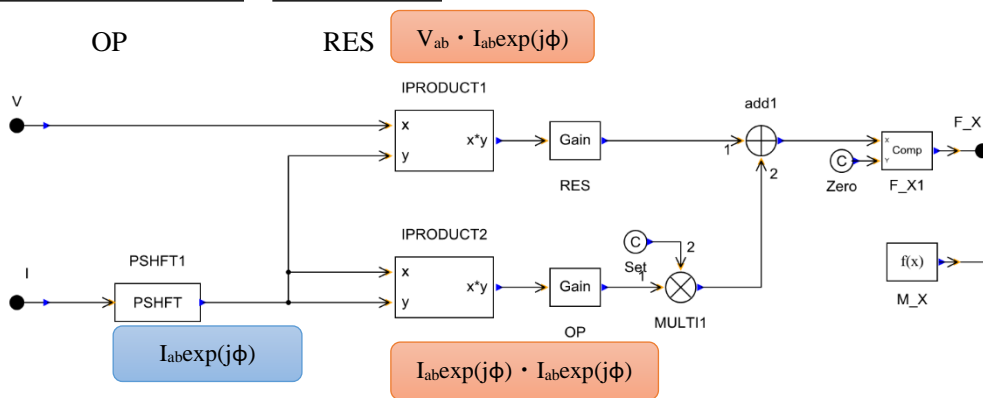


Figure 6 Modeling of reactance elements

## 5. Simulation

### [Objective]

To ascertain the responses of the distance relay (Mho relay and reactance relay) for short-circuit protection during internal and external faults.

### [Analysis conditions]

The analysis conditions are as follows.

- Calculation time step: 1 ms
- Calculation start time: 0 s
- Calculation end time: 0.3 s
- Display start time: 0.1 s
- Display end time: 0.3 s

### [Fault conditions]

- 2LS (Phase ab)
- Internal fault: Fault in the protection section of distance relay step 1
- External fault: Fault outside the protection section

### [Preconditions]

- The distance relay of phase ab is the target
- The current value (the value at the present moment) is used as the polarity voltage of the short-circuiting mode (the memory effect is not taken into account)
- A relay locking mechanism in the small current region is not taken into account
- The simulated range is restricted to a digital filter and relay operation only
- The settling values of the relay are as follows:
  - 44X1:  $1.097 \Omega$  [80% of the normal phase reactance (approximately  $1.367 \Omega$  in secondary side conversion value) of the self-protection section]
  - 44 M:  $4.101 \Omega$  [300% of normal phase reactance of self-protection section]
- A timer is not attached, and the operation is instantaneous.

However, relay calculations (window length required for a phase shift or other factor) take the necessary amount of time.

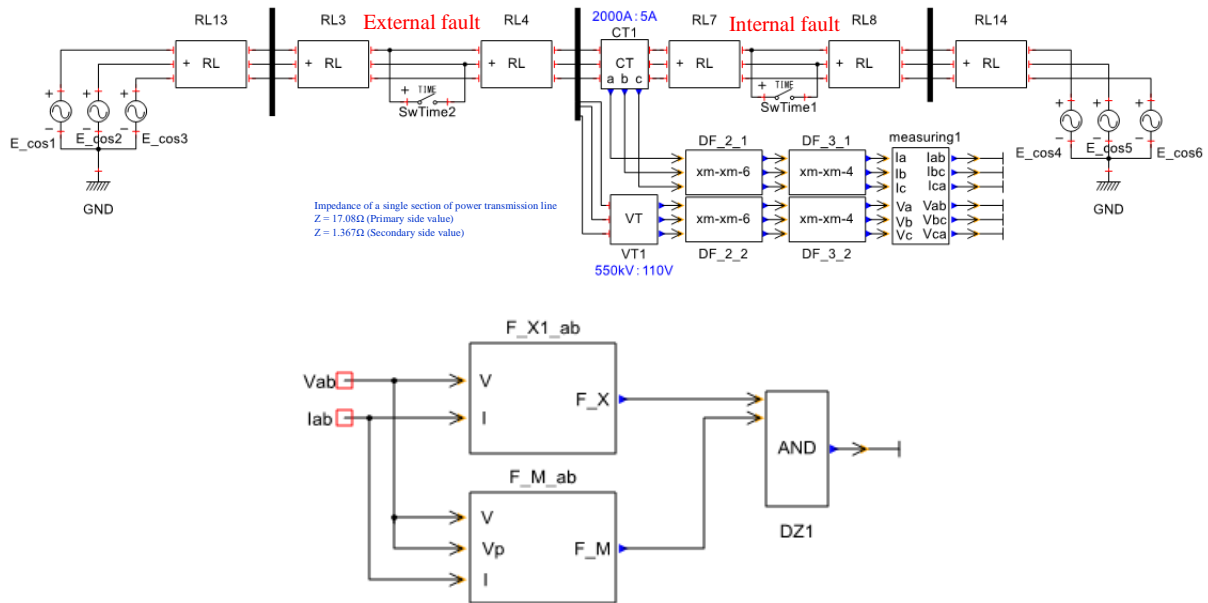


Figure 7 Analysis circuit and relay sequence

[Analysis Results]

Table 3 shows the results of the “observed relay impedance ( $Z_{RY}$ )” and “relay operation judgment” for distance relay step 1. The results of the observed impedance of the Mho relay ( $F\_M\_ab / M\_M$ ) and the observed impedance of the reactance relay ( $F\_X\ 1\_ab / M\_X$ ) are shown for the “observed relay impedance ( $Z_{RY}$ ).” The distance relay operates when the observed impedance seen from this relay exceeds the set value.

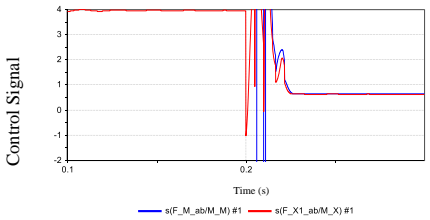
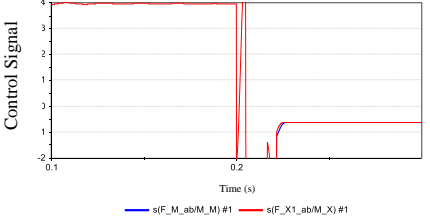
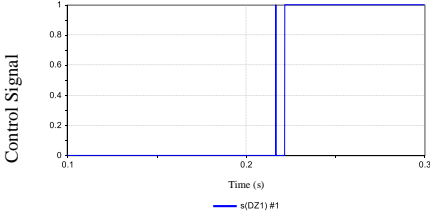
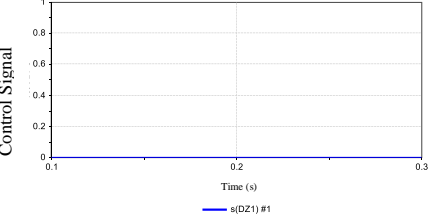
The result of the observed impedance of the relay shows a slight difference between the behaviors of the impedance of the Mho relay and the reactance relay. This is because their respective principle formulas, and in particular their maximum sensitivity angles, differ.

In the case of an internal fault, the impedance falls below the set value of the reactance relay (forward reach of  $1.097\ \Omega$ ) and is within the set value of the Mho relay (forward reach of  $4.101\ \Omega$ , and backward reach of  $0\ \Omega$ ), and hence it may be inferred that the distance relay is in operation. In contrast, in the case of an external fault, the impedance is lower than the set value of the reactance relay and the direction characteristic, namely, the Mho relay, falls outside the set value (facing the rear side) and hence it may be concluded that the relay is not in operation.

However, there is a delay from the occurrence of a fault to the relay operation, and it must be understood that this is the window length owing to the relay operation.

It is evident from these results that the distance relay is operative in the case of an internal fault and becomes inoperative in the event of an external fault, thus confirming that it is operating normally.

Table: Analysis results

	Internal fault	External fault
$Z_{RY}$		
Operati on flag		

End

Change log		
Date	Example file version	Content changes
2015/05/29	1.0	First edition created (for XTAP Version 2.01)

Examples of XTAP		No.	RELAY-02
Example Name	Coordinated Study of the Fault Current Interrupting Arcing Horn and Transmission Line Protection Relay		
Field	Overhead power transmission, line protection		
Literature	<ul style="list-style-type: none"> <li>● Otaka, Kameda, “Coordination between Fault Current Interrupting Arcing Horn and Transmission Line Protection Relay,” Central Research Institute of Electric Power Research Report H10009, May 2011</li> <li>● Otaka, Iwata, Tanaka, Goda, Central Research Institute of Electric Power Industry Report H06007, May 2007 “Development of Current Breaking Simulation Model for Fault Current Interrupting Arcing Horn (Part 2): Development and Application of Arc Conductance-Dependent Model”</li> <li>● Otaka, Iwata, Tanaka, Goda, Tada, Tomonaga, Uemura, Central Research Institute of Electric Power Industry Report H 05013, June 2006, “Development of Current Breaking Simulation Model of Fault Current Interrupting Arcing Horn: Construction of a Basic Arcing Model”</li> </ul>		
Overview	<p>The fault current interrupting arcing horn (referred to hereafter as AH) is a lightning protection device that instantly interrupts a fault current caused by a lightning strike and plays a significant role in the reduction of a power failure and instantaneous voltage drop. The short-circuit current interrupting type AH for 66/77-kV overhead power transmission lines is capable of interrupting fault currents of up to 10 kA within a single AC cycle. Typically, if the fault current is interrupted by an AH, there will be no need for a transmission line protection relay (Ry hereafter) to shut off the transmission line by opening the circuit breaker. However, it has been seen that Ry detects a failure and shuts off the transmission line even when the fault current has been interrupted by an AH.</p> <p>The present example analyzes the operations of an AH and Ry using the parameters of the fault occurrence point (distance from the relay installation point) and the AH current interruption time (0.5 cycles or one cycle), and aids their coordinated study to avoid the duplication of interruptions using an AH and Ry.</p>		

## Analysis Circuit and Conditions

Figure 1 shows the single-line diagram of the model system. The model is a 50 Hz, 66-kV system with a power source at one end, and the transmission line is assumed to be an ACSR 520 mm<sup>2</sup> cable, with a span length of 20 km. The back impedance is 12.1 mH and the fault current is 10 kA when a 3LG ground fault occurs at the nearest end of the substation (equivalent to the maximum interruption current of the AH). The neutral point of the transformer substation is grounded through a resistor (NGR) with a capacitance of 200 A.

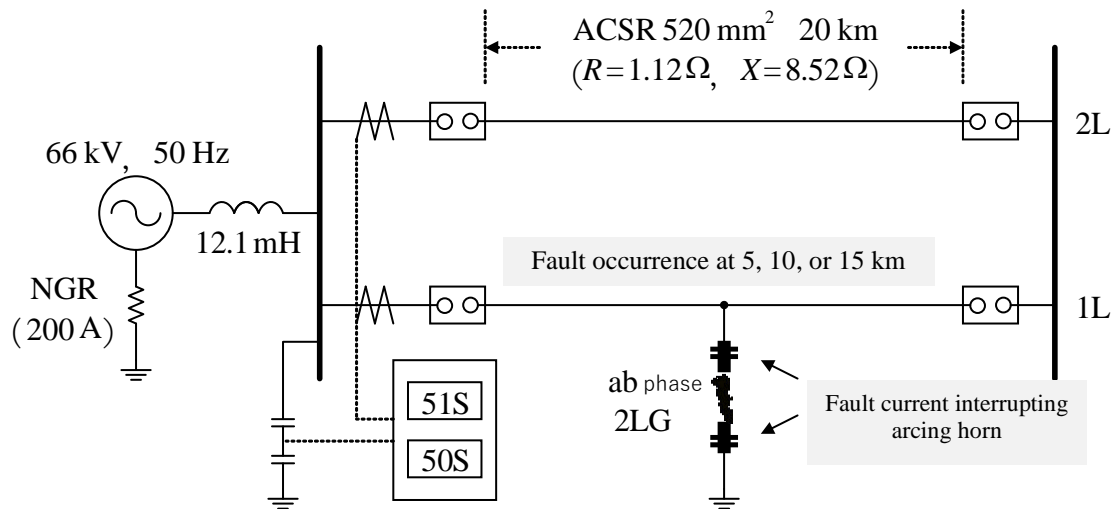


Figure 1 Single-line diagram of the model system

### [Analyzed Phenomenon]

Protection relays of a self-end judgment type are often installed for short-circuit/ground faults in the transmission line protection of a 66/77-kV system without back-up protection. In general, the fault detection time of Ry is faster for short-circuit faults, and a short-circuit relay is perhaps the only one that comes close to the current interruption time of an AH. Hence, the Ry studied in this example has two types of short-circuit relays applied for the main protection, namely, an overcurrent relay (51 S) and a distance relay (44 S).

The fault is assumed to be a 2 LG fault in the ab phase, its point of occurrence to be 5, 10 or 15 km from the relay installation point, and the AH current interruption time to be either 0.5 cycles or one cycle. The reason why an AH interrupts a fault current at 0.5 cycles in certain cases and at one cycle in other cases is due to the variations in the fault conditions (fault current, fault phase) and the surrounding environment (weather, equipment type).

The behavior of an AH and Ry at the time of a fault occurrence is analyzed based on these conditions.

[Fault Current Interrupting Arcing Horn Model]

We developed an AH current interrupting simulation model for the short-circuit current interruption of the 66/77-kV system using the current–voltage waveform obtained through a short-circuit current interruption test, the details of which are provided in the studies above.

This model combines the Cassie [1] and Mayr [2] models, which have been conventionally used as macroscopic arc models of circuit breakers, and is capable of accurately simulating the arc conductance generated between the arc horns from the time of a fault occurrence to the time of its removal.

Although an AH has variations in the current interruption time, as mentioned above, with XTAP, it is easier to consider the coordination with Ry if the zero point of the fault current interruption is clearly specified. For this reason, in the current interrupting simulation model of an AH, it has been made possible to select the first or second zero point for the occurrence of the fault current interruption. In specific terms, the Cassie model is used at the zero point at which the current needs to be continued, and the Mayr model is used only at the zero point where it is desirable to interrupt the current. An overview of the Cassie and Mayr models is provided in [3].

[ Overcurrent Relay Model]

Because the 2 LG current at the line end (20 km point) was 2,670 A, the value of 4,330 A, which is the value of the phase current of 2,500 A converted into a line current,  $(2,500 \times \sqrt{3})$ , was taken as the settling value of the overcurrent relay. The binary addition method [4] has been applied for an amplitude value calculation, and because this calculation algorithm includes the filter effect, the application of the digital filter operation has been omitted.

- Amplitude value calculation (binary addition method)

$$D_m = |I_m| + |I_{m-3}| + \frac{1}{2} \left| |I_m| - |I_{m-3}| \right| \dots\dots\dots (1)$$

$$D_{51S} = \frac{1}{k_{51S}} (D_m + D_{m-1} + D_{m-2}) \dots\dots\dots (2)$$

Here,  $D_{51S}$  is the calculated value of the overcurrent relay,  $k_{51S}$  is the gain of the amplitude generated in the process of the calculation, and  $I_m = I_{1m} - I_{2m}$  (line current). When  $D_{51S}$  exceeds the set value of 4,330 A, it becomes an Ry operation. The suffix  $m-T$  represents the “time before an electrical angle  $T \times 30^\circ$ .” For example,  $m-1$  represents a delay at an electrical angle of  $30^\circ$ , and  $m-3$  represents a delay at an electrical angle of  $90^\circ$ . The analog filter was not taken into consideration, and the confirmation time of the failure continuity confirmation counter was set to an electrical angle of  $60^\circ$ .

[ Distance Flow Relay Model]

To prevent the operation of a distance relay in response to a fault beyond the protected section owing to

an instrument transformer or an analog error of the relay itself, the protection range within which the main protection can be instantly cut off is set to approximately 80% of the entire protection section [5]. Hence, in the present example, the point at 80% of the distance from the relay installation point (distance of 16 km) was set as the protection range, and  $0.8 X = 6.81 \Omega$  was set as the settling value. Based on the actual commonly used relays that we have tested thus far, a product operation with a maximum sensitivity angle of  $75^\circ$  [4] was used for the amplitude value, and the differential filter [4] was used for the digital filter calculation.

- Amplitude value calculation (product operation with a maximum sensitivity angle of  $75^\circ$ )

$$D_{44S} = \frac{1}{k_{44S}} \frac{V_m^2 + V_{m-3}^2}{(I_m + I_{m-1})V_{m-3} - (I_{m-3} + I_{m-4})V_m} \dots\dots\dots (3)$$

- Digital filter calculation (differential filter)  $y_m = \frac{1}{2}(x_m - x_{m-6})$  (4)

Here,  $D_{44S}$  is the calculated value of the distance relay,  $k_{44S}$  is the gain of the amplitude value generated during the calculation,  $I_m = I_{1m} - I_{2m}$  (line current), and  $V_m = V_{1m} - V_{2m}$  (line voltage). When  $D_{44S}$  falls below the settling value of 6.81, it becomes an Ry operation. In addition,  $x_m$  is the input value of the digital filter, and  $v_m$  is the output value of the digital filter. An analog filter was not taken into consideration, and the confirmation time of the failure continuity confirmation counter was set to an electrical angle of  $60^\circ$ .

[Simulation of Transmission Lines]

The transmission line was an ACSR 520 mm<sup>2</sup> cable, with a span length of 20 km. For the sake of simplicity, the “ $\pi$ -type equivalent circuit line model” was used in this study.

[Analysis Conditions]

The analysis conditions are as follows.

- Calculation timestep: 0.1  $\mu$ s
- Calculation start time: 0 ms
- Calculation end time: 50 ms
- Display start time: 0 ms
- Display end time: 50 ms

The fault occurrence time and current interruption time can be specified by double-clicking on the AH part, and the system frequency and setting value can be specified by double-clicking on the Ry (51S, 44S) part.

[Example of XTAP Input]

The creation of this example using XTAP is illustrated in Figure 2. Because only 1L is used for the overcurrent relays and distance relays, a 2L simulation is omitted. AH and Ry (51 S, 44 S) were componentized, and the detailed models can be browsed by editing the component diagrams.

Example name: Coordinated study of the fault current interrupting arcing horn and transmission line protection relay

No: Relay-02 XTAB Example: Ver2.00, Example file: Ver 1.0

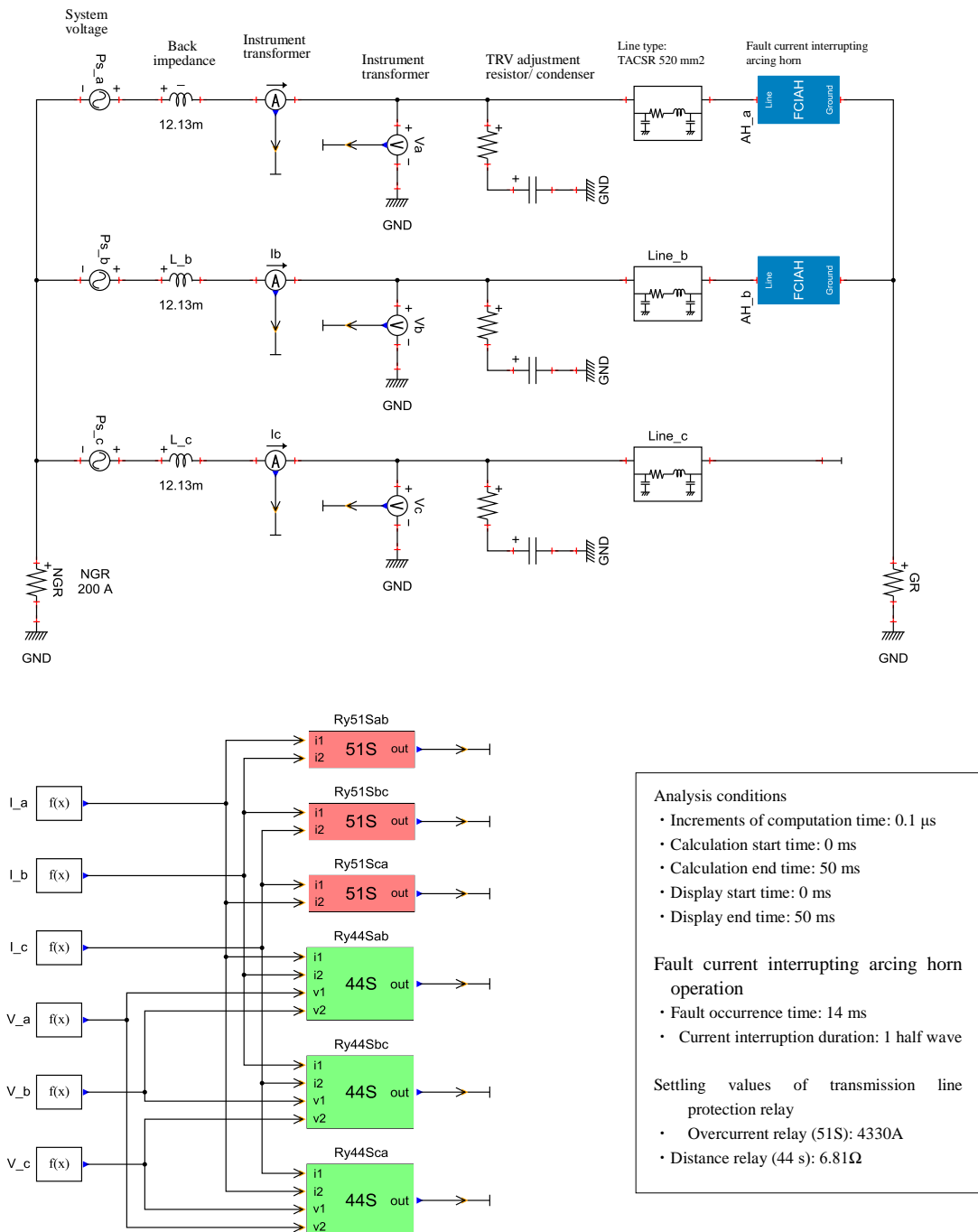


Figure 2 Example of XTAP input

## Analysis Results

The analysis results for the case in which the fault occurrence point is 10 km from the relay installation point and the AH current interruption time is set to 0.5 cycles and one cycle are shown here.

The first result is the case in which the AH current interruption time is set to 0.5 cycles. Figure 3 shows the current waveform, Figure 4 shows the voltage waveform, Figure 5 shows the 51S calculated value, Figure 6 shows the 51S output, Figure 7 shows the 44S calculated value, and Figure 8 shows the 44S output.

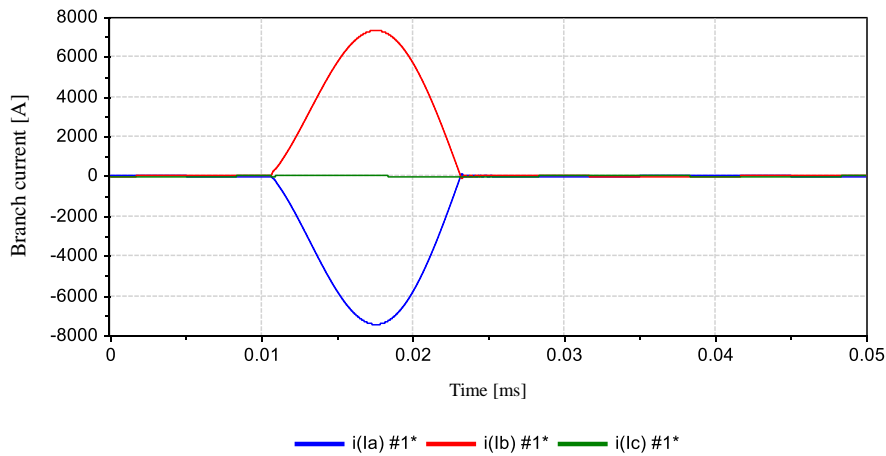


Figure 3 Current waveform at 0.5 cycle interruption

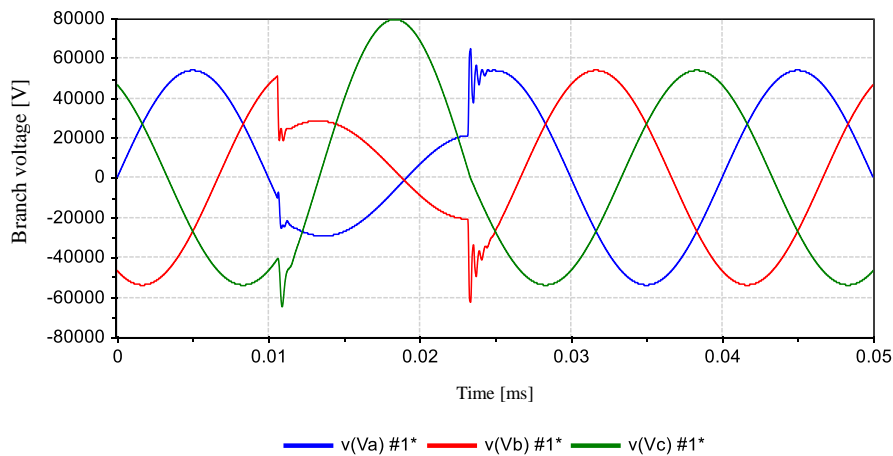


Figure 4 Voltage waveform at 0.5 cycle interruption

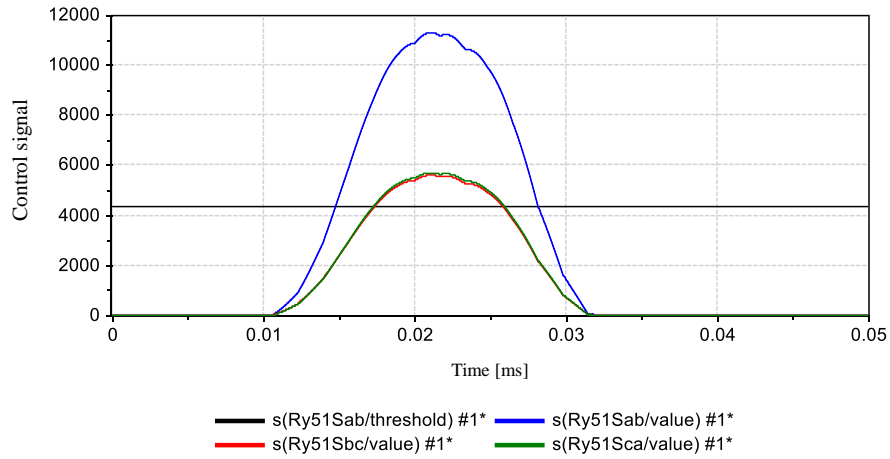


Figure 5 51S calculation value at 0.5 cycle interruption (the black line is the settling value)

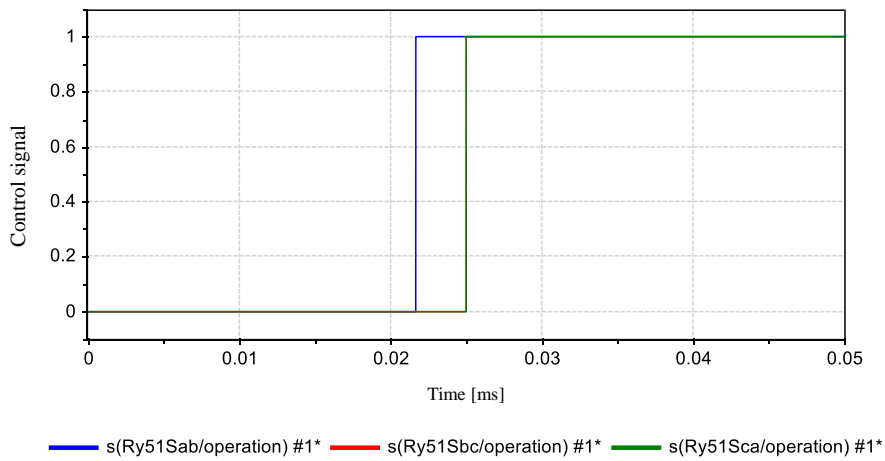


Figure 6 51S output at 0.5 cycle interruption

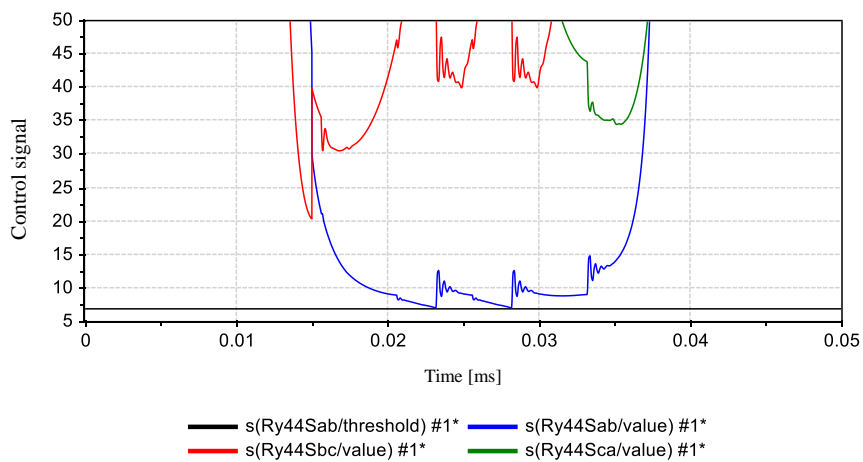


Figure 7 Calculated value of 44S at 0.5 cycle interruption (the black line is the settling value)

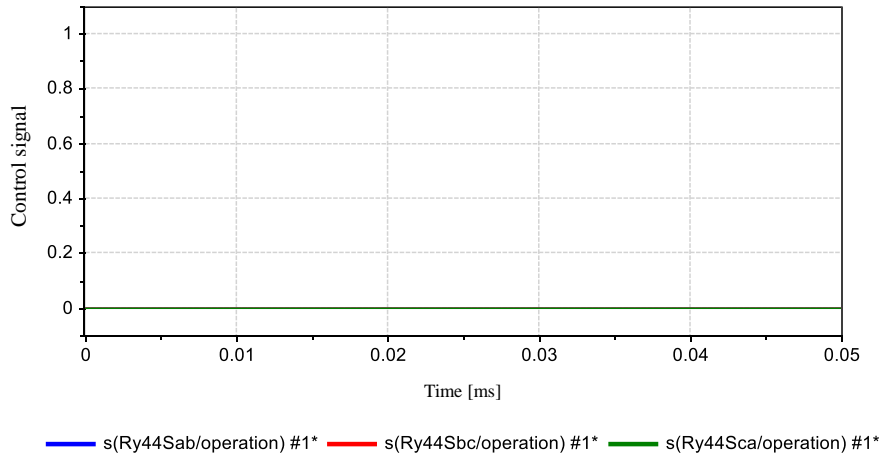


Figure 8 44S output at 0.5 cycle interruption

As can be seen from Figures 5 and 6, the calculated values of ab, bc, and ca phases for the overcurrent relay exceeded the settling value, resulting in an Ry operation. In contrast, Figures 7 and 8 show that, although the calculated value of the ab phase is momentarily below the settling value of the distance relay, it does not exceed the electrical angle of  $60^\circ$ , which is the confirmation time of the fault continuity check counter, and hence Ry does not operate.

Next, we look at a case in which the AH current interruption time is one cycle. Figure 9 shows the current waveform, and Figures 10–14 show the voltage waveform, 51S calculated values, 51S output, 44S calculated values, and 44S output, respectively.

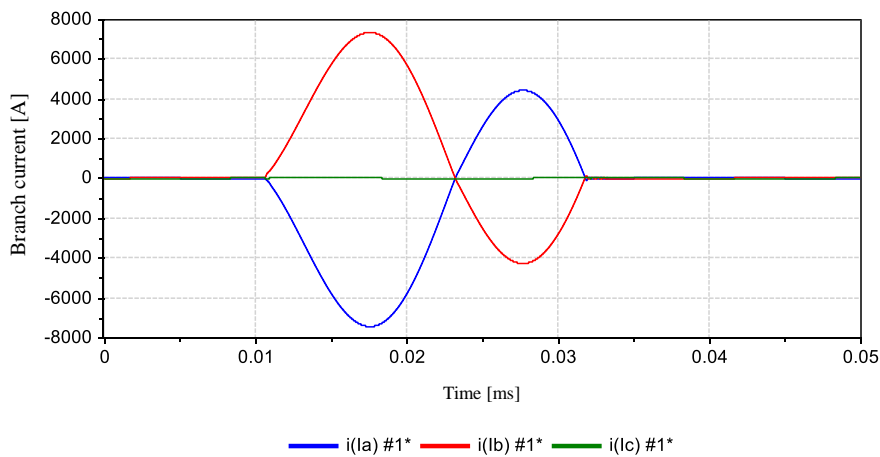


Figure 9 Current waveform at one cycle interruption

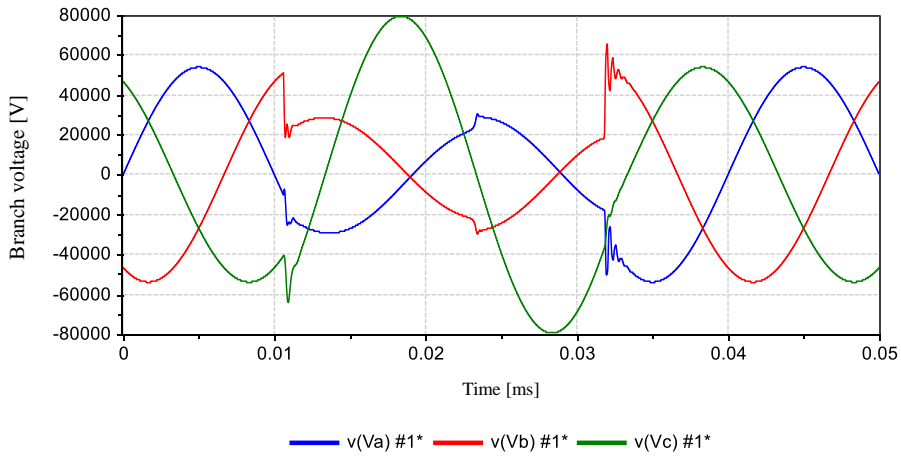


Figure 10 Voltage waveform at one cycle interruption

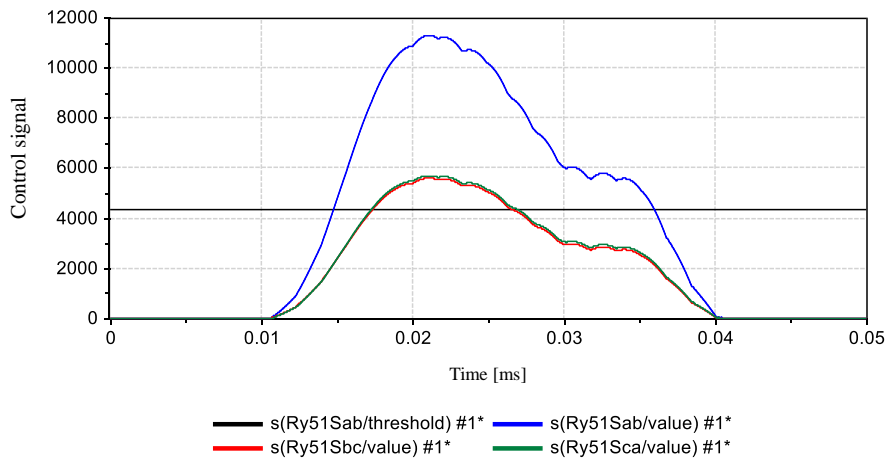


Figure 11 51S calculation value at one cycle interruption (the black line is the settling value)

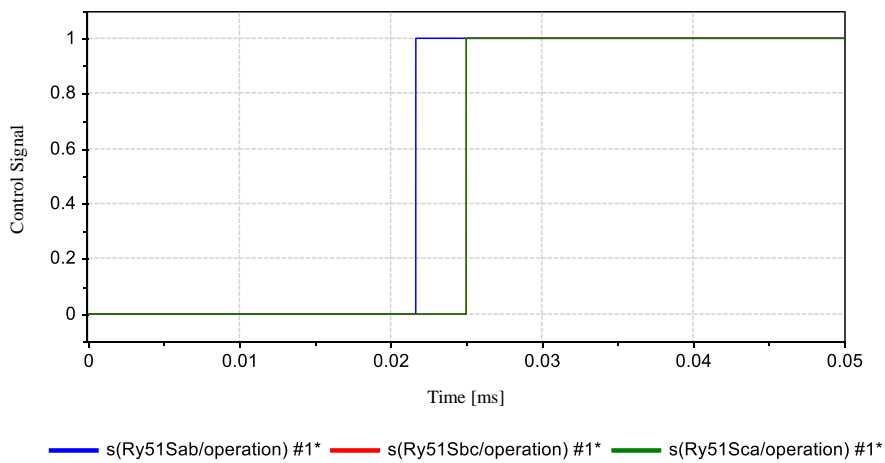


Figure 12 51S output at one cycle interruption

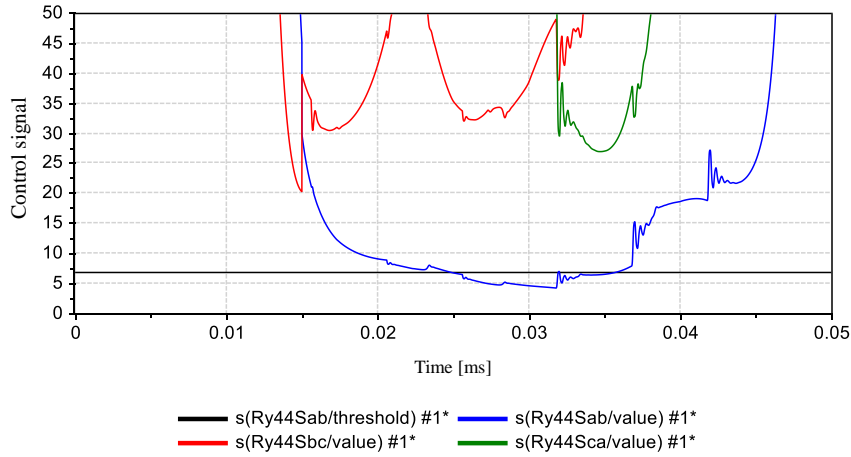


Figure 13 Calculated value of 44S at one cycle interruption (the black line is the settling value)

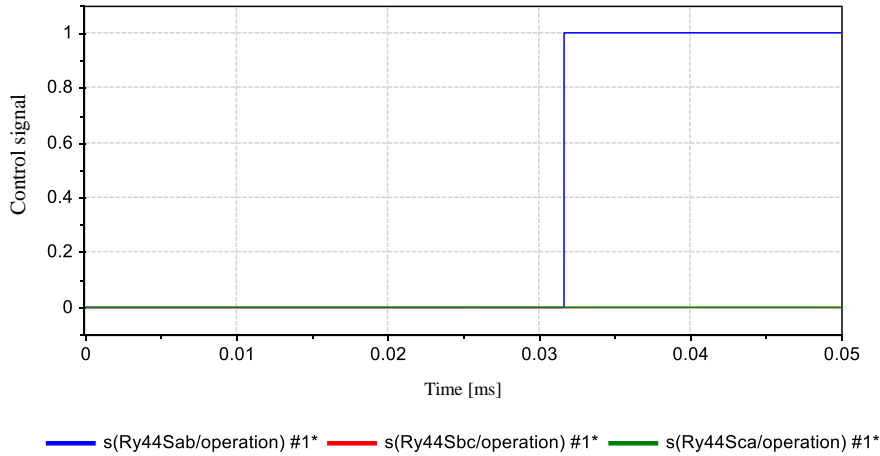


Figure 14 44S output at one cycle interruption

It can be seen from Figures 11 and 12 that, just as in the case of the 0.5 cycle interruption, the calculated values of the ab, bc, and ca phases for the overcurrent relay exceeded the settling value, resulting in an Ry operation. Figures 7 and 8 show that, although the calculated value of the ab phase is below the setting value of the distance relay, it does not exceed the electrical angle of  $60^\circ$ , which is the confirmation time of the fault continuity check counter, and hence Ry does not operate.

The needless Ry operations, including their occurrence when the fault occurrence point is set at 5 or 15 km from the relay installation point, are classified and shown in Table 1. In the table,  $\circ$  indicates that a needless operation has not occurred, whereas  $\times$  indicates the occurrence of a needless operation.

Table 1 Occurrence of needless operation of transmission line protection relay

Fault point	AH current interruption time	Needless operation of 51S relay				Needless operation of 44S relay			
		ab Phase	bc Phase	ca Phase	Total	ab Phase	bc Phase	ca Phase	Total
5 km	0.5 cycles	×	×	×	×	×	○	○	×
	1 cycle	×	×	×	×	×	○	○	×
10 km	0.5 cycles	×	×	×	×	○	○	○	○
	1 cycle	×	×	×	×	×	○	○	×
15 km	0.5 cycles	×	○	○	×	○	○	○	○
	1 cycle	×	○	○	×	○	○	○	○

From Table 1, it can be seen that, as a whole, the overcurrent relay tends to operate more than the distance relay. Moreover, if the fault occurrence point is close to the relay installation point, a needless Ry operation is liable to occur when the current interruption time of the fault current interrupting arcing horn is extended from 0.5 cycles to one cycle.

However, even if a coordinated operation using an Ry may be difficult to achieve, installing an AH is extremely effective as a countermeasure against lightning damage to an overhead transmission system because it helps reduce the equipment damage owing to the continuous current arc at the location of the fault occurrence. We anticipate the widespread use of an AH in the future.

## References

- [1] A. M. Cassie, "Arc Rupture and Circuit Severity: A New Theory," CIGRE Report, No.102 (1939)
- [2] O. Mayr, "Beiträge zur Theorie des statischen und des dynamischen Lichtbogen," Archiv für Electrotechnik, Vol. 37, pp. 588-608 (1943)
- [3] Institute of Electrical Engineers of Japan, "Handbook of Electrical Engineering (7th Edition)," Ohmsha Ltd., pp. 886-887 (2013)
- [4] Protection relay system of Basic Technical Investigation Committee: "Protection Relay System Basic System Technology," Technical Report of The Institute of Electrical Engineers of Japan, No. 641 (1997)
- [5] Ohoura: "Protection Relay System Engineering," Ohmsha Ltd., pp. 174-175 (2002)

End

Change log		
Date	Example file version	Content changes
2015/07/01	1.0	First edition created (for XTAP Version 2.01)

XTAP Examples		No.	MAC-01-A
<b>Example Name</b>	Synchronous Generator (Single-Line 3 LG-O Fault and Constant Excitation Occurring in a Single-Machine Infinite Bus System)		
<b>Field</b>	Power system applications		
<b>Literature</b>	<p>Because this example was created for this training course, there are no references.</p> <p>※ For the modeling and system characteristics of synchronous generators, refer to textbooks on electrical equipment and electric power systems engineering such as the following:</p> <ul style="list-style-type: none"> <li>• Technical Report No. 798 of the Institute of Electrical Engineers of Japan, “Application technology of synchronous machine constants,”</li> <li>• N. Akira, “Application of Power System Technology Calculation,” Denkishoin Ltd.,</li> <li>• C. Concordia, “Synchronous Machine Theory and Performance,” John Wiley and Sons, Inc.</li> </ul>		
<b>Overview</b>	<p>The target system of the analysis is a single-machine infinite bus system connected with one synchronous generator and an infinite bus by two parallel transmission lines.</p> <p>This example simulates the phenomenon of the occurrence of a three-phase ground fault in one of the lines of a parallel two-line transmission, which is eliminated through the operation of circuit breakers at both ends of the line, and analyzes the dynamic characteristics of the synchronous generator. The field voltage of the synchronous generator is assumed to remain constant.</p>		

## Analysis Circuit and Conditions

A single-line diagram of the analyzed system is shown in Figure 1. The figures in normal font in the diagram indicate the value of the impedance, and those in italics indicate the value of the specified flow condition.

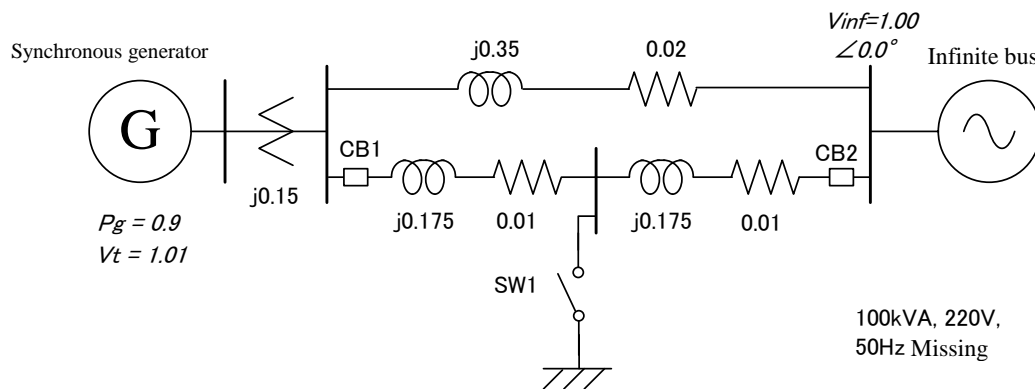


Figure 1 Analyzed system

### [Analysis Phenomenon]

In the model system shown in Figure 1, SW1 is closed at 0.5 s to generate a three-phase ground fault, and the fault is eliminated by opening CB1 and CB2 at 0.57 s.

The field voltage of the synchronous generator is set to a constant value (gain G2 of the AVR block is set to zero).

The machine input  $T_m$  is assumed to be given by  $T_m = T_{m0}/\omega$  with an initial value of  $T_{m0}$  and an angular velocity of  $\omega$ .

### [Synchronous Generator Model]

The synchronous generator model was constructed based on the Park equation. The rotor circuit consists of two axes, a d axis and a q axis. The saturation of the air-gap flux was not taken into consideration.

The generator constants used in this example are shown in Table 1. During the analysis, the circuit constants of the generator model (resistance and reactance values) are automatically calculated from the generator constant and assigned to the circuit elements.

During the steady state initialization of this example, the node to which the synchronous generator is connected is designated as PV, and the initial power flow on the system side is first calculated. The initial value of the internal variable of the generator is then automatically calculated to satisfy the various amounts of generator buses and set as the circuit element.

Table 1 Generator constants

Item	Value
Unit inertial constant [s]	$M = 8.05$
Synchronous reactance [pu]	$X_d = 1.86, X_q = 1.35$
Transient reactance [pu]	$X_d' = 0.44$
Initial transient reactance [pu]	$X_d'' = X_q'' = 0.37$
Transient time constant of short circuit [s]	$T_d' = 0.733$
Transient time constant of initial short circuit [s]	$T_d'' = T_q'' = 0.048$
Armature time constant [s]	$T_a = 0.29$
Armature leakage reactance [pu]	$X_L = 0.25$

[Circuit Elements Other than Synchronous Generator Model]

A sine wave power supply is used to simulate the infinite bus voltage. For simplicity, the transmission line was simulated by connecting the linear resistance and linear inductance in-series, and a linear inductance was used in the transformer.

[Analysis Conditions]

The analysis conditions are as follows:

	Overall	For an enlarged view of the instantaneous value
• Calculation time step	100 $\mu$ s	Same as the value on the left
• Calculation start time	0 s	Same as the value on the left
• Calculation end time	10 s	0.70 s
• Display start time	0 s	0.45 s
• Display end time	10 s	0.70 s
• Output frequency	10	1

[Example of XTAP Input]

An illustration showing the creation of the model system of Figure 1 using XTAP is indicated in Figures 2 and 3.

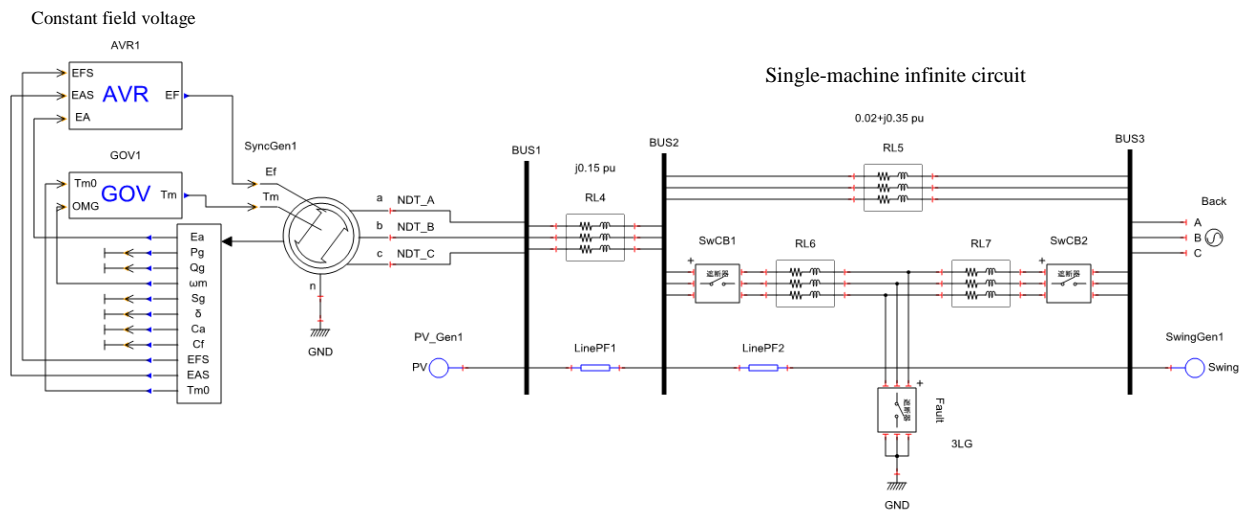
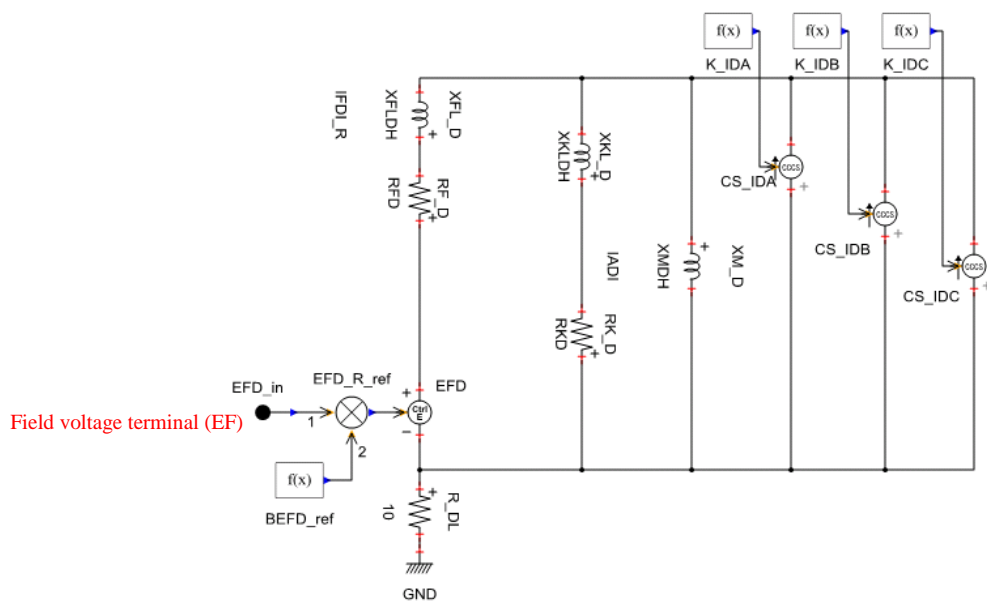
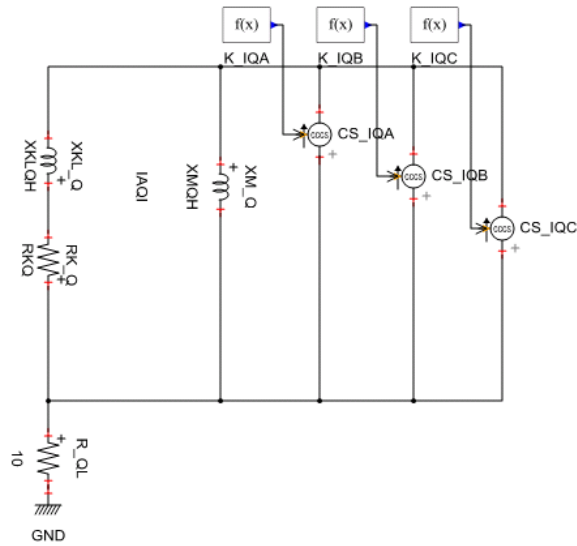


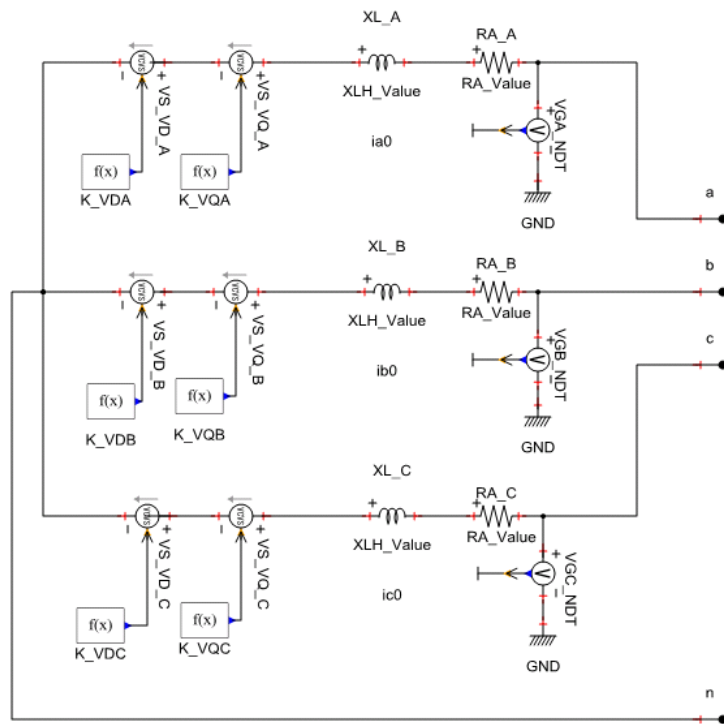
Figure 2 Model system created in XTAP



(a) d-axis circuit



(b) q-axis circuit



(c) Armature circuit

Figure 3 Synchronous generator model

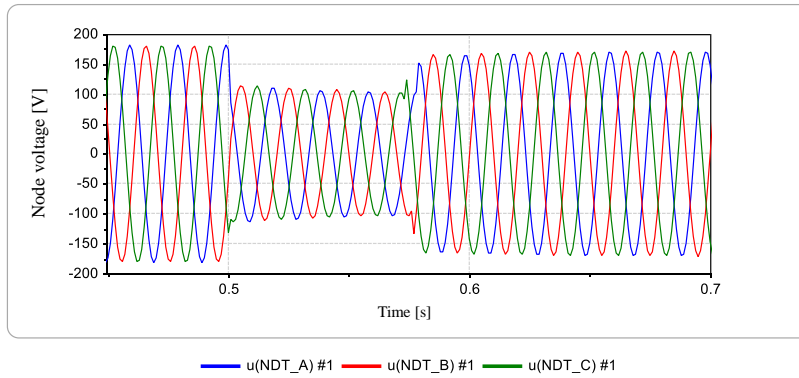
## Analysis Results

The results of executing this example using XTAP are shown in Figure 4.

Figure 4(a) shows the three-phase instantaneous waveform of the generator terminal voltage. The terminal voltage drops during a 3LG fault. Figure 4(b) shows the three-phase instantaneous waveform of the generator armature current. The transient DC component is superimposed over the fundamental wave AC component. Figures 4(c) and 4(d) show the instantaneous active and reactive powers calculated using an  $\alpha - \beta$  conversion. Owing to the influence of the transient DC component of the armature current, the vibration is superimposed immediately after the 3LG-O fault. In this case, the transient DC component is attenuated by several hundred milliseconds. Figure 4(e) shows the effective value of the terminal voltage, and Figure 4(f) shows the field voltage. Because the field voltage is kept constant in this example, when the system condition changes owing to a single open line, the terminal voltage drops instead of being maintained at 1.0 pu. Figure 4(g) shows the internal phase angle. Owing to the single open line, the impedance of the system increases, leading to a large internal phase angle.

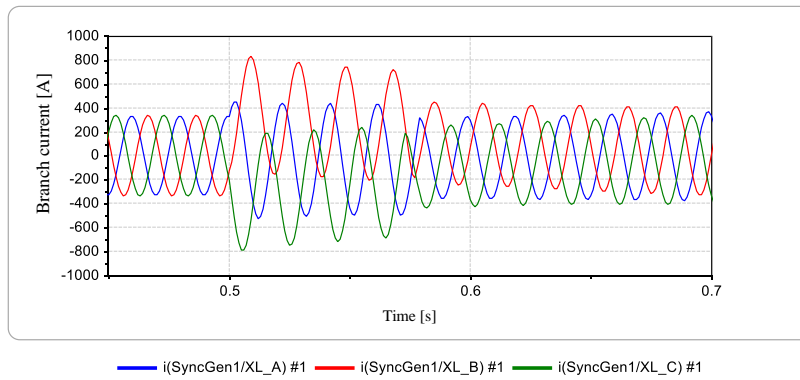
In addition, a back-swing phenomenon is observed in the speed deviation of the rotor of the generator (Figure 4 (h)). The relationship between the mechanical torque input and the electromagnetic torque output at this time is shown in Figure 4(i). The electromagnetic torque output fluctuates owing to the transient DC component, and as this torque remains greater than the mechanical torque input, the generator rotor decelerates.

MAC-01-A



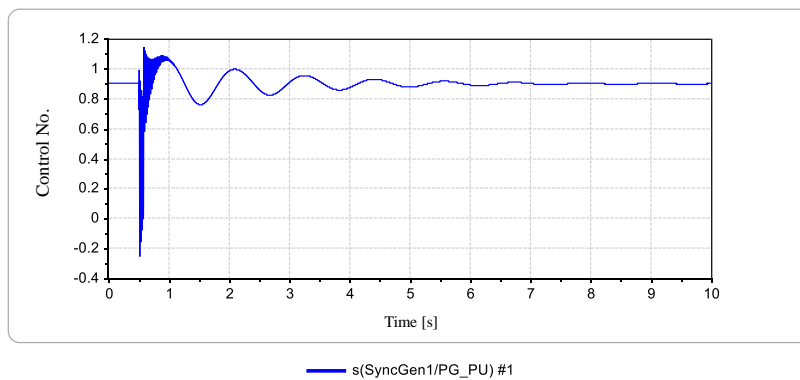
(a) Terminal voltage [V]

MAC-01-A



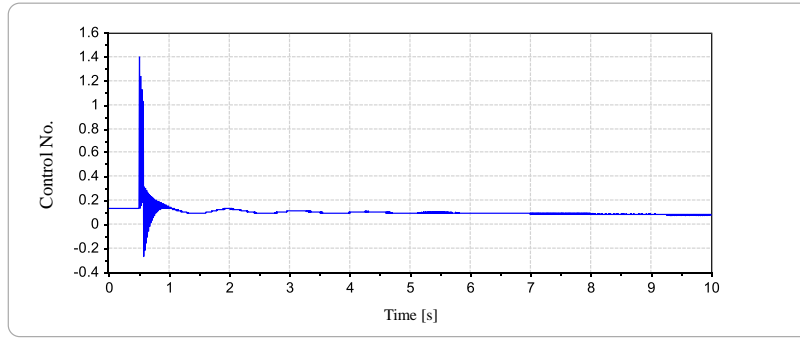
(b) Armature current [A]

MAC-01-A



(c) Active power [pu]

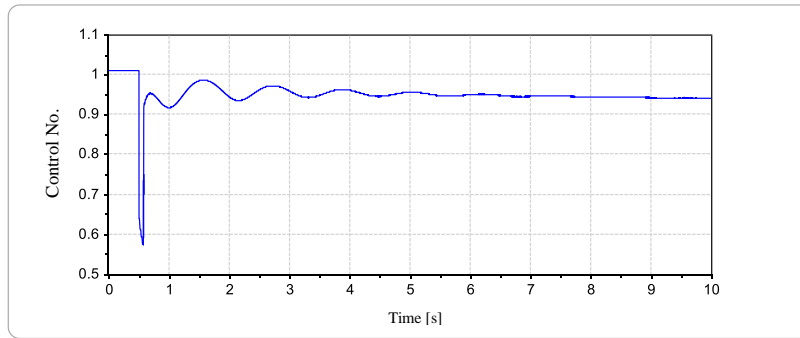
MAC-01-A



s(SyncGen1/QG\_PU) #1

(d) Reactive power [pu]

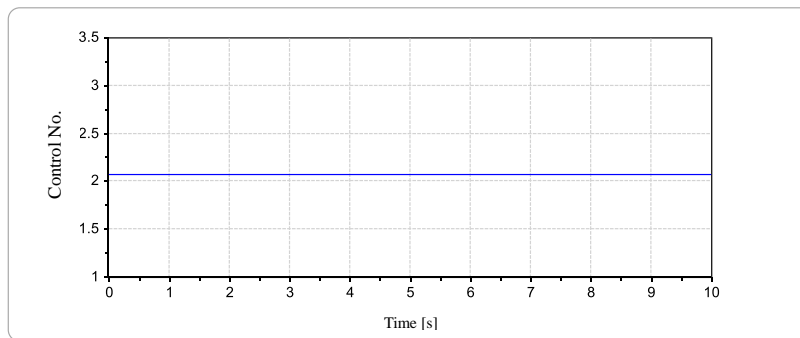
MAC-01-A



s(SyncGen1/EA\_PU) #1

(e) Effective value of terminal voltage [pu]

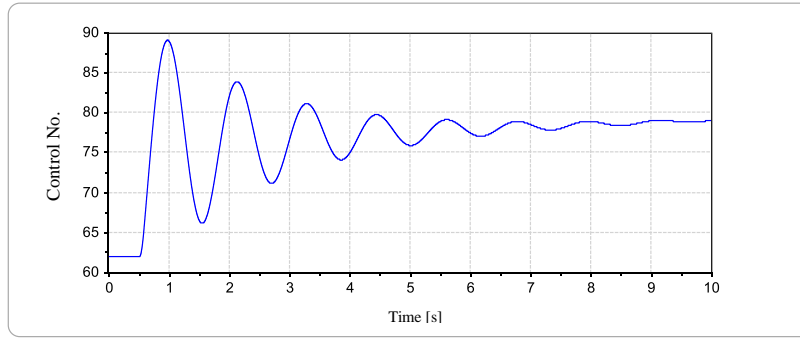
MAC-01-A



s(SyncGen1/EFD\_S) #1

(f) Field voltage [pu]

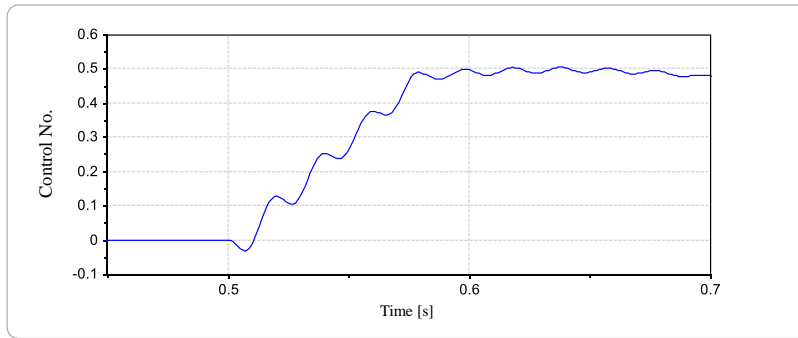
MAC-01-A



s(SyncGen1/AG\_DEG) #1

(g) Internal phase angle [deg.]

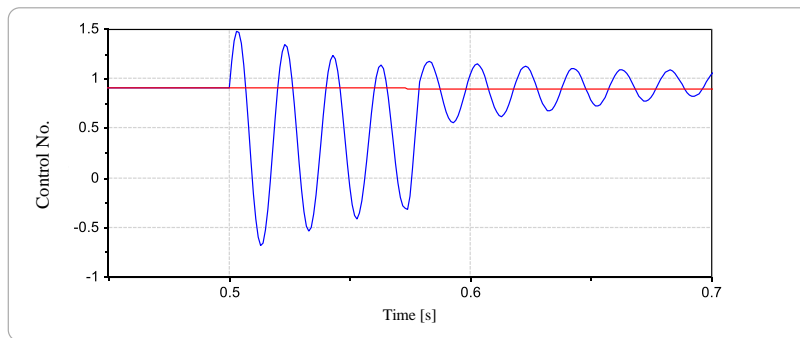
MAC-01-A



s(SyncGen1/SG\_PER) #1

(h) Speed deviation [%]

MAC-01-A



s(SyncGen1/TG) #1 s(SyncGen1/TM) #1

(i) Mechanical and magnetic torque [pu]

Figure 4 Analysis results using XTAP

## [Output Variables]

As a reference for creating a graph, the output variables set in the synchronous machine model of this example are summarized below.

◆ Node voltage	
• v(Sync_Gen1/VGA_NDT)	Terminal voltage [V]
◆ Branch current	
• i(Sync_Gen1/XFL_D)	Field current [puA]
• i(Sync_Gen1/XL_A)	Armature current [A]
◆ Branch voltage	
• v(Sync_Gen1/EFD)	Field voltage [puV]
◆ Control system	
• s(AVR1/EF_out)	AVR Block output [puV]
• s(AVR1/EFS_in)	Field voltage initial value [puV]
• s(GOV1/TM_GOV)	GOV Block output [puV]
• s(Sync_Gen1/AG_DEG)	Internal phase angle [deg]
• s(Sync_Gen1/CA_PU)	Armature current (Rms value) [pu]
• s(Sync_Gen1/CK_PU)	Braking current [pu]
• s(Sync_Gen1/EA_PU)	Terminal voltage (Rms value) [pu]
• s(Sync_Gen1/EFD_S)	Field voltage [pu]
• s(Sync_Gen1/IMD_S)	D-axis mutual reactance current [pu]
• s(Sync_Gen1/IMQ_S)	D-axis mutual reactance current [pu]
• s(Sync_Gen1/IG_D)	D-axis current [pu]
• s(Sync_Gen1/IFD_S)	Field current [pu]
• s(Sync_Gen1/IKD_S)	D-axis damper current [pu]
• s(Sync_Gen1/IKQ_S)	Q-axis damper current [pu]
• s(Sync_Gen1/IG_Q)	Q-axis current [pu]
• s(Sync_Gen1/PG)	Active component of electrical output [W]
• s(Sync_Gen1/PG_PU)	Active component of electrical output [pu]
• s(Sync_Gen1/QG)	Reactive component of electrical output [Var]
• s(Sync_Gen1/QG_PU)	Reactive component of electrical output [pu]
• s(Sync_Gen1/SG_PER)	Speed deviation [%]
• s(Sync_Gen1/TG)	Electromagnetic torque [pu]
• s(Sync_Gen1/TM)	Mechanical torque [pu]
• s(Sync_Gen1/V_NDT)	Terminal voltage (Rms value) [V]

End

Change log		
Date	Example file version	Content changes
2014/11/19	2.0	Modified for XTAP Version 2.00 Reconnection of PV designated generator bus parts consequent to the change in parts
2013/04/19	1.3	Change of fault occurrence time by improving the initial calculation value
2012/07/19	1.2	Modified for XTAP Version 1.20
2011/10/18	1.1	Modified for XTAP Version 1.11
2010/07/16	1.0	First edition created (for XTAP Version 1.10)

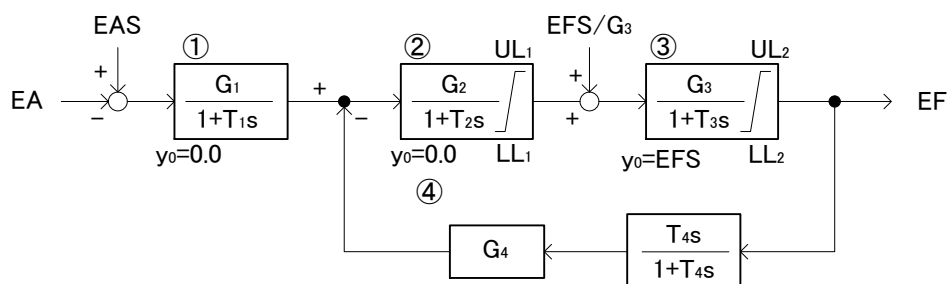
XTAP Examples		No.	MAC-01-B
<b>Example Name</b>	Synchronous Generator (Single-Line 3 LG-O Fault Occurring in a Single-Machine Infinite Bus System with AVR)		
<b>Field</b>	Power system applications		
<b>Literature</b>	<p>Because this example was created specifically for this training course, there are no references.</p> <p>※ For the modeling and system characteristics of synchronous generators, refer to textbooks on electrical equipment and electric power systems engineering. Example reference materials are provided in MAC-01-A.</p> <p>AVR was created with reference to the model LAT = 1 of “Power System Dynamics Analysis Program (Y Method).”</p> <ul style="list-style-type: none"> <li>• Technical Report No. 754 of the Institute of Electrical Engineers “Standard Model of Electric Power System,” p. 41</li> </ul>		
<b>Overview</b>	<p>The target system of the analysis is a single-machine infinite bus system connected with a single synchronous generator and an infinite bus using two parallel line transmission lines.</p> <p>This example simulates the occurrence of a three-phase ground fault in one of the lines of a parallel two-line transmission line that is eliminated through the operation of circuit breakers at both ends of the line, and analyzes the dynamic characteristics of the synchronous generator. An automatic voltage regulator (AVR) is used to control the field voltage.</p>		

## Analysis Circuit and Conditions

[Analysis Phenomenon]

An AVR is added to the synchronous generator discussed in the example MAC-01-A. For other analysis conditions, see this example.

An AVR is a device that controls the field voltage in such a way that the terminal voltage remains constant. The AVR block used in this example is shown in Figure 1. An AVR can be applied by setting the gain  $G2$  to  $0.0 \rightarrow 1.0$ .



Example constants:  $G1 = 1.0$ ,  $T1 = 0.0$ ,  $G2 = 1.0$  (using AVR control) or  $0.0$  (constant excitation),  $T2 = 0.2$ ,  
 $UL1 = 100.0$ ,  $LL1 = -100.0$ ,  $G3 = 100.0$ ,  $T3 = 2.0$ ,  $UL2 = 4.0$ ,  $LL2 = 0.0$ ,  $G4 = 0.1$ ,  $T4 = 0.5$   
 ( $G4$  is set to  $0.2$  when LAT of Y method is 1)

Figure 1 AVR block

When using the control system, it is necessary to set the initial value of each block such that the desired initial command value is output. In this example, setting the initial value of block ③ to EFS, and the initial values of blocks ① and ② to zero, makes the initial command equal to EFS. Because the value of EFS is automatically calculated inside the synchronous generator model and output to the measurement terminal of the synchronous generator model, the control system can be connected to this terminal.

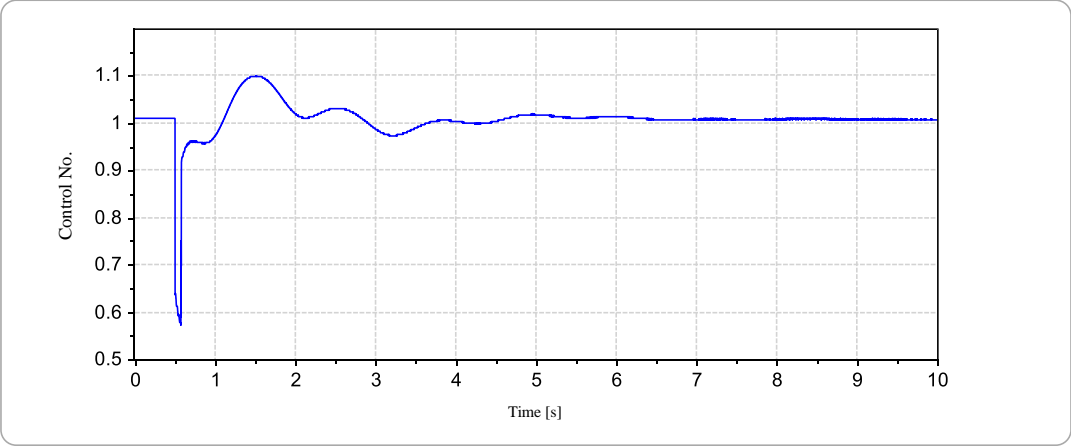
## Analysis Results

The results of executing this example using XTAP are shown in Figure 4.

When compared with the waveform of example MAC-01-A, the field voltage in this example is seen to vary significantly owing to the function of the AVR, and after a 3 LG-O fault, the terminal voltage of the

generator returns to the same value as prior to the fault.

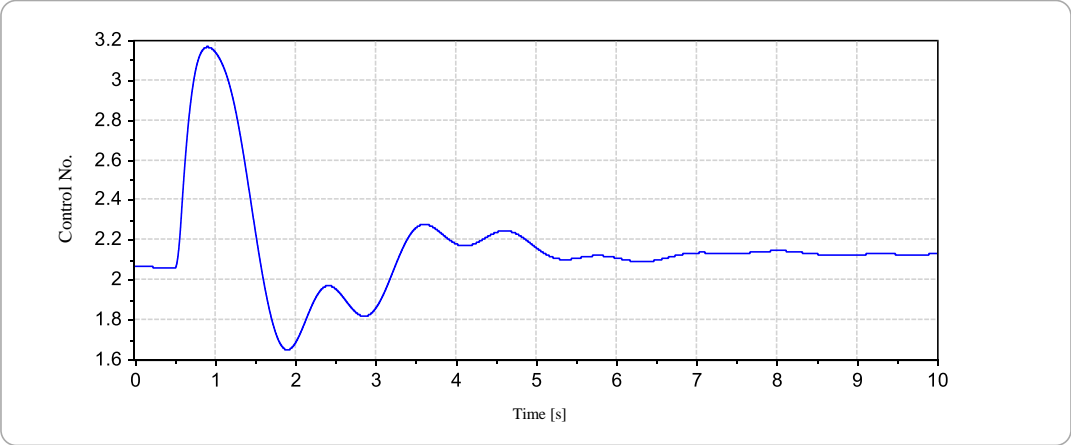
MAC-01-B



s(SyncGen1/EA\_PU) #1

(a) Effective value of terminal voltage

MAC-01-B



s(SyncGen1/EFD\_S) #1

(b) Field voltage

Figure 2 Analysis results using XTAP

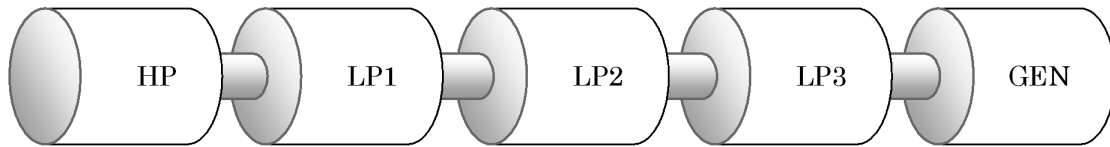
End

Change log		
Date	Example file version	Content changes
2014/11/19	2.0	Modified for XTAP Version 2.00 Reconnection of PV designated generator bus parts consequent to the change of parts
2013/08/21	1.4	Modified AVR diagram of the example title (Figure 1)
2013/04/19	1.3	Change in fault occurrence time by improving initial value calculation
2012/07/19	1.2	Modified for XTAP Version 1.20
2011/10/18	1.1	Modified for XTAP Version 1.11
2010/07/16	1.0	First edition created (for XTAP Version 1.10)

XTAP Examples		No.	MAC-01-C
<b>Example Name</b>	Synchronous Generator (Torsional Torque Simulation)		
<b>Field</b>	Power system applications		
<b>Literature</b>	<p>Because this example was created for this training course, there are no references. The following references are available as examples of the axis system constants. The present example was created with reference to [1].</p> <p>[1] Okamoto et al., "Evaluation of the Effect of Circuit Breaker Opening/Closing Control on Generator/Turbine Shaft System," Document of the Joint Study Group on Electric Power Technology /Electric Power System Technology, PE-99-101, PSE-99-98</p> <p>[2] "First Benchmark Model for Computer Simulation of Subsynchronous Resonance," IEEE Trans. Power Apparatus and Systems, Vol. PAS-96, No. 5, pp. 1565-1572, 1977</p> <p>[3] J.F. Goossens et al, "Full Scale Short Circuit and Other Tests on the Dynamic Torsional Response of Rodenhuize NR 4-300 MW – 3000 RPM Turbogenerator Part II," IEEE Trans. PAS, Vol. PAS-100, No. 9, pp. 4174-4185, 1981</p>		
<b>Overview</b>	<p>The target system of the analysis is a single-machine infinite bus system, which is connected to one synchronous generator and an infinite bus using two parallel line transmission lines.</p> <p>This example simulates the phenomenon of the occurrence of a three-phase ground fault in one of the lines of a parallel two-line transmission, which is eliminated by the operation of the circuit breakers at both ends of the line, and analyzes the torsional torque of the synchronous generator.</p>		

## Analysis Circuit and Conditions

The shaft configuration and constants of the generator being analyzed are shown in Figure 1.



	High-pressure turbine	Low-pressure turbine 1	Low-pressure turbine 2	Low-pressure turbine 3	Generator
M:	0.37 s	1.69 s	1.83 s	1.71 s	2.65 s
K:		21.4	150.2	112.5	144.1

(shaft stiffness in pu torque/electrical rad)

Figure 1 Shaft configuration and constants

### [Analysis Phenomenon]

The torsional torque at the time of a 3LG-O fault is simulated using the model “Synchronous generator (d1q1, considering torsional torque),” which considers the axis system.

### [Axis System Data]

The axis system data of Figure 1 are input into the synchronous machine model. The input screen is shown in Figure 2.

Turbine1	Turbine2	Turbine3	Turbine4	Turbine5	Turbine6	Generator	Excitation System
0.0	0.0	0.37	1.69	1.83	1.71	2.66	0.0
0.0	0.0	0.35	0.21	0.21	0.23		
0.0	0.0	21.4	150.2	112.5	144.1	0.0	
0.0	0.0	0.0	0.0	0.0	0.0	0.0	0.0
0.0	0.0	0.0	0.0	0.0	0.0	0.0	0.0

Note  
 When you input data, please keep in mind the following:  
 Input data from generator side to turbine side without any blanks.  
 When the turbine is not used, the unit inertia constant input 0.  
 Sharing ratio of output power's total amount must equal 1.  
 When damping effect is ignored, self and mutual damping coefficient input 0.

Figure 2 Shaft data input screen of synchronous generator

[Configuration of the Shaft System Model]

(1) Calculation procedure

The various amounts of the shaft system of the generator are calculated through the following steps.

- ① Calculation of pu conversion and initial value of input constant
- ② Calculation of torsional torque and damping torque
- ③ Calculation of input torque into each mass point and output torque from each mass point
- ④ Calculation of angular velocity  $\omega$  and angle of rotation  $\theta$  of each mass point

(2) Equations of torque

Using the constant after a pu conversion, the equations of torque may be defined as follows. The reference value for the unit method of torque is the rated capacitance of the generator. Subscript  $x$  indicates the number of mass points.

- Inertia torque  $TQM_x[\text{pu}]$   $TQM_x = LMT_x \cdot \frac{d\omega_x}{dt}$
- Torsional torque  $TQS_x[\text{pu}]$   $TQS_x = CKTP_x \cdot (\theta_x - \theta_{x+1})$
- Self-damping torque  $TQDS_x[\text{pu}]$   $TQDS_x = RDSP_x \cdot \omega_x$
- Mutual damping torque  $TQDM_x[\text{pu}]$   $TQDM_x = RDMP_x \cdot (\omega_x - \omega_{x+1})$

(3) Calculation of angular velocity  $\omega$  and angle of rotation  $\theta$  of mass points

The difference between the input torque and output torque is the inertia torque at each mass point. The change in the rotational velocity  $\omega$  (speed deviation  $Sg$ ) can be obtained from this relationship. Here, the initial value of  $\omega$  is the rated angular velocity (1 [pu]), and the initial value of  $Sg$  is set to zero. The following equation is obtained by taking the example of turbine 2.

$$\begin{aligned} (\text{Input to turbine 2}) &= (\text{inertia torque of turbine 2}) + (\text{output torque of turbine 2}) \\ TQIN_2 &= TQM_2 + TQOT_2 \end{aligned}$$

$$LMT_2 \frac{d\omega_2}{dt} = (TQIN_2 - TQOT_2)$$

$$S_{g2} = \frac{d\omega_2}{dt} = \frac{1}{LMT_2} (TQIN_2 - TQOT_2)$$

Here,  $\omega$  and  $\theta$  can be calculated from the following equations.

- Angular velocity  $\omega_2 = S_{g2} + \omega_{INIT2} = S_{g2} + 1.0$
- Angle of rotation  $\theta_2 = \int S_{g2} dt + \theta_{INIT2}$

## Analysis Results

The results of executing this example using XTAP are shown in Figures 3–5.

Figure 3 shows the angle of rotation of each mass point. During the initial state, the input side (the left side of Figure 1) is larger than the generator side. After a system fault, the entire shaft system accelerates while generally maintaining this relationship.

Figure 4 shows the angular velocity of each mass point. Although the mass points rotate at the same rated angular velocity (1 [pu]) before a system fault, they show different angular velocity fluctuations after the fault.

Figure 5 shows the torsional torque between the mass points. The value of the torque between adjacent mass points on the output side (the right-hand side of Figure 1) is shown for each mass point. The result in this example is zero because the generator (mass point 7) is a terminal (there is no mass point on its right). A constant torque is transmitted from the input side to the generator side before the system fault, whereas a torsional vibration is generated after a fault.

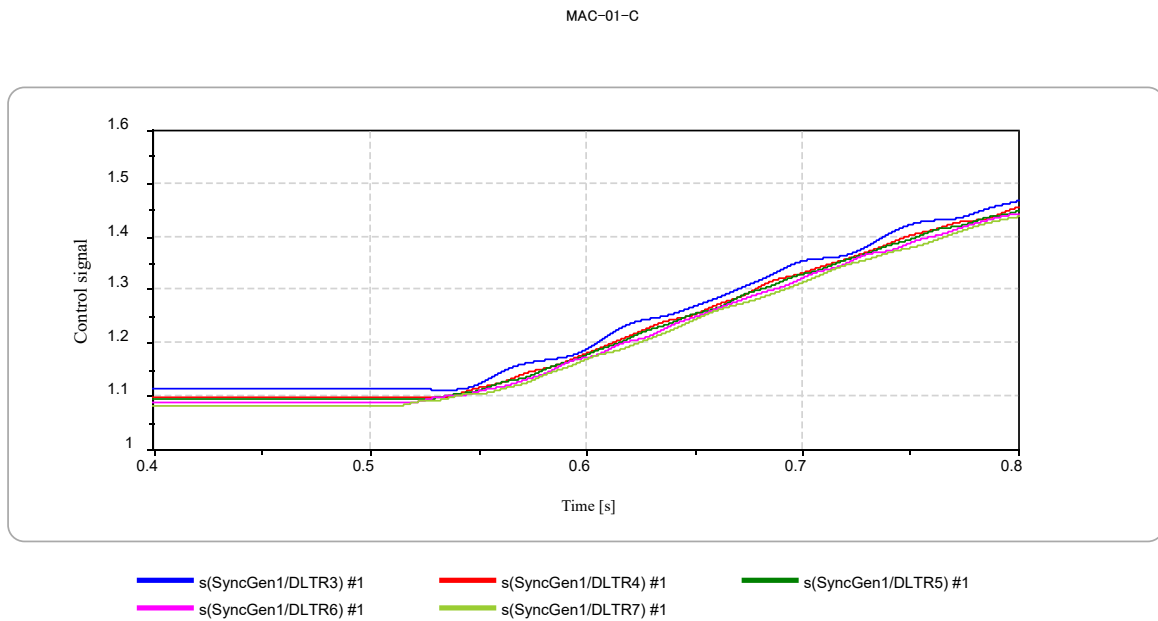
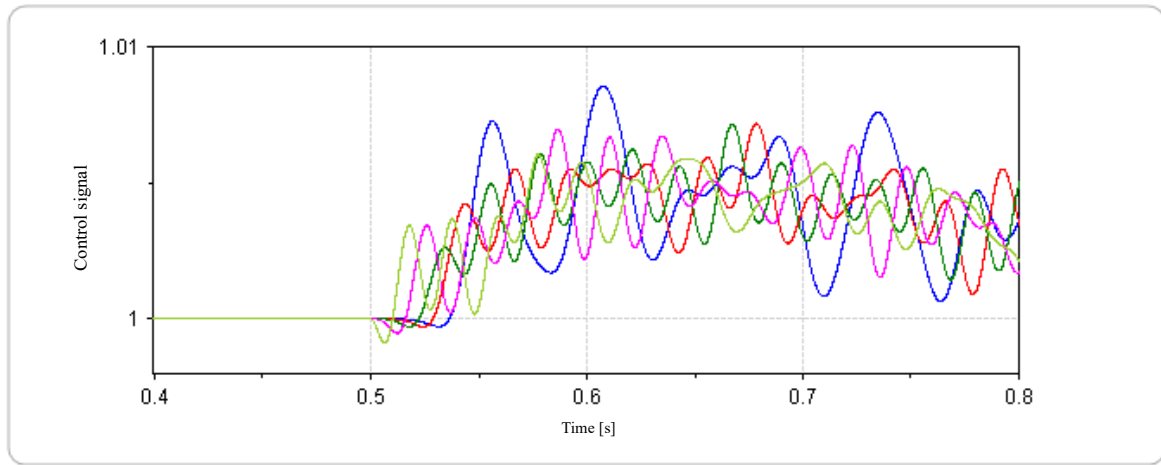


Figure 3 Angle of rotation of each mass point [rad]

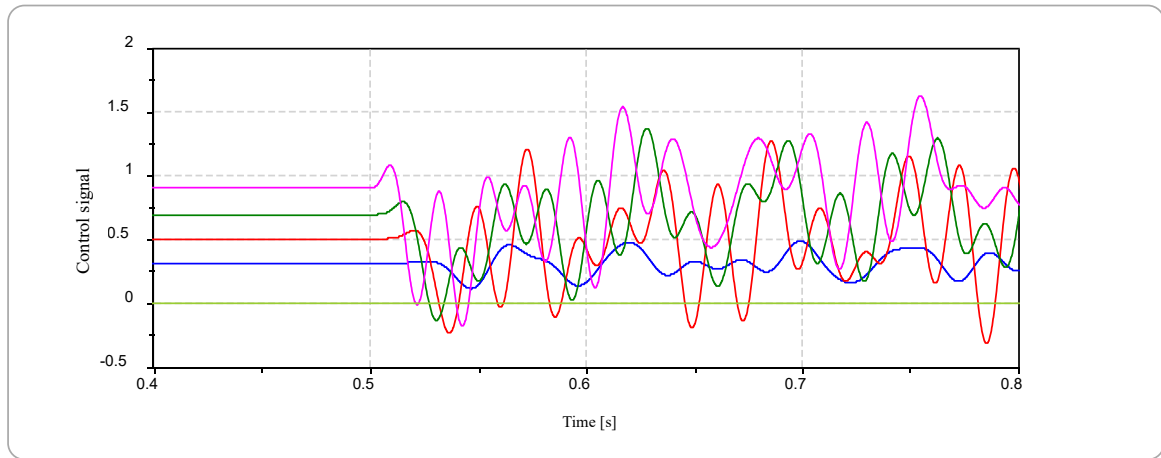
MAC-01-C



— s(SyncGen1/OMG3) #1    — s(SyncGen1/OMG4) #1    — s(SyncGen1/OMG5) #1  
— s(SyncGen1/OMG6) #1    — s(SyncGen1/OMG7) #1

Figure 4 Angular velocity of each mass point [pu]

MAC-01-C



— s(SyncGen1/TQS3) #1    — s(SyncGen1/TQS4) #1    — s(SyncGen1/TQS5) #1  
— s(SyncGen1/TQS6) #1    — s(SyncGen1/TQS7) #1

Figure 5 Torsional torque of each mass point (between adjacent mass points on the right-hand side in Figure 1)

End

Change log		
Date	Example file version	Content changes
2021/11/11	2.3	Modified for XTAP Version 2.30
2014/11/19	2.0	Modified for XTAP Version 2.00 Reconnection of PV designated generator bus parts consequent to a change in parts
2013/04/19	1.3	Change of fault occurrence time by improving initial value calculation Combined with the power flow conditions of MAC-01-A, B
2012/07/19	1.2	Modified for XTAP Version 1.20
2010/10/18	1.0	First edition created (for XTAP Version 1.11)

XTAP Examples		No.	MAC-01-D
<b>Example Name</b>	Synchronous Generator (Considering Magnetic Saturation) (Single-Line 3 LG-O Fault Occurring in a Single-Machine Infinite Bus System with AVR Control)		
<b>Field</b>	Power system applications		
<b>Literature</b>	<p>Because this example has been created for this training course, there are no references.</p> <p>※ For the modeling and system characteristics of synchronous generators, refer to textbooks on electrical equipment and electric power systems engineering. Examples of reference materials are provided in MAC-01-A. The AVR was created with reference to the model LAT = 1 of “Power System Dynamics Analysis Program (Y Method).”</p> <ul style="list-style-type: none"> <li>• Technical Report No. 754 of the Institute of Electrical Engineers “Standard Model of Electric Power System,” p. 41.</li> </ul>		
<b>Overview</b>	<p>The target system of the analysis is the single-machine infinite bus system connected with one synchronous generator and an infinite bus using two parallel line transmission lines.</p> <p>The need to increase the magnetomotive force by increasing the field current is ascertained when considering the magnetic saturation.</p>		

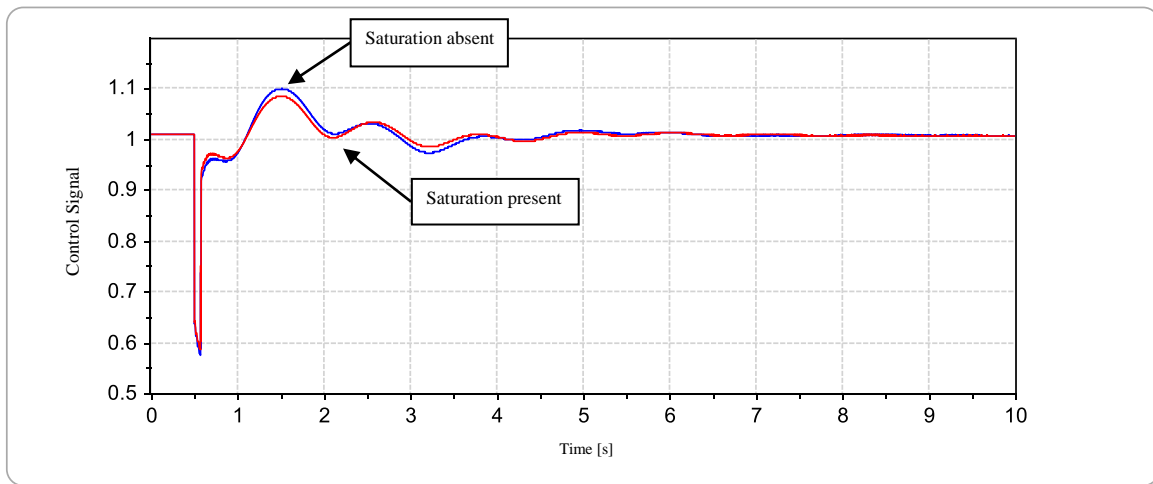
## Analysis Circuit and Conditions

[Analysis Phenomenon]

The synchronous generator of example MAC-01-B is replaced with parts that consider the magnetic saturation characteristics. For other analysis conditions, see example MAC-01-B.

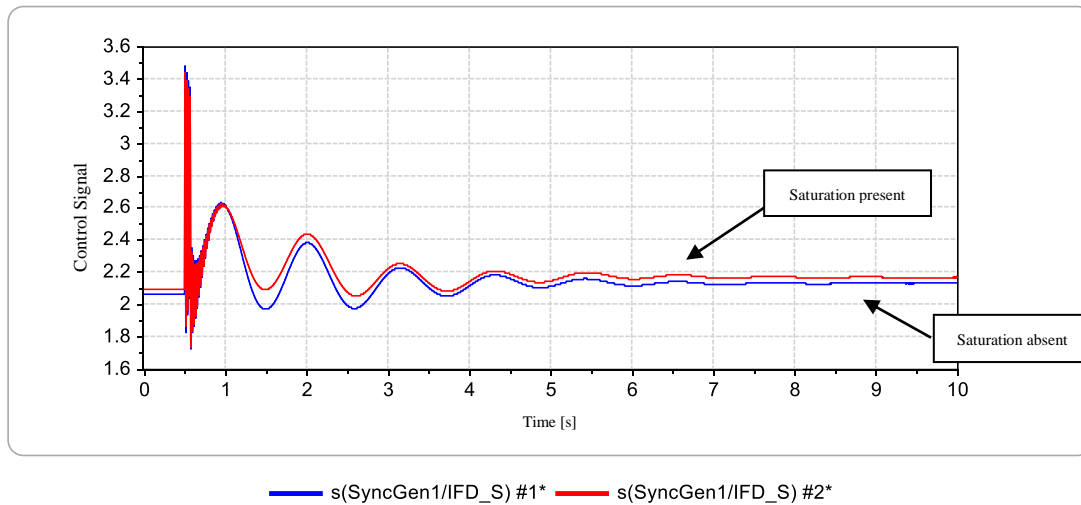
## Analysis Results

MAC-01-D



— s(SyncGen1/EA\_PU) #1\* — s(SyncGen1/EA\_PU) #2\*

(a) Terminal voltage



(b) Field current

Figure 1 Analysis results using XTAP

Figure 1 shows the analysis results. Figure (a) shows the terminal voltage of the synchronous generator, and Figure (b) shows the field current.

A terminal voltage of 1.01 [pu] and an active power output of 0.9 [pu] are set as the power flow conditions.

A comparison of the fluctuations in the transient terminal voltage in Figure (a) indicates that the fluctuation is smaller in the event of magnetic saturation than in its absence.

A comparison of the field currents during the initial state and a steady state after a fault shown in Figure (b) indicates that, for the same terminal voltage and active power output, the need to increase the magnetomotive force by increasing the field current is greater in the presence of magnetic saturation than in its absence, as the air gap flux decreases owing to a saturation.

End

Change log		
Date	Example file version	Content changes
2015/10/27	2.1	Change to the method considering saturation characteristics
2014/11/19	2.0	Modified for XTAP Version 2.00 Reconnection of PV designated generator bus parts consequent to the change in the parts
2013/08/21	1.1	Improved initial value calculation and simulation method of magnetic saturation Combined with the power flow conditions of MAC-01-A, B
2010/07/19	1.0	First edition created (for XTAP Version 1.20)

XTAP Examples		No.	MAC-02
Example Name	3 LG-O Simulation of Induction Motor		
Field	Basic calculation (power systems)		
References	N. Kibo, T. Noda, K. Takenaka, "Development of Instantaneous Value Simulation Method of an Induction Motor for transient phenomena analysis," CRIEP Report R 08022, June 2009		
Overview	<p>A3 LG - O simulation of an induction motor is calculated in this example.</p> <p>The present example has the following objectives: 1) to ascertain that, in the event of a change in the system voltage owing to a system fault such as a 3 LG, the active and reactive powers continue to fluctuate even after the removal of the fault, and 2) to verify through the waveform that, unlike a synchronous machine, an induction motor is not very likely to turn into the supply source of a short-circuit current, as its current becomes attenuated during the fault period.</p> <p>Please look up the references for further details such as the equipment constants. In addition, please consult the references for a comparison of the results of analog simulator tests, as well as a comparison of XTAP, EMTP, and Y method results.</p>		

## Analysis Circuits and Conditions

Figure 1 shows the analysis circuit

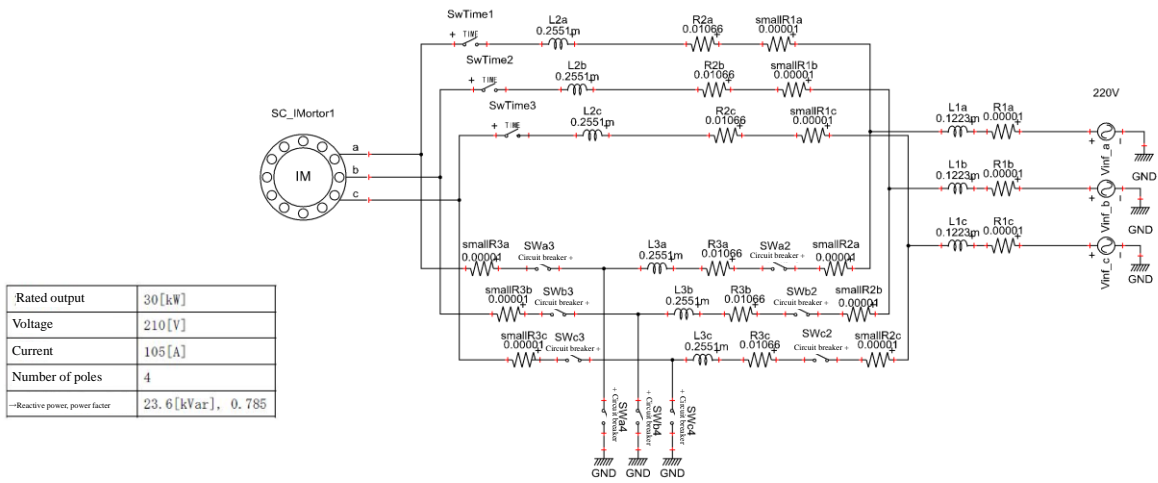


Figure 1 Analysis circuit

[Basic conditions]

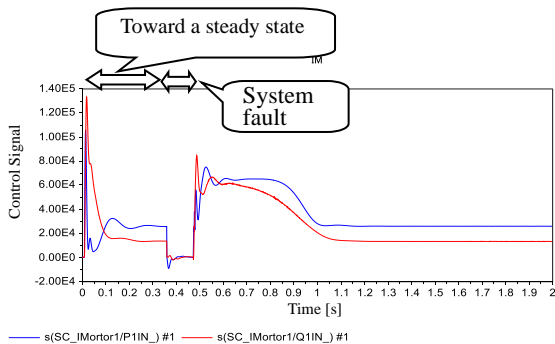
$t = 0.01$ : IM parallel to the system

$t = 0.04$ : Addition of load torque  $T_L = 0.78$

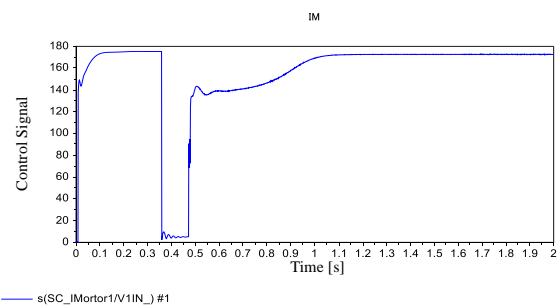
$t = 0.36$ : Occurrence of system fault

$t = 0.47$ : Clearing of system fault      Instantaneous drop period 110 ms = 0.11 s

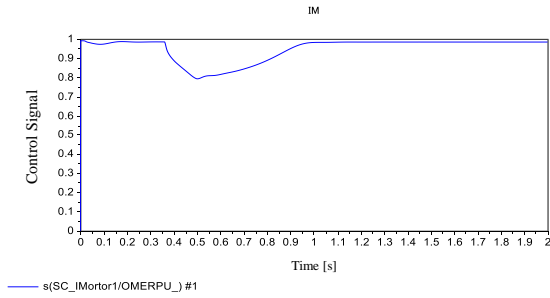
## Analysis Results



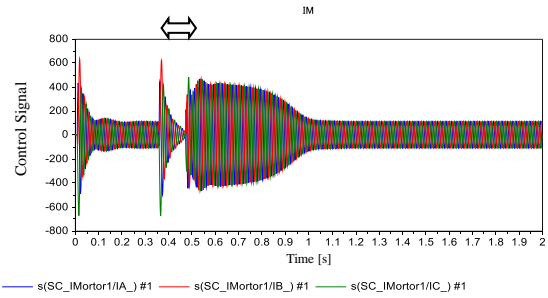
Induction machine PQ[W, Var]



Terminal voltage of induction machine [V] (Phasevoltage)

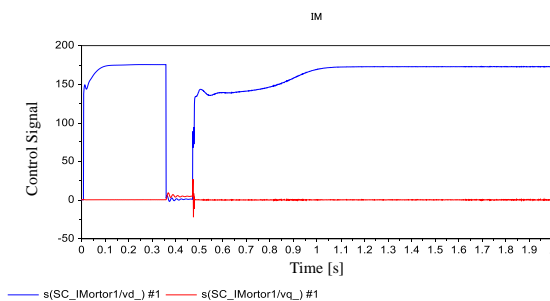


Induction machine  $\omega_r$ [pu]

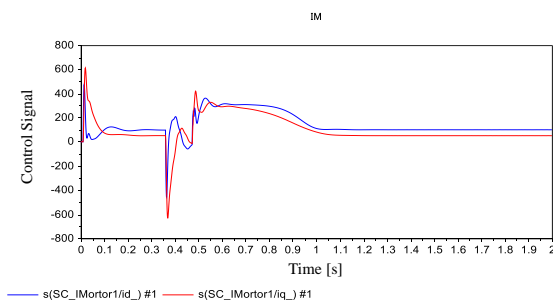


Three-phase current of induction machine [A]

○ The secondary side of the induction motor is short-circuited and can be viewed as a variable RL load from the standpoint of the electric power system. The three-phase current of the induction motor shows that, unlike a synchronous machine, the induction motor is not very likely to turn into the supply source of a short-circuit current as its current becomes attenuated during the fault period. Further, being viewed as a load, the rotational speed decreases when the amount of active power received from the power system decreases during the fault period (see  $\omega_r$ ). Even after the fault is eliminated, the loss of the rotating body increases owing to the change in slip, and hence  $\omega_r$  does not return quickly to a value of 1 pu (depending on the load torque characteristic of the induction motor).



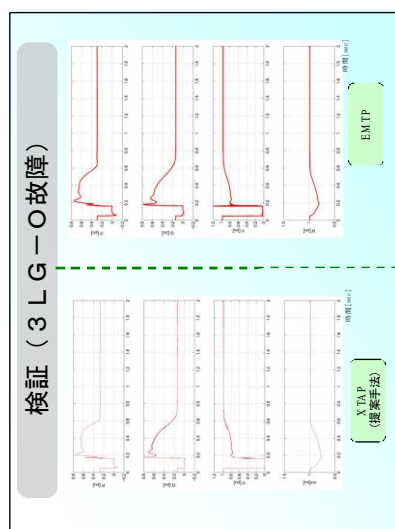
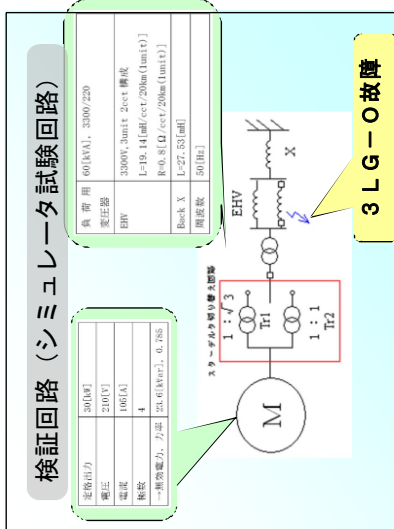
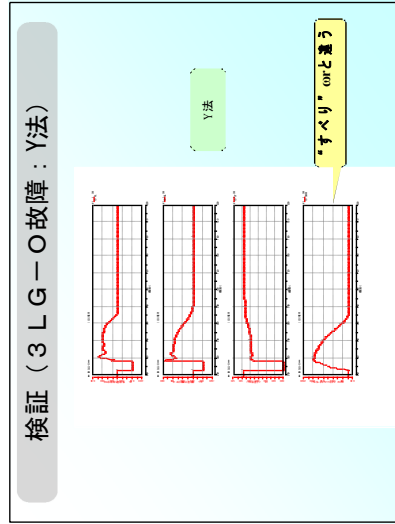
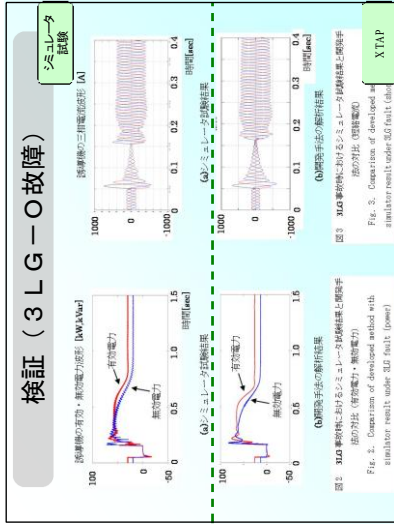
$V_d, V_q$ [pu]



$I_d, I_q$ [pu]

The above shows the voltage/current waveform of the dq axis in the induction motor model. Because the dq axis is selected such that  $V_q$  becomes zero, the terminal voltage of the induction machine naturally becomes the  $V_d$ .

# Comparison of Simulator Test, EMTF Analysis, and Y Method Results (in Japanese)



Change log		
Date	Example file version	Content changes
2021/11/11	2.30	Modified for XTAP Version 2.30
2014/11/19	2.0	Modified for XTAP Version 2.00
2012/07/05	1.2	Modified for XTAP Version 1.20
2011/09/02	1.1	Modified for XTAP Version 1.11
2010/08/30	1.0	First edition created (for XTAP Version 1.10)

XTAP Examples		No.	PS-01-A
Example Name	Simulation of the WEST 10 System of the Institute of Electrical Engineers of Japan		
Field	Power systems analysis		
References	<p>(1) Committee for Standardization of Benchmark Power System Models, “Standard Benchmark Power System Models,” Technical Report No. 754, 1999, the Institute of Electrical Engineers of Japan.</p> <p>(2) T. Noda, H. Takizawa, T. Nakajima, “A Study of Electromagnetic Transient Simulations Using IEEJ’s West-10 Benchmark Power System Model,” Proc. of International Conference on Power Systems Transients (IPST) 2015, Paper #35, Cavtat, Croatia, 2015. Downloadable from <a href="http://www.ipstconf.org">www.ipstconf.org</a></p> <p>(3) T. Noda, O. Sakamoto, Y. Aki, “Acceleration of Power System Instantaneous Value Analysis by Single-Phase Effective Value Simulation of Remote System,” Journal of the Institute of Electrical Engineers of Japan, Vol. 135, No. 8, pp. 502-510, 2015.</p>		
Overview	<p>The 60-Hz system of Japan is a comb-type linking of the systems of several electric power companies through 500-kV transmission lines in the east-west direction and extends more than 1,000 km. This system with ten generators is simulated using the WEST 10 system of the Institute of Electrical Engineers proposed in [1]. Although the WEST 10 system was originally developed as a model system for an effective value analysis (transient stability analysis), in the present example, an instantaneous value analysis using XTAP is attempted. Further, in the presented set of examples, the results of an instantaneous value analysis using XTAP are compared with the results of an effective value analysis based on CPAT developed in our company, and appear to show a proper agreement. Please consult [1] for details of the WEST 10 system, and [2] for a comparison with the effective value analysis results.</p>		

Analysis Circuit and Results

Figure 1 shows a schematic diagram of the WEST 10 system. The system frequency is 60 Hz. All ten generators are simulated using a generator model with one damping circuit each for the *d* and *q* axes, the generator constants of which are typically used for thermal power plants with a large capacitance. The inertial constant of each

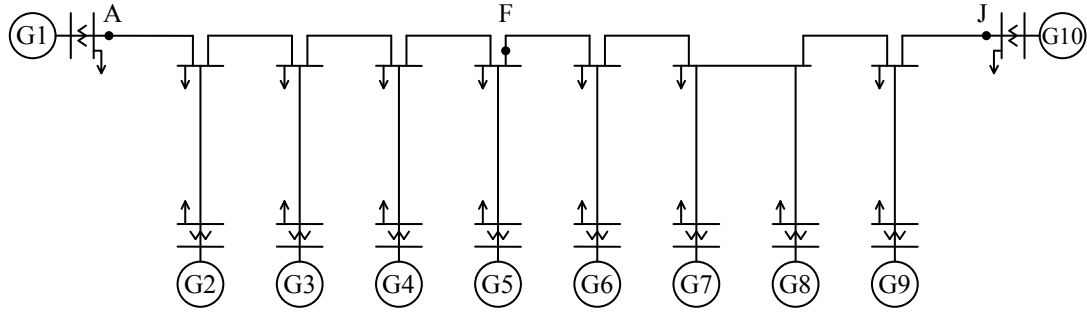


Figure 1 Benchmark power system model of the “WEST 10 System” of the Institute of Electrical Engineers

generator model is 7 s, and each generator has a speed governor system model for the thermal and nuclear power, as well as a rotary exciter model. The impedance of the step-up transformer of each generator is 0.14 pu based on its own rating, with a tap ratio set to 1. The lines connecting the substations are double-circuit transmission lines of 100 km each, and the power lines connecting the power plants and substations are double-circuit transmission lines of 50 km each. The power line of G8 alone has a length of 100 km. The load is simulated using a model with the following characteristics: When the load end voltage is  $V_L$ , the active power has a constant current characteristic of  $V_L \geq 0.7$  pu, and a constant impedance characteristic of  $V_L < 0.7$  pu. The reactive power is a constant impedance characteristic regardless of  $V_L$ . Two cases, namely, a daytime section (under a peak load) and a night section (under a light load), are considered for the power flow conditions, and the power flow conditions of each generator and each load are specified for each section. The impedances of each transmission line and transformer in each section are also set.

An instantaneous value analysis requires more detailed model data than an effective value analysis. Because the WEST 10 system was originally designed for an effective value analysis (transient stability analysis), the data are insufficient for an instantaneous value simulation. Therefore, the following settings were made regarding the missing data in the instantaneous value simulation. The rated voltage of the generator was set to 22 kV, and the neutral point was grounded through a 0.1  $\Omega$  resistor, assuming the ground resistance of the power plant. The Y -  $\Delta$  connection was used in the transformer, with the generator side having a 22-kV  $\Delta$  connection, and the transmission side having a 500-kV Y connection. The neutral point of the Y connection was connected to a 0.1  $\Omega$  resistor, assuming the ground resistance of the preceding power station. Regarding the transmission line, although it would be ideal to carry out a realistic simulation using a distributed constant line model with constant parameters, or a frequency-dependent distributed constant line model, a  $\pi$ -type equivalent circuit model (1 stage) without interphase coupling was applied in this study. A realistic analysis taking into consideration the coupling between phases, the propagation phenomena of traveling waves, and the frequency-dependence of the line constants are topics for a future study.

Assuming a one-line three-wire ground fault (fault duration of 70 ms) at points A, F, and J in Figure 1 as a system fault, the daytime and nighttime sections were calculated for each case. The computational time step was set to 100  $\mu$ s for XTAP and 10 ms for CPAT.

Figure 2 shows the WEST 10 system created using XTAP for the lines described above.

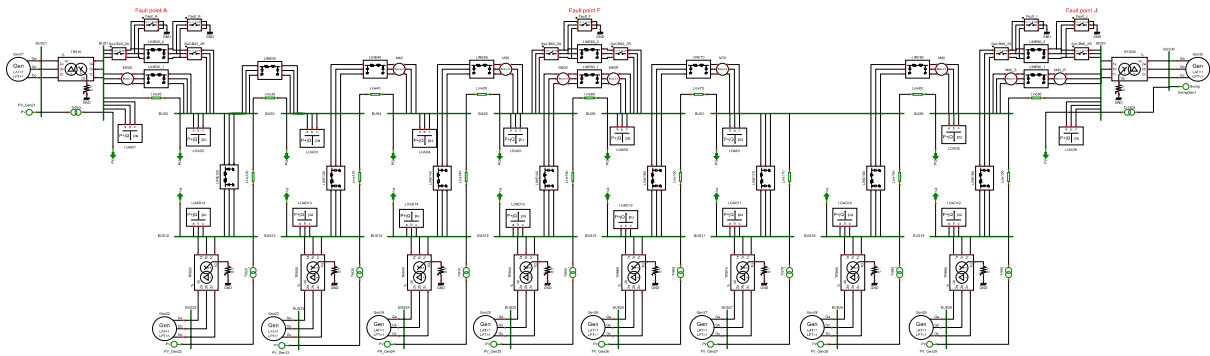


Figure 2 WEST 10 system created using XTAP

## Analysis Results

The analysis results are shown in Figures 3–5. In addition to the results of an instantaneous value analysis using XTAP, the figure also shows the results of the effective value analysis by CPAT for comparison. The calculation results indicate that the instantaneous value analysis results from XTAP are in good agreement with the results of the effective value analysis using CPAT for both the daytime and nighttime sections in the cases of ground faults occurring at points A and F. The results of the ground fault at point J are generally in agreement, but with certain differences. Figure 6 shows the calculation results of the fault current waveform using XTAP. Because a DC component is superimposed over the current of phase b, there is no current zero point (zero missing) up to approximately 70 ms after the fault. Eventually, a zero point is reached for the first time and the fault current cuts off only at approximately 100 ms after the occurrence of the fault. As a result, in the instantaneous value analysis, the fault duration time of only the b phase is approximately 100 ms, which differs from the results of the effective value analysis. In the case of the daytime section of the ground fault at point J, shown in Figure 5 (a), a significant difference appears in that, although generators G 6 through G 9 are not out-of-step in the CPAT results, they are out-of-step in the XTAP results.

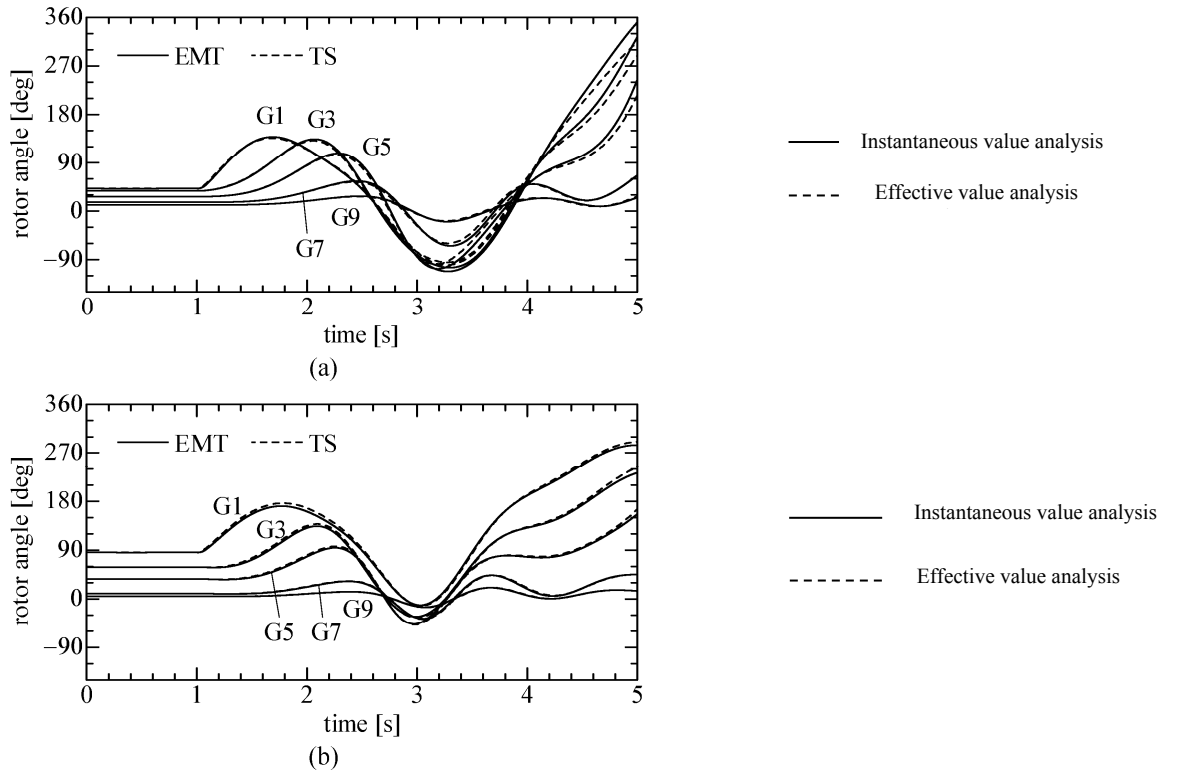


Figure 3 Comparison of the results of instantaneous value analysis using XTAP and effective value analysis using CPAT

Ground fault: A, (a) daytime and (b) nighttime sections

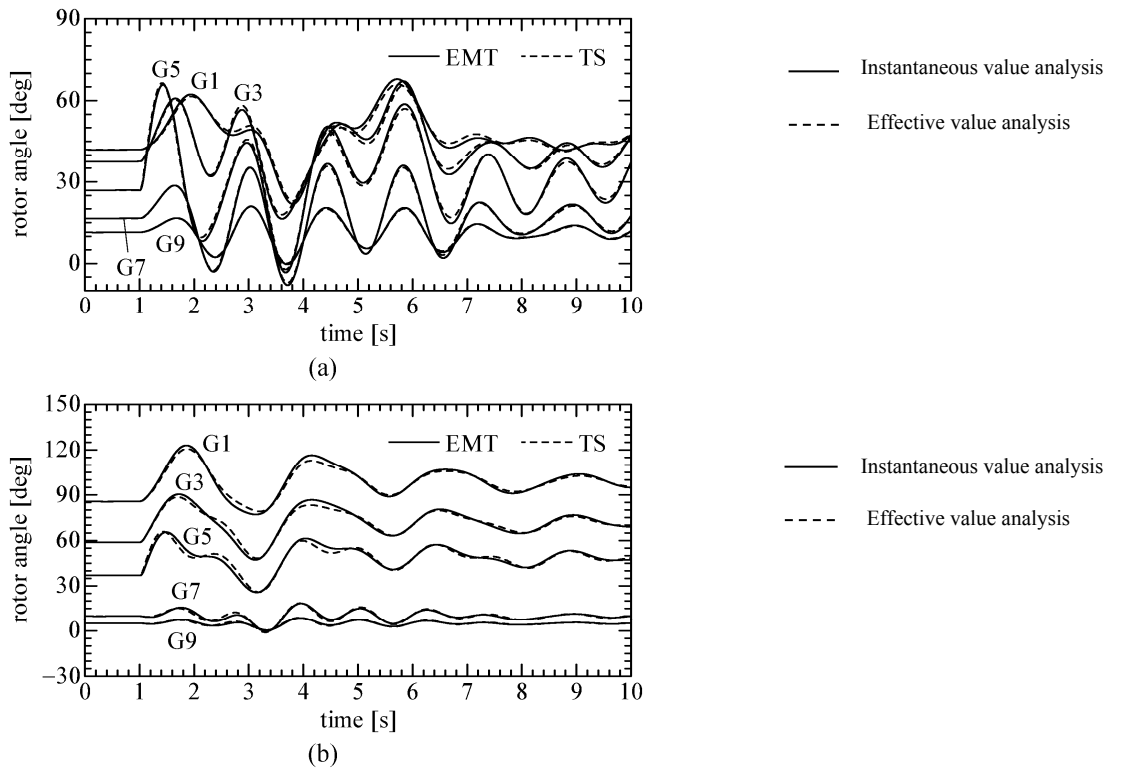


Figure 4 Comparison of the results of instantaneous value analysis using XTAP and effective value analysis using CPAT

Ground fault: F, (a) daytime and (b) nighttime sections

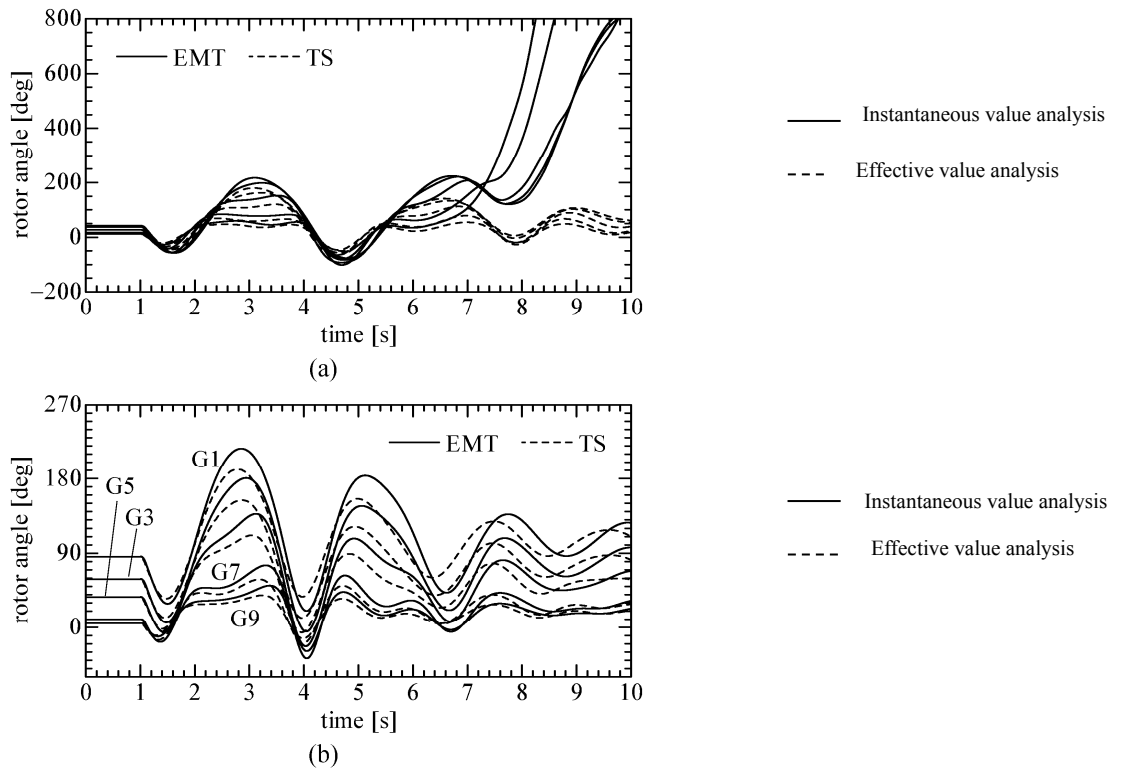


Figure 5 Comparison of the results of instantaneous value analysis using XTAP and effective value analysis using CPAT

Ground fault: J, (a) daytime and (b) nighttime sections

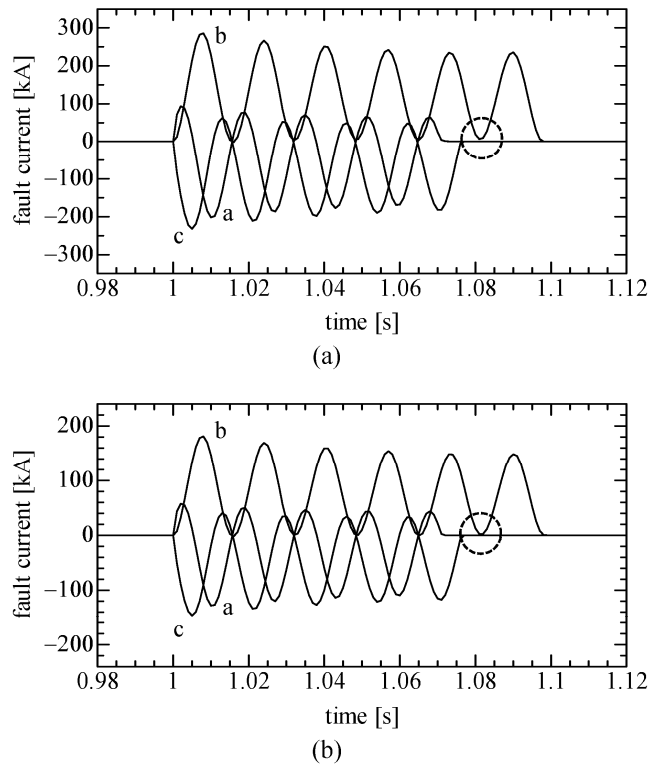


Figure 6 Ground fault current waveform at ground point J: (a) daytime and (b) nighttime sections

Change Log		
Date	Example File Version	Content changes
2015/09/24	2.0	First edition created (for XTAP Version 1.10)
2021/03/04	2.1	Changed the load model to a model that can acquire power-flow calculation information. Change the example name.

XTAP Exercises		No.	PS-02-A
<b>Exercise Name</b>	Simulation of EAST 10-Machine Power System of the Institute of Electrical Engineers of Japan (IEEJ)		
<b>Field</b>	Power system analysis		
<b>References</b>	<p>[1] IEEJ Technical Committee on Standardization Model of Power System, “Standardized Model of Power System,” IEEJ Technical Report No. 754, 1999 in Japanese.</p> <p>[2] T. Noda, H. Takizawa and T. Nakajima, “A Study of Electromagnetic Transient Simulations Using IEEJ's West-10 Benchmark Power System Model,” Proc. of International Conference on Power Systems Transients (IPST) 2015, Paper # 35, Cavtat, Croatia, 2015 (available for download from <a href="http://www.ipstconf.org">www.ipstconf.org</a>)</p> <p>[3] T. Noda, O. Sakamoto, R. Yonezawa, “Enhancement of Electromagnetic Transient Analysis of Remote Power Systems Using Single-phase Phasor-based Model,” IEEJ Transactions B, Vol. 135, No. 8, pp. 502-510, 2015.</p>		
<b>Summary</b>	<p>The core of Japan’s 50-Hz grid is a 500-kV transmission line loop. The IEEJ's EAST 10-machine power system described in reference [1] simulates this grid by means of a 10-machine power system. While the EAST 10-machine power system is a model grid primarily intended for effective value analysis (transient stability analysis), this exercise involves its use for transient analysis using the XTAP simulator.</p> <p>More information about the modeling method of power system for transient analysis is provided in references [2] and [3] and in XTAP Example PS-01. Details of the EAST 10-machine power system are provided in reference [1].</p>		

## Analysis Circuit and Conditions

Figure 1 shows the circuit diagram of the EAST 10-machine power system modeled on XTAP. The power system operates at 50 Hz. The models for all 10 generators include damper circuits on the  $d$  and  $q$  axes respectively, with generator constants specified for thermal, hydro, and nuclear power generators. The inertia constants are 8 seconds for the thermal and nuclear power generator models and 10 seconds for the hydro generator models.

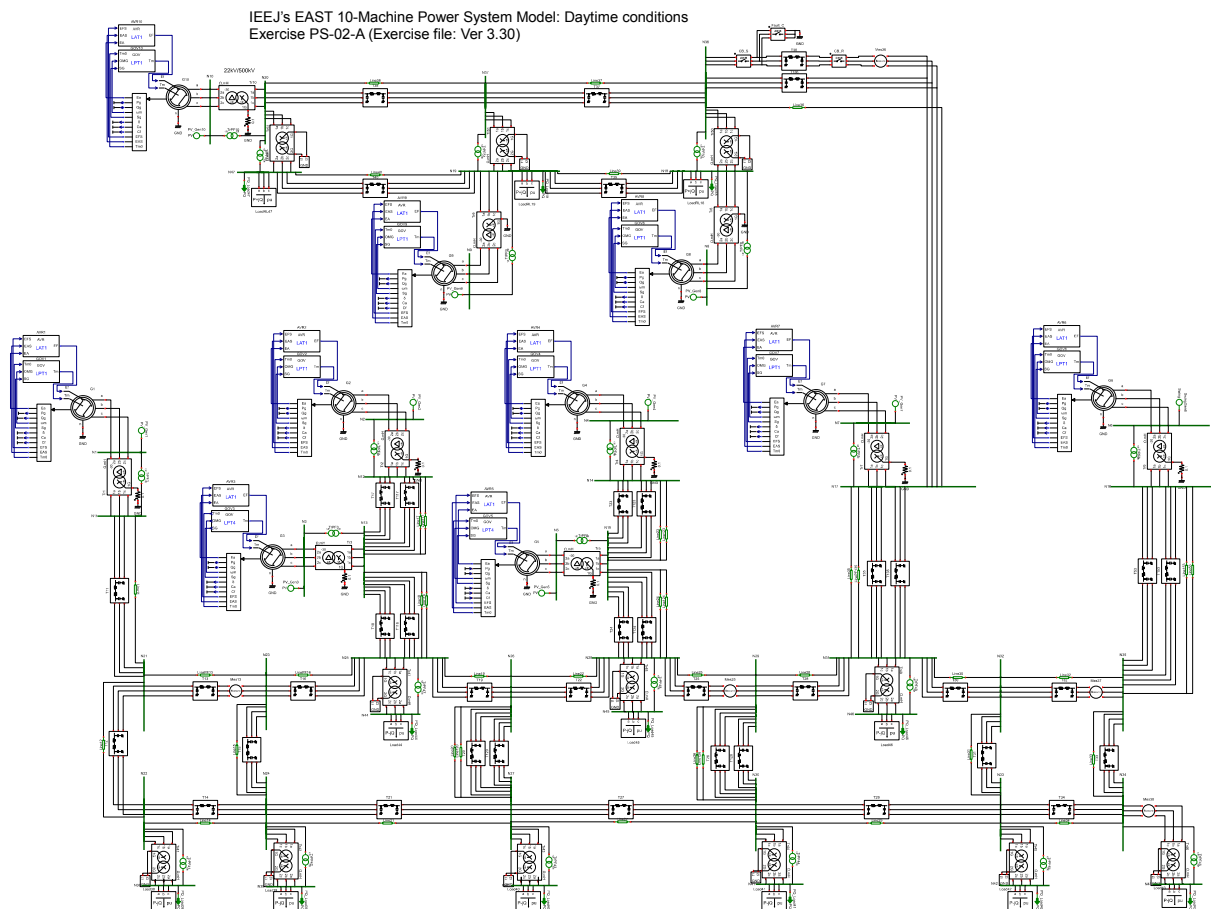


Figure 1 IEEJ's EAST 10-Machine Benchmark Power System Modeled on XTAP

The step-up transformers for all 10 generators have impedances of 0.14 pu (based on machine capacity) but different tap ratios. Dual transmission lines are used throughout and the loop length is 1,960 km. The loads are modeled as having constant impedance for both active and reactive powers. (This differs from reference [1] where the loads are modeled as having constant current for active power above a certain voltage.) Daytime load flow conditions were assumed.

Transient analysis requires more detailed model data than is needed for effective value analysis. This means that, because the EAST 10 power system model was primarily developed for the purpose of effective value analysis (transient stability analysis), it lacks some data needed for transient analysis modeling. Thus, as was done for XTAP example PS-01 for the WEST 10 power system, this missing data was specified as follows.

- Generator rated voltage was set as 22 kV.
- The step-up transformers were specified as Y- $\Delta$ -connected, with a 22 kV  $\Delta$  connection on the generator side and a 500 kV Y connection on the transmission line side. Also, a 0.1  $\Omega$  resistance was connected to the Y-connected neutral to replicate the power plant ground resistance.
- The 500 / 275 kV transformers were specified as Y-Y connected with a 0.1  $\Omega$  neutral resistance.
- For the transmission lines, while a more realistic simulation using a constant-parameter or frequency-dependent distributed constant model might be desirable, a (single-stage)  $\pi$  equivalent circuit model without mutual interaction between lines was used in this example.
- A grid fault was simulated as a three-phase ground fault on the N36 bus of one transmission line (duration: 70 ms) and this was calculated for each case under daytime and nighttime conditions. The calculation time step in XTAP was set at 100  $\mu$ s.
- The loads were modeled as a resistance and inductance (or capacitance in the case of capacitive loads) in series, with the respective resistance and inductance (or capacitance) values being simulated by a model in which the load was controlled to have constant impedance characteristics for both active and reactive powers regardless of the voltage across the load ( $V_L$ ).

## Analysis Results

Figure 2 shows the time waveforms for the rotor angles in generators 1, 7, 8, and 10 (relative to generator 6, which was set as the swing node). Along with the results of transient analysis using XTAP, the results of effective value analysis by CPAT are also provided for comparison. The results show good agreement between the XTAP transient analysis and CPAT effective value analysis. As this case involved generator step-out (loss of synchronism), the CPAT analysis terminated at approximately 5.8 seconds. Accordingly, while the CPAT and XTAP results diverge from 5 seconds onwards, their agreement prior to this time is good.

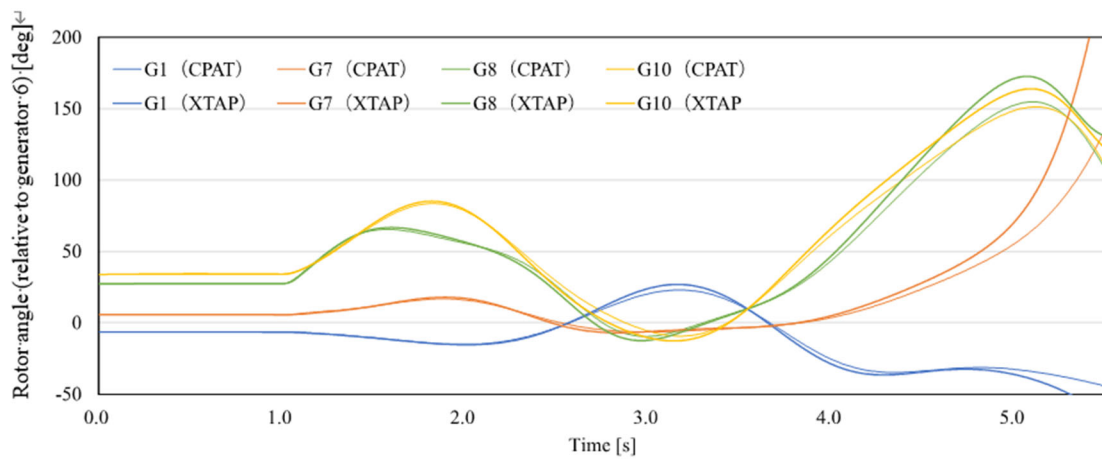


Figure 2 Comparison of Results of Transient Analysis Using XTAP and Effective Value Analysis Using CPAT

Revision History		
Date	Exercise File Version	Revision Details
2021/03/04	1.0	Initial document

Examples of XTAP		No.	CB-01
Example Name	Current Breaking Simulation of 66-Kv Fault Current Interrupting Arcing Horn		
Field	Overhead power transmission, power quality		
Literature	<ul style="list-style-type: none"> <li>● Central Research Institute of Electric Power Industry Report H05013 “Development of current breaking simulation model of fault current interrupting arcing horn: Construction of a basic arcing model”</li> <li>● Central Research Institute of Electric Power Industry Report H06007 “Development of current breaking simulation model for fault current interrupting arcing horn (Part 2): Development and application of arc-conductance dependent model”</li> </ul>		
Overview	<p>A 66-kV fault current interrupting arcing horn is a lightning protection device that helps control a power outage by cutting off short-circuit currents of up to 10 kA within a single AC cycle. However, unlike lightning arresters used for a power transmission that utilize the nonlinear resistance characteristics of zinc oxide elements, a short-circuit current circulates with almost the same magnitude despite being within a single AC cycle and impacts the power system by leading to an instantaneous drop in voltage.</p> <p>This example assumes a case in which a three-phase ground fault (3 LG) has been cleared using a fault current interrupting arcing horn and analyzes the current–voltage waveform at the location where the arcing horn is installed and at the substation serving as a power source. In addition, because a fault current interrupting arcing horn may interrupt the current at the first (0.5 AC cycle) or second (one AC cycle) zero point, this analysis was designed to specify the zero point at which the current is cut off.</p>		

## Analysis Circuit and Conditions

Figure 1 shows a single-line diagram of the model system conducting a current breaking simulation of a fault current interrupting arcing horn; the poles of the 66-kV transmission line are as shown in Figure 2.

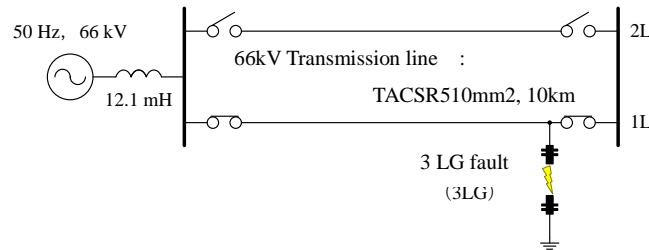


Figure 1 Single-line diagram of the model system

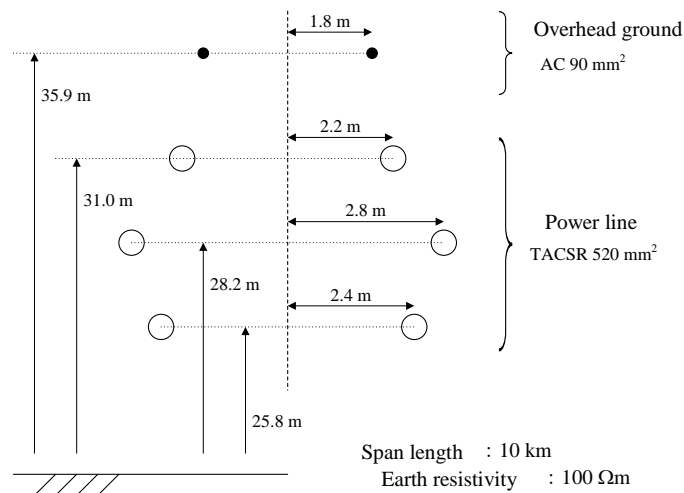


Figure 2 Poles of the 66-kV transmission line

The model is a 50 Hz, 66 kV system with a power source at one end, where the transmission line is assumed to be an ACSR 520 mm<sup>2</sup> cable, with a span length of 10 km. Although it is a double-circuit transmission line, the circuit breaker on the 2L side is open, and only the 1L side is used. The back impedance is 12.1 mH, and the short-circuit current is 10 kA, when a three-phase ground fault occurs at the nearest end of the substation (equivalent to maximum cutoff current of fault current interrupting arcing horn).

### [Analyzed Phenomenon]

In this example, a three-phase ground fault (3 LG) occurring in the terminal tower of transmission line 1L is simulated. The tower is fitted with a fault current interrupting arcing horn, and it is assumed that the current of each phase is cut off at the second zero point (one cycle of AC) after the occurrence of a fault.

Please refer to the two documents mentioned above for the current breaking simulation model of the fault current interrupting arcing horn. As shown in Figure 3, it is possible to simulate the arc conductance between the arc horns from the occurrence of a fault up to its clearing using a combination of the Cassie and Mayr models, which are widely used as macroscopic arc models of circuit breakers.

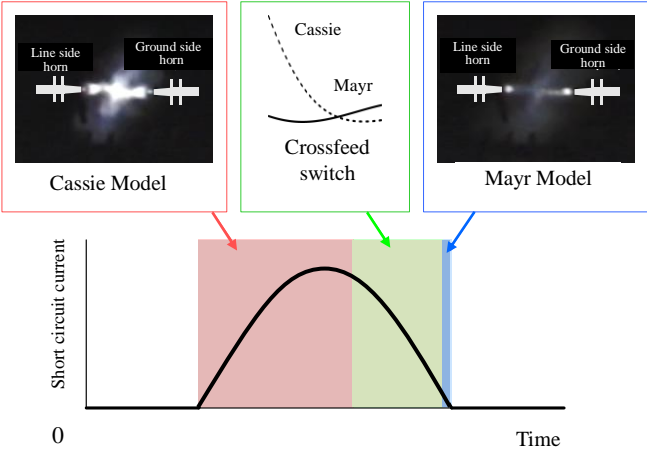


Figure 3 Current breaking simulation model of fault current interrupting arcing horn

[Creation of a Transmission Line Model]

As shown in Figure 2, the transmission line studied consists of a 90 mm<sup>2</sup> AC overhead ground wire and a 520 mm<sup>2</sup> TACSR power line. For simplicity, a “fixed-parameter distributed constant circuit” is used in this example.

[Analysis conditions]

The analysis conditions are as follows.

- Calculation timestep: 0.1 μs
- Calculation start time: 0 ms
- Calculation end time: 50 ms
- Display start time: 0 ms
- Display end time: 50 ms

Further, the time of occurrence of a fault and the current interruption time can be specified by double-clicking on the part (FCIAH) of the fault current interrupting arcing horn. In the present example, the following settings are applied.

- Time of fault occurrence: 14 ms
- Current interruption time: 2 half waves (current is cut off at the second zero point from the fault occurrence)

[Example of XTAP Input]

The creation of this example using XTAP is illustrated in Figure 4.

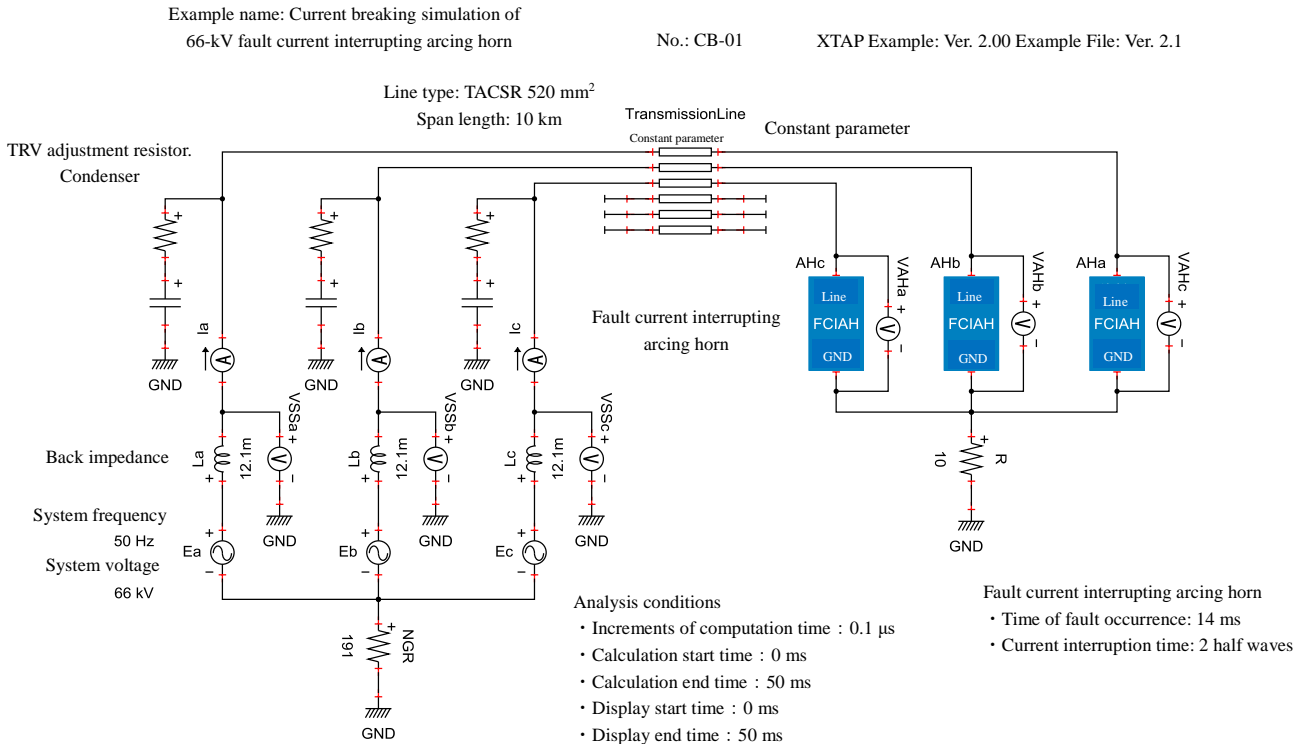


Figure 4 Example of XTAP input

## Analysis Results

First, the execution results of XTAP for the present example are shown in Figure 5.

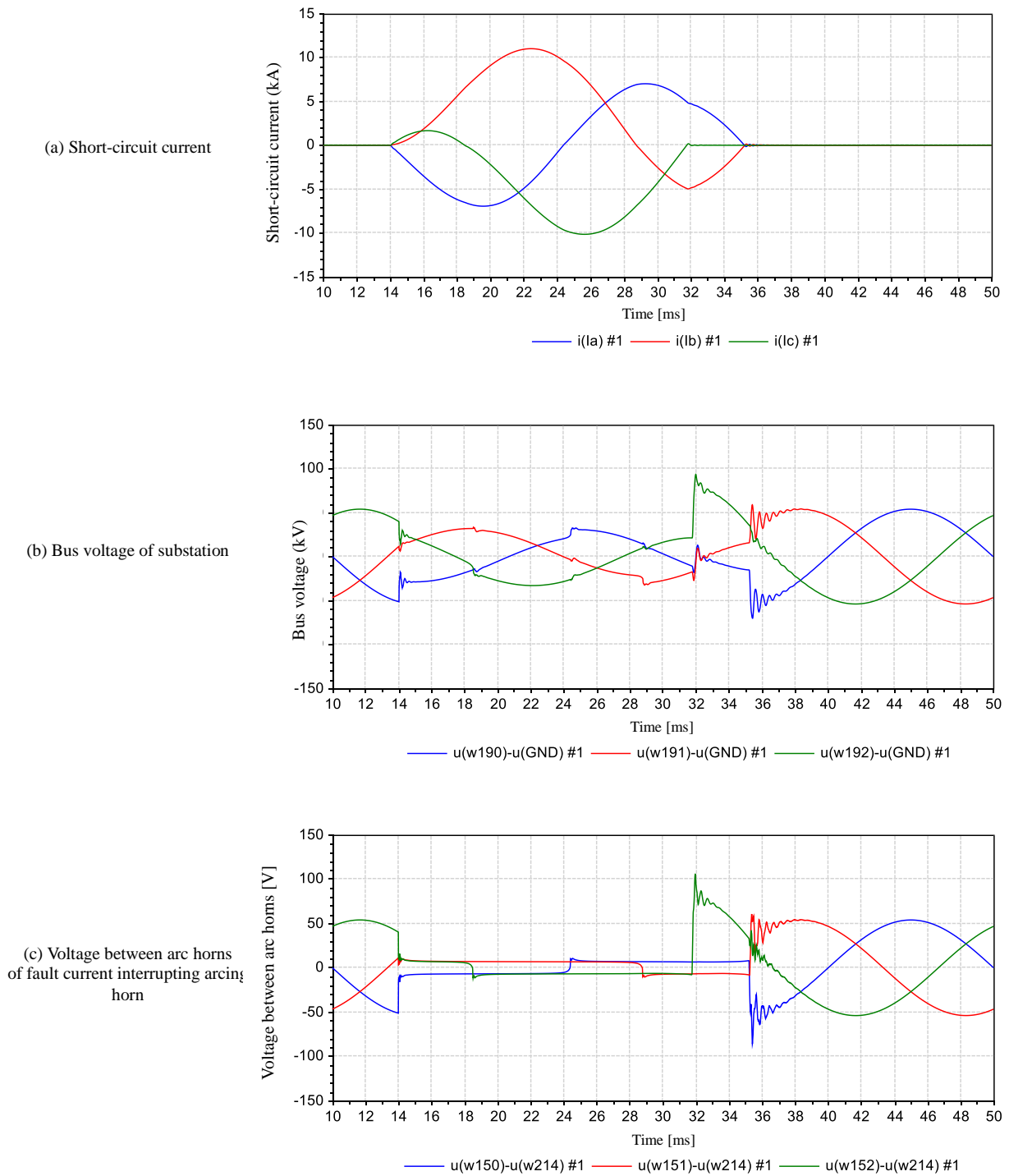


Figure 5 XTAP execution result (current interruption time of fault current interrupting arcing horn: 2 half waves)

Next, the execution results from XTAP when the current interrupting time of the fault current interrupting arcing horn is set to 1 half wave (when the current is interrupted at the first zero point from the occurrence of a fault) are as shown in Figure 6.

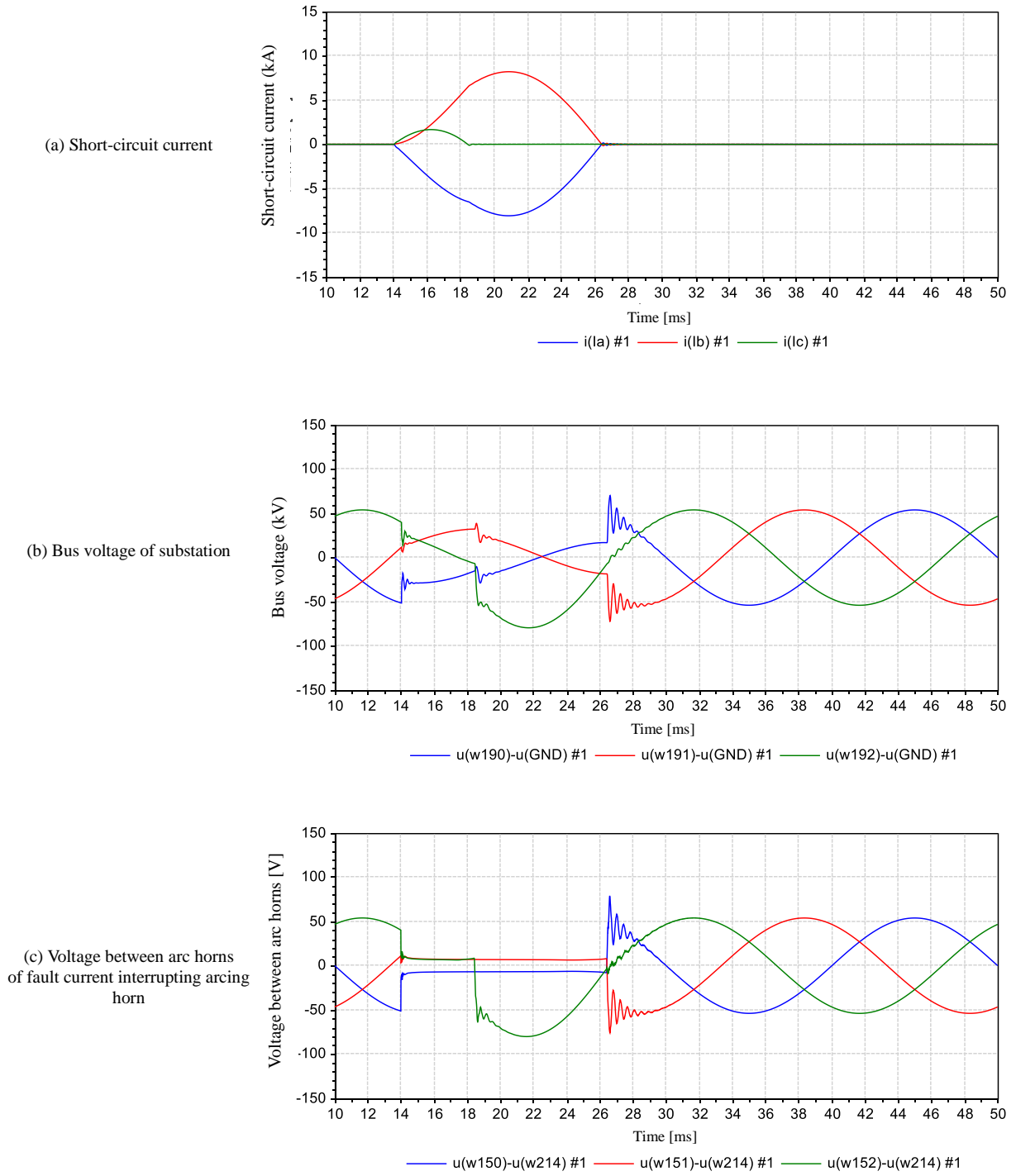


Figure 6 XTAP execution result (current interruption time of fault current interrupting arcing horn: 1 half wave)

End

Change log		
Date	Example file version	Content changes
2015/07/29	2.1	Name of example changed from PQ - 03 to CB - 01
2014/11/19	2.0	Modified for XTAP Version 2.00 Recalculated line constant consequent to change of XTLC
2014/08/19	1.2	Rectified certain problems
2012/07/19	1.1	Modified for XTAP Version 1.20
2011/10/18	1.0	First edition created (for XTAP Version 1.11)

XTAP Examples		No.	CB-02
Example Name	Analysis of Terminal Short-Circuit Breaker and Capacitive Current Switching in 154-Kv System		
Field	Basic calculation (electric power system)		
Literature	<ul style="list-style-type: none"> <li>● Noda, Ohtaka, Yonezawa, Matsumoto, Matsubara, Kuzuna, “Investigation into Instantaneous Value Analysis and Transient Phenomena Analysis Methods for Electric Power System and Analysis Example using XTAP (Part 1): Analysis of switching surge overvoltage,” Central Research Institute of Electric Power Research Report H12005, June 2013</li> <li>● Application Guidelines for the Revised Standards of AC Circuit Breakers and Special Committee for the Investigation of Cut Off Duty in Electric Power Systems, “Circuit Breaker Standard JEC-2300 Application Guide: Survey on Interruption of Electric Power System and Background of Revision of Standards,” Technical report of The Institute of Electrical Engineers of Japan, No. 1200, September 2010</li> </ul>		
Overview	<p>When the circuit breaker installed in a substation interrupts the current, a transient recovery voltage (TRV) having an oscillating component ranging from several hertz to several kilohertz is generated between the poles of the circuit breaker. The TRV is a very important parameter in discussing the current interrupting performance and insulation recovery characteristics of a circuit breaker. Further, because a power system exhibits various behaviors depending on its configuration and constants, an instantaneous value analysis is effective in studying the TRV.</p> <p>In this example, an analysis of the “Break Terminal Fault interruption” (CB-02-BTF.xsf), which breaks a fault occurring within the vicinity of the circuit breaker in a 154-kV system, and an analysis of the “Small Capacitive Current Breaker” (CB-02 - CCS.xsf), which shuts off the capacitor bank connected to the substation tertiary circuit, are carried out.</p>		

## Analysis Circuit and Conditions

A single-line diagram of the model system is shown in Figure 1. The current value in the figure represents the value of the short-circuit current flowing from the power source. The target of the analysis is the substation T shown in the figure.

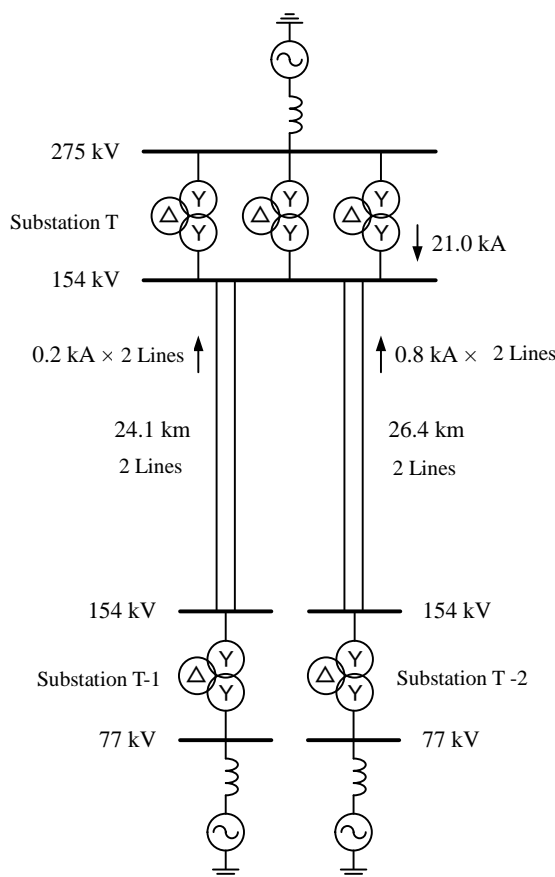


Figure 1 Single-line diagram of model system

### [Phenomenon Being Analyzed]

As mentioned above, when the circuit breaker interrupts the current, a TRV with a vibration component ranging from several hertz to several kilohertz is generated between the poles, which is a very important parameter in discussing the current interrupting performance and insulation recovery characteristics of a circuit breaker. Based on the breaking phenomenon, various test methods have been defined for an evaluation of the TRV. These are described in detail in JEC-2300-2010 “AC circuit breaker” in accordance with the standards of the Japanese Electrotechnical Committee of the Institute of Electrical Engineers of Japan (JEC), and in IEC 62271-100 “High-voltage switchgear and control gear - Part 100: Alternating-current circuit-breaker” in accordance with the standards of the International Electrotechnical Commission (IEC).

The breaking of a fault occurring within the vicinity of the circuit breaker, as shown in Figure 2, is called a terminal short-circuit fault interruption (hereinafter referred to as a breaker terminal fault (BTF)). Because

a BTF has the maximum current flowing from the rear power source, it may be stated that it has the main responsibility of protecting the power system from ground and short-circuit faults. Here, it is assumed that a fault occurring within the vicinity of the substation T is broken by the circuit breaker installed on its secondary side.

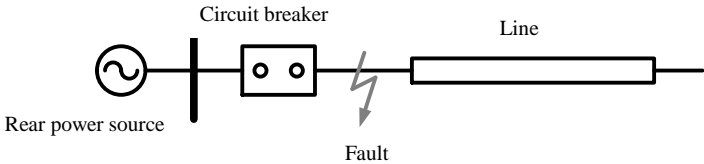


Figure 2 Illustration of terminal short-circuit fault

A case in which the capacitor bank is cut off, as is shown in Figure 3, is called capacitive current switching. Figure 4 shows the current and voltage waveforms at the time of a capacitive current switching. When the circuit breaker interrupts the current, the crest value of the circuit breaker terminal voltage  $U_T$  remains as the DC voltage  $U_L$  on the load side (line or capacitor bank side) and a 1-cos type voltage, which is the difference between  $U_T$  and the voltage  $U_S$  of the power supply side, which appears as the inter-electrode voltage  $U_{CB}$  of the circuit breaker. Because an interrupting current is small compared with a short-circuit current and ground fault current, a current interruption may be completed even when the breaker poles are not sufficiently opened. If a high recovery voltage occurs in such a state, it may exceed the dielectric strength between the poles of the circuit breaker, leading to the possibility of a re-ignition. In particular, when the breaker re-ignites near the crest value of the inter-electrode voltage, a very high overvoltage may occur, and caution is therefore necessary. Here, it is assumed that the circuit breaker installed on the tertiary side of substation T cuts off the capacitor bank connected at that end.

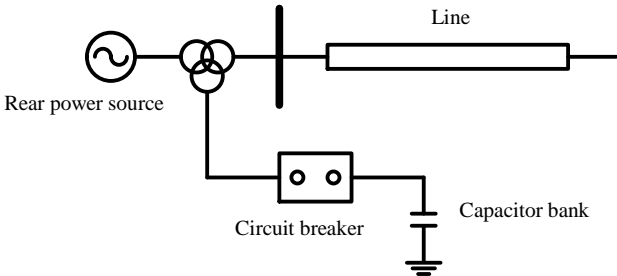


Figure 3 Illustration of capacitive current switching

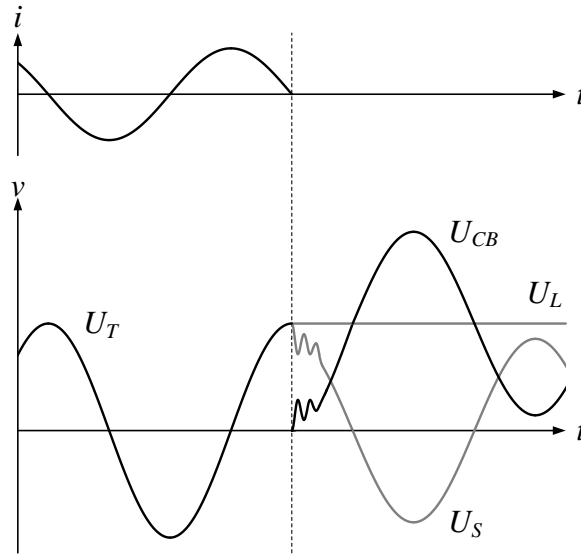


Figure 4 Illustration of TRV waveform of capacitive

[Power Supply Simulation]

Based on [1], the power source, resistance, and inductance of the primary side of substation T; the secondary side of substation T-1; and the secondary side of substation T-2 were set to match the short-circuit current values. Because the power factor of the power supply circuit is not known, the resistance and inductance were adjusted such that the decay time constant of the DC component ( $\tau = L / R$ ) will be 45 ms. In addition, the resistances and capacitances were inserted in parallel such that the TRV of the blocking first phase corresponds to JEC-2300-2010.

[Transformer Simulation]

The capacity, winding resistance, and leakage inductance were set based on [2], and the capacitance was set based on [3]. The neutral point is directly grounded on the 275-kV side and resistance grounded on the 154- and 77-kV sides.

[Line Simulation]

The type of electric wire used was determined based on the data of the 154-kV standard transmission line listed in [4].

A 810 mm<sup>2</sup> TACSR wire was used for the power lines (two conductors) and a 90 mm<sup>2</sup> AC wire was used for the overhead ground wire, the ground resistivity of which was 100 Ωm. The simulation was conducted using a frequency-dependent line model, the sample range of which was 0.1 Hz to 10 MHz, and the samples size was 400.

[Busbar Simulation]

Because the ground capacitance of individual devices was not known, each bus was collectively provided with a ground capacitance of 40,000 pF.

[Capacitor Bank Simulation]

A 60-MVA capacitor bank was installed in the tertiary circuit of the transformer of substation T. In line with JIS C 4902 (1998) “High pressure and special high-voltage phase advancing capacitor and accessory equipment,” a 6% series reactor was also installed for the capacity of the capacitor bank.

[Analysis Conditions]

The analysis conditions are shown in Table 1.

Table 1 Analysis conditions

	Analysis of Break Terminal Fault interruption	Analysis of capacitive current switching
Increment in calculation time	0.1 $\mu$ s	1 $\mu$ s
Calculation start time	0 ms	0 ms
Calculation end time	200 ms	100 ms
Display start time	40 ms	20 ms
Display end time	160 ms	80 ms

[Example of XTAP Input]

An illustration showing the creation of this example using XTAP is provided in Figure 5.



## Analysis Results

First, the analysis of a BTF interruption in a line from substation T to substation T-1 was carried out. Let us consider a case in which a short-circuit failure occurs at 50 ms in a one-line three-phase ground fault near substation T, and the circuit breaker of the substation opens at 150 ms. Figure 6 shows the current waveform of the circuit breaker, and Figure 7 shows the TRV waveform of the first phase of interruption (c phase). The TRV was a four-parameter waveform of multiple frequencies, where the crest value  $u_c$  was 249 kV, and the crest time  $t_2$  was 307  $\mu$ s.

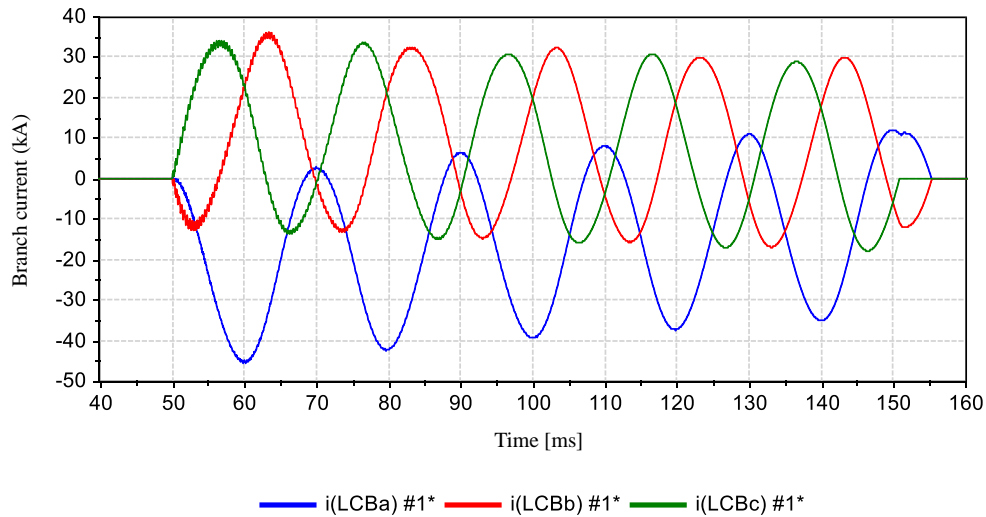


Figure 6 Current waveform of circuit breaker

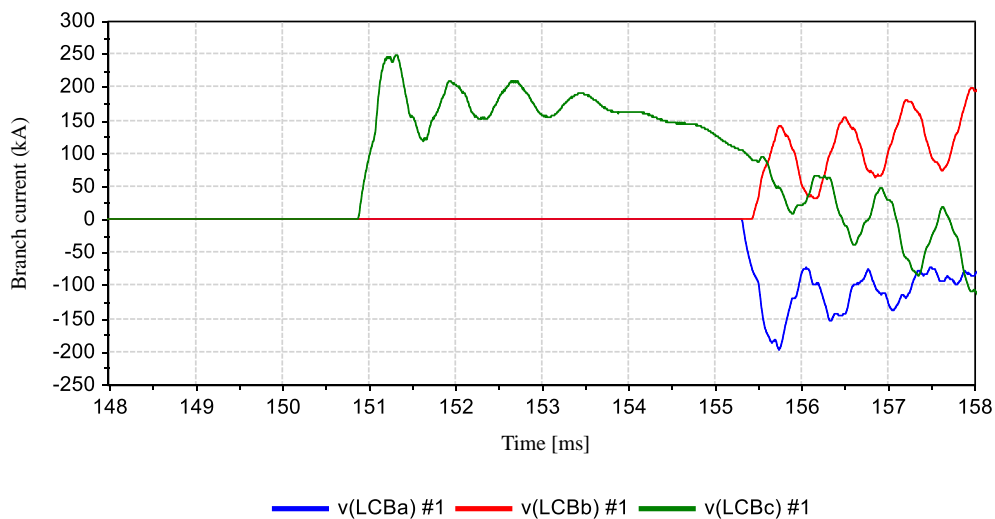


Figure 7 TRV waveform at the time of BTF interruption

Next, an analysis of the capacitive current switching in the tertiary circuit of the transformer of substation T was conducted. We considered a case in which the circuit breaker on the tertiary side of the transformer opens at 50 ms and interrupts the current flowing through the capacitor bank. Figure 8 shows the current waveform flowing through the circuit breaker, and Figure 9 shows the TRV waveform generated in the circuit breaker. The breaking current was 719 A. The TRV crest value of the first phase of interruption (c phase) is 64.2 kV, which is 2.40-times higher than the ground voltage crest value, namely, 26.8 kV, of the tertiary circuit of the transformer.

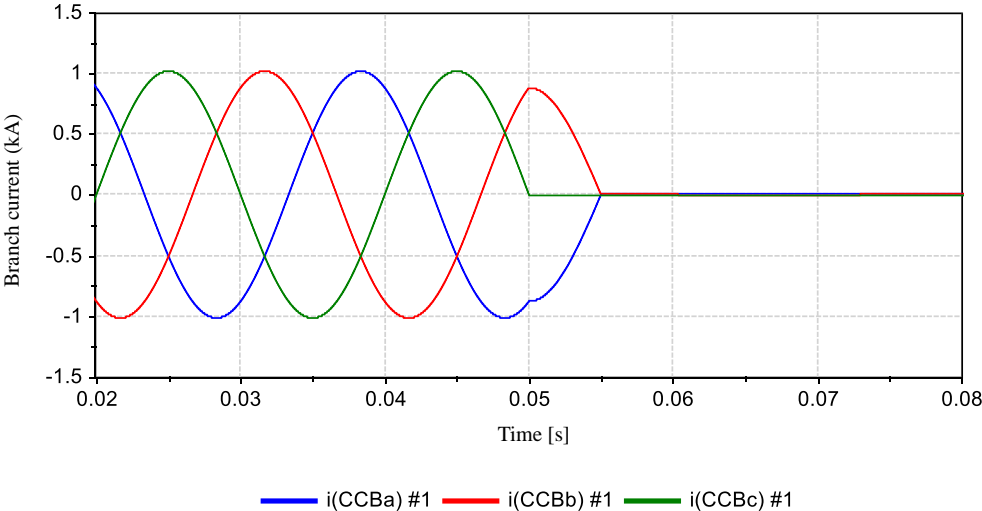


Figure 8 Current waveform at the time of capacitive current switching

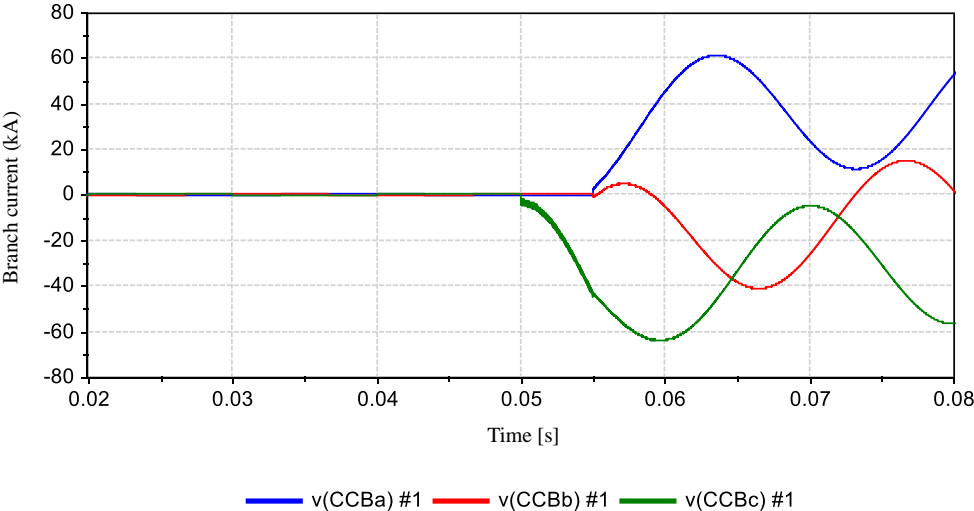


Figure 9 TRV waveform at the time of capacitive current switching

## References

- [1] IEEE Working Group 15.08.09, "Modeling and analysis of system transients using digital programs," IEEE PES Special Publication, TP-133-0, 1998
- [2] Japan Electrical Engineers Association Home Page, <http://www.jeea.or.jp/course/contents/03102/>, as of January 2013
- [3] Modeling research committee for sophistication of lightning surge evaluation of The Institute of Electrical Engineers, "Modeling for Sophistication of Lightning Surge Evaluation," Technical Report of The Institute of Electrical Engineers of Japan, No. 704, November 1998
- [4] Lightning Protection Design Committee, Power Generation and Transformation Subcommittee, "Lightning Protection Design Guide on Transformer Substation and Underground Transmission Line," Central Research Institute of Electric Power Industry Report General Report, T 40, December 1995

End

Change log		
Date	Example file version	Content changes
2015/07/29	2.1	Name of example changed from STRV-01 to CB-02 Fixed bugs in three-phase three-wire transformer
2014/11/19	2.0	Recalculated line constant consequent to change of XTLC
2013/08/08	1.0	First edition created (for XTAP Version 1.21)

XTAP Example Collection		No.	SLD-01
Example Name	Flashover Analysis of 6.6-kV Distribution Line		
Field	Lightning surge analysis, overvoltage analysis		
References	<p>For general information on the lightning protection design of medium-voltage lines, refer to the following.</p> <ul style="list-style-type: none"> <li>➤ “Distribution Line Lightning Protection Design Guide,” Comprehensive Report T69, Central Research Institute of Electric Power Industry</li> </ul> <p>For information on the analytical model of concrete poles, refer to the following.</p> <ul style="list-style-type: none"> <li>➤ “Development of Distribution Line Lightning Surge Analysis model for Steep Wave Lightning Current,” Research Report H07002, Central Research Institute of Electric Power Industry</li> </ul>		
Outline	<p>Flashover may occur due to lightning overvoltages caused by direct lightning strikes on medium-voltage distribution lines. Hence, it is necessary to protect the medium-voltage distribution line from lightning by effectively installing lightning protection equipment, such as an overhead ground wire and surge arrester. In this example, we show the lightning surge analysis model to calculate the overvoltage across the insulators when lightning directly strikes a medium-voltage power distribution line with the overhead ground wire.</p> <p>With XTAP, because the concrete pole, phase conductor, pole-mounted transformer, and other models necessary for a lightning surge analysis of power distribution lines are registered as components, through their combination, a lightning surge analysis of medium- and low-voltage power distribution lines becomes possible.</p>		

## Analysis Circuit and Conditions

Figure 1 shows the analysis circuit and arrangement of each conductor. The analysis line is a single-circuit 6.6 kV medium-voltage distribution line with a diameter of 40 m. Both ends of the line are terminated with matching resistors to prevent the unintended reflection. The calculations assume a lightning strike on a utility pole located in the center of the line.

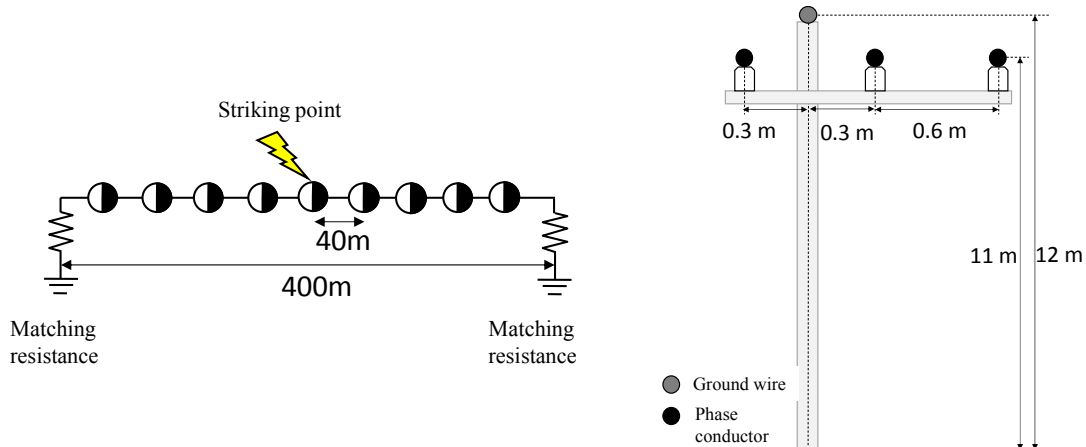


Figure 1 Topology of examined line.

Each equipment of the distribution line is modeled in the following way.

➤ Phase conductor

Calculate the line constants of each conductor shown in Figure 1 by means of XTLC, a line constant calculation program provided with XTAP.

For the case of focusing only on flashover, as in this example, the calculation frequency of the line constants can be set to about 100 kHz using the constant parameter distribution constant parameter line model (CP-Line), which is accurate enough for practical use.

In this example problem, the calculation frequency and ground resistivity are set to 100 kHz and 100  $\Omega\text{m}$ , respectively.

Note that in cases where a long calculation time is required, such as the surge arrester failure calculation, it is necessary to use the calculation using the frequency-dependent line model (FD-Line).

➤ Concrete pole model

For direct lightning surge analysis, the grounding conductor and the reinforcing bar of the concrete pole are often modeled by a single-phase lossless constant-parameter line model.

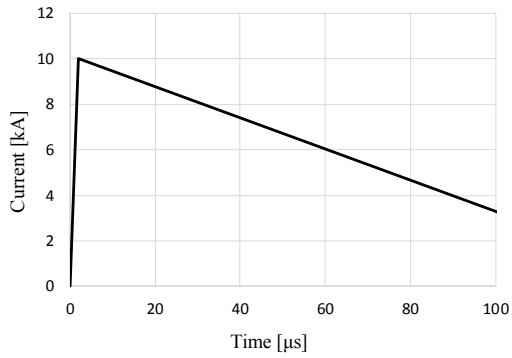
In this example, a constant parameter line model (CP-line) is used to simulate the surge impedance of the concrete pole and the grounding conductor

➤ Lightning current waveform

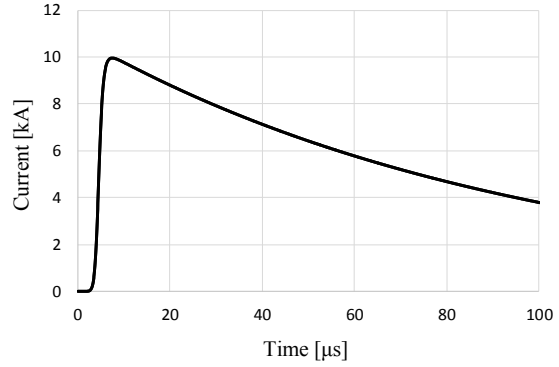
Lightning current waveforms are often modeled by a triangular waveform as shown in Figure 2(a). On the other hand, in recent research current waveforms represented by the Heidler function (Figure 2(b)), are also often used as a more realistic waveform.

Heidler function is expressed by the following function. ( $n=1$ ,  $\eta_1=0.92$ ,  $n_1=10$ ,  $\tau_1=4.6 \times 10^{-6}$ ,  $\tau_2=95.1 \times 10^{-6}$  in Figure 2(b) )

$$i(t) = \frac{I_{01}}{\eta_1} \times \frac{(t/\tau_{11})^{n_1}}{1 + (t/\tau_{11})^{n_1}} \exp(-t/\tau_{21}) + \frac{I_{02}}{\eta_2} \times \frac{(t/\tau_{12})^{n_2}}{1 + (t/\tau_{12})^{n_2}} \exp(-t/\tau_{22}) + \dots + \frac{I_{0n}}{\eta_n} \times \frac{(t/\tau_{1n})^{n_n}}{1 + (t/\tau_{1n})^{n_n}} \exp(-t/\tau_{2n})$$



(a) Triangular waveform



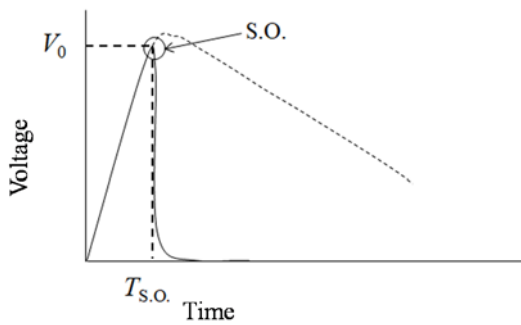
(b) Heidler function waveform

Figure 2 Lightning current waveform(Wavefront duration: 2  $\mu$ s, Wavetail duration: 70  $\mu$ s)

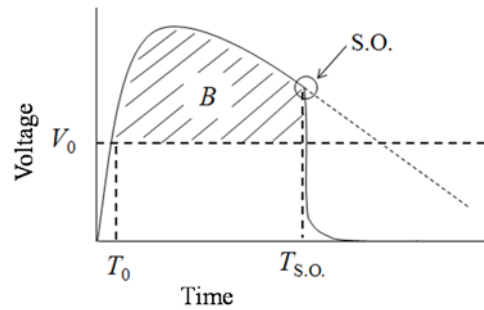
In this example, lightning channel impedance is assumed to be 1000  $\Omega$  in this example.

➤ Flashover of insulator

The integral method model is used in this example to simulate the flashover of a distribution insulator. In this model, flashover occurs when the integral value  $B$  of the portion of the voltage waveform generated in the insulator above  $V_0$  exceeds a threshold value. Although the integral method model is inferior to the constant voltage model in terms of simplicity, it is suitable for multiphase flashover analysis because it can take into account the influence of insulator voltage waveform. In this example, the flashover model constant ( $V_0 = 135$  kV,  $B = 0.065$ ) is set based on the lightning impulse test results.



(a) Constant voltage model



(b) Integral Method model

Figure 3 Overview of insulator flashover model

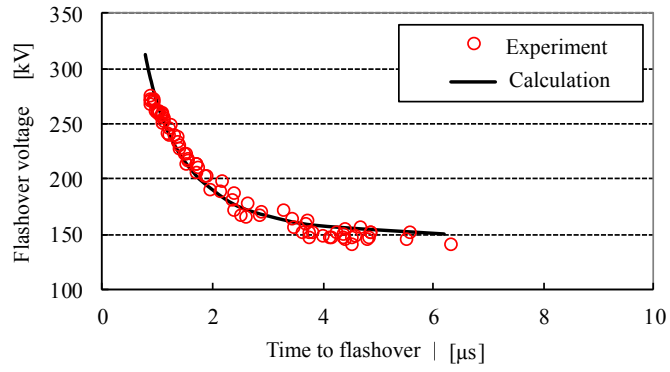


Figure 4 Example of  $V-t$  characteristics of a distribution insulator.

In this example, a surge arrester for medium voltage distribution line is represented by a nonlinear resistor with series gap. The discharge voltage of series gap is set to be 29 kV and the  $V-I$  characteristic of nonlinear resistor is set as shown in Figure 4.

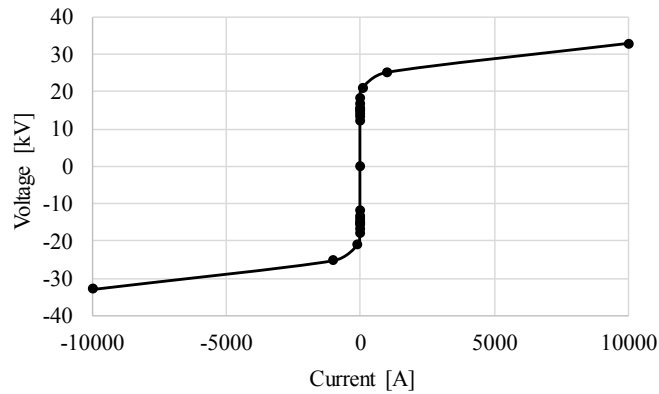


Figure 5  $V-I$  characteristics of surge arrester.

Figure 6 shows this example problem configured on XTAP under the above calculation condition.

Example Name : Flashover Analysis of 6.6-kV Distribution Line  
No. SLD-01

Waveform of lightning current: triangular waveform  
Flashover model: integration method model  
Surge arrester: installed

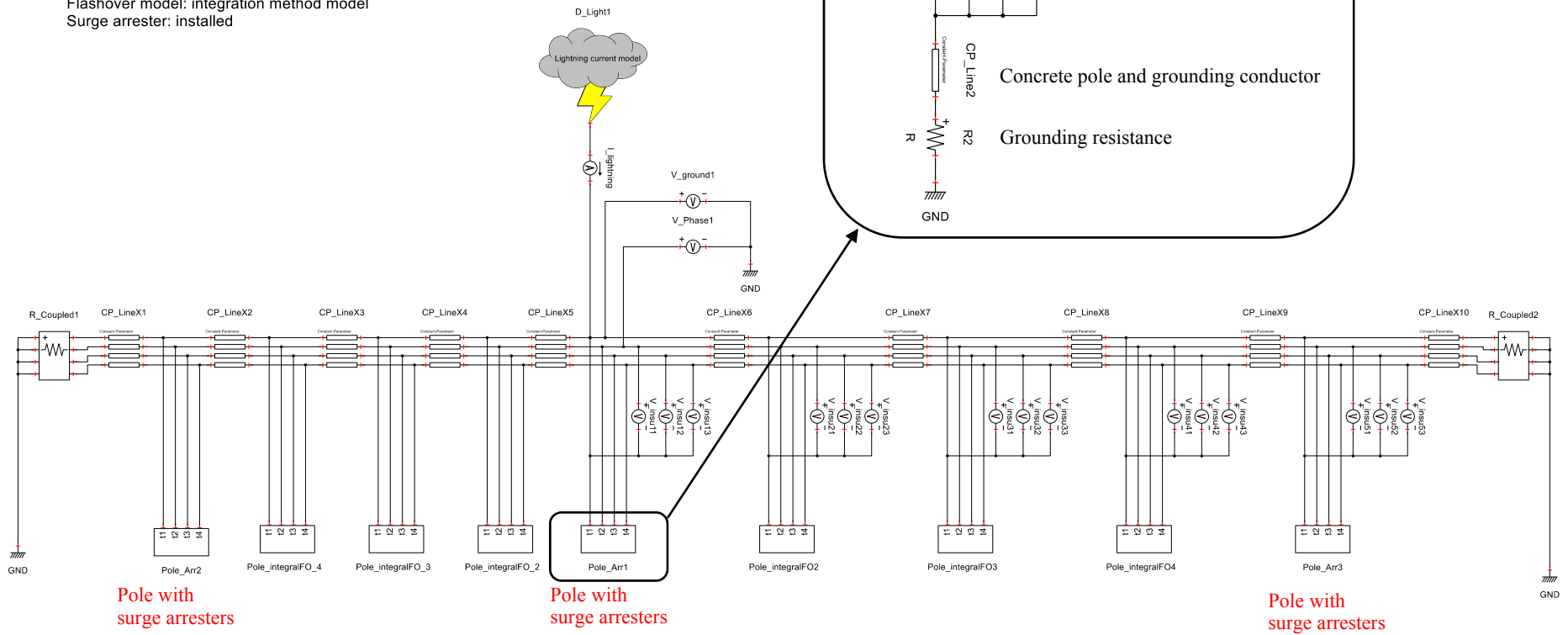


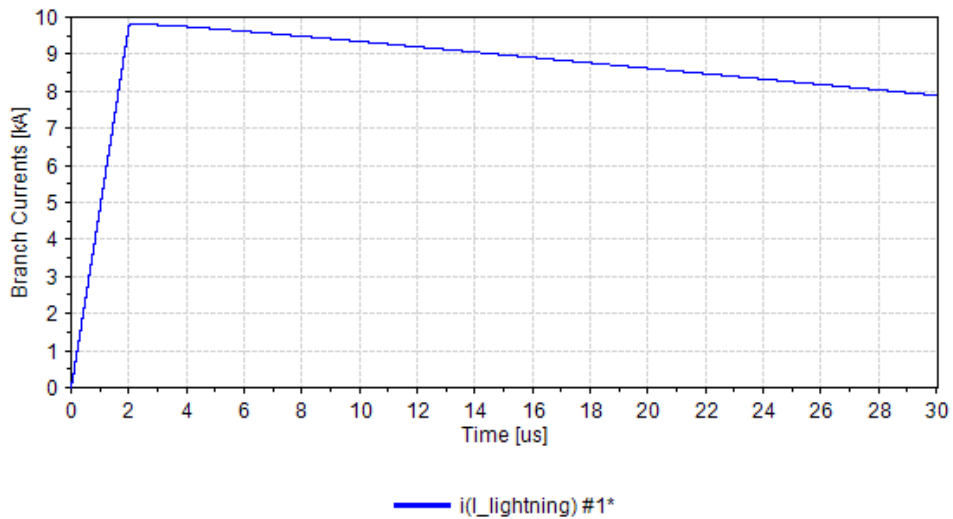
Figure 6 Overview of calculation model in XTAP.

## Calculation results

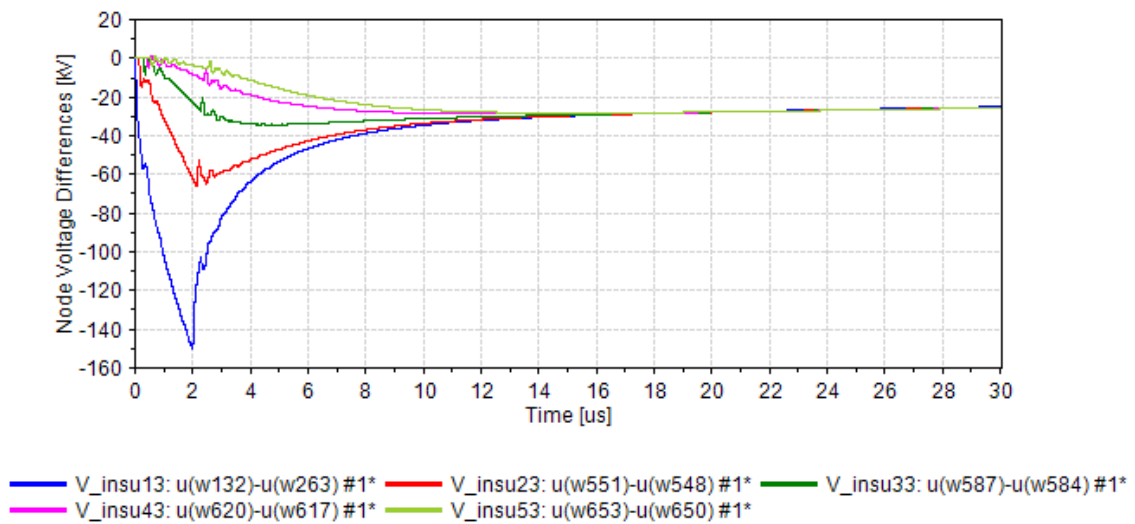
Figures 7 and 8 show the calculated results of the lightning current waveforms and the voltage across the insulators on poles 1 through 5. Figures 7(b) and 8(b) show the voltage between the insulators without surge arresters. The insulator voltage obtained by the triangular waveform is larger than the insulator voltage obtained by Heidler function waveform. From this, it can be understood that when evaluating the conservative side (where the insulator voltage is calculated to be larger), the strike current should be modeled as a triangular wave. As shown in Figs. 7(c) and 8(c), the insulator voltage at the lightning struck pole ( $V_{\text{insu13}}$ ) is suppressed by the installation of surge arresters.

Figure 9 shows the flashover voltage waveform when the lightning current is a triangular wave. The flashover current value increases from 15 kA to 50 kA due to the installation of surge arresters. Also, the location of the flashover point has changed from Pole No. 1 to Pole No. 3.

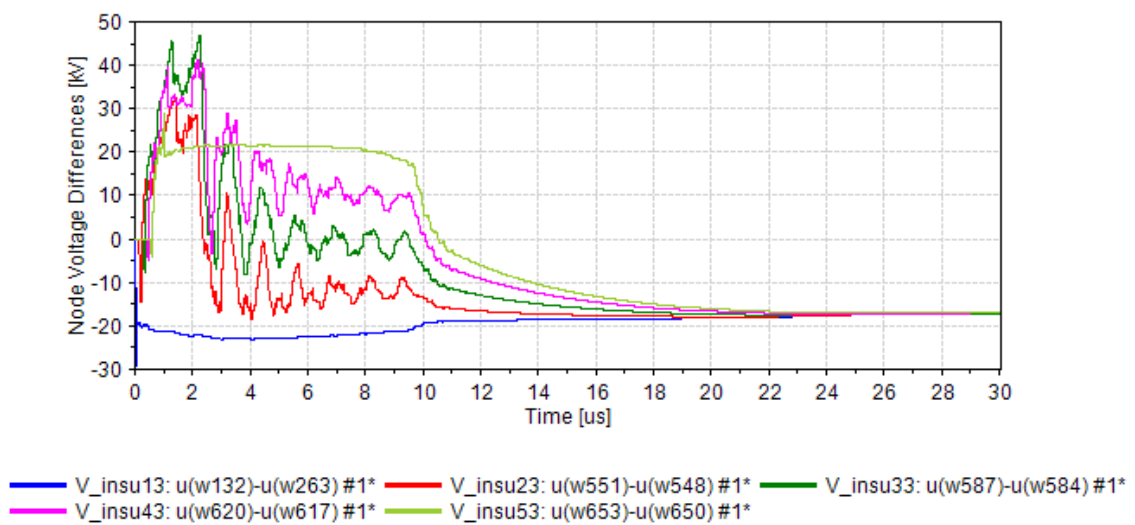
In this example, only 1-phase flashover is calculated, but since the 6.6 kV distribution line in Japan is an ungrounded neutral system, lightning outages do not usually occur with 1-phase flashover. For this reason, in lightning outage rate calculations, multi-phases flashover is often considered to be lightning outage.



(a) Lightning current waveform

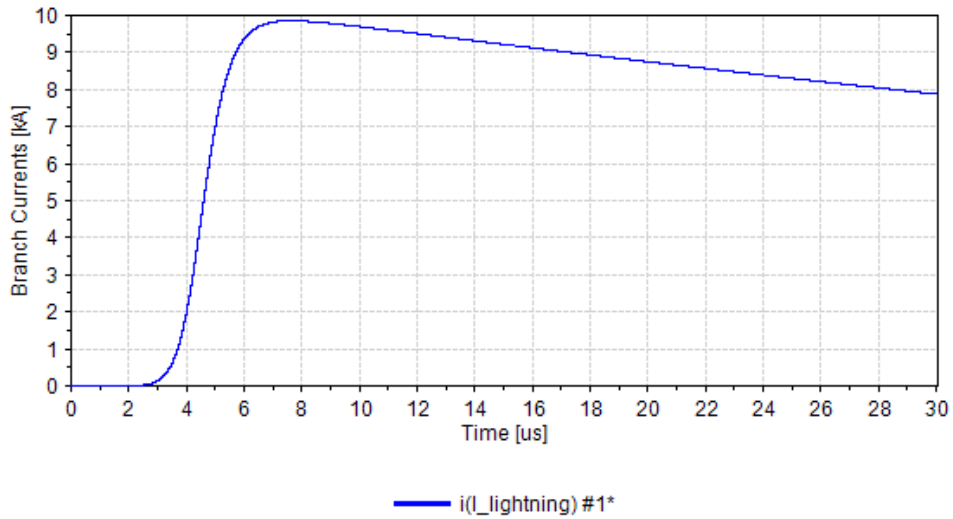


(b) Insulator voltage from Pole. No.1–No.5 (without surge arrester)

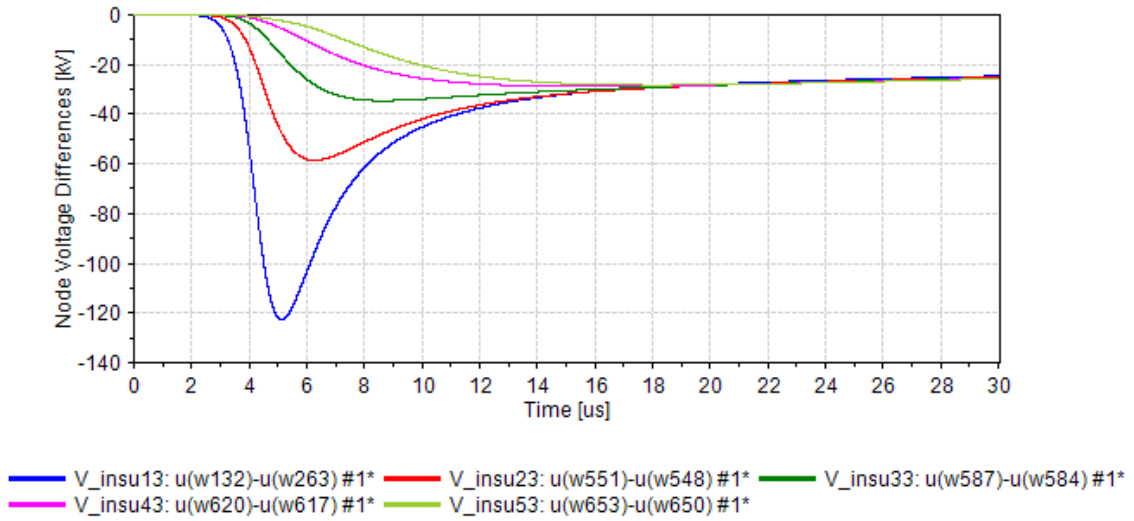


(c) Insulator voltage from Pole. No.1–No.5 (with surge arrester)

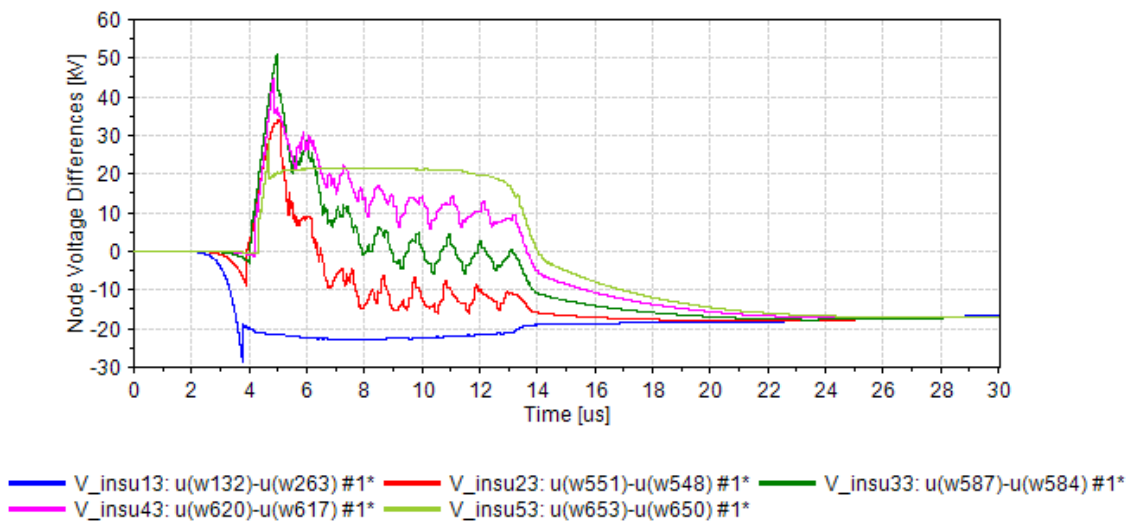
Figure 7 Calculation results obtained by the triangular lightning current waveform



(a) Lighting current waveform

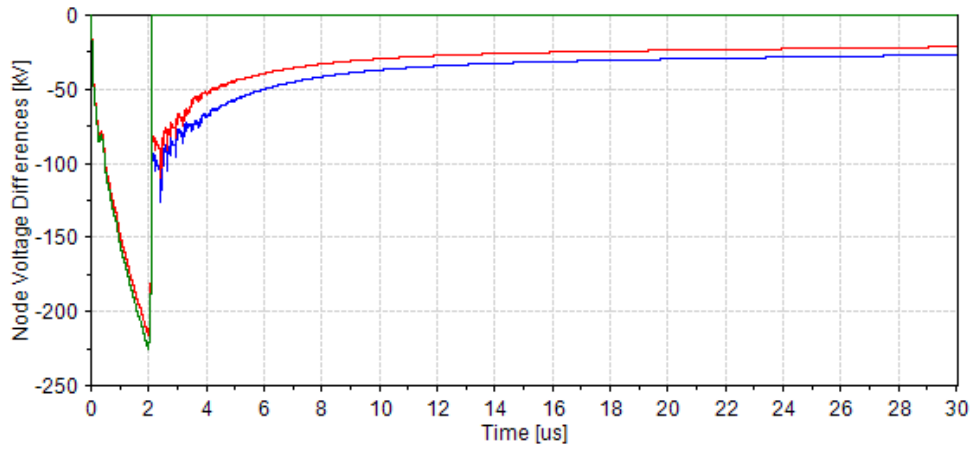


(b) Insulator voltage from Pole. No.1–No.5 (without surge arrester)



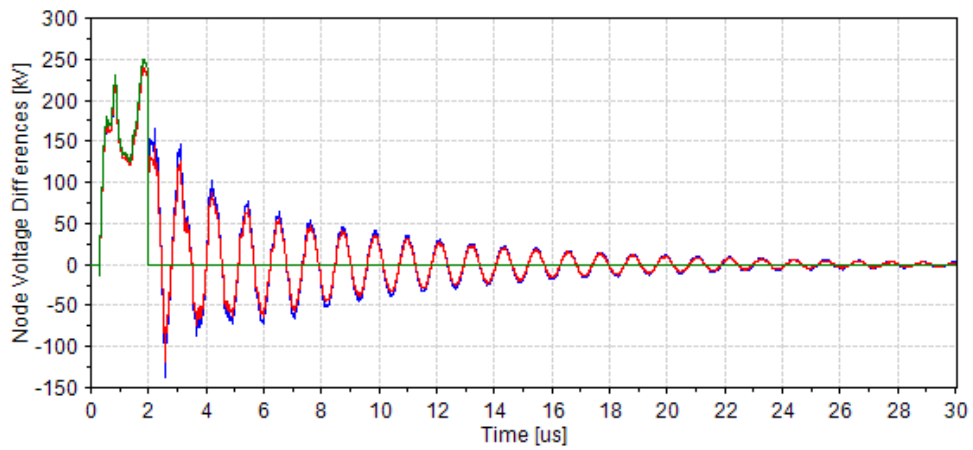
(c) Insulator voltage from Pole. No.1–No.5 (with surge arrester)

Figure 8 Calculation results obtained by the Heidler function lightning current waveform



— V\_ins11: u(w130)-u(w263) #1\* — V\_ins12: u(w131)-u(w263) #1\* — V\_ins13: u(w132)-u(w263) #1\*

(a) Case without surge arrester (Peak value of lightning current: 15 kA, Flashover at Pole No. 1)



— V\_ins31: u(w585)-u(w584) #1\* — V\_ins32: u(w586)-u(w584) #1\* — V\_ins33: u(w587)-u(w584) #1\*

(b) Case with surge arrester (Peak value of lightning current: 50kA, Flashover at No. 3)

Figure 9 Insulator voltage when the flashover occurs obtained by the triangular lightning current waveform.

END

Revision History		
Date	Example File Version	Content Changes
2022/12/13	2.1	Corrected the flashover current value to 50kA when lightning arrestors are installed.
2022/08/03	2.1	Revised example contents with addition of analytical models such as lightning current waveforms represented by Heidler functions and a flashover model represented by the integration method.
2014/11/19	2.0	Update for XTAP Ver. 2.00 Recalculation of line constants following the change in XTLC
2012/08/30	1.2	Update for XTAP Ver. 1.20
2011/09/08	1.0	Creation of first edition (for XTAP Ver. 1.11)

XTAP Example Collection		No.	SLD-02
<b>Example Name</b>	Lightning Surge Aspects Occurring in Secondary Side of a Pole-mounted Transformer During Lightning Strike on a Distribution Line		
<b>Field</b>	Lightning surge analysis, overvoltage analysis		
<b>References</b>	<p>For information on the analytical models of pole-mounted transformers, service lines and indoor wiring, see the following.</p> <ul style="list-style-type: none"> <li>· Honda, Noda, Asakawa, Shindo, Yokoyama, Abiko, “Improvements to a Transient Simulation Model of Pole-Mounted Distribution Transformers,” Journal of the Institute of Electrical Engineers of Japan, B, Vol. 124, No. 9, pp. 1169-1176 (2004)</li> <li>· Matsuura, Noda, Nakamura, Sakai, “Modeling of Service Drop-Wires and Interior Wiring Cables for Lightning Surge Analysis,” Journal of the Institute of Electrical Engineers of Japan, B, Vol.130, No. 2, pp. 246-258 (2010)</li> </ul>		
<b>Outline</b>	<p>With the recent progress of our highly information-oriented society, damage to consumer equipment from lightning is on the rise. Even in power distribution systems, the number of electronic devices that are driven at low voltages is increasing. It is therefore important to accurately grasp the aspects of a lightning overvoltage (current) occurring in low-voltage distribution lines and consumer appliances after the watt hour meter (WHM) at the time of a lightning strike on a distribution line. In this example, we calculate the lightning overvoltage occurring on the WHM and the lightning current flowing into consumer appliances when lightning directly hits a distribution line.</p> <p>With XTAP, because the power line, pole-mounted transformer, and other models necessary for a lightning surge analysis of low-voltage distribution lines are registered as components, through their combination, a lightning surge analysis of low-voltage distribution lines becomes possible.</p>		

## Analysis Circuit and Conditions

In this example, we examine the occurrence of a lightning surge on the secondary side of a pole-mounted transformer when a lightning strike occurs on a concrete pillar equipped with a pole-mounted transformer. It should be noted that, despite there being two types of grounding methods for pole-mounted transformers and lightning arresters, namely, “individual grounding” in which each grounding is separately secured, and “shared grounding” in which the grounding is combined, herein, we examine “shared grounding” only.

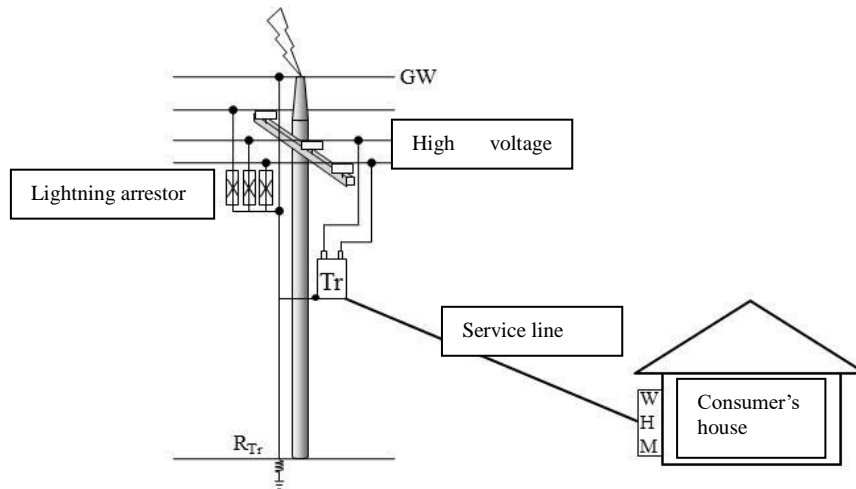


Figure 1 Conceptual diagram of lightning surge analysis from the secondary side of pole-mounted transformer

### · Analytical Model of Concrete Pillar

In the lightning surge analysis of a distribution line, because a concrete pillar and pulled grounding line are often regarded as a single conductor, they are usually simulated using a constant single-phase distributed line. In this study, we adopt a simple concrete pillar model in which a constant single-phase distributed line is divided into three positions (pole head, high-voltage cross-arm, and pole-mounted transformer equipment positions). (Because a concrete pillar model capable of accurately calculating the lightning over-voltage of a high-voltage distribution line up to the order of  $n$  seconds is registered in XTAP, its use is sufficient when calculating high-voltage distribution lines only.)

Further, for overhead ground lines and high-voltage distribution lines, a model that calculates the line constants with the arrangement shown in Figure 2 is generally prepared, and can be used in the calculations by simply determining the line length.

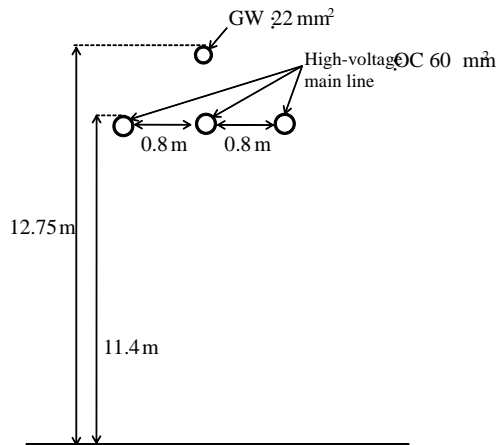


Figure 2 Conductor arrangement in high-voltage distribution line

· Analytical Model of a Pole-mounted Transformer

For pole-mounted transformers, an analytical model that can accurately calculate the transition voltage from the primary side to the secondary side has been prepared in XTAP (there are two types of models with different winding structures). The pole-mounted transformer model has connection points at the primary side terminal, secondary side terminal, and the chassis ground, and can be used in the calculations by simply connecting them.

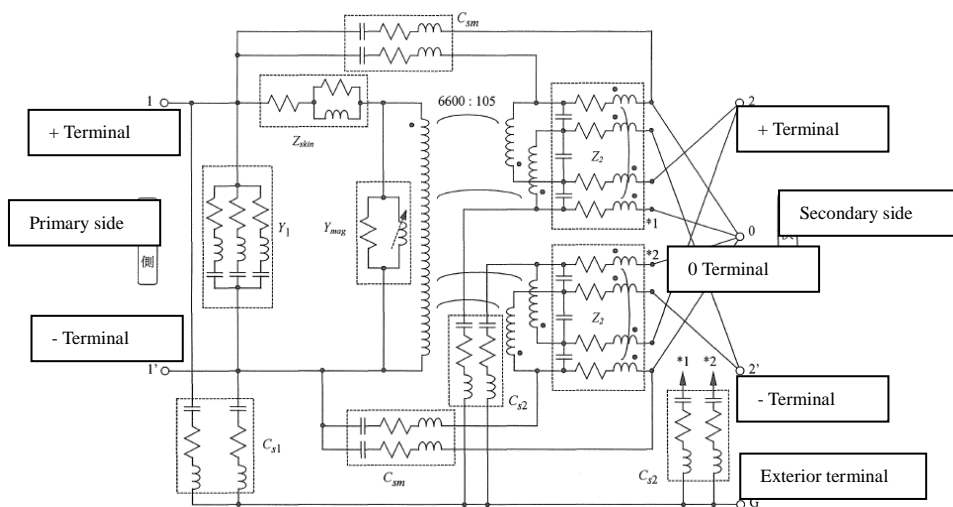


Figure 3 Example of the analytical model of pole-mounted transformer

· Analytical Model of Service Line and Indoor Wiring

In the DV electric wires used for service lines and VVF cables used for indoor wiring, because the distance between conductors is small, the mutual coupling becomes strong. It is therefore difficult to obtain the accurate values of the line constants through a simple calculation using XLTC. In XTAP, a service line model in which the line constants are obtained when considering this mutual coupling has been prepared and can be used for the calculations by simply determining the line length.

· Analytical Model of WHM

There are two types of WHM: mechanical and electronic. Between them, a mechanical WHM is usually omitted because it does not have an influence on the lightning surge analysis. In contrast, in an electronic WHM, a varistor (ZnO lightning protection element) is installed between the lines, and is often simulated by simply inserting a non-linear resistance between the lines simulating the V-I characteristics. In this example, both mechanical and electrical WHMs are studied.

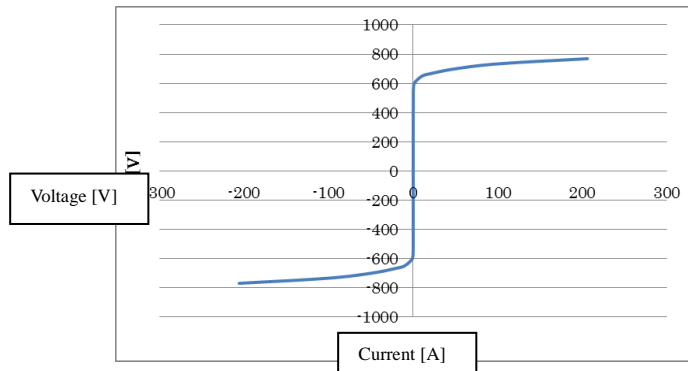
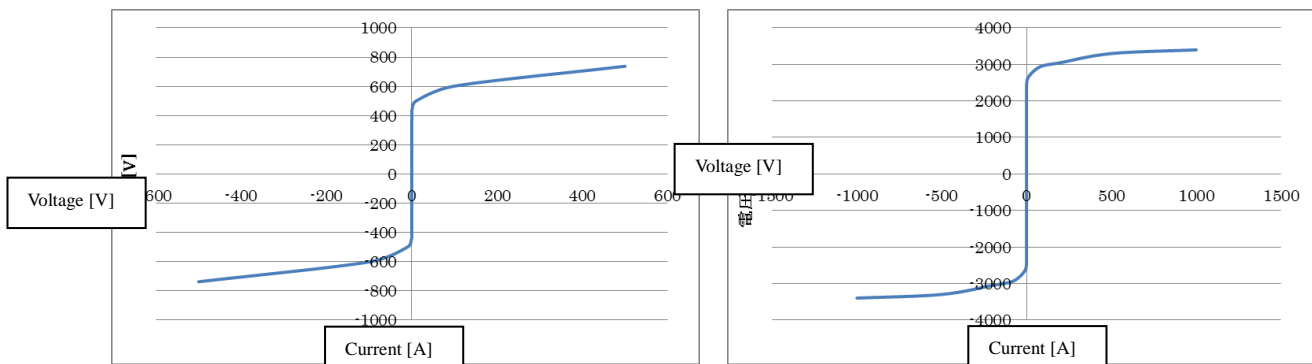


Figure 4 Example of V-I characteristics of varistor between the lines of electronic WHM

· Analytical Model of Consumer Home

Because the detailed circuit of a consumer home is unknown in most cases, it is difficult to create a standard model. Hence, in this analysis, as a simplified simulation, we conducted the calculation by assuming a house connected to two grounding devices (an air conditioner and a washing machine, namely, an inter-line varistor and a ground varistor) at the end of a VVF cable (10 m).



(a) Inter-line varistor

(b) Ground varistor

Figure 5 Example of the V-I characteristics of varistor used in consumer equipment

- Other Analysis Conditions
- Lightning current:  $1/70 \mu\text{s}$  Ramp wave, Crest value: 10 kA, Lightning impedance:  $1000 \Omega$
- Ground resistance of the lightning arrester:  $30 \Omega$  (in a lightning-struck pillar, the grounding of the lightning arrester and pole-mounted transformer is shared)
- Calculation step time: 1 ns
- Calculation start time:  $0 \mu\text{s}$

- Calculation end time: 10  $\mu$ s

Figure 6 shows the construction of this example using XTAP under the above conditions.

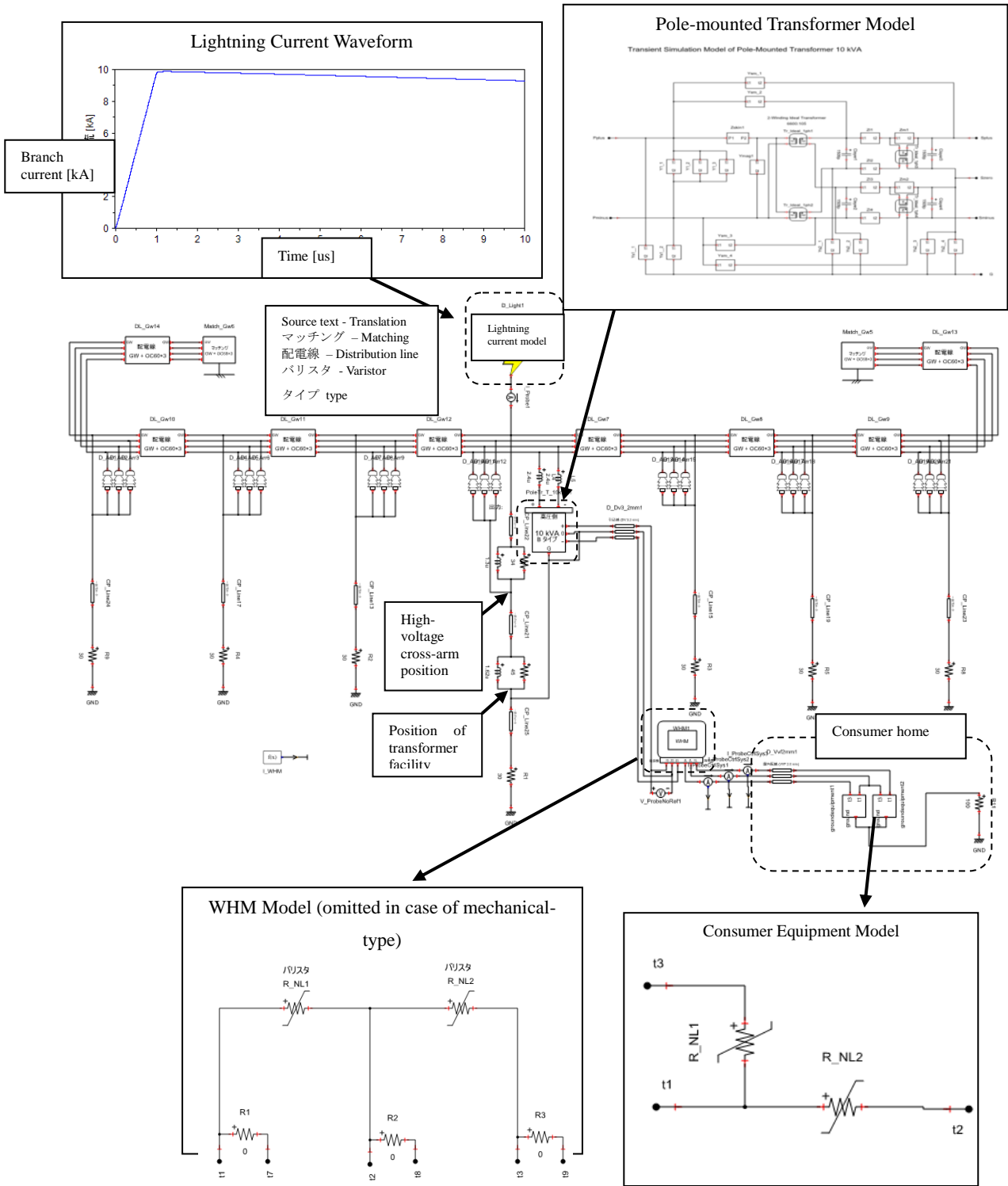
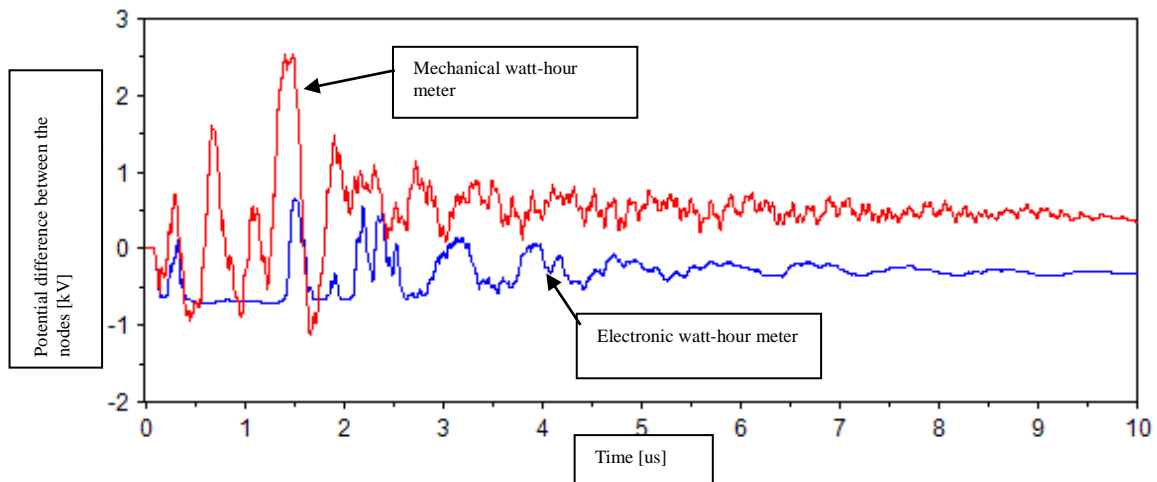
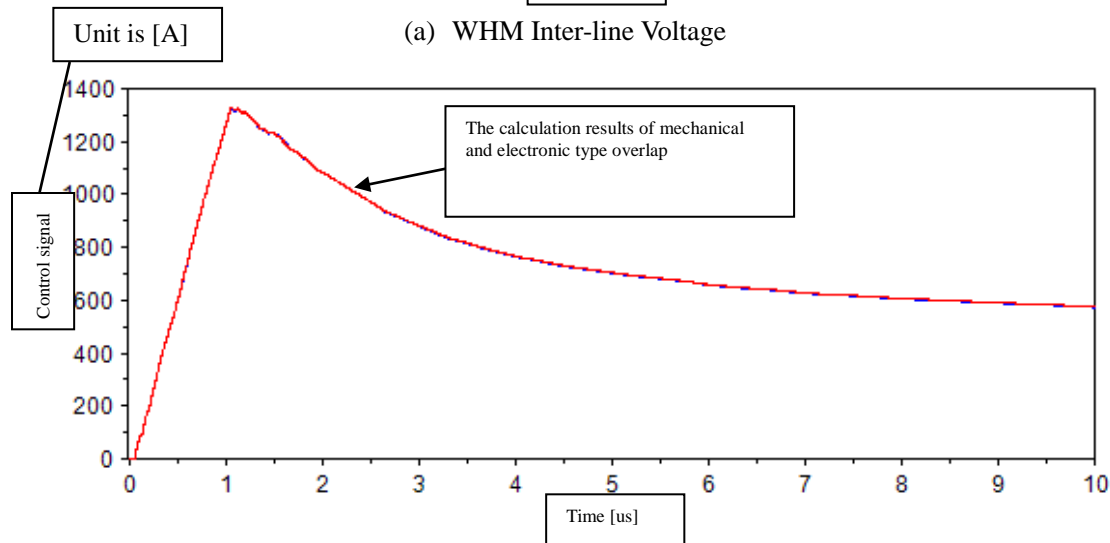


Figure 6 Example of XTAP input

## Analysis Results



(a) WHM Inter-line Voltage



(b) Current flowing into the consumer home (three lines together)

Figure 7 Analysis results using XTAP

From the calculation results, it can be seen that with an electronic WHM, the lightning overvoltage generated between lines can be suppressed to the limit voltage by the varistor. However, unlike conventional mechanical measuring instruments, because electronic WHMs have inbuilt circuit boards such as a CPU that are vulnerable to lightning (see the references below for examples), from this result alone, it cannot be stated that the lightning protection performance of electronic instruments is better than that of mechanical instruments; rather, it is necessary to examine factors other than the overvoltage (induction voltage generated inside the instrument) obtained from the circuit calculation.

· Studies on the Lightning Protection Performance of Electronic Watt-hour Meters

Asakawa, Furukawa, Takahashi, Ishimoto: "The Factors and Counter Measures of Failures in Electronic Watt-Hour Meters Caused by Lightning: An Experimental Study on Electromagnetic Interference Prevention Method," Journal of the Institute of Electrical Engineers of Japan, B, Vol. 131, No. 9, pp. 793-800 (2011)

END

Revision History		
Date	Example File Version	Content changes
2014/11/19	2.0	Revision for XTAP Version 2.00
2012/10/03	1.1	Correction owing to an error in the simulation method of electronic instruments
2012/09/18	1.0	Creation of first edition (for XTAP Version 1.20)

<b>XTAP Example Collection</b>		<b>No.</b>	SLS-01
<b>Example Name</b>	Lightning Surge Calculation of 500-kV Air-insulated Substation		
<b>Field</b>	Lighting surge analysis of substations, overvoltage analysis		
<b>References</b>	Central Research Institute of Electric Power Supply Industry, Comprehensive Report T40, “Lightning Protection Design for Power Stations, Substations, and Underground Transmission Lines”		
<b>Outline</b>	<p>A lightning surge overvoltage is one of the important factors in the insulation design of transmission lines and power generation substation equipment.</p> <p>In this example, we calculate the surge propagation pattern for the case of a lightning strike occurring on the first steel tower of a 500-kV air-insulated substation (the first tower when viewed from the substation) and the lightning current entering the power line from a reverse flashover, until it reaches the main transformer in the substation. This corresponds to the first case (circuit symbol A) of Table III-3-1 (p.84) of the lightning protection design guide mentioned in the reference column above. The modeling methods for all equipment in the substation, the transmission lines, and the system voltage are as recommended by the lightning protection design guide (however, for the transmission line, a fixed constant line model is used instead of a frequency-dependent line model).</p> <p>For XTAP Ver. 1.11, all models described in the lightning protection design guide are provided as components (which can be downloaded from the support site) for each voltage class, and in Ver. 1.2 and later, they are expected to become standard equipment. By combining these components, it is possible to easily create data cases for a lightning surge analysis. In this analysis example, although only circuit symbol A of Table III–3–1 (p. 84) of the lightning protection design guide is described and provided as an example file SLS-01A.xsf, circuit symbols B through V are also provided as example files SLS-01B.xsf through SLS-01V.xsf.</p>		

## Analysis Circuit and Conditions

In this example, we calculated the surge propagation for a case of lightning striking the first steel tower of a 500-kV air-insulated substation, and the lightning current entering the power line from a reverse flashover reaching the main transformer in the substation.

Specifically, the first case (circuit symbol A) in Table III-3-1 (p. 84) of the lightning protection design guide mentioned in the reference column above is described as an example.

The first steel tower is the first tower when seen from the substation. Because the overvoltage in the substation becomes the most severe when a lightning strike occurs on this tower, for a typical analysis, a lightning strike of the first steel tower is assumed. Figure 1 shows the conceptual diagram of the lightning surge calculation in the air-insulated substation. From here, we describe the phenomenon until the lightning current reaches the main transformer, as shown in the figure.

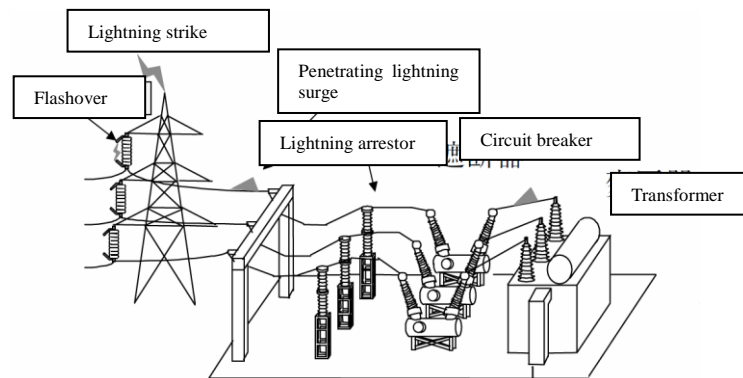


Figure 1 Conceptual diagram of lightning surge calculation in air insulated substation

### [Reverse Flashover Phenomenon]

As shown in Figure 1, if a lightning strike occurs on a steel tower, the potential of the body of the tower increases owing to the impedance of the steel tower itself (called the surge impedance of the tower) and the ground impedance of the tower-foot, and becomes higher than the potential of the power line. When the potential difference between the upper phase arm and the power line exceeds the flashover voltage of the arcing horn, a flashover occurs in the upper phase, and the lightning current penetrates the power line. Because a flashover occurs owing to the arm potential becoming higher than that of the power line, this is called a “reverse” flashover. In addition, because the flashover of an arcing horn is a phenomenon in which a discharge path is formed owing to a leader progressing between the horns, it occurs within a short time of microseconds or less. However, the horns will be gradually short-circuited within a finite time. It should be noted that, owing to the branching of the current into the overhead ground wire, the current entering the steel tower decreases, thus suppressing the potential increase of the steel tower. At the same time, the

lightning current branching toward the overhead ground wire increases the potential of the power line through electromagnetic induction, further suppressing the voltage between horns.

To accurately simulate the potential increase of a steel tower described above, a steel tower is simulated using a four-stage model created based on a comparison with the measurement results. The ground resistance is set to a severe condition of  $10 \Omega$ , which is the upper limit of the control value. The transmission line, including the overhead ground wire, is simulated using a distributed constant line model, and four spans between the first and fifth towers are simulated. For locations away from the fifth tower, a condition in which the line continues infinitely is simulated through matching with a polyphase resistance equivalent to the characteristic impedance (surge impedance) of the transmission line. Although the influence of steel towers far from the fifth tower is ignored, because the traveling waves propagated beyond the fifth steel tower never return through a reflection within the observation time, even if ignored, no influence on the analysis results will occur. Further, the system voltage is simulated by connecting a 500-kV three-phase voltage source through a polyphase resistor for matching. Because the system voltage influences the voltage between the upper-phase horns, it also influences the flashover. The flashover phenomenon is simulated through a smooth short-circuiting of the horns by connecting a leader model consisting of a combination of an inductance and a switch between the horns.

#### [Surge Propagation at the Substation]

The lightning current entering the power line owing to a reverse flashover becomes a traveling wave (surge) and propagates to the substation through the service line, as shown in Figure 1. In the substation, because lightning arrestors, circuit breakers, potential transformers, current transformers, and bushings are connected to the busbar, the traveling wave propagating through the busbar is influenced by the impedance of these devices, eventually reaching the main substation. Progressive wave components higher than the limit voltage are negatively reflected at the arrestors and positively reflected at the terminal end of the busbar. Further, in the potential transformers, current transformers, and bushings, only a steep portion of the waveform is negatively reflected owing to the capacitance. Thus, a complex reciprocal reflection phenomenon occurs on the busbar. It should be noted that, a portion of the lightning current branches toward the overhead ground wire at the top of the first steel tower, which travels up to the anchoring steel at the entrance of the substation and becomes negatively reflected.

The busbar is simulated using a single-phase distributed constant line, and the lightning arrestor is simulated using a nonlinear resistance having its voltage–current characteristics ( $v$ – $i$  characteristics). The electrostatic capacitances of the potential transformers, current transformers, bushings, and main transformer are simulated along with the capacitance. Although a transformer is often considered to experience inductance, when conducting an analysis on the order of microseconds, such as a lightning surge analysis, the impedance of inductance  $\omega L$  becomes an extremely large value, which can be ignored, and the inductance of the capacitance  $1/\omega C$  between the windings and iron core, and between the windings, becomes relatively small and thus dominant. This capacitance is called the penetration capacity of the transformer. The circuit breaker is simulated as a short distributed constant line if it is in a closed state and

simulated with a capacitance in an open state. The anchoring steel is also simulated as a distributed constant line.

#### [Modeling Details]

For the modeling details, refer to the lightning protection design guide (however, for the transmission line, a fixed parameter line model is used instead of a frequency-dependent line model)

#### [Analysis Conditions]

The analysis conditions are as follows.

- Calculation time step            1.0 ns
- Calculation end time            10.0  $\mu$ s
- Display start time                0.0  $\mu$ s
- Display end time                 10.0  $\mu$ s

#### [Example of XTAP Input]

An instance of creating this example using XTAP is shown in Figure 2.

## Analysis Results

The results of executing this example using XTAP are shown in Figures 3 and 4.

## Remarks

In this analysis example, although only the case of the circuit symbol A of Table III-3-1 (p. 84) of the lightning protection design guide mentioned in the reference column is explained and provided as the example file SLS-01A.xsf, note that the cases of circuit symbols B through V are also provided as example files SLS-01B.xsf through SLS-01V.xsf.

END

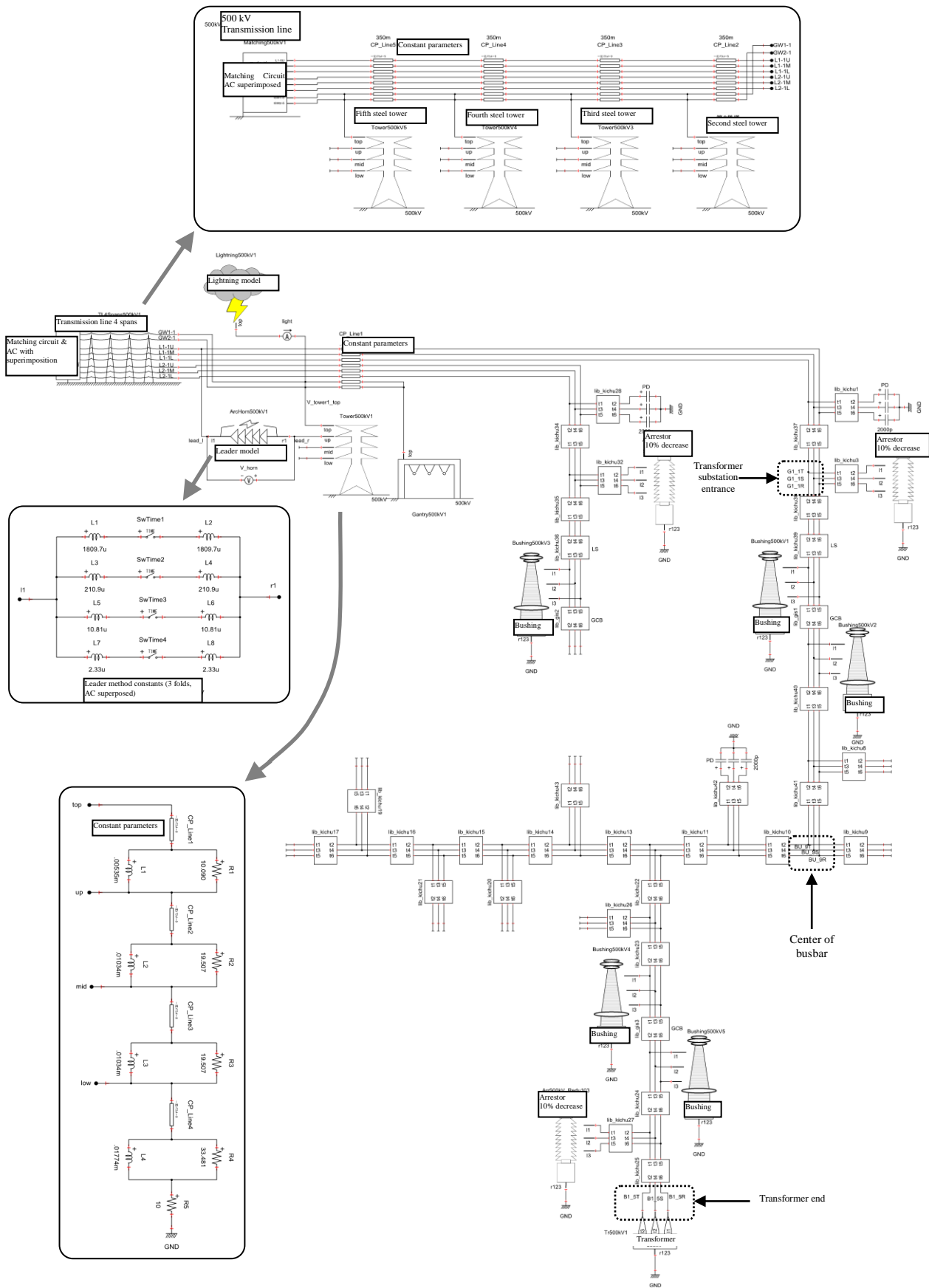
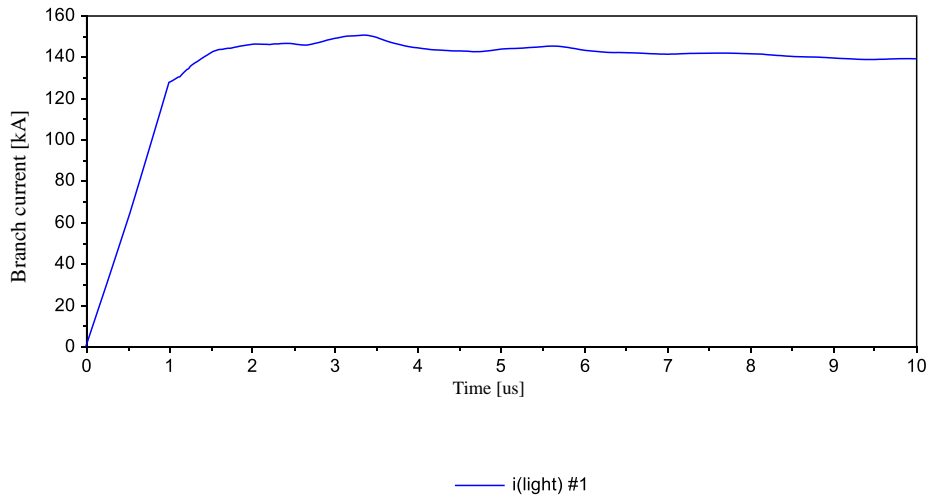
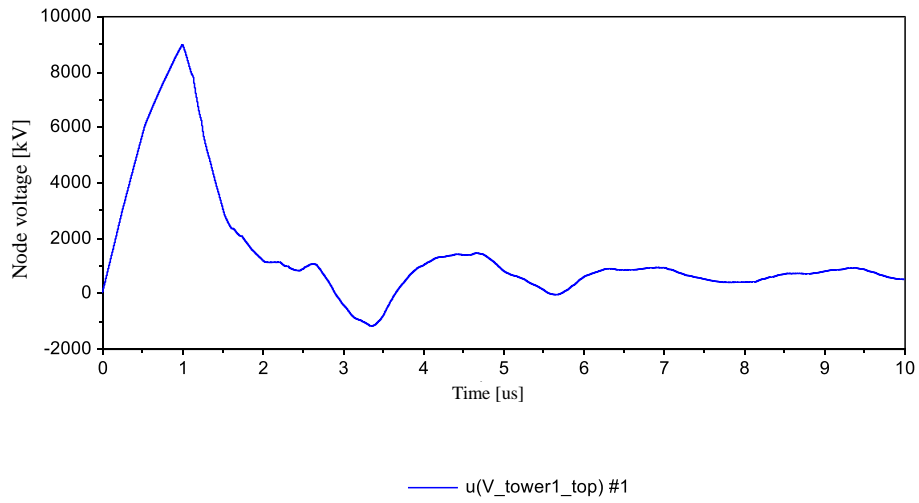


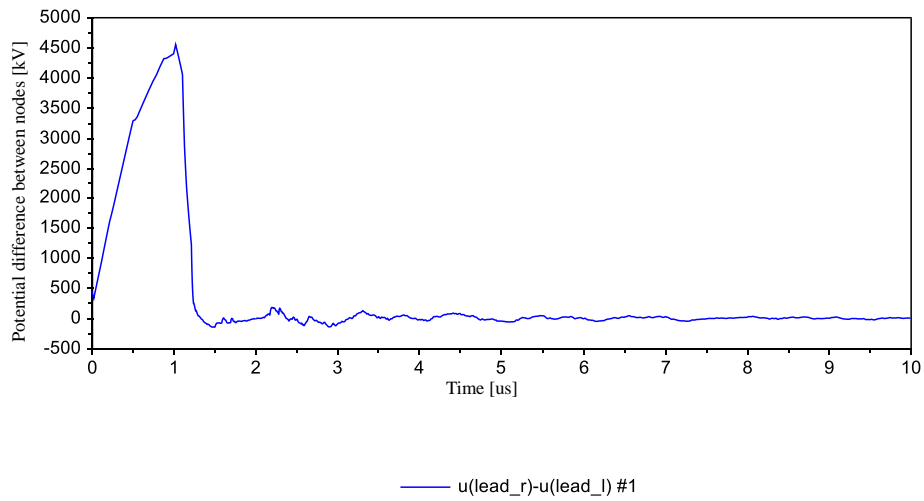
Figure 2 Example of XTAP input



(a) Lightning current waveform

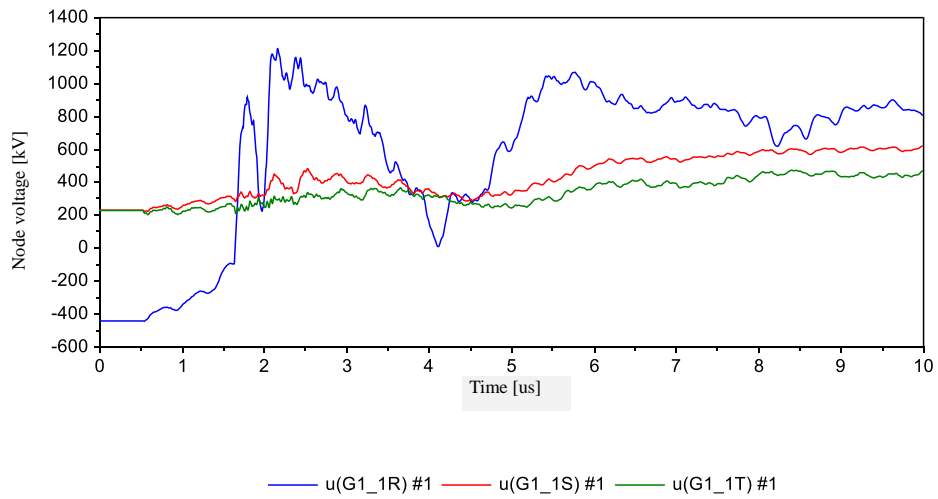


(b) Tower-top potential rise waveform

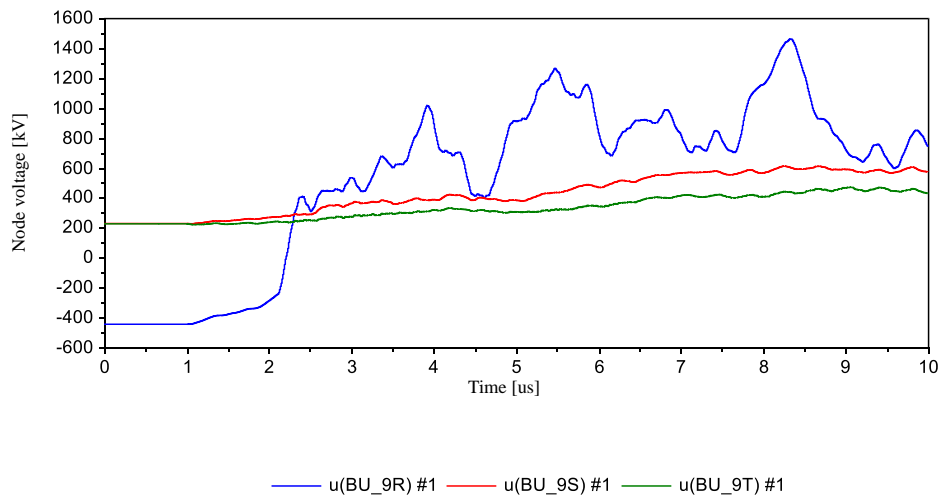


(c) Waveform of voltage between horns

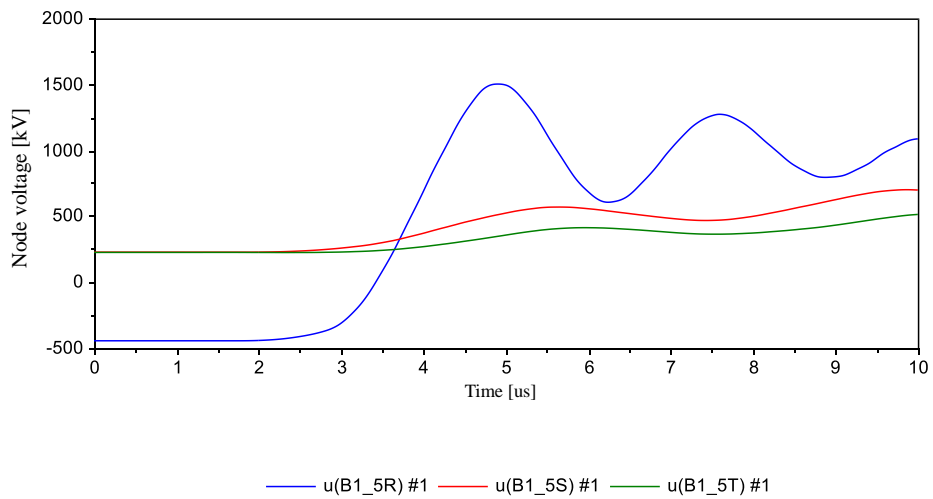
Figure 3 Results of analysis using XTAP (part 1)



(a) Busbar voltage waveform (substation entrance)



(b) Busbar voltage waveform (center of the bus)



(c) Busbar voltage waveform (transformer end)

Figure 4 Results of analysis using XTAP (part 2)

Revision History		
Date	Example File Version	Content changes
2014/11/19	2.0	Revision for XTAP Ver. 2.00 Recalculation of line constants according to the changes in XTLC
2012/07/19	1.2	Revision for XTAP Version 1.20
2011/12/15	1.1	Revision of explanation (addition of cases for circuit symbols B through V)
2011/10/25	1.1	Revision for XTAP Version 1.11
2010/07/16	1.0	Creation of the first edition (for XTAP Version 1.10)

XTAP – Example collection		No.	SSW-01
Example Name	Switching Surge Calculation of a 500-Kv Vertically Arranged Double-Circuit Transmission Line		
Field	Switching surge calculation		
References	<p>Because this example was created specifically for this induction course, there are no reference documents.</p> <p>* For general information on the switching surge calculation, please refer to the following.</p> <p>Central Research Institute of Electric Power Industry, Comprehensive Report 121, “Study on Switching Over-voltages in Power Systems”</p>		
Outline	<p>A switching surge overvoltage is one of the important factors in determining the insulation level of the transmission lines and power station/substation equipment.</p> <p>In this example, an input surge calculation is conducted on a 500-kv vertically arranged double-circuit transmission line, which is commonly used in Japan.</p> <p>Assuming a 500-kV transmission line connecting an upper substation and a lower substation, the waveform of the overvoltage generated at the start and end of the line is calculated when the circuit breaker of the first line (1L) is closed at the upper substation. In the actual 500-kV system, to reduce the input surge overvoltage, the resistance input method is adopted (first, energization is applied with a resistance of a few 100 Ω, and the resistance is then short-circuited after approximately 10 ms to complete the input). However, in this example, we tried setting the input with no resistance allowing the travelling wave phenomenon to be easily understood. In addition, a frequency-dependent line model that takes into consideration the skin effect of the electric line and ground, as well as their frequency characteristics, is used.</p>		

## Analysis Circuit and Conditions

Figure 1 shows a skeleton diagram of the system in which an input surge calculation is conducted, and Figure 2 shows the assembly of a 500-kV transmission line.

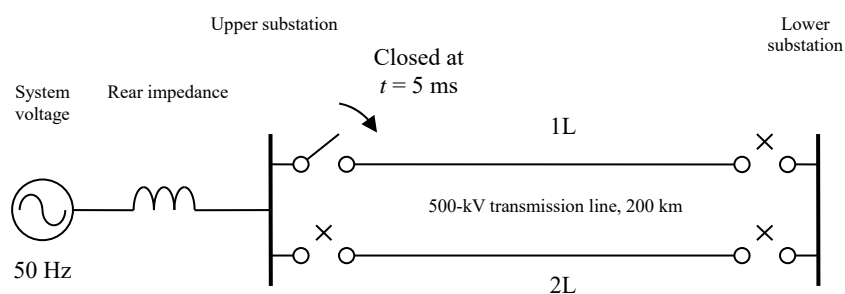


Figure 1 Skeleton diagram of a grid in which an input surge calculation is conducted

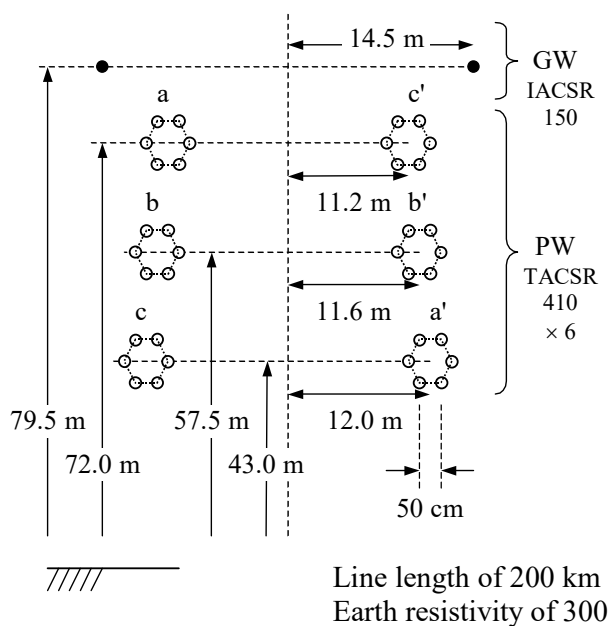


Figure 2 Assembly of 500-kV vertically arranged double-circuit transmission line

Further, the assembly in Figure 2 is same as that of example TL-02.

### [Analysis Phenomenon]

When closing the 1L circuit breaker at the upper substation, a voltage is applied to the starting-edge of the transmission line 1L. If the closing timing is close to  $90^\circ$  of the system

voltage (sine wave) in any one of the three phases, a large voltage will be applied to that phase. In this example, assuming a system frequency of 50 Hz, an initial part of phase-a of the system voltage of  $0^\circ$ , and a circuit breaker closing time  $t$  of 5 ms, phase-a of 1L is set to the peak value, which is the most severe input condition. Because it is difficult to intuitively understand the travelling wave phenomenon on a constant multi-phase distributed line, we tentatively consider only a single-phase distributed constant line, namely, phase-a of 1L. The voltage applied at phase-a of 1L propagates along the transmission line as a travelling wave and reaches the remote end after approximately 670  $\mu\text{s}$  (as estimated from the line length with the propagation speed being the speed of light). Because the remote end has an open condition (impedance of  $\infty$ ), the traveling wave voltage that reaches the end is specularly reflected and generates a double overvoltage. This overvoltage is generated between the inter-electrode gap of the circuit breaker in the lower substation 1L, which is under an open condition, and between the insulators of the bus bar and the transmission line within the vicinity, which becomes a problem in terms of the insulation design. The travelling wave is then reflected back and forth along the transmission line and displays an oscillatory waveform determined by the line length. In lines other than phase-a of 1L, an induced voltage is generated, which is also reciprocally reflected.

Considering the above description, at the time of normal operation, although an overvoltage of twice the ground voltage peak value will be generated, in practical terms, the overvoltage value varies depending on the skin effect of the electric wire and ground, its frequency characteristics, and the induction phenomena with other phases and other lines. Moreover, when another transmission line is connected to the busbar of the upper or lower substation, the reciprocating reflection phenomenon occurring in these lines is also superimposed, resulting in a more complex overvoltage waveform. Because it is almost impossible to obtain such an overvoltage waveform through manual calculations, a program such as XTAP is required. During the actual input surge analysis, taking into consideration the randomness of the circuit breaker input timing, a Monte Carlo calculation (a statistical calculation) is conducted. Although the current XTAP does not have a function to automate this process, such a function is expected to be added in the near future.

[Line Model Preparation]

A frequency-dependent line model that takes into consideration the skin effect of the electric wire and ground, as well as the frequency characteristics, is used. Because it is identical to

the line used in example TL-02, please refer to that example.

[Circuit Elements other than the Line Model]

A “SIN wave voltage generator” is used for the system voltage simulation. By calculating the inductance equivalent as 5%, taking 50 Hz, 500 kV, and 1000 MVA as the base, the impedance behind the upper system is set to 39.8 mH. For the circuit breaker, a “switch with a circuit breaker logic” is used, and its input is set at time  $t = 5$  ms.

[Analysis conditions]

The analysis conditions are as follows:

- Calculation time step                      10.0  $\mu$ s
- Calculation end time                      20.0 ms
- Display start time                      0.0 ms
- Display end time                      20.0 ms

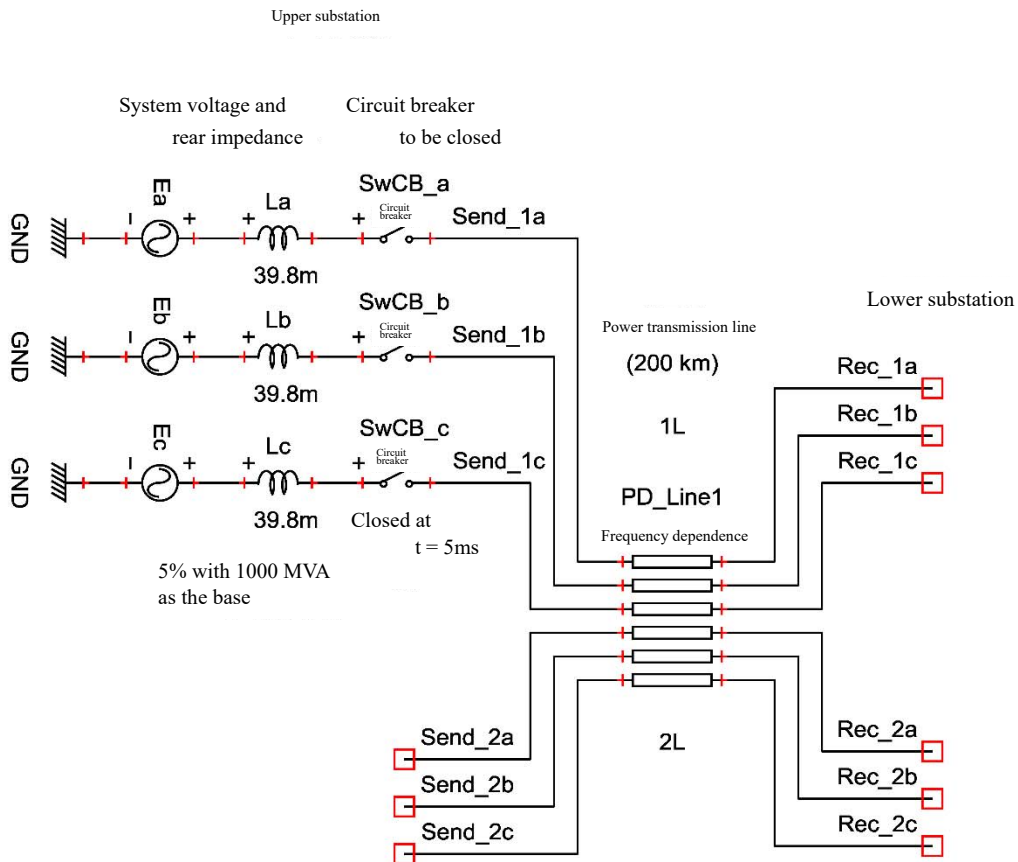
[XTAP Input Example]

Figure 3 shows an example of creating this example using XTAP.

Analysis Results

The results of this example executed using XTAP are shown in Figures 4 and 5.

END



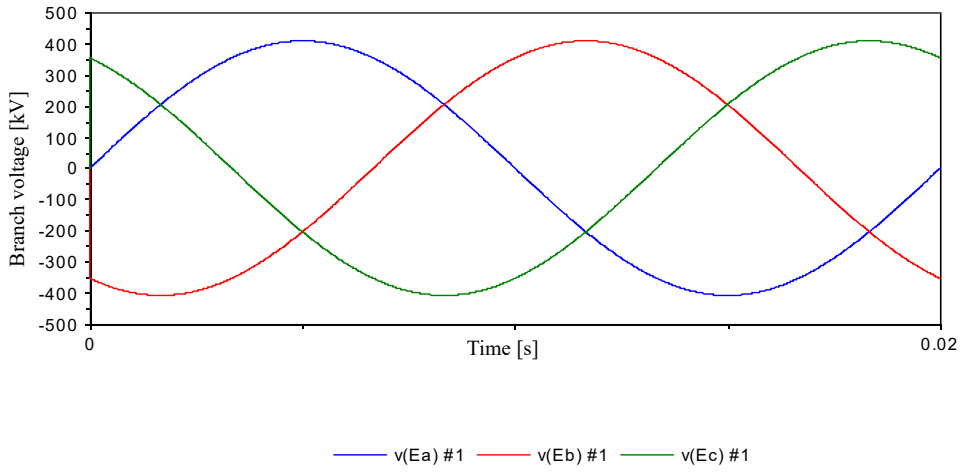
**Analysis conditions**

Calculation time step:10.0μs  
 Calculation end time:20.0ms  
 Display start time:0.0ms  
 Display end time:20.0ms

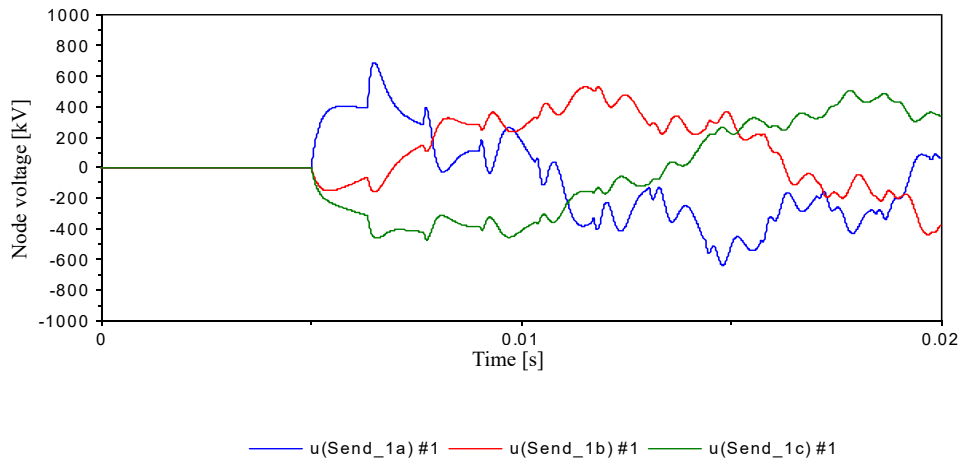
Line constants are calculated using XTLC under the following conditions

- \* Frequency-dependent line model
- \* Frequency samples 0.1 Hz to 10 MHz(400 points)
- \* For the pillar assembly, refer to the example table

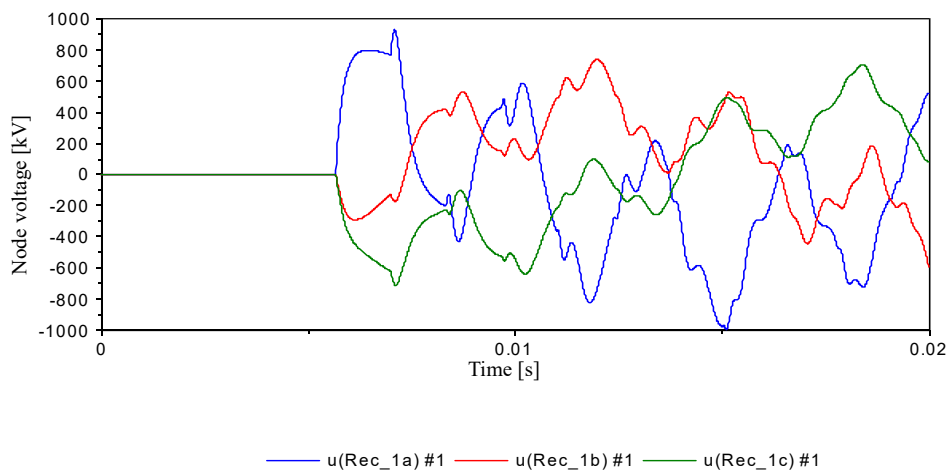
Figure 3 Example of XTAP input



(a) System voltage waveform

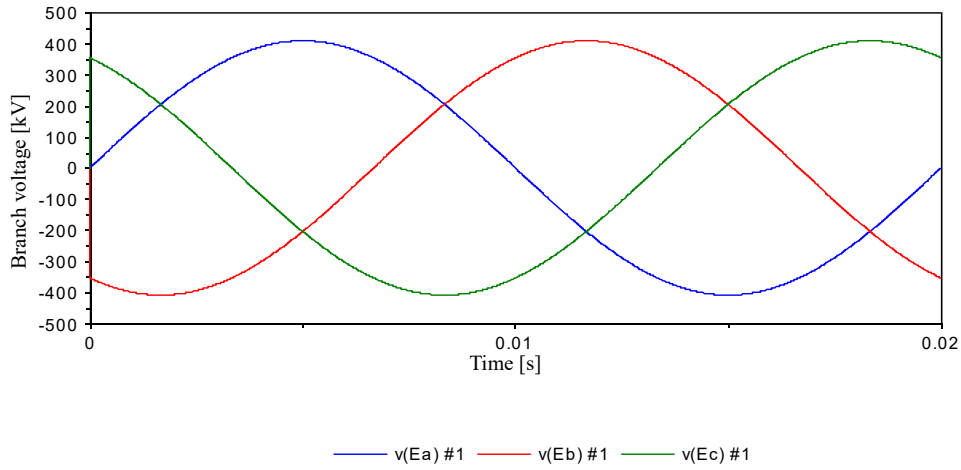


(b) 1L Starting-edge voltage waveform

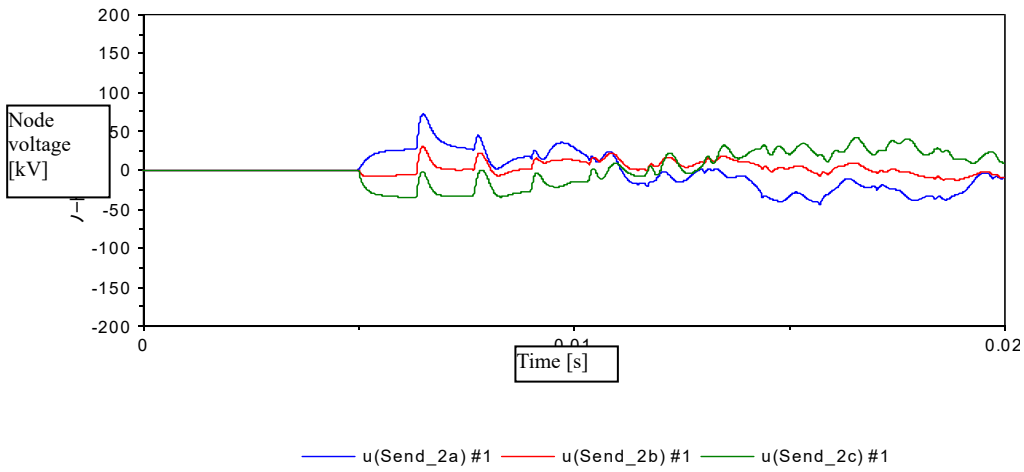


(c) 1L Remote-end voltage waveform

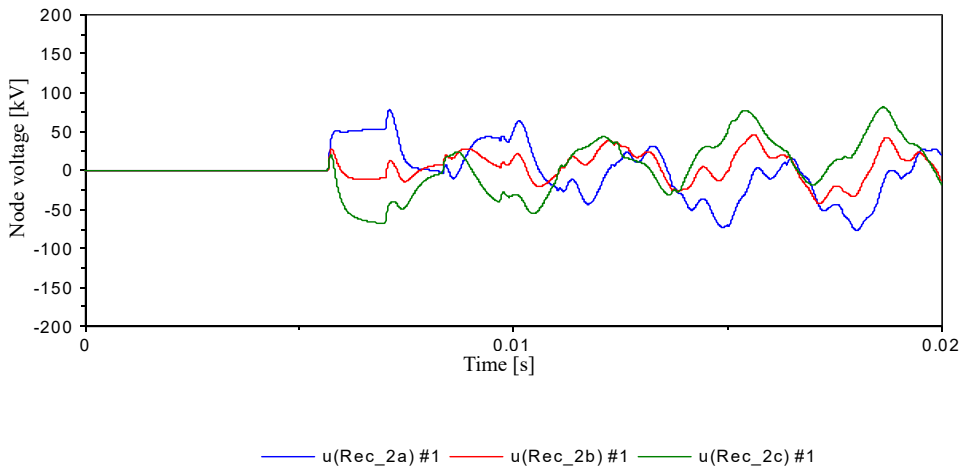
Figure 4 XTAP analysis results (1L voltage waveform)



(a) System voltage waveform



(b) 2L Starting-edge voltage waveform



(c) 2L Remote-end voltage waveform

Figure 5 XTAP analysis results (2L voltage waveform)

Revision History		
Date	Example file Version	Content changes
2014/11/19	2.0	Update for XTAP Version 2.00 Recalculation of line constants owing to changes in XTLC
2012/07/19	1.2	Update for XTAP Version 1.20
2011/10/18	1.1	Update for XTAP Version 1.11 The line constant file was modified because the number of valid digits of XTLC was modified.
2010/07/16	1.0	Initial version created (for XTAP Version 1.10)

<b>XTAP Example Collection</b>		<b>No.</b>	SSW-02
<b>Example Name</b>	Switching surge Analysis of a 275-kV System		
<b>Field</b>	Switching surge calculation, switching surge calculation, overvoltage analysis		
<b>References</b>	“Review of Simulation Methods for Electromagnetic Transients in Power Systems and Simulation Cases Using XTAP (Part 1) Switching Transient Overvoltage Simulations,” Survey Report H12005, Central Research Institute of Electric Power Industry		
<b>Outline</b>	After elucidating the concept of a switching surge, the principle of occurrence, and the simulation method of each element of the power transmission system, we introduce an example switching surge analysis of a 275-kV system using XTAP (excerpted from the above reference).		

# 1 Switching surge

## 1.1 Concept [5]

When newly starting the operation of a power transmission line or restarting the operation after construction, voltage is applied to the power line by keeping the transmission line without a load and closing the circuit breakers on the power supply side.

Further, when ground faults occur in the transmission lines from lightning strikes or similar events, the circuit breakers on both sides of the line are temporarily opened to remove the continuous current arc owing to a ground fault, and the circuit breakers are closed again to resume the power transmission (called reclosing). Thus, when applying voltage to a power transmission line, it is often kept without a load. When applying voltage to a no-load transmission line, an overvoltage called a switching surge occurs in the line. Therefore, the insulation of the transmission line must be designed to withstand the overvoltage owing to this switching surge.

The magnitude of the overvoltage owing to a switching surge depends significantly on the supply voltage at the moment when the circuit breaker is closed. Because a circuit breaker is a device that applies the opening and closing of the electrodes using a mechanical mechanism, its operation is slower compared to the commercial frequency and the variation is also large. That is, because the phase of the supply voltage at the moment the circuit breaker is closed cannot be predicted, it is reasonable to think that it is determined (randomly) based on probability. Therefore, in the study of the actual switching surge, the switching surge calculations are conducted a number of times by randomly changing the closing timing of the circuit breaker, and the result is displayed in

the form of a cumulative frequency distribution of the generated voltage, as shown in Figure 1. In this way, it is possible to evaluate the probability of occurrence of a certain overvoltage. A method for obtaining the statistical results based on many simulations conducted when randomly changing the parameters described above is called the Monte Carlo method. Although the maximum value of the generated voltage tends to increase as the number of simulations increases, the value at which the generation probability reaches 2% tends to be a constant regardless of how frequently the number of simulations is greater than or equal to a certain value. Hence, this value is often used as the representative figure. The value at which the generation probability becomes 2% is called the “2% value.” The cumulative frequency distribution of the generated voltage is often plotted on a type of graph called a normal probability plot, as shown in Figure 1. In this type of plot, the vertical axis is scaled such that the plotted points become a straight line in the case of a normal distribution.

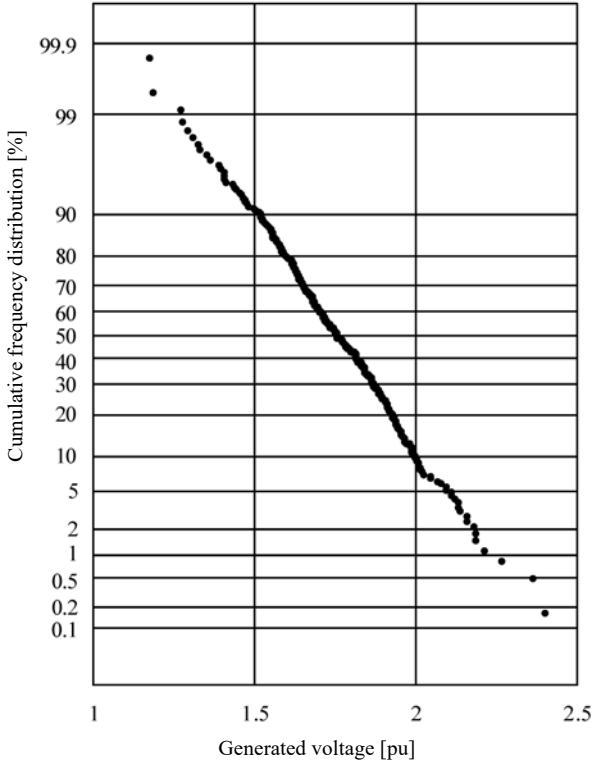


Figure 1 Cumulative frequency distribution of voltages generated by switching surge

An overvoltage from a switching surge is often represented as a multiple of the nominal voltage when the ground wave peak value is 1, which is called the overvoltage multiple. It is important to note that, although pu is used as the unit, it is unrelated to the pu used in a system analysis (where the effective value of line voltage is set to 1). Strictly speaking, the term “switching surge” must be used as a generic name for not only for a switching surge but also for a surge generated by the opening and closing of a switch, such as a cut-off surge or capacitor switching surge. However, the term “switching surge” is commonly used in the sense of a switching surge. Hence, the above-mentioned overvoltage multiple is also called as a switching surge multiple.

1.2 Principle of Switching Surge Generation

An overvoltage from a switching surge can be broadly classified into two types: one occurring as an oscillation phenomenon of the inductance of the power supply side and the capacitance of the transmission side, and the other caused by a specular reflection of the progressive waves propagating on the transmission line at the open far end. The former occurs when the line can be treated as a lumped constant capacitance because the inductance of the line is small whereas the capacitance is large, such as with a cable line. In contrast, the latter occurs when the distribution constant characteristics of the line become remarkable, such as in a long-distance overhead

power transmission line. From now, we will explain these circuit phenomena.

First, we will describe the switching surge phenomenon occurring as the oscillation phenomenon of the power source side inductance and transmission line capacitance [1]. We assume that, in a power station or a substation, a no-load transmission line is energized by closing the circuit breakers. The power source on the upper side of the circuit breaker is simulated using a sine wave voltage source  $e(t) = E \sin(\omega t + \theta)$  and an inductance  $L$  connected in-series. Assuming that the transmission line can be regarded as the capacitance of the lumped constants, it is simulated with capacitance  $C$ . The equivalent circuit of the above is illustrated in Figure 2. When the circuit breaker  $S$  is closed at  $t = 0$  under the conditions of the initial phase of the power supply  $\theta$  at  $90^\circ$  and the residual voltage of the transmission line at zero, the voltage  $v$  of the transmission line is given by the following equation.

$$v(t) = \frac{E}{1 - \omega^2 LC} \left( \cos \omega t - \cos \frac{1}{\sqrt{LC}} t \right) \quad (1)$$

In the above equation, the first term corresponds to a steady supply voltage, and the second term corresponds to the oscillation owing to  $L$  and  $C$ . It should be noted that, in the above calculations, because the losses in the power supply side and the transmission line are ignored, the second term does not attenuate. In reality, however, it attenuates because of the losses. As an example, when calculated according to equation (1) for the case of  $\omega = 2\pi 60$ ,  $L = 15$  mH, and  $C = 2$   $\mu$ F (for an underground cable of a few kilometers), Figure 3 is obtained as the waveform of the transmission line voltage  $v$  (voltage value normalized using  $E$ ). It can be observed that the voltage owing to an  $LC$  oscillation is superimposed on the supply voltage. Usually, because the value of  $\omega^2 LC$  in equation (1) is much smaller than 1, it is understood that the peak value of  $v$  reaches approximately  $2E$  (that is, 2 pu).

In equation (1), the amplitude of the term owing to the  $LC$  oscillation of the second term is approximately equal to the voltage applied before closing the circuit breaker  $S$ . This holds well even when there is a residual voltage in the transmission line. For instance, assuming that the circuit breaker was opened at the moment when the

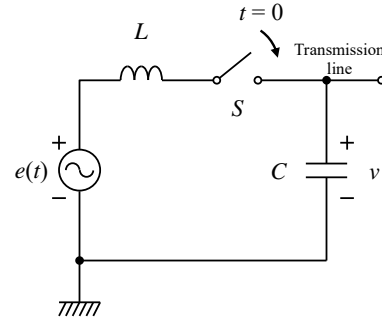


Figure 2 Equivalent circuit for energization of a no-load transmission line (lumped constant capacitance approximation)

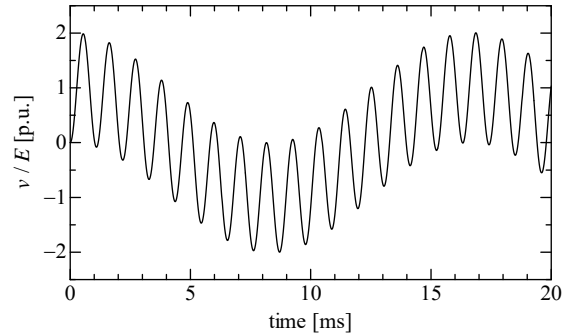


Figure 3 Voltage waveform when energizing a no-load transmission line (lumped constant capacitance approximation)

power supply reached a negative peak value, namely,  $-E$ , if the circuit breaker is closed at  $\theta = 90^\circ$  from the state in which the residual voltage of  $V_0 = -E$  exists in the transmission line, as the voltage waveform  $v$  of the transmission line starts from  $-E$  and oscillates at an amplitude of approximately  $2E$ , it takes a peak value of approximately  $3E$  (3 pu).

Next, we describe the switching surge phenomenon occurring from the specular reflection of progressive waves propagating along the transmission line at the open far end. In the same manner as above, the no-load transmission line is energized by closing the circuit breakers in the power station or substation. The power source on the upper side of the circuit breaker is simulated using a sine wave voltage source  $e(t) = E \sin(\omega t + \theta)$  and an inductance  $L$  connected in-series. The transmission line is simulated using a no-loss distributed constant circuit with a line length  $l$ , propagation velocity  $c$ , and characteristic impedance  $Z_0$ . The equivalent circuit is shown in Figure 4. We assume that the circuit breaker  $S$  is closed at  $t = 0$  under the conditions of the initial phase of the power supply  $\theta = 90^\circ$ , and the residual voltage of the transmission line is zero. In this case, because the voltage of the power supply increases in a step form, it is considered a step wave with amplitude  $E$  immediately after  $t = 0$ . Because the waveform of voltage  $v_1$  at the starting edge of the transmission line is obtained by dividing the voltage of the step wave by  $L$  and  $Z_0$ , it becomes a stepped waveform with an amplitude  $E$  vanishing at a time constant of  $L/Z_0$ . This waveform  $v_1$  propagates along the transmission line as a traveling wave and reaches the remote end after a propagation time of  $\tau = l/c$ . According to the distributed constants circuit theory[6], because a voltage wave is specularly reflected at the open end producing twice the voltage, a voltage of  $2E$  (2 pu) is generated at the remote end of the transmission line. Further, after time  $\tau$ , the specular reflected traveling wave reaches the starting edge. Because the impedance of the power supply side is only  $L$ , which is small, the voltage wave is almost negatively reflected at the starting edge, and thereafter this reciprocating reflection repeats. Although the supply voltage was considered a step wave immediately after  $t = 0$ , because it changes to a sinusoidal wave when viewed over the long term, the voltage actually generated on the transmission line is the sinusoidal supply voltage superimposed through the above-mentioned reciprocating reflection. As an example, assuming an overhead power transmission line equivalent to 100 km, the waveform of the remote-end voltage  $v_2$  is calculated using  $\omega = 2\pi 60$ ,  $L = 50$  mH,  $l = 100$  km,  $c = 300$  m/ $\mu$ s, and  $Z_0 = 400$   $\Omega$  when applying the Bergeron method [2], the results of which are shown in Figure 5 (the voltage values are normalized by  $E$ ). The reciprocating reflection resulting in a peak voltage of approximately 2 pu at the remote end is superimposed over the supply voltage. In the above calculation, because the losses in the power supply side and the transmission line are ignored, the reciprocating reflection continues. However, considering the losses, the reciprocating reflection will gradually attenuate. Therefore, the peak voltages occurring near 9 and 17 ms are actually much smaller, and the first peak near 1 ms is often the maximum value. The spike-like voltage waveform of the portion surrounded by the dotted line in Figure 5 is generated owing to a sudden change in the current flowing through the inductance  $L$  when the traveling wave returning from the remote end reaches the starting edge. It should be noted that, because the transmission line is treated herein as a distributed constant circuit, in the initial phase of the reciprocating reflection of the traveling wave, oscillations with a period of  $4\tau$  were observed owing to the reciprocating reflection phenomenon. In contrast, as the frequency decreases, the behavior of the open-ended distributed constant circuit approaches the capacitance. In other words, when the high-frequency components are

lost by repeated reciprocating reflections, the oscillation period approaches a value determined by the inductance and capacitance of the transmission line added to the inductance of the power source side (for details of this phenomenon, refer to Section 2.3.2 of [5]).

Because the concept of a residual voltage is the same as that of the switching surge, which occurs as the oscillation phenomenon of the inductance of the power supply side and transmission line capacitance described above, it is omitted herein.

### 1.3 Residual Voltage and Input Conditions

As mentioned in the previous section, an overvoltage from a switching surge varies depending on the magnitude of the residual voltage. Therefore, in an actual analysis, to reproduce a realistic residual voltage, it is necessary to set the input conditions according to the operation of the actual equipment. The input conditions used in the analysis of [7] are shown below.

- (1) Three-phase input – Under this analysis condition, the input is simulated in a state where there is no residual voltage in the transmission line, such as when newly starting the operation of a power transmission line or restarting the operation of the power transmission line after construction. Using a circuit breaker of the load-end under an open condition, the three phases of the circuit breaker on the supply side are closed concurrently. When parallel lines are in operation, the induced voltages from these lines will be superimposed.
- (2) Three-phase reclosing – Under this analysis condition, we simulate the cutoff and reclosing of all three phases of the circuit breaker together in the transmission lines where accidents have not occurred. After cutting off all three phases at both ends of the transmission line, using the circuit breaker at the load-end in an open state, the three phases of the circuit breaker at the power supply side are all closed concurrently. Normally, because a large residual voltage remains during all three phases, it gives the most severe

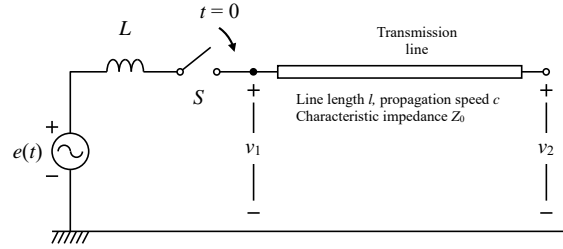


Figure 4 Equivalent circuit for energization of a no-load transmission line (simulation using a no-loss distributed constant circuit)

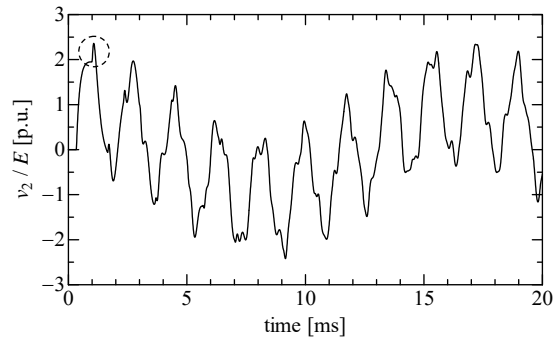


Figure 5 Remote-end voltage waveform when energizing a no-load transmission line (simulation using a no-loss distributed constant circuit)

overvoltage. Because this analysis condition includes the cutoff and reclosing of the transmission lines where accidents have not occurred, such a voltage does not exist during an actual switching operation. However, it is used to obtain the most severe overvoltage as a reference value.

- (3) Selective reclosing – This analysis condition is for ultra-high voltage transmission lines where both ends of the transmission line are cut off only for the phase that caused the accident. The circuit breaker at the load end is kept as is, whereas the circuit breaker at the supply side is switched on.

Furthermore, when analyzing a specific case, the analysis is conducted by setting the residual voltage assumed for the case without being limited to the above three conditions.

#### 1.4 Simulation of the Power Supply Side

Both ends of power transmission lines are usually connected to a power generation station, a substation, or a switching station. Among the two ends of the power transmission line, the circuit breaker at the power supply side is closed and a switching surge is generated. When considering an exclusion of the lightning arrestors and transmission lines of other routes, which are described later, if the power supply side is a power plant, there will be a power generator and a step-up transformer behind the circuit breaker. If the power supply side is a substation, there will be a transformer behind the circuit breaker and transmission lines further spreading the system. If the power supply side is a switching station, there will be transmission lines directly behind the circuit breaker from where the system spreads.

If the power supply side is a power station or a substation, the system behind the circuit breaker is often simulated using an equivalent circuit, as shown in Figure 6. This equivalent circuit is a simplified circuit that simulates the voltage generated by the system behind the circuit breaker and its impedance. The three-phase voltage sources, namely,  $e_a(t)$ ,  $e_b(t)$ , and  $e_c(t)$ , simulate the sinusoidal voltage generated in the busbar of the power source side with the circuit breaker to be closed under an open condition. Further, the impedances  $Z_1$  and  $Z_n$  simulate the impedance of the system behind the circuit breaker. In contrast, when the power source side is a switching station, the transmission line behind the circuit breaker is simulated as a transmission line model using the method described in section 1.5, and the power station before or the substation after is simulated using the equivalent circuit shown in Figure 6. For the tip of a transmission line or a switching station, we first simulate the transmission line up to the power station or substation as the transmission line model. For a switching station, the reason for simulating the transmission line behind it as a transmission line model is that the transmission line at the instant the circuit breaker is closed appears to have a characteristic impedance corresponding to a resistance of several hundreds ohms, which may result in an error in the equivalent circuit shown in Figure 6.

Although the amplitude of the three-phase voltage source can be easily obtained from the operating value, the resistance and impedance of the impedances  $Z_1$ , and  $Z_n$  will become a problem. In the guidelines[8] compiled by the IEEE Working Group on a switching surge analysis,  $Z_n$  is omitted (short-circuited), and the resistance and impedance of  $Z_1$  are determined from the short-circuit capacity of the system behind the circuit breaker. In other words, the short-circuit impedance is obtained from the positive-phase equivalent circuit of the system behind the circuit breaker. Taking its real part as the resistance and the value obtained by dividing the imaginary part by  $\omega$  (namely,  $2\pi f$ , where  $f$  is the commercial frequency) as the inductance, we obtain  $Z_1$ . However, in the guidelines [9] compiled by the CIGRE Working Group, the impedance of the rear system is obtained by adding the impedances of the generator, transformer, and transmission lines that are present behind the circuit breaker, taking into consideration the zero-phase impedance. Because the equivalent circuit of the generator is complex, it is simulated by approximating the  $d$ -axis sub-transient reactance  $X_d''$ . In addition, because the positive-phase component impedance obtained through an integration corresponds directly to  $Z_1$ , the resistance and inductance can be obtained from the real and imaginary parts. Taking the zero-phase impedance obtained through an integration as  $Z_0$ , the value of  $Z_n$  is obtained from

$$Z_n = \frac{1}{3}(Z_0 - Z_1) \quad (2)$$

The resistance and inductance values are obtained from its real and imaginary parts. Further, in the CIGRE guidelines, the frequency-dependent effect, that is, the effect of the increase in the resistance component of the generator and transformer, as the frequency increases, is taken into consideration, and the typical frequency characteristics of the generator and transformer are indicated. Because transformers, transmission lines, and generators are present behind the circuit breaker, it is not easy to obtain their comprehensive frequency characteristics. Moreover, it is also not easy to obtain the frequency characteristics of each generator or transformer. However, if the frequency characteristics of the system behind the circuit breaker are roughly

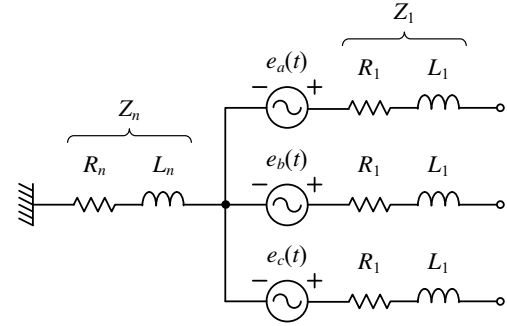


Fig. 6 Equivalent circuit of the power supply side

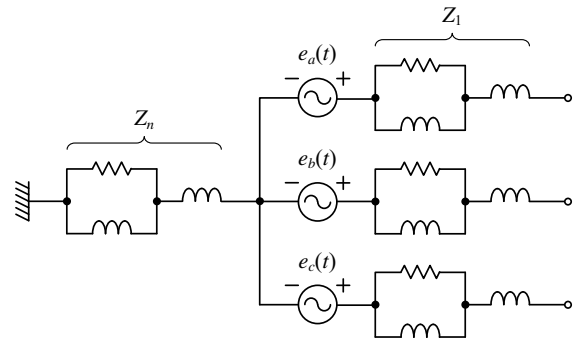


Figure 7 Equivalent circuit of the power supply side considering its frequency dependence

known, the frequency-dependent effect can be approximated [3], [10] using an equivalent circuit similar to that shown in Figure 7.

In equation (2) above, the imaginary part of  $Z_0 - Z_1$  may become negative in certain cases, and a simulation using the inductance may become impossible. To handle this problem, a simulation method using an ideal Y- $\Delta$  transformer for coupling is introduced in [9]. If the neutral point of the transformer behind the circuit breaker is directly grounded, it becomes  $Z_0 = Z_1$ , and  $Z_n$  can be omitted (short-circuited).

Reference [5] compares the calculation results of the case in which the value of inductance  $L$  is only the leakage inductance of the transformer just behind the circuit breaker, and the case in which it is the inductance obtained from the short-circuit capacity of the system behind the circuit breaker, with the measured results. An actual measurement was carried out at the Shikoku Electric Power Nagagawa trunk line and Kansai Electric Power Okutataragi trunk line, and in both cases, it was concluded that the calculation results closer to the actual measurements can be obtained if  $L$  is simulated using only the leakage inductance of the transformer just behind the circuit breaker. Although this conclusion may not be necessarily consistent with the IEEE or CIGRE guidelines, as an important research result, we introduce it here. From this, conducting a calculation by changing the inductance as a parameter is considered realistic in an actual analysis.

When conducting a detailed analysis, instead of using the equivalent circuits of Figures 6 and 7, the system behind the circuit breaker may also be assembled and analyzed.

## 1.5 Simulation of Transmission Line

In a switching surge calculation, it is necessary to accurately reproduce the phenomena from the peak voltage observed immediately after closing the circuit breaker until it settles at the supply voltage of the commercial frequency after the attenuation of the reciprocating reflection and  $LC$  oscillation. In other words, because it is necessary to reproduce within the line model characteristics of a wide frequency range, from the commercial frequency to a high frequency corresponding to the peak voltage, it is standard to use a frequency-dependent line model. However, when a switching surge occurs as an oscillation phenomenon of the power supply side inductance and transmission line capacitance described in the first half of Section 1.2, such as when the line to be energized is a comparatively short underground cable, a sufficient level of accuracy can be obtained using a constant parameter line model. Because the capacitance of the transmission line does not have a frequency-dependent effect, in such a case, the frequency used to calculate the line constants does not significantly affect the calculation results.

Because two or more lines assembled in the same tower will have a relatively large mutual induction between them, they are simulated as a single transmission line model. When considering the mutual induction between two or more transmission lines running parallel within the neighborhood, all lines are integrated into a single transmission line model. In a switching surge analysis, to simulate the line from the start to end as a single line model, the line constants are usually calculated when assuming an average pillar assembly over the entire span. Further, when the presence of the overhead ground wire is considered, it is eliminated from the matrix of the line constants. In XTAP, frequency-dependent line models with span lengths of 25, 50, 75, and 100 km are prepared

for each standard pillar assembly of each voltage class introduced in [4]. When the pillar assembly and span length differ from these, the analyst must create a frequency-dependent model using the line constant calculation routine, XTLC, included in XTAP. At that time, it is recommended to set the samples of the line constant calculation frequency to 400 points within the range of 0.1 Hz to 10 MHz.

## 1.6 Simulation of Lightning Arrestor

In recent years, zinc-oxide type lightning arrestors have been used not only to suppress a lightning surge overvoltage, but also a switching surge overvoltage [7], [11]. In addition to the non-linear voltage-current characteristics, which are the basic characteristics of a zinc-oxide type lightning arrestor, the limiting voltage slightly increases for sharp waves within an order of  $\mu\text{s}$ . However, even in a lightning surge analysis targeting a steeper phenomenon as compared to a switching surge analysis, because the influence of the sharp wave characteristics is insignificant in the analysis of a system of 500 kV or less, it is ignored. That is, the zinc-oxide type lightning arrestor is simulated using only a non-linear resistance that reproduces the non-linear voltage-current characteristics [4]. In the lightning surge analysis of a 1,000 kV system, there are examples in which the sharp wave characteristics are taken into consideration [12], [13].

As the target phenomenon of the analysis is gentle in the case of a switching surge analysis as compared to a lightning surge analysis, it is natural to ignore the sharp-wave characteristics of a zinc-oxide type lightning arrestor and simulate it using only the nonlinear resistance. The representative voltage-current characteristics of a zinc-oxide type lightning arrestor are summarized in [4], and their models are available in XTAP. Grasping the processing energy of the arrestor that follows the switching surge is also an important item of an analysis. Because the available voltage-current characteristics may be the upper limit of the actual arrestor characteristics, it is necessary to take this into consideration when analyzing the processing energy.

## 1.7 Simulation of Transmission Line on Another Route

In an analysis of a switching surge overvoltage, because the circuit breaker at the far end of the transmission line to be analyzed is open, there is no need to simulate the remote system. If there is a zinc-oxide type arrestor at the service line entrance of the substation at the far-end side, it may be simulated. Meanwhile, in the starting-edge of the transmission line, it is necessary to simulate the following equipment. First, the system present in the power supply side of the circuit breaker to be closed, in other words, the system behind the circuit breaker, is simulated using the equivalent circuit shown in Figure 6 or 7, as described in Section 1.4. If there is a zinc-oxide type arrestor in the line side of the substation at the starting-edge, it must be simulated. In addition, if a power transmission line of another route is connected to the busbar on the line side of the substation (which is hereinafter simply referred to as the “transmission line of another route”), it must be simulated.

The simulation of the transmission line of another route is not easy. Because the analysis is carried out under the assumption that the transmission line of another route is normally operated, the problem is to determine how far the system extending further from its far end must be simulated. Although an example that deeply examines this problem has not been found, a simulation is usually conducted through the following procedure. First, following the transmission line of another route and examining the type and length of the transmission line, the substation whose influence on the analysis results is large is determined, and the simulation is conducted in detail up to that substation. The transmission lines falling under the scope of this detailed simulation are simulated as they are as transmission line models using the procedure described in Section 1.5. The transformers in the substations along the way are simulated, including the secondary side, using the procedure described in example SSW-03. Further, if there is a lightning arrester installed at the substation, it needs to be simulated. Systems far from the substation located at the end of the detailed simulation range are simulated using the appropriate equivalent circuits, while taking into consideration whether the system seen from there is a power source or a load. For example, in the case of the power source, the equivalent circuit in Figure 6 or 7 is often used. The values of the source voltage  $E$  and the impedances  $R$  and  $L$  in the equivalent circuit are obtained using the method described in Section 1.4. In contrast, if there is a load far from the terminal substation, the equivalent circuit shown in Figure 8 is used in the IEEE guidelines [8]. In this equivalent circuit, the impedance of the transmission line and the transformer up to the actual load is expressed by  $R_s$  and  $L_s$ , the effective power of the load is expressed by the resistance  $R_p$ , and the reactive power is expressed by the inductance  $L_Q$  (if the value of the reactive power is negative, it is simulated using capacitance  $C_Q$ ). The simulation method stated here is just an example, and in practice, the analyst makes a judgement individually and then conducts a simulation. Further, because it is not easy to specify the range of the system that must be simulated in detail, in reality, trial switching surge calculations are conducted to observe the influence. Hence, this is often determined through trial and error.

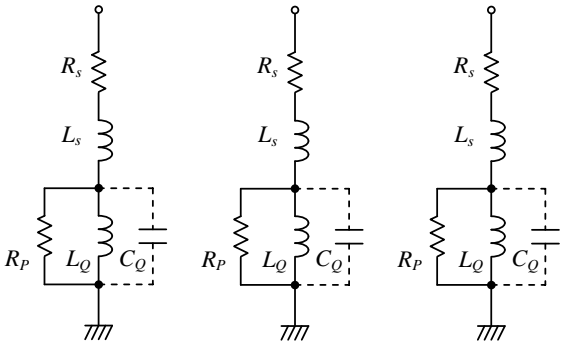
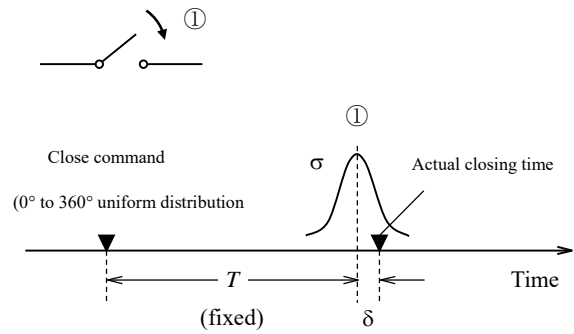


Figure 8 Equivalent circuit of a load

## 1.8 Simulation of Circuit Breaker and Statistical Calculation

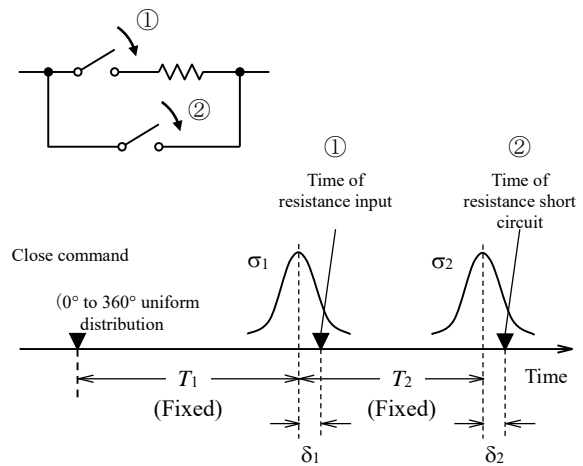
As described in Section 1.1, the magnitude of the switching surge overvoltage is statistically evaluated from the results of the multiple switching surge calculations conducted by randomly changing the closing timing of the circuit breaker. Therefore, the circuit breaker is simulated as an ideal switch that can randomly change the closing timing for each simulation.

First, we describe the simulation of a circuit breaker that does not have an input resistance. As shown in Figure 9(a), a close command is first given to the circuit breaker. The timing at which this close command is issued is assumed to be evenly distributed between  $0^\circ$  and  $360^\circ$  of the phase of the power supply voltage, and in the simulation, it is determined using a uniformly distributed random number. Next, taking the point in time after a certain time  $T$  has elapsed from the close command as a reference, the time until the electrodes inside the circuit breaker really connect is assumed to fluctuate according to the normal distribution with a standard deviation of  $\sigma$ . This fluctuation is generated using a random number following a normal distribution. Taking the inherent variation of the simulation resulting from the random number generation as  $\delta$ , the ideal switch that simulates the circuit breaker will close at the instant  $T + \delta$  has elapsed from the close command. In the above,  $T$  is the average value of the time required for the electrodes inside the circuit breaker to connect after the close command is issued. Although a close command is simultaneously given to the three-phase circuit breaker, because  $\delta$  is generated using random numbers for each phase, the values in the three phases differ.



(a) No input resistance

A circuit breaker with an input resistance is simulated as follows. Similar to the case of closing with no-resistance, a close command is given to the circuit breaker, and its timing is determined using a random number uniformly distributed between  $0^\circ$  and  $360^\circ$  of the phase of the supply voltage, as shown in Figure 9(b). Next, taking the point in time after a certain time  $T_1$  has elapsed after the close command as a reference, the time until the resistance is actually turned on is assumed to fluctuate according to the normal distribution with a standard deviation of  $\sigma_1$ . Further, taking the time point after a certain time  $T_1 + T_2$  has elapsed after the close command as a reference, the time until the resistance is really short-circuited is assumed to fluctuate



(b) With input resistance

Figure 9 Simulation of circuit breakers

according to the normal distribution with a standard deviation of  $\sigma_2$ . These two fluctuations are generated as random numbers that follow their respective normal distributions. Taking the inherent variation of the simulation obtained as a result of a random number generation as  $\delta_1$  and  $\delta_2$ , the ideal switch for turning on the resistance is closed when  $T_1 + \delta_1$  has elapsed from the close command, and the ideal switch for short-circuiting the resistance is closed when  $T_1 + T_2 + \delta_2$  has elapsed from the close command. Here,  $T_1$  is the average value of the time necessary for turning on the resistance after the close command is issued, and  $T_1 + T_2$  is the average value of the time required for short-circuiting the resistance after the close command is issued. Although a close command is simultaneously given to the three-phase circuit breaker, because  $\delta_1$  and  $\delta_2$  are generated by random numbers for each phase, the values in the three phases differ.

In [5], by conducting experiments on the closing timing of the circuit breakers, it has been concluded that the variations follow a normal distribution, and there are no differences owing to the type or voltage class of the circuit breaker. Further, the standard deviation of the variations was between 0.5 and 1.5 ms, and the average was approximately 1 ms. However, because a considerable amount of time has elapsed since the experiment was conducted, whether the above findings can be applied to the latest circuit breaker is unknown.

Because XTAP is equipped with statistical calculation functions (functions applying a Monte Carlo simulation) that automatically conduct numerous switching surge calculations by providing random numbers to the timing of the close command and the variation of the closing circuit breaker, the calculation of the cumulative frequency distribution of the maximum value of the generated voltage is automated.

## 1.9 Example Analysis using XTAP

We introduce an example of calculating a switching surge overvoltage generated when power transmission line 1 is energized in a 275-kV system, as shown in Figure 10. The system on the power supply side of substations 1, 3, and 4 was simulated using the equivalent circuit shown in Figure 6. In the calculation of the switching surge, all voltage source components in the equivalent circuit were set to a 275-kV three-phase power supply of the same phase, and thus the tidal current does not become a problem. If the conditions are set such that the tidal currents do not occur, a Ferranti effect will occur, and the evaluation will become rigorous. For the impedance part of the equivalent circuit, we calculated the respective inductance values from the assumed short circuit capacities and added realistic resistance values. These resistance and inductance values are shown in Figure 10. Assuming that the transmission lines 1, 2, and 3 are overhead lines with the standard assembly stated in [4] and the earth resistivity as 100  $\Omega\text{m}$ , we conducted the simulation using a frequency-dependent line model. The lengths of transmission lines 1, 2, and 3 were 100, 50, and 70 km, respectively, and the samples of the line constant calculation frequency at the time of the creation of the frequency-dependent line model were set to 400 points within the range of 0.1 Hz to 10 MHz. The circuit breaker to be closed was the circuit breaker 1 at the substation-1 side of transmission line 1, and the circuit breaker was assumed to have no input resistance, as shown in Figure 9(a). The average time from the close command to the time of closing  $T$  was set to 10 ms, and the variation in the closing time  $\sigma$  was set to 1.5 ms. Moreover, in this analysis, we assumed the condition in which there is no lightning arrester. Figure 11 shows the data created by XTAP.

Using these, we conducted 300 simulations by taking the timing at which the close command is issued as a random number uniformly distributed between  $0^\circ$  and  $360^\circ$  of the power supply phase. The calculation time step was set to  $0.5 \mu\text{s}$  from the propagation time of the transmission line. Figure 12 shows the maximum value of the voltage generated at the end of transmission line 1 (substation 2 side) in pu plotted on a normal probability plot (taking the peak of the nominal voltage to ground as 1 pu). Here, the largest among the maximum values of the voltage waveform of each phase was taken. From Fig. 12, the 2% value, which is the maximum value of the generated voltage corresponding to a cumulative frequency of 2%, is approximately 2.7 pu. Figure 13 shows a plot of the voltage waveforms of each phase corresponding to the 2% value. From the figure, it can be confirmed that the maximum voltage is generated in the b-phase.

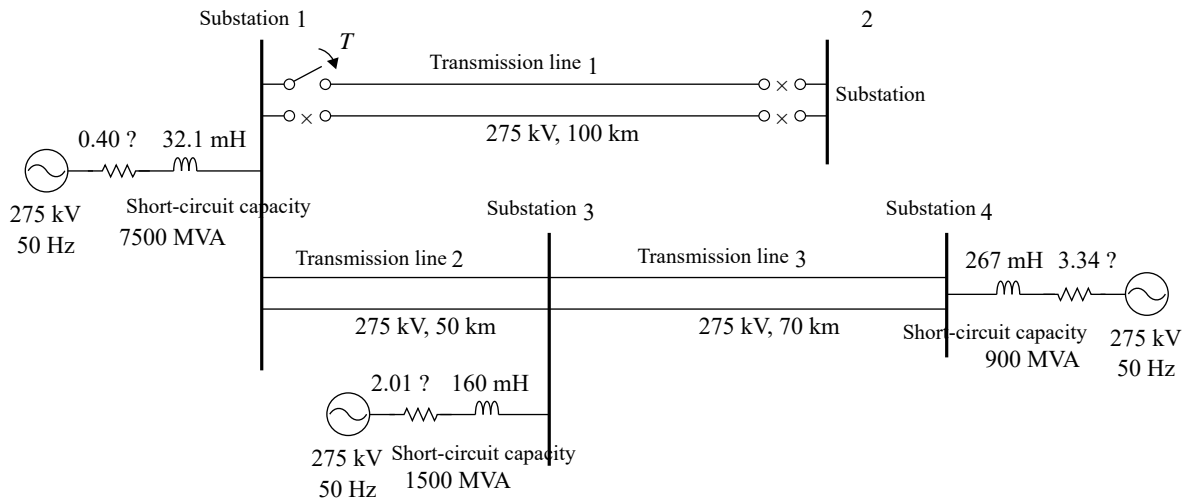


Figure 10 Example circuit for switching surge calculation

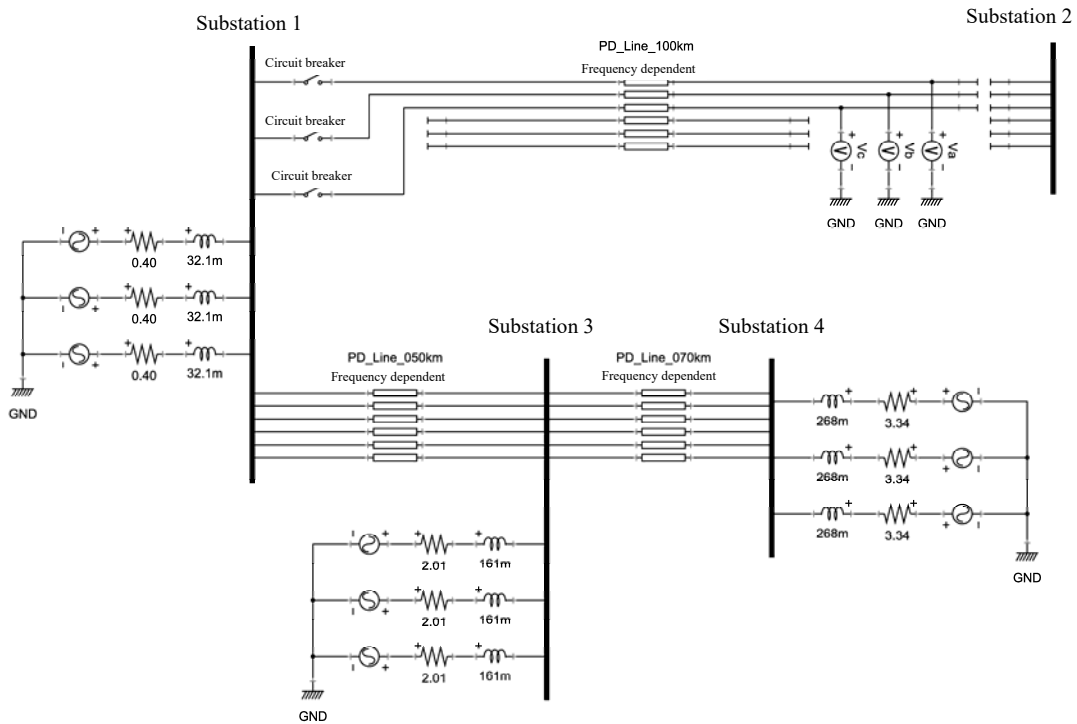


Figure 11 XTAP data for switching surge calculation

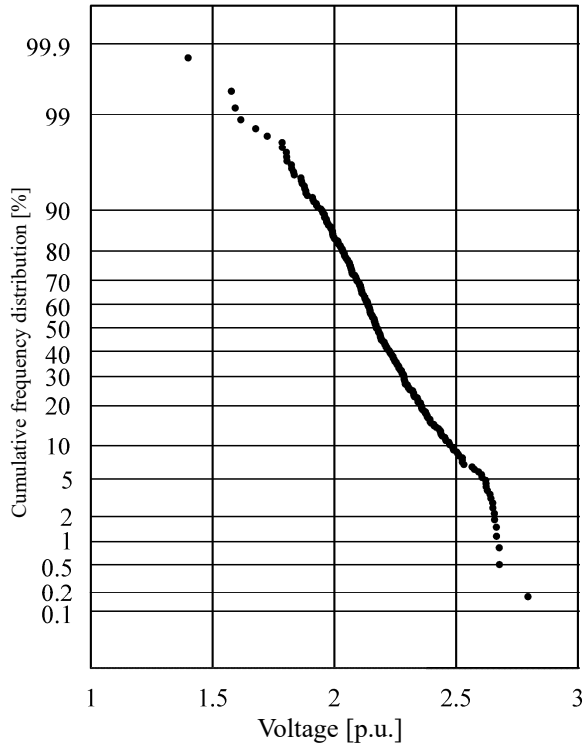
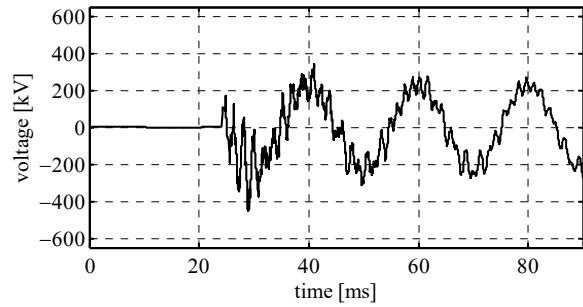
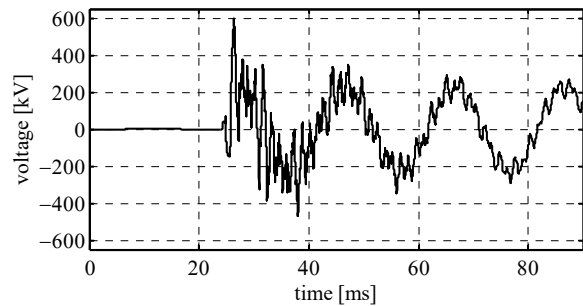


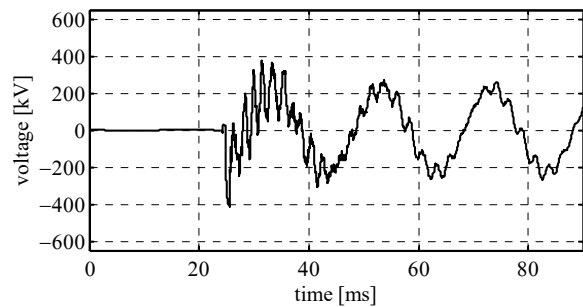
Figure 12 Cumulative frequency distribution of the voltages generated at the end of transmission line 1



(a) Phase-a voltage



(b) Phase-b voltage



(c) Phase-c voltage

Figure 13 Waveforms of the voltages generated at the end of transmission line 1 in the case corresponding to the 2% value

#### Reference

- [1] T. Kono, "Theory of System Insulation," Corona Publishing Co., Ltd. 1984.
- [2] H. W. Dommel, "Digital computer solution of electromagnetic transients in single- and multiphase networks," IEEE Trans., Power Apparatus and Systems, Vol. PAS-88, No. 4, pp. 388–399, Apr. 1969.
- [3] T. Noda, "Identification of a multiphase network equivalent for electromagnetic transient calculations using partitioned frequency response," IEEE Trans., Power Delivery, Vol. 20, No. 2, pp. 1134–1142, Apr. 2005.
- [4] Lightning Protection Design Committee, Power station and Substation Sub-working group, "Guide to Lightning Protection Design for Power Stations, Substations and Underground Transmission Lines," Central Research Institute of Electric Power Industry, Comprehensive Report T40, December 1995.  
\* This document was revised to the following document  
Lightning Risk Research Committee, Power Station and Substation Lightning Risk Sub-Working Group, "Guide to Lightning Protection Design of Power Stations, Substations and Underground Transmission Lines (rev. 2011)," Central Research Institute of Electric Power Industry, Comprehensive Report H06, September 2012.
- [5] T. Ono, "Study on Switching Over-voltages in Power Systems," Central Research Institute of Electric Power Industry, Comprehensive Report 121, January 1985.

- [6] A. Ametani, "Distributed Parameter Circuit Theory," Corona Publishing Co., Ltd., 1990.
- [7] H. Matsubara, T. Ono, H. Motoyama, "Reduction of Switching Overvoltage on Transmission Lines," Central Research Institute of Electric Power Industry, Report T87085, Aug 1988
- [8] IEEE Working Group 15.08.09, "Modeling and analysis of system transients using digital programs," IEEE PES Special Publication, TP-133-0, 1998.
- [9] CIGRE Working Group 13.05, "The calculation of switching surges," ELECTRA, No. 32, pp. 17–42, 1974.
- [10] T. Noda, M. Takasaki, "A sub-network reduction method for the calculation of electromagnetic transients in a power system (Part 1)," Research Report T03013, March 2004
- [11] T. Watanabe, S. Funabashi, J. Sadakaji, "A method of switching surge analysis for 1000 kV power transformation equipment and results," IEE Japan, Switching Protection and High-voltage Research Group SP-94-47, HV-94-118, 1994.
- [12] J. Takami, S. Okabe and E. Zaima, "Lightning surge overvoltages at substations due to backflashover with assumed lightning current waveforms based on observations," IEEE Trans., Power Delivery, Vol. 25, No. 4, pp. 2958–2969, Oct. 2010.
- [13] J. Takami, S. Okabe and E. Zaima, "Study of lightning surge overvoltages at substations due to lightning strokes to phase conductors," IEEE Trans., Power Delivery, Vol. 25, No. 1, pp. 425–433, Jan. 2010.

END

Revision History		
Date	Example file version	Content changes
2014/11/19	2.0	Update for XTAP Version 2.00 Recalculation of line constants following the changes in XTLC
2013/08/20	1.0	Creation of the first edition (for XTAP Version 1.21)

<b>XTAP Example Collection</b>		<b>No.</b>	<b>SSW-03</b>
<b>Example Name</b>	Analysis of Input Surge Owing to Block Energization during Large-scale System Restoration		
<b>Field</b>	Large-scale system restoration, input surge calculation, switching surge calculation, overvoltage analysis		
<b>Reference</b>	“Review of Simulation Methods for Electromagnetic Transients in Power Systems and Simulation Cases Using XTAP (Part 1): Switching Transient Overvoltage Simulations,” Central Research Institute of Electric Power Industry, Study Report H12005.		
<b>Outline</b>	After describing the concept, the principle of occurrence, and the simulation method of each element of the transmission system for the case of an input surge owing to block energization during a large-scale system restoration, we introduce an example analyzing a 500/275-kV line using XTAP (excerpted from the above document).		

# 1 Input Surge Owing to Block Energization during Large-scale System Restoration

## 1.1 Concept , [2]

When a power outage occurs across a system of a power company within the entire area (hereinafter referred to as a “complete outage”), it is necessary to restore the system by starting from the voltage of the adjacent interconnected power company or from a self-starting generator. When adding voltage to a normal transmission line, as described in example SSW-02, we conduct an operation of setting the power transmission line to a no-load and turning on the circuit breaker at the power supply side for each transmission line. However, when restoring a complete outage, because a large amount of time is needed until restoration if the lines are energized one by one, as in the case of a normal voltage addition, we follow a procedure in which the system is divided into several blocks and the blocks are energized individually [3] (in this case, each block is set to no-load). Because many transmission lines and substations are included in a single block, the length of the transmission line becomes long, and its inductance and capacitance also increase. Further, the inductance and capacitance of the transformers in the substation add to this. Thus, in the case of energizing each block, as the stored electromagnetic energy increases owing to an increase in the equivalent inductance and capacitance, problems of an overvoltage and the processing energy of the arrestors tend to occur more frequently compared to the case of adding voltage to each line [4]. Therefore, for the purpose of examining the appropriate block division during a

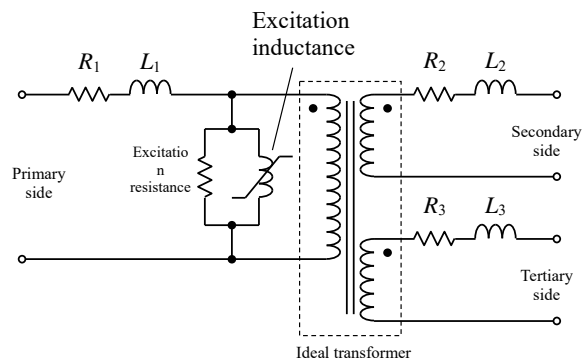
large-scale system restoration, and to grasp the overvoltage and processing energy of the arrestors in the determined block division, it is necessary to analyze the input surge phenomenon from a block energization.

### 1.2 Simulation of Each Element

The method of analysis of the input surge generated through block energization for a large-scale restoration is basically the same as the analysis method of the normal input surge described in SSW-02. However, considering the substation equipment included in the energized block, it is necessary to simulate the transformers and phase-modifying equipment not present in the normal input surge analysis. Therefore, beginning from the next section, we will describe the method for simulating the transformers and phase-modifying equipment.

### 1.3 Transformer Simulation

The transformer is simulated using the “basic equivalent circuit of a transformer,” which is a well-known circuit available in text books. Figure 1 shows its one-phase component. The equivalent circuit is composed of a winding resistance, leakage inductance, excitation resistance, excitation inductance, and an ideal transformer. In the case of a two-winding transformer, the leakage inductance is either equivalently placed on the primary side or divided between the primary and secondary sides in an appropriate ratio. In the case of a three-winding transformer, as the leakage inductances between the primary and secondary sides, secondary and tertiary sides, and tertiary and primary sides are given as the test results, the inductances of the primary, secondary, and tertiary sides are calculated from these data and used. The leakage inductance on the secondary side often has a negative value, and when this value is used as is, a numerical instability may occur in the simulation in certain cases [5]. In some cases, it is recommended to input a small positive inductance value while conducting an analysis using XTAP. Assuming the excitation resistance as linear, the resistance obtained from the result of the no-load test at the rated voltage is set. Simulating the



$R_1, L_1$ : Resistance and leakage inductance of the primary winding  
 $R_2, L_2$ : Resistance and leakage inductance of the secondary winding  
 $R_3, L_3$ : Resistance and leakage inductance of the tertiary winding

\* The figure above shows a one-phase component of a three-winding transformer. In the case of a two-winding transformer, the tertiary winding is not needed.

Figure 1 Fundamental equivalent circuit of a transformer

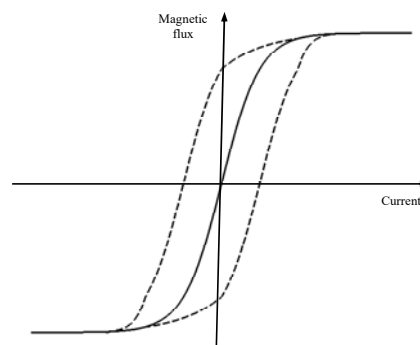


Figure 2 Hysteresis characteristics of iron core

excitation inductance as non-linear, saturation characteristics (current–magnetic-flux characteristics) of the iron core provided by the manufacturer is set. If the saturation characteristics of the iron core provided by the manufacturer also include the hysteresis characteristics, the characteristics passing through the center is used as shown in Figure 2. In this manner, the equivalent circuit for the phase of a transformer is obtained. This is prepared for the three phases, connected in patterns such as Y– $\Delta$  or Y–Y– $\Delta$ , and taken as the transformer model. In XTAP, because models of these three-phase transformers have been prepared in advance, an analyst does not have to apply the wiring (however, the excitation inductance is simulated as an exterior non-linear inductance).

#### 1.4 Simulation of the Phase-modifying Equipment

In the course of a large-scale system restoration, when energizing the blocks of the system one by one, each block is set to no-load. Therefore, to prevent a steady overvoltage owing to the Ferranti effect after energization, a shunt reactor, which is a type of phase-modifying equipment, may be added in certain cases [1], [4]. As shown in Figure 3, in the shunt reactor model, each phase of the reactor is simulated using a series connection of the inductance and resistance representing a loss, and these models are connected and used as the actual machine. If the saturation characteristics of the iron core is available, the inductance is taken as non-linear. Because shunt reactors are connected to the tertiary side of the main transformer, even in the model, they are connected in the same way as the actual machine. In addition, because the models of the shunt reactors are already available in XTAP, the analyst does not need to build an equivalent circuit.

#### 1.5 Harmonic Overvoltage

In the block energization during a large-scale system restoration, a sustained harmonic overvoltage with low attenuation occurs owing to a different principle from the input surge overvoltage explained here, of which studies are ongoing in Japan and abroad [4], [6]. This is an overvoltage caused by the flow of the excitation inrush current of the transformer at the timing that strengthens the natural vibration at each cycle when the natural frequency of the block to be energized matches an integral multiple of the lower order of the commercial frequency. Because the natural vibration is excited as long as the above-mentioned timing is met, and the damping is small as long as the block that is energized is on a no-load, the attenuation is small.

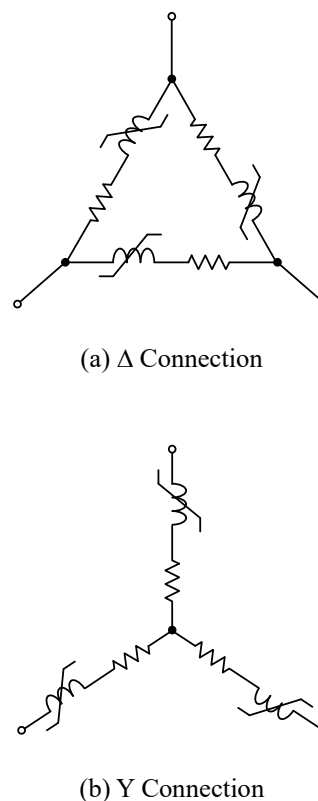
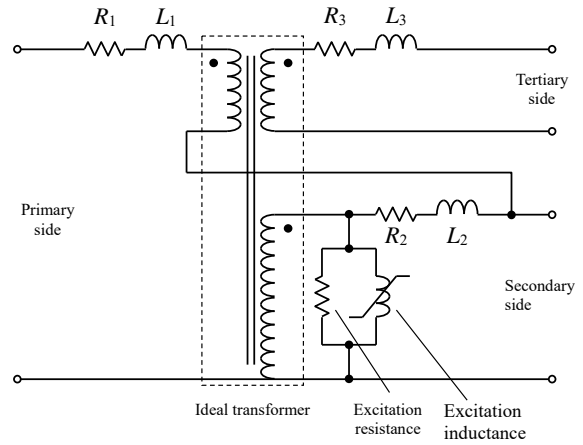


Figure 3 Shunt reactor models

## 1.6 Example of Analysis using XTAP

Considering the 500/275-kV system shown in Figure 4 as one of the blocks during a complete outage restoration, we calculate the overvoltage generated at the time of energizing this block. The power source side of the circuit breaker to be closed is simulated using the equivalent circuit of example SSW-02 shown in Figure 7, taking into consideration the frequency characteristics. Here, assuming the frequency characteristics to be same as the characteristics of a transformer with a 500-MVA capacity indicated in the CIGRE guidelines [7], the constants of the equivalent circuit are calculated from the assumed short circuit capacity (10,000 MVA) (the calculated constants of which are shown in Figure 4).



$R_1, L_1$ : Resistance and leakage inductance of the primary winding  
 $R_2, L_2$ : Resistance and leakage inductance of the secondary winding  
 $R_3, L_3$ : Resistance and leakage inductance of the tertiary winding

\* The above figure shows one phase in the case of a three-winding transformer

Figure 5 Basic equivalent circuit of an autotransformer

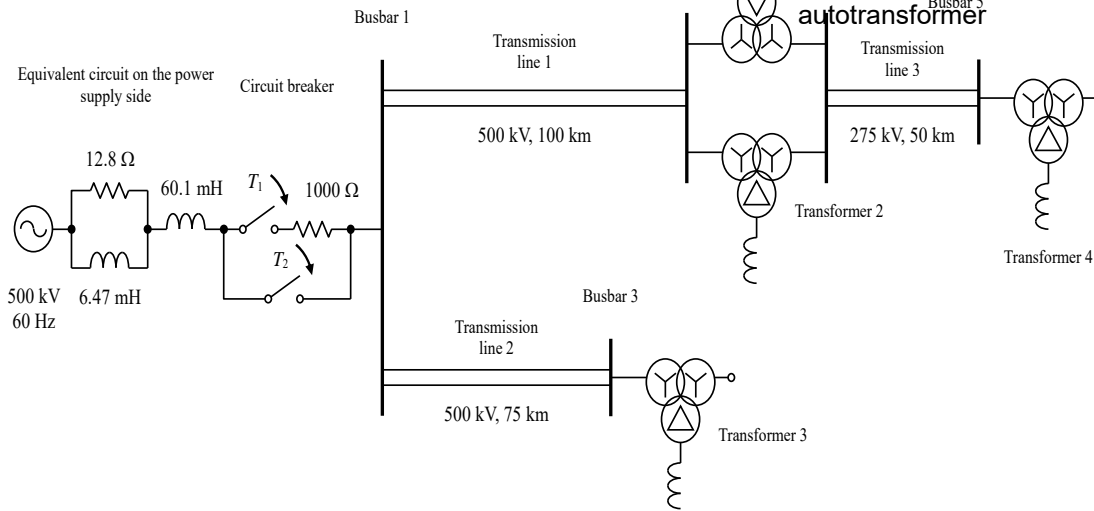


Figure 4 Example circuit for the calculation of input surge owing to block energization

Because the circuit breaker to be closed has the closing resistance of example SSW-02 shown in Figure 9(b), the value of the input resistance is set to 1,000  $\Omega$ .

The average time  $T_1$  from the close command to the resistance input, and the average time  $T_2$  from the resistance input to the resistance short-circuit, are both set to 10 ms, and the variation of the resistance input  $\sigma_1$  and the variation of the resistance short-circuit  $\sigma_2$  are both set to 1.5 ms. Transmission lines 1 and 2 are both 500-kV overhead transmission lines with lengths of 100 and 75 km, respectively. Further, transmission line 3 is a 275-kV overhead transmission line with a length of 50 km. Assuming the pillar assembly of the transmission lines to be the standard pillar assembly in [8], and the earth resistivity as 100  $\Omega\text{m}$ , we simulated the assembly using a frequency-dependent model. The line constant calculation frequency samples for the creation of the frequency-dependent model are set to 400 points within the range of 0.1 Hz to 10 MHz. Transformers 1, 2, and 3 are 500-, 275-, and 77-kV autotransformers, respectively, having the same constants, and are simulated using the equivalent circuit shown in Figure 5. Although the basic concept of this equivalent circuit is the same as the basic equivalent circuit of a transformer described in Section 1.3, compared with Figure 1, this is modified to an autotransformer connection where the low-voltage side of the primary winding and secondary winding are common. Transformer 4 is a three-winding transformer of 275/77/22 kV, which is simulated using the basic equivalent circuit of Figure 1. In all transformers, the saturation characteristics of the excitation inductance is set to a two-line approximation, as shown in Figure 6. Further, it is assumed that shunt reactors are connected to the tertiary side of each transformer, and are simulated using the  $\Delta$ -connection model shown in Fig. 3 (a). For simplicity, the inductance and resistance values are calculated from the assumed capacity without considering the non-linear characteristics of the reactor. The constants of the transformer and the shunt reactor above are shown in Table 1. The lightning was simulated using a non-linear resistor having the characteristics of a 30% reduced high-performance lightning arrester described in [8]. Regarding the installation location and quantity, a resistor was installed on buses 1 through 5. The XTAP data thus created are shown in Figure 7.

Using these data, we conducted 300 simulations with the timing at which the close command is issued as a random number uniformly distributed between  $0^\circ$  and  $360^\circ$  of the power supply phase. The calculation time increment is set to  $0.5 \mu\text{s}$ . Figure 8 shows the maximum value of the voltage generated in bus 5 plotted in pu on a normal probability plot (taking the peak of the nominal voltage to ground as 1 pu). Here, the largest among the maximum values of the voltage waveforms of each phase was taken as the maximum. From Figure 8, the 2% value, which is the maximum value of the generated voltage corresponding to a cumulative frequency of 2% is approximately 1.8 pu. A plot of the voltage waveform of each phase of the case corresponding to this 2% value is shown in Figure 9. In the case corresponding to the 2% value, it can be confirmed that the maximum voltage is generated in phase-b.

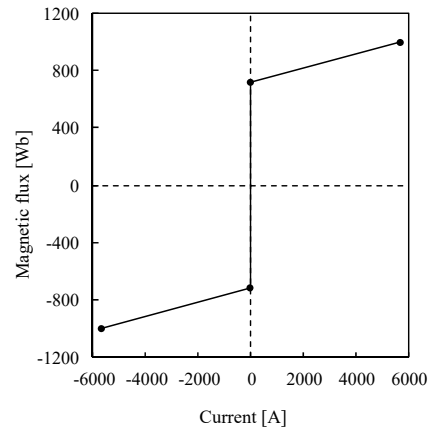


Figure 6 Saturation characteristics of excitation inductance

Table 1 Transformer and shunt-reactor constants used in analysis

(a) Transformers 1–3

$R_1$	0.152 $\Omega$	$L_1$	87.6 mH
$R_2$	0.227 $\Omega$	$L_2$	17.8 mH
$R_3$	0.178 $\Omega$	$L_3$	4.30 mH
Excitation resistance		400 k $\Omega$	

(b) Transformer 4

$R_1$	0.756 $\Omega$	$L_1$	60.2 mH
$R_2$	0.237 $\Omega$	$L_2$	0.001 mH
$R_3$	0.0484 $\Omega$	$L_3$	1.93 mH
Excitation resistance		150 k $\Omega$	

(c) Shunt-reactor

Transformers 1–3 (per phase)			
$R$	0.741 $\Omega$	$L$	590 mH
Transformer 4 (per phase)			
$R$	0.121 $\Omega$	$L$	96.3 mH

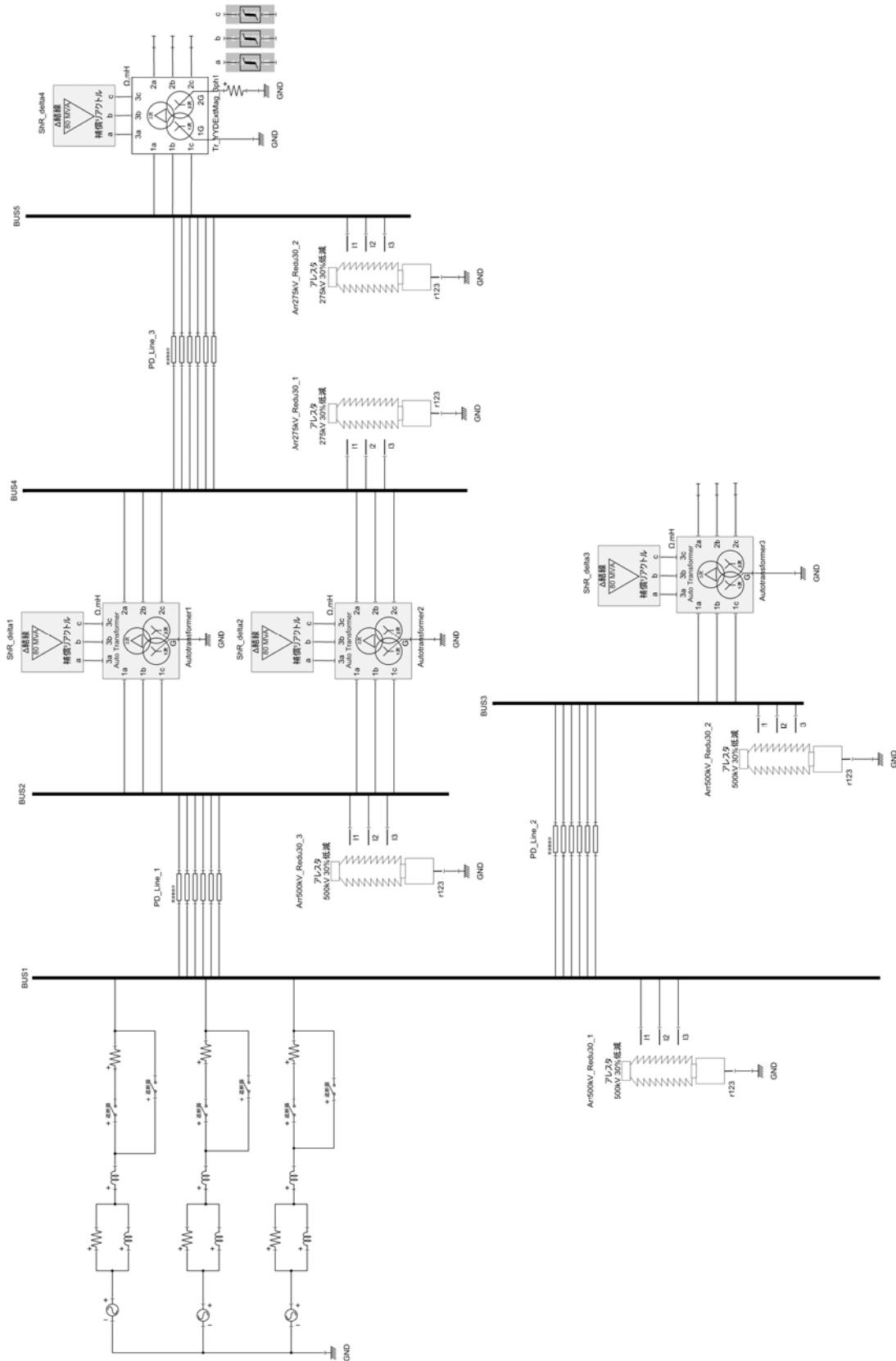


Figure 7 XTAP data for the calculation of input surge owing to block energization

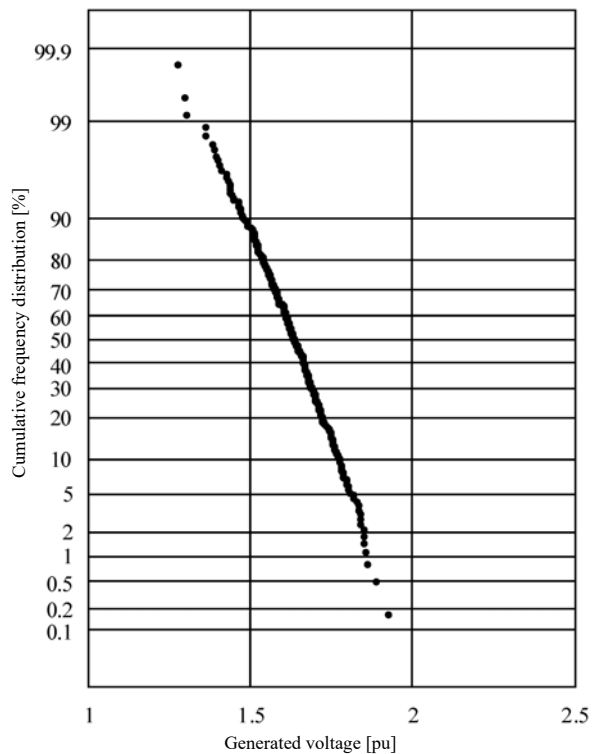
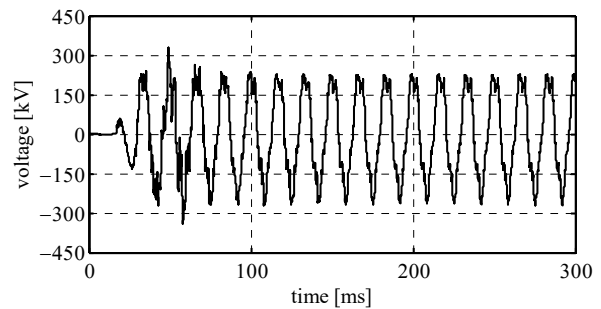


Figure 8 Cumulative frequency distribution of the voltages appearing in busbar 5

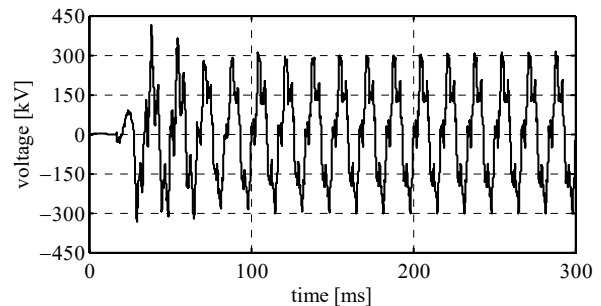
### References

- [1] M. M. Adibi, "Power system restoration: Methodologies & implementation strategies," IEEE Press, 2000.
- [2] M. M. Adibi and L. H. Fink, "Restoration from cascading failures," IEEE Power & Energy Magazine, pp. 68-77, Sep./Oct. 2006.
- [3] M. M. Adibi and R. J. Kafka, "Power system restoration issues," IEEE Computer Applications in Power, Vol. 4, No. 2, pp. 19-24, Apr. 1991.
- [4] M. M. Adibi, R. W. Alexander and B. Avramovic, "Overvoltage control during restoration," IEEE Trans., Power Systems, Vol. 7, No. 4, pp. 1464-1470, Nov. 1992.
- [5] X. Chen, "Negative inductance and numerical instability of the saturable transformer component in EMTP," IEEE Trans., Power Delivery, Vol. 15, No. 4, pp. 1199-1204, Oct. 2000.
- [6] K. Furukawa, T. Funakoshi, T. Kawachino, S. Takasaki, T. Shimojo, K. Hirayama, T. Sogabe, T. Shimamura, S. Nohara, "Transient overvoltage in a high-voltage transformer and countermeasures to prevent overvoltage under applied voltage at black start," IEEJ Journal B, Vol 125, No. 1, pp. 53-64, 2005.
- [7] CIGRE Working Group 13.05, "The calculation of switching surges," ELECTRA, No. 32, pp. 17-42, 1974.
- [8] Lightning Protection Design Committee, Power station and Substation Sub-working group, "Guide to Lightning Protection Design for Power Stations, Substations and Underground Transmission Lines," Central Research Institute of Electric Power Industry, Comprehensive Report T40, December 1995.

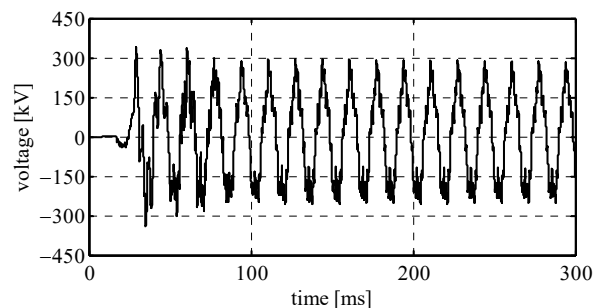
\* This document was revised to the following document.



(a) Phase-a voltage



(b) Phase-b voltage



(c) Phase-c voltage

Figure 9 Waveforms of the voltages appearing at bus 5 for a 2% value

Lightning Risk Research Committee, Power Station and Substation Lightning Risk Sub-Working Group, "Guide to Lightning Protection Design of Power Stations, Substations and Underground Transmission Lines (rev. 2011)," Central Research Institute of Electric Power Industry, Comprehensive Report H06, September 2012.

END

Revision History		
Date	Example File Version	Content changes
2014/11/19	2.0	Update for XTAP Version 2.00 Recalculation of line constants owing to the change in XTLC
2013/09/09	1.0	Creation of the first edition (for XTAP Version 1.21)

<b>XTAP Example Collection</b>		<b>No.</b>	<b>SSW-04</b>
<b>Name of the Example</b>	Comparison of the Ground-fault Surge Analysis of a 500-kV Power Transmission Line with the Actual Measurements		
<b>Field</b>	Ground fault surge calculation, switching surge calculation, overvoltage analysis		
<b>References</b>	Central Research Institute of Electric Power Industry, Survey Report H12005, “Review of Simulation Methods for Electromagnetic Transients in Power Systems and Simulation Cases using XTAP (Part 1): Switching Transient Overvoltage Simulations”		
<b>Outline</b>	We describe the concept of a ground-fault surge, its principle of occurrence, and the method of simulation of each element in the power transmission system, and introduce an example of the ground-fault surge analysis of a 500-kV transmission line using XTAP (excerped from the above reference).		

# 1 Ground-Fault Surge

## 1.1 Concept [1]-[4]

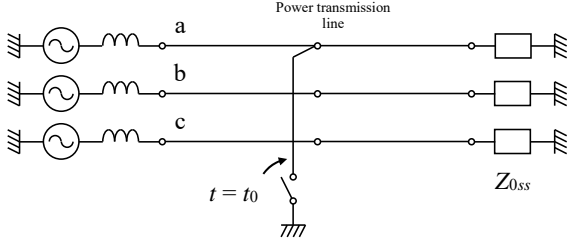
When a ground-fault occurs in the transmission lines from a lightning strike or similar event, an overvoltage occurs during a healthy phase. In the case of multi-line transmission lines, an overvoltage also occurs in each phase of the circuits other than the circuit where the fault occurred. This is called the ground-fault surge. If the insulation level of the transmission line is inadequate, there is a risk of a one-phase ground fault accident progressing into a multi-phase or a multi-circuit ground fault accident. Hence, from this perspective, an overvoltage needs to be considered during the insulation design. In particular, if an overvoltage from an input surge is kept low by a resistance input or by the effect of arrestors in the substation, the ground-fault surge becomes a problem in the insulation of the transmission lines. Because an overvoltage from a ground-fault surge is an overvoltage that occurs in transmission lines rather than in substations, the unavailability of an effective suppression method such as the installation of an arrester is also a feature.

Herein, we briefly summarize the difference of this concept from the input surge. As described in example SSW-02, the magnitude of an input surge overvoltage is statistically evaluated from the results of numerous input surge calculations conducted by randomly changing the closing timing of the circuit breaker. Specifically, in the case of no closing resistance, the magnitude of the input surge overvoltage is determined based on the timing of the close command as well as the closing timing of the three circuit breakers that is stochastically determined based on this timing. If a closing resistance is present, the magnitude of the input surge overvoltage is determined based on the timing of the close command as well as the close timing of the six circuit breakers

stochastically, which is also determined based on this timing. Further, the timing of the close command is also determined stochastically. Thus, because the magnitude of the input surge overvoltage depends on the multiple timings that are stochastically determined, the probability of occurrence of the combination of the closing timing that can cause a maximum overvoltage is extremely low. Therefore, rather than finding the maximum value of the overvoltage whose occurrence frequency is extremely low, it is considered reasonable to conduct a statistical evaluation. In contrast, in the case of a ground-fault surge analysis, because the problem is a single-line ground-fault that occupies the majority of ground-fault accidents, the phase of the power supply voltage that causes the ground-fault is gradually changed to obtain the maximum value of the overvoltage. Although the timing at which the event that causes a ground-fault, such as lightning, is probabilistic, it does not depend on stochastically determined multiple timings, as in the case of an input surge, but depends only on the timing at which a single-line ground fault occurs. Hence, it is considered that the ground-fault at the phase that gives the maximum overvoltage may be sufficient. Usually, an overvoltage becomes maximum when a ground-fault occurs just after the instant when the power supply voltage of the ground-fault phase attains the peak value.

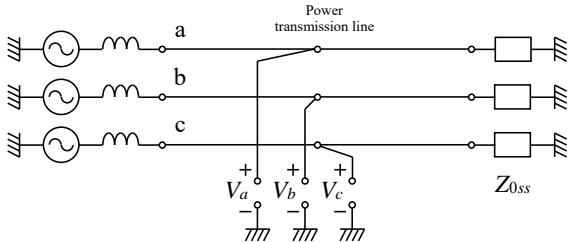
1.2 Principle of Occurrence of Ground-fault Surge [1], [2], [4]

The mechanism of occurrence of a ground-fault surge can be easily understood by considering it as the overlap of a transient voltage caused by a ground-fault of a steady voltage from a source voltage. The steady voltage corresponds to the voltage before the occurrence of the ground-fault. However, considering a transmission line where the source voltage is virtually zero and the voltage occurring in the ground-fault phase before the



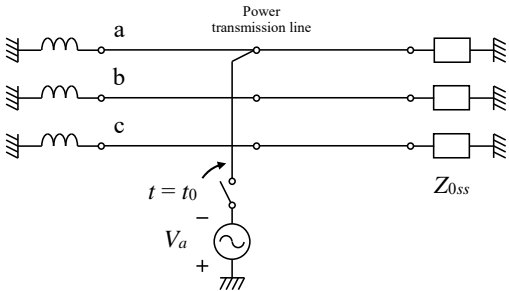
(a) Ground-fault of phase-a at  $t = t_0$

||



(b) Steady voltage

+



(c) Transient voltage

- \* A ground fault is assumed to be at the center of the transmission line
- \* The impedance of the power supply side is simply displayed with only the inductance
- \*  $Z_{0ss}$  is the combined value of the characteristic impedance of the transmission line connected to the load side substation

Figure 1 Mechanism of occurrence of ground-fault surge

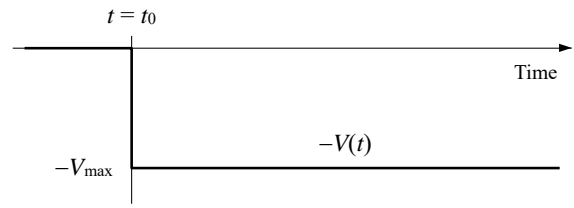
ground-fault is  $+V(t)$ , the transient voltage is the voltage occurring in each phase when a voltage of  $-V(t)$  is superposed on the ground-fault phase at the time of the ground fault.

Considering the superposition of the steady voltage and the transient voltage, the voltage of the ground-fault phase will become zero (ground-fault condition) owing to the cancellation of  $+V(t)$  by  $-V(t)$ , and the voltage of the healthy phases will be the sum of the transient voltage generated by applying  $-V(t)$  to the ground-fault phase and the steady voltage. Taking the case of a ground-fault of phase-a of a single-circuit transmission line as an example, Figure 1 shows an illustration of the mechanism of occurrence of the above-mentioned ground-fault surge.

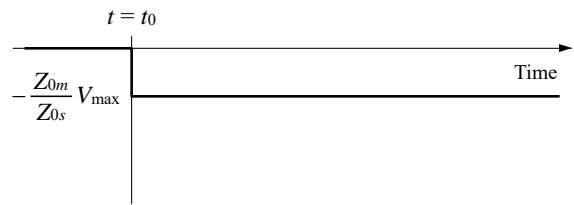
Here, we discuss the transient voltage component in more detail. Because the largest overvoltage is generated when a ground fault occurs at the center of the transmission line owing to reasons to be described later, we consider the ground fault to be at the center of the transmission line. First, the transient voltage component of the ground-fault surge is the voltage that occurs in each phase when the voltage in the ground-fault phase before the ground-fault is  $+V(t)$  and when a voltage of  $-V(t)$  is applied on the ground-fault phase at the time of occurrence of the ground fault, when considering a transmission line with a source voltage of virtually zero. For example, if the ground-fault occurs when the voltage of the ground-fault phase has a positive peak value,  $-V(t)$  rises stepwise from zero to the negative peak value  $-V_{\max}$ , and thereafter varies sinusoidally. However, because the overvoltage in question occurs within a time region shorter than a cycle of the commercial frequency,  $-V(t)$  can be approximately regarded as a step wave rising from zero to  $-V_{\max}$  without any problem, as shown in Figure 2(a). When such a step wave is applied to the ground-fault phase at the center of the transmission line where the supply voltage is virtually taken as zero, an overvoltage represented by the following equation occurs during the induction phase.

$$V_m = -\frac{Z_{0m}}{Z_{0s}} V_{\max} \quad (1)$$

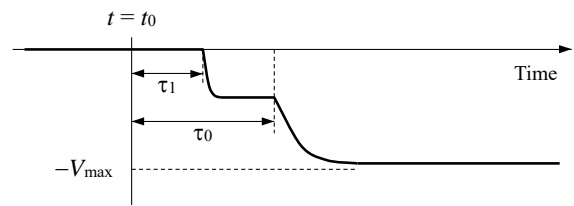
However,  $Z_{0s}$  is the component of the ground-fault phase of the characteristic impedance matrix, and  $Z_{0m}$  is the mutual component between the induction phase in focus and the ground-fault phase of the same matrix; in addition, although  $Z_{0m}/Z_{0s}$  depends on the type and arrangement of the line, it normally takes a value of between 0.1 and 0.35. From the above, the waveform of the voltage  $V_m$  of the induction phase at the center of the transmission line can be illustrated, as shown in Figure 2(b). Next, we consider the waveform of this surge when it has propagated to a point of distance  $x$ . It is known that when a surge propagates along a transmission line, it splits into several line waves and ground return waves. A line wave is a propagation mode where the forward and return paths of the current flow are the phase conductors of the transmission line and the propagation speed is almost equal to the speed of light. Precisely, although several line waves exist, for simplicity, we collectively refer to them as a line wave. In contrast, the ground return wave is a propagation mode where the three phase conductors of the transmission line are collectively taken as the current forward path and the ground is taken as the return path. The propagation speed of the ground return path is approximately 90% of the speed of the line wave. Taking the propagation speeds of the line wave and the ground return wave as  $v_1$  and  $v_0$  respectively, the time required for the arrival of the line wave and the ground wave to point P at distance  $x$  from the ground-fault point is  $\tau_1 = x/v_1$  and  $\tau_0 = x/v_0$ , respectively. That is, at point P, as shown in Figures 2(c), and 2(d), the line wave arrives at a time  $\tau_1$  after a ground-fault, after which the ground return wave arrives after the time  $\Delta\tau = \tau_0 - \tau_1$  has elapsed. Because the line wave that arrives earlier takes the ground-fault phase as the forward path and the induction phase as the return path, the



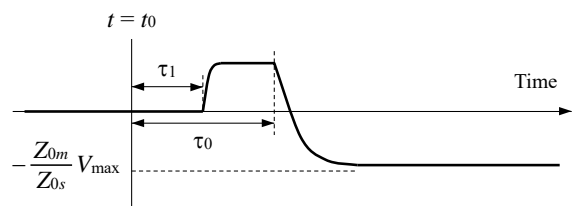
(a) Voltage of ground-fault phase at ground-fault point



(b) Voltage of induction-phase at ground-fault point



(c) Voltage of ground-fault phase at point P



(d) Voltage of induction phase at point P

Figure 2 Branching phenomenon

voltage of the induction phase is opposite in polarity to the ground-fault phase. The earth return wave has the same polarity because both the ground-fault phase and the induction phase are forward paths. Therefore, during  $\Delta\tau$  when the line wave has arrived, if the induction phase has an opposite polarity to the ground-fault phase, that is, when  $-V(t)$  is a step wave that rises negatively, as currently considered, a positive surge occurs. If the underground cable and many overhead transmission lines are connected to the busbars of the substations (or the power stations) at both ends of the transmission lines, and if the condition in which the characteristic impedance seen from the transmission line causing the ground-fault is sufficiently small is satisfied, the line wave surge with a positive polarity will return to the center of the transmission line as a negative surge owing to a negative reflection at both ends of the busbars. At this time, because the source voltage of the ground-fault phase is near the positive peak, the source voltage of the induction phase is negative, and hence, a negative overvoltage determined by the surge impedance shown in Figure 2(b) is superimposed. Here, a negative surge that is negatively reflected from both sides of the above-mentioned transmission line is superimposed, and further, when the surge is reflected at the ground-fault point, the negative surge of the inductance phase increases. In detailed surge calculations, the overvoltage of inductance phase can theoretically bridge up to a maximum of approximately 2 pu. However, this is the most severe case in which the ground fault occurs exactly at the center of the transmission line, and the condition in which the characteristic impedances of the busbars at both ends of the transmission line are extremely small was satisfied. The ground-fault surge occurring in reality will be smaller. The reason why the overvoltage reaches the maximum when the ground-fault occurs at the center of the transmission line is because the line wave surge negatively reflected from both sides of the transmission line is superimposed at the same timing.

Because the propagations of multiple line-waves are not the same, the propagation of few tens of kilometers causes a difference of approximately a few  $\mu\text{s}$  in the propagation time. Thus, although it depends on the line length, protrusions on the order of a few  $\mu\text{s}$  to a few tens of  $\mu\text{s}$  occur in the voltage waveform, which may become the peak value. However, because the duration of these protrusion-like voltages is within the time range of the lightning surge rather than the switching surge, considering the characteristics ( $V-t$  characteristics) where the insulation performance of the insulator becomes higher as the time of voltage application becomes shorter, it can be ignored as a switching surge-like overvoltage.

### 1.3 Simulation of Each Element

The simulation of each element in the ground-fault surge calculation can be basically considered similar to the input surge calculation described in example SSW-02. Similar to the case of an input surge calculation, the difficulty is to determine how far the system must be simulated. Basically, we follow each transmission line from both ends of the transmission line to be analyzed, and simulate in detail up to those substations that are determined to have a large influence on the analysis results, taking into consideration the type and length of the transmission line, as described in example SSW-02 of section 1.7. The systems far from the substation located at the end of the detailed simulation range are simulated with the appropriate equivalent circuits, considering whether the system seen from there is a power source or a load. Because it is not easy to specify the range of the

system that must be simulated in detail, in reality, trial ground-fault surge calculations are conducted to observe its influence. Hence, it is often determined through trial and error. In the calculation of a ground-fault surge, because the calculation results will be toward the severe side as the impedance of both ends of the transmission line becomes smaller, upon knowing that the results of the severe side can be obtained, a practical way to connect a voltage source and a small impedance on both the ends of the line is also possible.

#### 1.4 Example Analysis using XTAP

We introduce an example of calculating the ground-fault surge overvoltage for the case of a ground-fault occurring in phase-b of the first circuit, exactly at the center of power transmission line A, in the 500-kV power transmission system shown in Figure.

Here, G1 and G2 are the power stations simulated using the equivalent circuit of Figure 6 in the example SSW-02. The value of the inductance is calculated from  $X_d''$  of the assumed generator and the impedance of the step-up transformer. Here, G3 and G4 are the contracted representations of the systems far from busbars 3 and 4, respectively, and are simulated using the equivalent circuit of example SSW-02 shown in Figure 6. Assuming that the power source frequency is 60 Hz and the tidal current does not affect the overvoltage, the phases of the four three-phase voltage are assumed to be the same. Assuming all power transmission lines to be standard columns for 500 kV, as mentioned in [6], and the ground resistivity to be 100  $\Omega\text{m}$ , the simulation is conducted using a frequency-dependent line model. Samples of the line constant calculation frequency for creating the frequency-dependent line model were set to 400 points within the range of 0.1 Hz to 10 MHz. The ground-fault resistance, which simulates the arc resistance at the time of a ground-fault and the tower foot grounding resistance, is set to 1  $\Omega$ . For the sake of simplicity, the load was not simulated. The XTAP data simulated in this manner are shown in Figure 4. Using these data, we conducted a simulation by changing the timing at which the ground-fault occurs from 0° to 180° of the phase of the power source voltage in increments of 1°, and determined the characteristics of the maximum overvoltage with respect to the phase of the power source at the time of occurrence of the ground-fault. The pu (the peak value of the nominal voltage to the ground is 1 pu) of the results is shown in Figure 5. Because the protrusion-like voltage waveform generated by the propagation time difference between multiple line waves is also simulated, the calculation time step is taken as 1  $\mu\text{s}$ . From Figure 5, if the ground-fault occurs when the phase of the power source is 50°, the generated overvoltage attains the maximum value. Figure 6 shows the voltage waveforms of each phase calculated under this condition. The maximum overvoltage is generated in phase-c of the first line. The file name of this example is SSW-04-A.xsf.

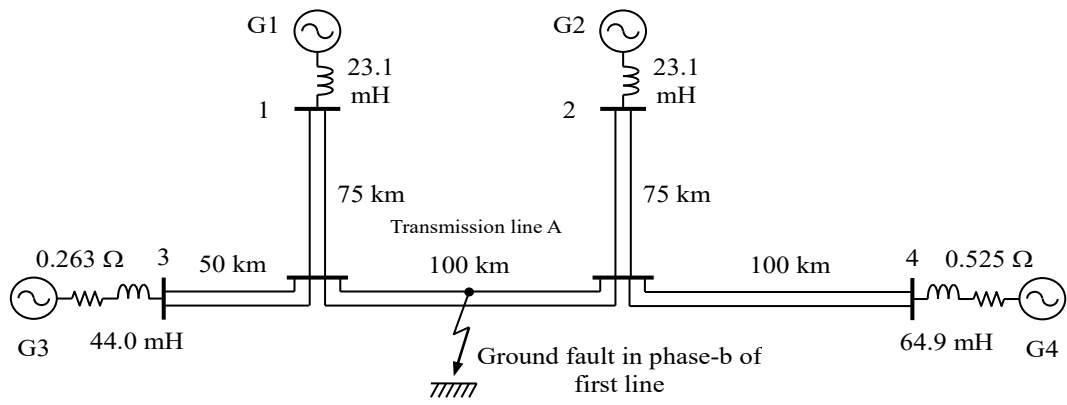


Figure 3 Example circuit of ground-fault surge calculation

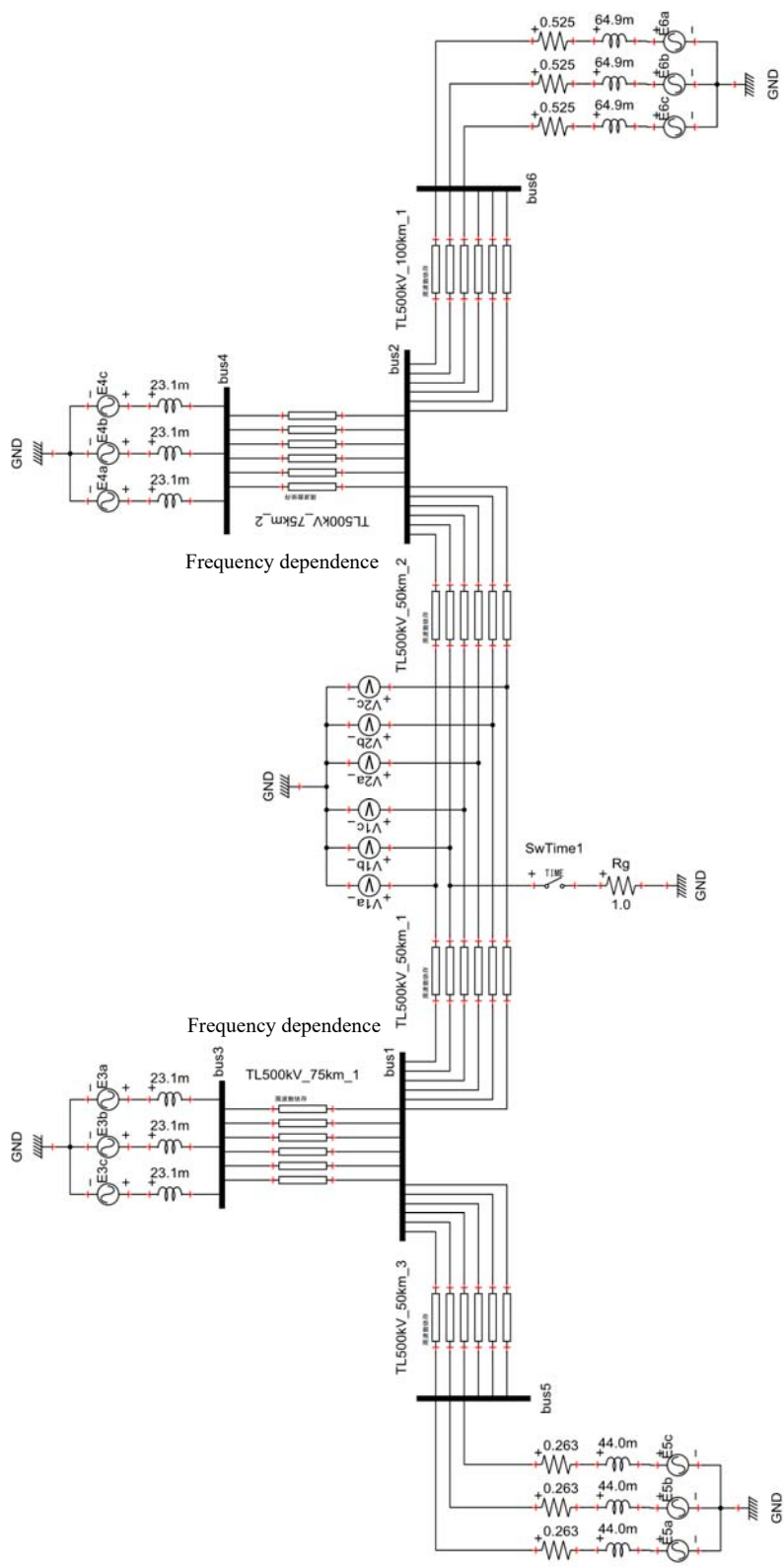


Figure 4 XTAP data for ground-fault surge calculation

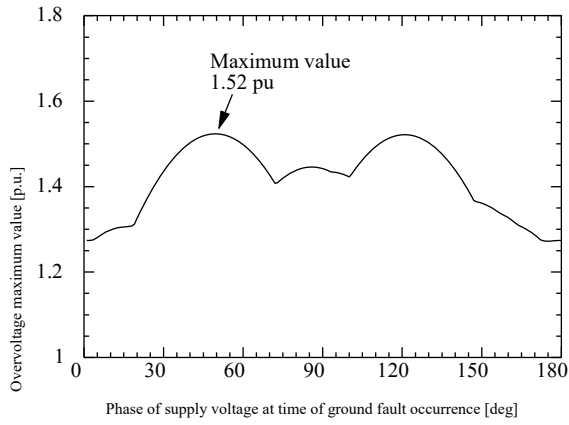
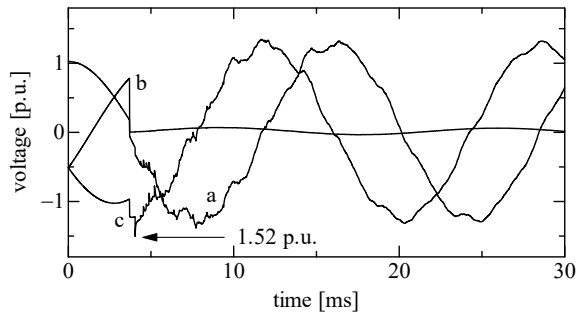
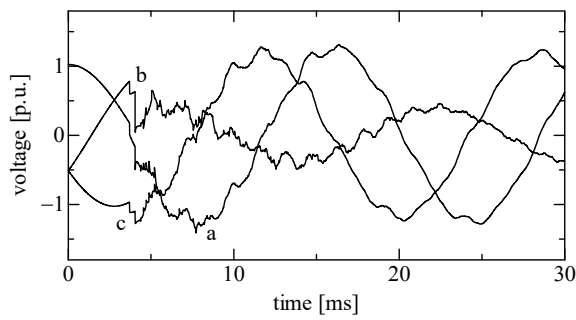


Figure 5 Maximum voltage versus phase of source voltage at time of occurrence of ground-fault



(a) First circuit

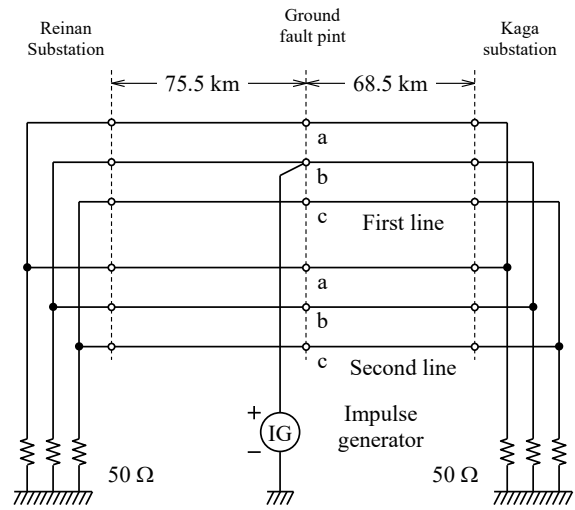


(b) Second circuit

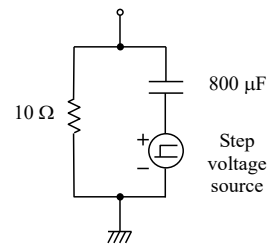
Figure 6 Calculation results at the time of occurrence of ground-fault when the phase of the source voltage is  $50^\circ$

## 1.5 Comparison with Actual Measurement Results

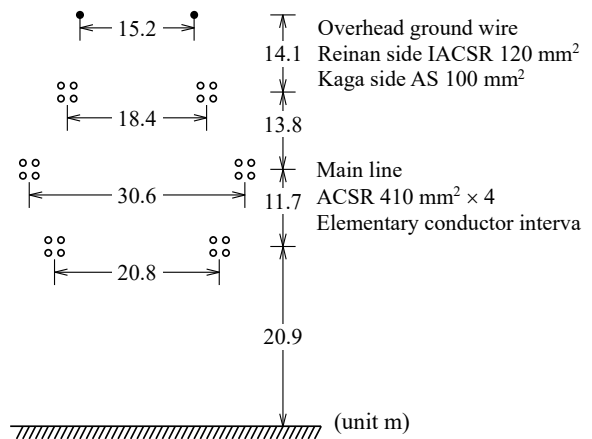
To reproduce the results of the ground-fault surge test [5] conducted at the 500-kV Kaga-Reinan line connecting the Hokuriku Electric Power Kaga Substation and Kansai Electric Power Reinan Substation, we introduce an example simulation using XTAP. As described in Section 1.2, the transient voltage component generated by a ground-fault surge is obtained as the voltage generated when the voltage of the ground-fault phase before the ground-fault is  $+V(t)$  and when a voltage of  $-V(t)$  is applied to the ground-fault phase at the time of occurrence of the ground-fault, when considering a transmission line where the source voltage is virtually zero. Therefore, in this surge test, the source voltage is made zero by grounding each phase of the busbars in both ends of the Kaga-Reinan line to an impedance, and a voltage corresponding to the above-mentioned  $-V(t)$  is applied to the ground-fault phase at the ground-fault point such that only the transient voltage component is generated. The impedance that grounds each phase of the busbars at both ends of the line simulates the impedance of the system far from it in a simple manner, and herein we compare the actual measurement result with the calculation result when this is set to a resistance of  $50\ \Omega$ . Figure 7 shows the test circuit, the equivalent circuit of the impulse generator used for the voltage application, and the conductor arrangement of the Kaga-Reinan line. The ground-fault point is not the exact center of the line but is only 3.5 km from the center toward the Kaga Substation side. Further, the phase of the ground-fault is phase-b of the first line. Figure 8 shows the XTAP simulation data of this test circuit. The transmission lines are



(a) Test circuit



(b) Equivalent circuit of impulse generator



(c) Conductor arrangement of Kaga-Reinan line

Figure 7 Ground-fault surge test at Kaga-Reinan line

simulated using a frequency-dependent line model, and the frequency samples for a constant line calculation were set to 400 points within the range of 0.1 Hz to 10 MHz. The calculation time step of the simulation was set to 0.5  $\mu$ s. Figure 9 shows the results of the actual measurement, and Figure 10 shows the calculation results. Including the protrusion-like voltage waveform caused by the difference in the propagation time of multiple line waves, the calculation results agree well with the actual measured results. The file name of this example is SSW-04-B.xsf.

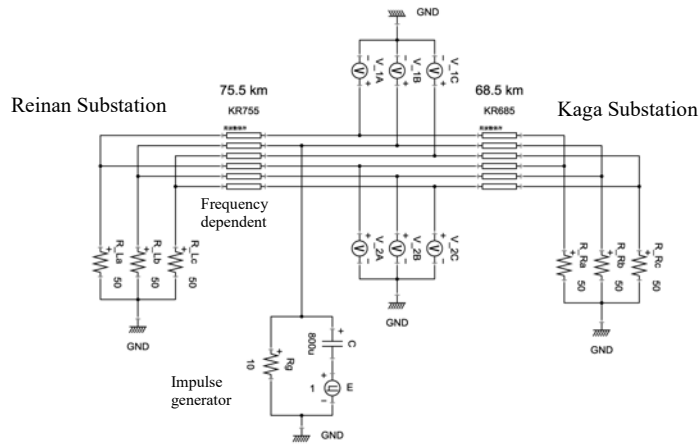


Figure 8 XTAP data reproducing the ground-fault surge test of Kaga-Reinan line

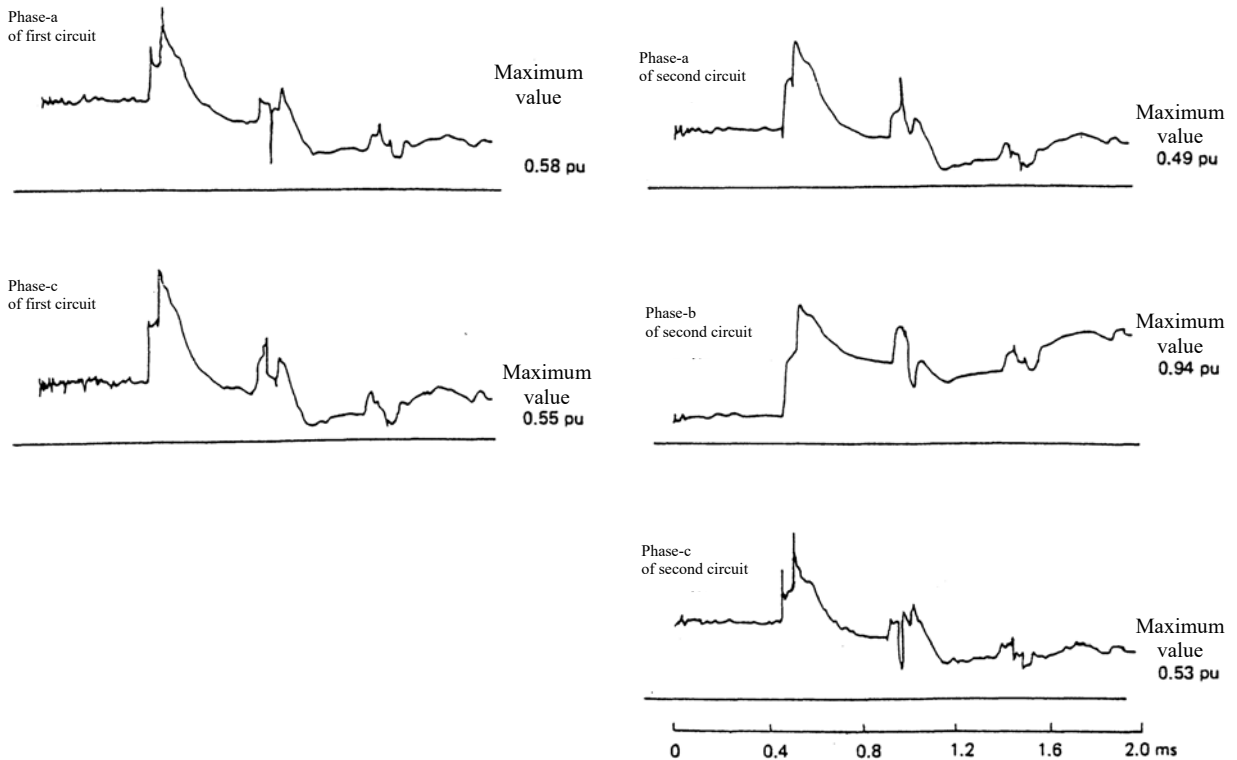


Figure 9 Measured results of ground-fault surge test at Kaga-Reinan line

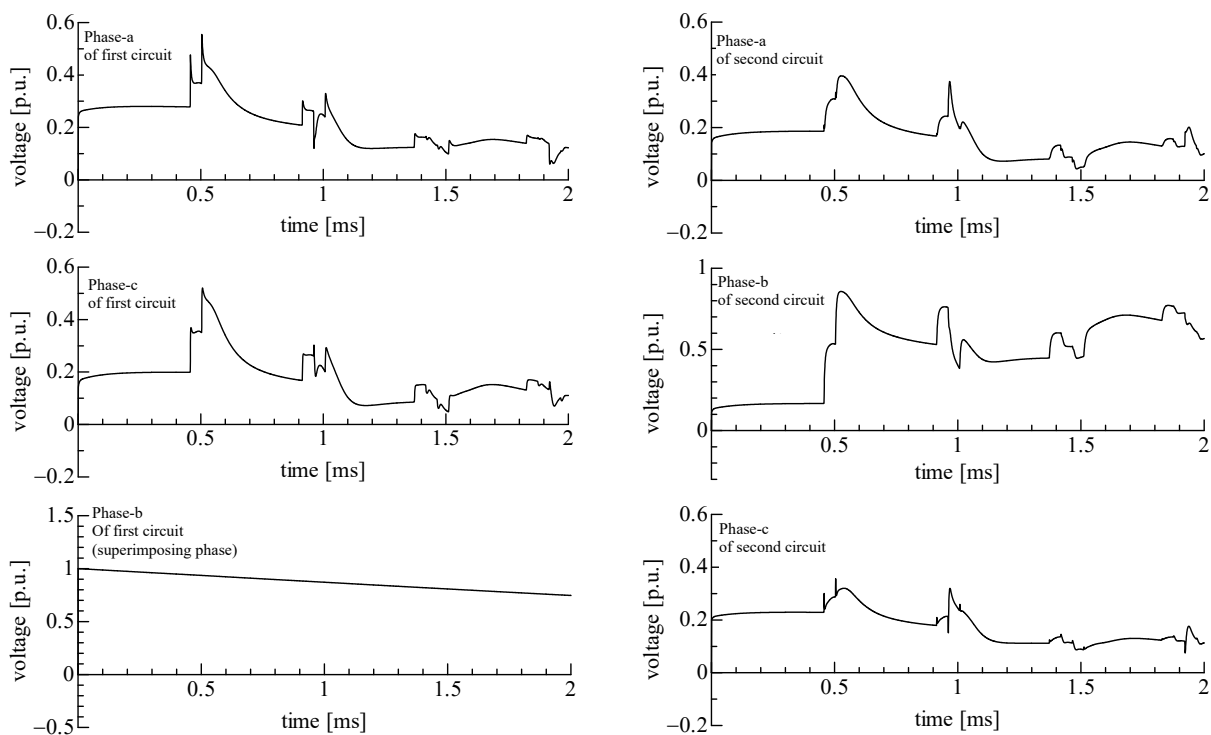


Figure 10 Calculation results of Kaga-Reinan line ground-fault surge test using XTAP

## References

- [1] T. Kono, "Theory of System Insulation," Corona Publishing Co., Ltd. 1984.
- [2] T. Ono, "Study on Switching Over-voltages in Power Systems," Central Research Institute of Electric Power Industry, Comprehensive Report 121, January 1985.
- [3] T. Watanabe, S. Funabashi, J. Sadakaji, "A method of switching surge analysis for 1000 kV power transformation equipment and results," IEE Japan, Switching Protection and High-voltage Research Group SP-94-47, HV-94-118, 1994.
- [4] E. W. Kimbark and A. C. Legate, "Fault surge versus switching surge: A study of transient overvoltages caused by line-to-ground faults," IEEE Trans., Power Apparatus and Systems, Vol. PAS-87, No. 9, pp. 1762-1769, Sep. 1968.
- [5] T. Ono, H. Matsubara, "Prediction of Fault Surge with TNA," Central Research Institute of Electric Power Industry, Research Report 177042, March 1978
- [6] Lightning Protection Design Committee, Power station and Substation Sub-working group, "Guide to Lightning Protection Design for Power Stations, Substations and Underground Transmission Lines," Central Research Institute of Electric Power Industry, Comprehensive Report T40, December 1995.

\* This document was revised to the following document

Lightning Risk Research Committee, Power Station and Substation Lightning Risk Sub-Working Group, "Guide to Lightning Protection Design of Power Stations, Substations and Underground Transmission Lines (rev. 2011)," Central Research Institute of Electric Power Industry, Comprehensive Report H06, September 2012.

END

Revision History		
Date	Example File Version	Content changes
2014/11/19	2.0	Update for XTAP Version 2.00 Recalculation of line constants owing to change in XTLC
2013/09/09	1.0	Creation of first version (for XTAP Version 1.21)

<b>XTAP Example Collection</b>		<b>No.</b>	SSWD-01
<b>Example Name</b>	Ground-fault Surge Propagation Analysis of a 6.6-kV Power Distribution Line		
<b>Field</b>	Ground fault surge analysis		
<b>References</b>	<p>(1) Electric Technology Research Association, Advanced Technical Committee on Distribution Automation Technology, “Advancements in Power Distribution Automation Technology,” Vol. 72, No. (2016)</p> <p>(2) Kyushu Electric Power Co., Ltd., Kyushu Technosystems Co., Ltd., The Method of Calculating Surge Propagation Speed in Accident Point Locating System, Japanese Patent No. 5085111, 2012.11.28</p>		
<b>Outline</b>	<p>At present, if a ground-fault accident occurs in a distribution line, it takes a significant amount of time to locate the accident site. To solve this problem, various ground fault location methods have been proposed. In this example, we describe the principle of standardization using the “ground-fault surge arrival time difference analysis method,” which is one of the ground-fault location standardization methods. Next, we describe the modeling of various types of power distribution equipment and finally conduct a ground-fault surge propagation analysis of the system created by combining the modeled distribution equipment. Based on the results, we study the standardization using the “ground-fault surge arrival time difference analysis method.”</p>		

## 1 Ground-fault Surge Arrival Time Difference Analysis Method

### 1.1 Standardization Principle

In the ground-fault surge arrival time difference analysis method, the surge wave caused by a ground-fault is measured using sensors located at two points between which the ground-fault location is sandwiched, and the ground-fault location is determined from the difference in the arrival time [1]. As shown in Figure 1, when a ground-fault accident occurs in a distribution line, a ground-fault surge propagates along the distribution line from the fault point to both the power supply side and the load side. A ground-fault surge is basically a zero-phase component that takes each phase of the electric line as the forward path and the ground (or the overhead ground wire) as the return path. It is assumed that the ground-fault occurs in a section of length  $l$  [m] sandwiched between two sensor-equipped switches, and that the

ground-fault surge is detected by these two switches. Taking the time detected by the sensor equipped switch closer to the ground-fault point (near side) as  $t_1$  and the time detected by the sensor equipped switch far from the ground-fault point (far side) as  $t_2$ , the difference in the arrival time is  $\Delta t = t_2 - t_1$  [ $\mu\text{s}$ ]. At this time, if the surge propagation velocity  $v$  [ $\text{m}/\mu\text{s}$ ] in the section is known, the distance from the far-side sensor to the ground-fault, that is, the standard distance  $x$  [ $\text{m}$ ], can be obtained from equation (1).

$$x = \frac{v\Delta t + l}{2} \quad (1)$$

Here, according to the distributed constant circuit theory, if the distribution line does not have any incidental facilities, the surge propagation speed will be close to the speed of light (300  $\text{m}/\mu\text{s}$ ). However, in actual distribution lines, because the measured surge waveform is complexly distorted owing to the occurrence of branching, as well as the characteristics of various distribution equipment and current detection sensors, the speed calculated from the difference in surge arrival time is different from the speed of light. Although this propagation speed is referred to as the “apparent surge propagation speed,” for simplicity, we refer to it as the “surge propagation speed” in this example.

To know the surge propagation speed within the section that differs from the speed of light, it is not practical to conduct an artificial ground-fault test in an actual distribution line. Therefore, the method shown in Figure 2 is used, in which the switch outside the target section is operated, and from the difference in arrival time measured when the switching surge caused by this passes through the section, the surge propagation velocity  $v$  [ $\text{m}/\mu\text{s}$ ] within the section is calculated.

Thus, the surge propagation velocity within the section is calculated in advance, and at the time of a ground-fault, this surge propagation velocity is substituted in equation (1) to standardize the ground fault location. Please note that this method is patented [2].

As mentioned above, the surge propagation velocity  $v$ , which changes depending on the branching, and the characteristics of various accessory power distribution equipment and current detection sensors, can be considered an important parameter that directly influences the accuracy of the standardization.

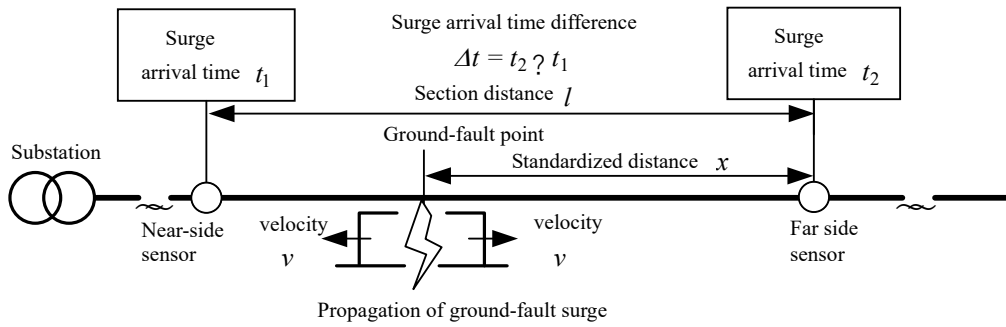


Fig. 1 Standardization principle of ground-fault surge arrival time difference analysis method

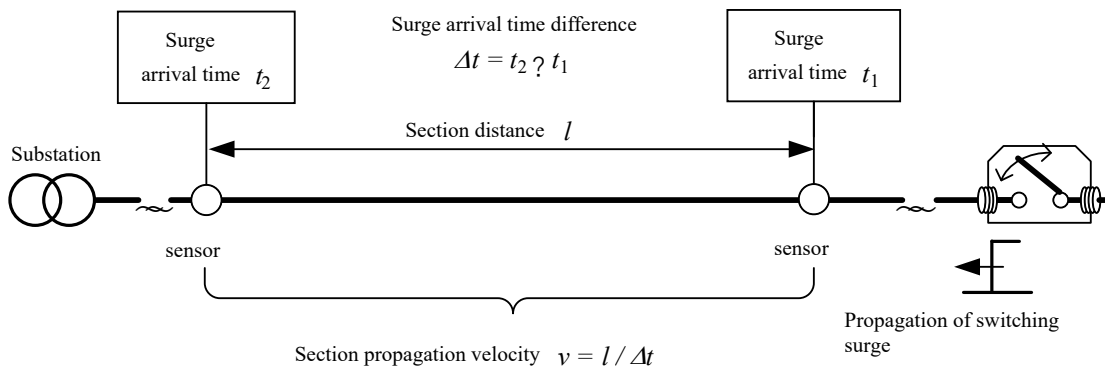


Figure 2 Acquisition of surge propagation speed

## 1.2 Modeling of Various Distribution Equipment

As mentioned earlier, the surge propagation velocity of the power distribution line varies depending on the branching, as well as the characteristics of various distribution equipment and the current detection sensors. Further, this surge propagation velocity has a significant influence on the standardization accuracy of the ground-fault surge arrival time-difference analysis method. Hence, to examine the realistic accuracy of the standardization, it is necessary to reproduce the model of the actual distribution line by reproducing the branching on the analysis program, and conduct a simulation taking into consideration the characteristics of the various distribution equipment and current detection sensors. To do so, an analysis model must first be created for the various distribution equipment and current detection sensors. In the ground-fault surge arrival time-difference analysis method, focusing on the point in which the standardization of the ground fault location is conducted using the zero-phase component of the ground-fault surge, we modeled the following distribution equipment that influences the zero-phase circuit by the ground capacitance. The modeling of each distribution facility is described in Sections 1.3 and 1.4. Furthermore, in Section 1.5, we describe the modeling of the current detection sensor used to measure the ground-fault surge.

- Distribution line (overhead ground wire and cable portion)
- Pole-mounted transformer and high-voltage receiving transformer

### 1.3 Modeling of Distribution Line

To analyze the surge propagating from the ground-fault point, it is necessary to treat the distribution line as a distributed constant circuit. Therefore, we created the distribution line model, as shown in Figure 3, using the fixed parameter distributed constant line model. The earth resistivity is taken as  $100 \Omega\text{m}$ , and the line constant calculation frequency is taken as  $100 \text{ kHz}$ . For an overhead ground wire, the concrete pillars are arranged such that the overhead ground wire is grounded once every  $200 \text{ m}$  or less. The grounding resistance was set to  $40 \Omega$ , and an impedance of  $12 \mu\text{H}$  of the ground wire was also simulated.

A fixed parameter distributed constant line model was also used for the cable portion, and its line constant was calculated using XTLC. Similar to the overhead ground wire, one end of the metal sheath in the cable part is grounded with a grounding resistance of  $40 \Omega$  through an inductance of  $12 \mu\text{H}$  simulating the inductance of the grounding wire.

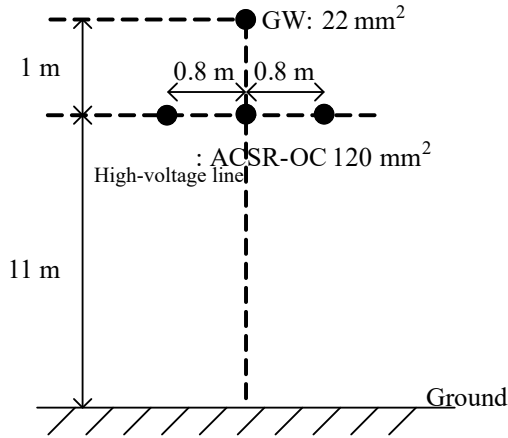


Figure 3 Pillar assembly of high-voltage cable and overhead ground wire

### 1.4 Modeling of Pole-mounted Transformer and High-voltage Receiving Transformer

From the viewpoint of simulating the surge response corresponding to the zero-phase component, the capacitance between the primary winding and the casing is considered to be the most important factor in the modeling of the pole-mounted transformer and high-voltage receiving transformer. Therefore, this capacitance was proportionally allocated to the primary side terminals and connected between the casing, and the resistance corresponding to the load on the secondary side was connected between the primary side terminals. The models of the pole-mounted transformer and high-voltage receiving transformer created in this manner are shown in Figures 4 and 5, respectively. For the capacitance between the primary winding and the casing, from the capacitance value actually measured on a pole-mounted transformer with a capacity of  $5$  to  $50 \text{ kVA}$ , an approximate equation of the following formula was created, of which the capacitance value  $C_s$  [pF] was determined from the transformer capacity  $S_{rate}$  [kVA] (the capacity of the power receiving transformer is the contract capacity).

$$C_s = 21.64 \cdot \ln(S_{rate}) + 22.42 \quad (2)$$

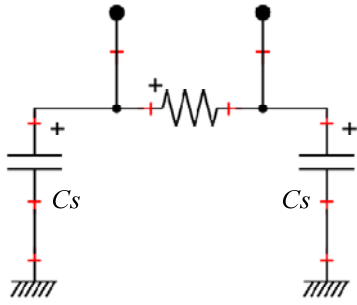


Figure 4 Pole-mounted transformer model

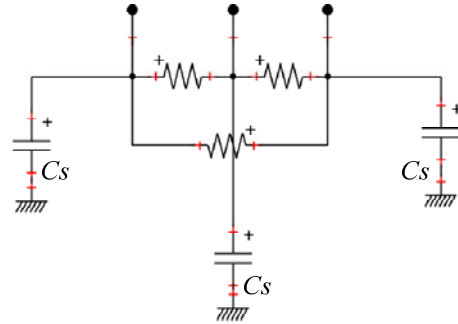


Figure 5 High-voltage receiving transformer model

## 1.5 Modeling of Current Detection Sensor

For the purpose of measuring the zero-phase current, a zero-phase current transformer (ZCT) is incorporated in the sensor-equipped switch. Because the primary purpose of the ZCT is to measure the zero-phase current at a commercial frequency, it is not designed to measure high-frequency components accurately. Therefore, by applying a lowpass filter (LPF) with a cut-off frequency of 100 kHz in the ZCT output, the frequency characteristic of the ZCT is simulated. Furthermore, by adopting an LPF, variations in the frequency characteristics based on the type and individual differences of the ZCT can be avoided.

## 2 Analysis Circuit and Conditions

Figure 6 shows the 6.6-kV distribution system to be analyzed. Here, we assume a case in which the ground fault occurs at a location sufficiently far from the distribution substation. In this system, three sensors, from sensor 1 on the substation side to sensor 3 at the end, are installed uniformly at a distance of 2,000 m from each other, and the section between sensors 1 and 2 is called Section A, whereas the section between sensors 2 and 3 is called Section B. Using this system, we conducted an analysis of the ground-fault surge propagation and examined the standardization using the “ground-fault surge arrival time difference analysis method.”

The other analysis conditions are as follows.

- Calculation time step: 10 ns
- Ground-fault occurrence time: 1  $\mu$ s
- Ground-fault phase: Phase-a
- Calculation start time: 0  $\mu$ s
- Calculation end-time: 40  $\mu$ s

Distribution substation  
system voltage and background impedance

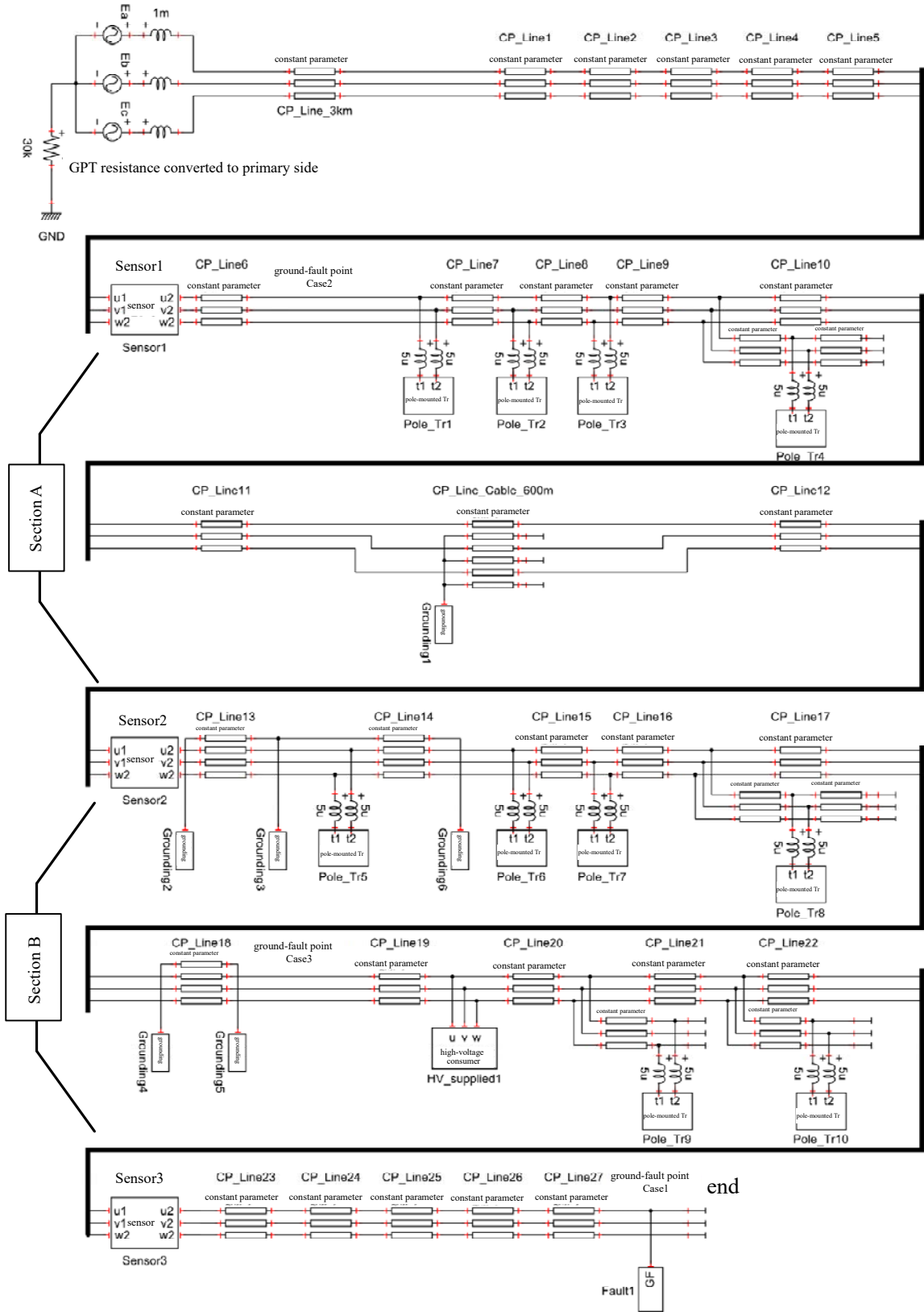


Figure 6 Analysis circuit

(when the ground-fault point is set to the point at the end of the system, as in Case 1)

### 3 Calculation of Section Propagation Velocity

To calculate the standardized distance using the ground-fault surge arrival time-difference analysis method, it is first necessary to calculate the propagation velocity  $v$  of each section from the arrival time difference when a surge is from the outside of the section targeted by the ground-fault location standardization sandwiched between the sensors. In an actual distribution line, the above-mentioned method of operating the switch outside the target section and calculating the propagation velocity of the section from the arrival time difference of the switching surge will not cause a ground-fault, which can hinder the supply. In a simulation study, it is easy to cause a ground-fault. Therefore, propagation velocity  $v$  of each section is obtained by causing a ground-fault at the end of the system, indicated as “ground-fault point Case 1,” and determining the ground-fault surge propagating from the ground-fault point toward the substation side. The instant at which the sensor output exceeds 0.3 A is determined as the surge arrival at each sensor, and the section propagation velocity is calculated from the time difference.

Figure 7 shows the analysis results of the case in which the ground-fault occurred at the point indicated as “ground-fault point Case 1.” From the figure, the propagation velocity  $v_A$  of Section A calculated from the surge arrival time difference of 21.69  $\mu\text{s}$  was approximately 92 m/ $\mu\text{s}$ , and the propagation velocity  $v_B$  of section B calculated from the arrival time difference of 7.49  $\mu\text{s}$  was approximately 267 m/ $\mu\text{s}$ , which indicates that the propagation velocity of the sections differs significantly. The difference is due to the cable portion. Owing to the influence of the large ground capacitance of the cable, a surge reflection occurs, and the surge passing through the cable greatly decreases. Therefore, in Section A, which has the cable portion, the propagation velocity decreases significantly.

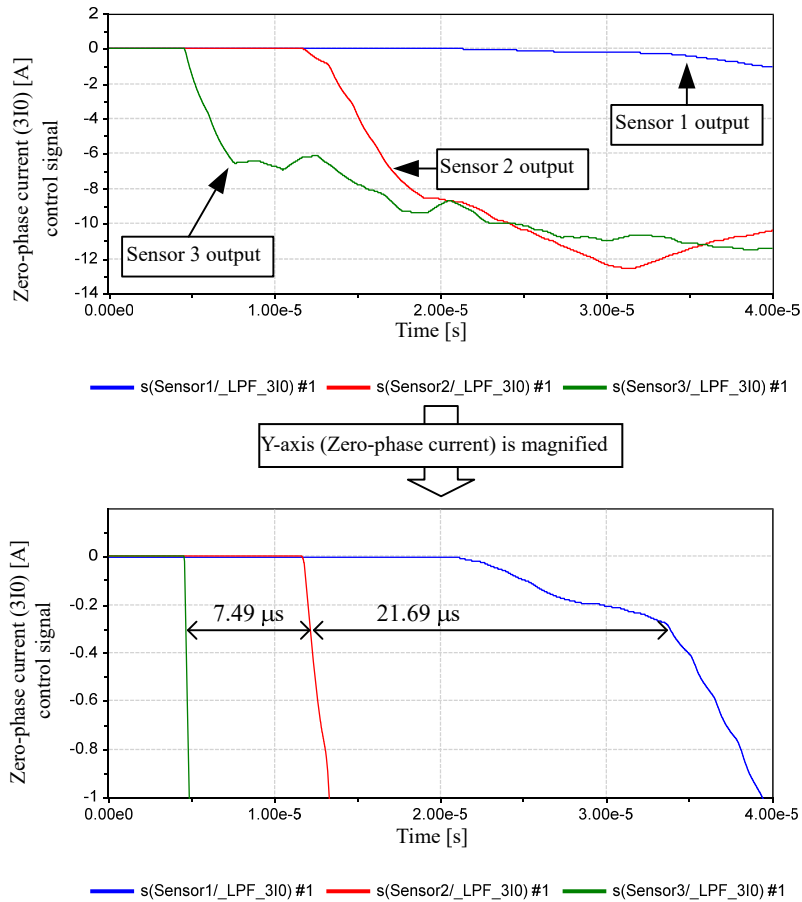


Figure 7 Output of each sensor and surge arrival time difference when ground-fault occurs at “ground-fault point Case 1”

## 4 Standardization of Ground-fault Location

### 4.1 Standardization of Ground-fault Location in Section A

In this section, using the propagation velocity  $v_A$  of Section A calculated above, we apply a standardization for a case in which a ground-fault occurs at the location indicated as “Ground-fault point Case 2” in Section A. From the analysis results shown in Figure 8, the difference in surge arrival time  $\Delta t$  between sensors 1 and 2 is 12.10  $\mu\text{s}$ . From this result, when calculating the standardized distance  $x$  by substituting  $v (= v_A = 92 \text{ m}/\mu\text{s})$  and  $\Delta t (= 12.10 \mu\text{s})$  in equation (1), the ground-fault point is determined to be at 1,557 m from sensor 2. In the analysis setting, because the location set as the ground-fault point (true value) is 1,800 m from sensor 2, the error of the standardized distance is 243 m, and its error rate is 14%.

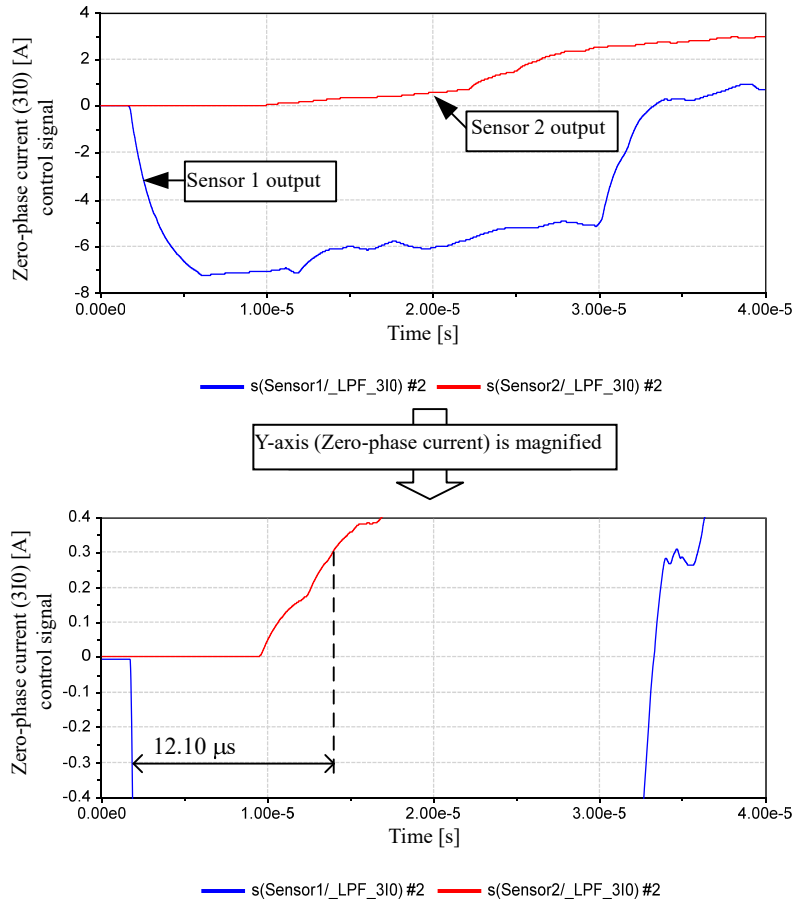


Figure 8 Output of sensors 1 and 2 and difference in surge arrival time when the ground-fault occurs in “ground-fault point Case 2”

#### 4.2 Ground-fault Point Standardization in Section B

In this section, using the propagation velocity  $v_B$  of Section B calculated above, we apply a standardization for the case in which a ground-fault occurs at the location indicated as “Ground-fault point Case 3” in Section B. From the analysis results shown in Figure 9, the difference in surge arrival time  $\Delta t$  between sensors 2 and 3 is 1.31  $\mu\text{s}$ . From this result, when calculating the standardized distance  $x$  by substituting  $v$  ( $= v_B = 267 \text{ m}/\mu\text{s}$ ) and  $\Delta t$  ( $= 1.31 \mu\text{s}$ ) in equation (1), the ground-fault point is determined to be 1,175 m from sensor 2. In the analysis setting, because the location set as the ground-fault point (true value) is 1,200 m from sensor 2, the error of the standardized distance is 25 m, and its error rate is 2%.

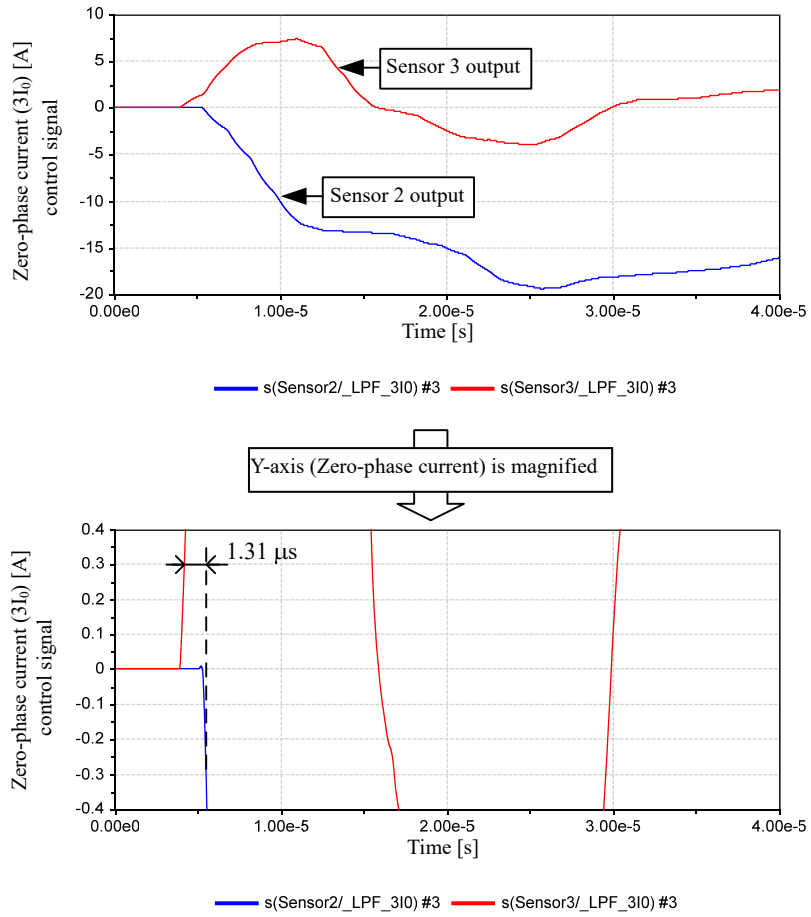


Figure 9 Outputs of sensors 2 and 3 and the difference in surge arrival time when a ground-fault occurs at “Ground-fault point Case 3”

END

Revision History		
Date	Example File Version	Content changes
2017/08/25	1.0	Creation of first edition (for XTAP Version 2.01)

XTAP Example Collection		No.	STL-01
<b>Name of the Example</b>	Simulation of Surge Propagation of a 500-kV Horizontally-arranged Single Circuit Transmission Line		
<b>Field</b>	Surge analysis (overvoltage analysis), line model		
<b>References</b>	Central Research Institute of Electric Power Industry, Research Report H07005 A Transmission Line Model for Electromagnetic Transient Analysis Based on the Frequency Region Partitioning Algorithm		
<b>Outline</b>	<p>In various surge analyses (overvoltage analyses), it is important to accurately simulate the surge (high-voltage traveling wave) propagating through the transmission lines and underground cables. For an accurate simulation of a surge, an accurate verification of the transmission line model used in the instantaneous value analysis is indispensable.</p> <p>In this example, we compare the results of a surge propagation characteristic test conducted on a 500-kV horizontally arranged single circuit transmission line (Azumo main line of Tokyo Electric Power), and the results of a surge propagation simulation conducted by modeling the transmission line using a frequency-dependent line model of XTAP. Because the results agree well, it can be understood that the frequency-dependent line model of XTAP has a sufficient analysis accuracy.</p>		

## Analysis Circuit and Conditions

Figure 1 shows the assembly of the 500-kV horizontally arranged single circuit transmission line to be analyzed, and Figure 2 shows the results of the surge propagation characteristic test.

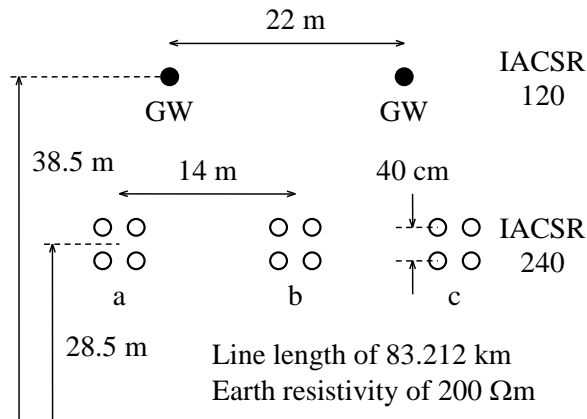


Figure 1 Assembly of 500-kV horizontally arranged single line transmission line

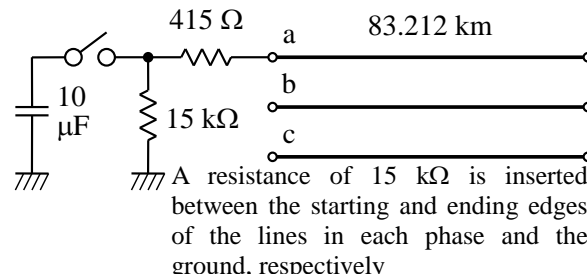


Figure 2 Surge propagation characteristic test circuit

#### [Analysis Phenomenon]

When a surge propagates on a  $n$ -phase transmission line, its waveform can be broken down into  $n$  propagation modes. Such a three-phase transmission line can be broken down into a first line-wave mode, a second line-wave mode, and a ground return mode. The first line-wave mode is a propagation mode where both ends of the power line (phase-a and phase-c) are set as the forward and return paths, respectively, and the second line-wave mode is a propagation mode where both ends of the power line (phase-a and phase-c) are the forward paths, and the central power line (phase-b) is set as the return path. Because the current flows through the conductors in both the forward and return paths, the attenuation is small, and the propagation speed is almost the speed of light. In contrast, in ground return mode, because the three power lines form the forward path and the ground becomes the return path, the current flows through the ground. Hence, the attenuation is large, and the propagation speed is less than the speed of light.

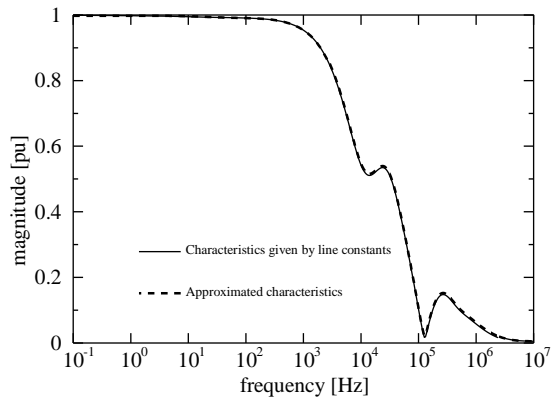
As shown in Figure 2, when a voltage charged in a capacitor is applied to the starting edge of a phase, a rectangular voltage is applied. As the rectangular voltage propagates along the transmission line, it splits into the above three modes (the branching phenomenon), and at the far-end, the arrival of the two line-wave modes can be first observed followed by the arrival of the ground return mode.

#### [Creation of the line model]

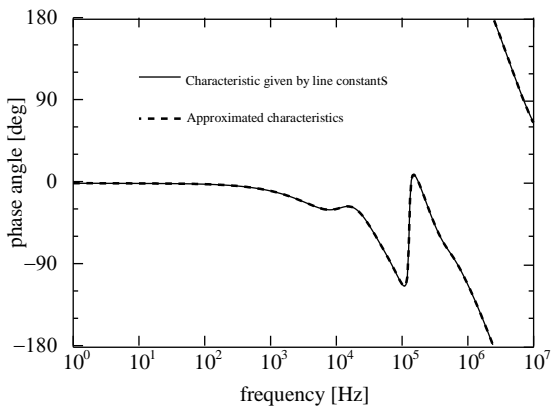
Using the line constant calculation program XTLC included in XTAP, and inputting the pillar assembly shown in Figure 1, we create a frequency-dependent line model (for the different types of line models, refer to the “Modeling of Transmission/Distribution Lines and Underground Cables”). By using the frequency-dependent line model, the skin effect of the transmission lines and ground and its frequency characteristics (which causes the branching phenomenon) can be reproduced.

The conditions for creating a frequency-dependent line model are as follows. We input the pillar assembly in Figure 1 and the parameters below to create the model file of the frequency-dependent line model (.xmf). At this time, from the graph displayed on the screen, we confirm whether the frequency characteristics of the line calculated using XTLC from the pillar assembly (frequency characteristics of the propagation function and the characteristic admittance) match the frequency characteristics of the line model (Figures 3 and 4).

- Frequency range: 0.1 Hz to 10 MHz
- Number of frequency samples: 400 points
- Earth resistivity: 200  $\Omega\text{m}$

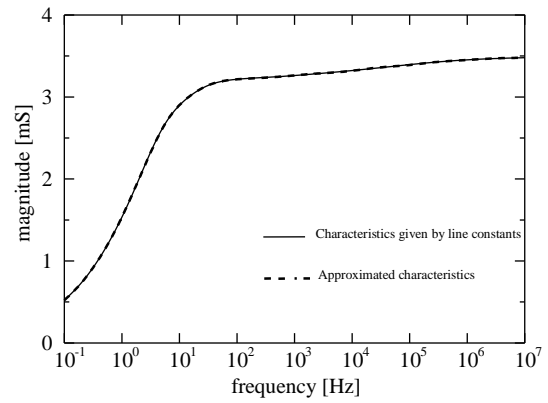


(a) Absolute value characteristics

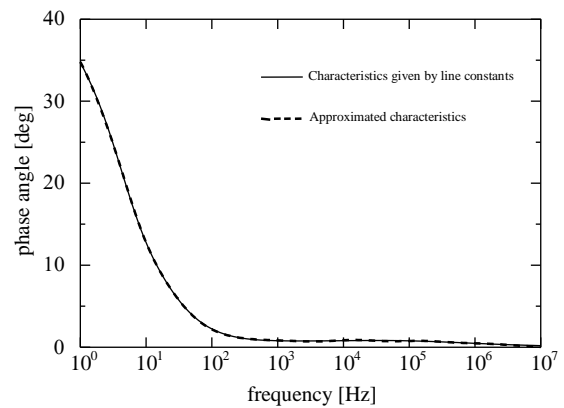


(b) Phase characteristics

Figure 3 Approximation of frequency characteristics of the propagation function matrix component (1, 1)



(a) Absolute value characteristics



(b) Phase characteristics

Figure 4 Approximation of frequency characteristics of the characteristic admittance matrix component (1, 1)

[Surge Propagation Simulation]

Creating the circuit shown in Figure 2 using XTAP, we apply an instantaneous value analysis. We set the transmission line to a frequency-dependent line model and double-click it to specify the model file (.xmf) created in advance in XTLC.

[Analysis Conditions]

The analysis conditions are as follows:

- Calculation time step            0.2  $\mu$ s
- Calculation start time            0 ms
- Calculation end time            0.5 ms
- Display start time            0.2 ms
- Display end time            0.5 ms

[Example of XTAP Input]

An instance of creating this example on XTAP is shown in Figure 5.

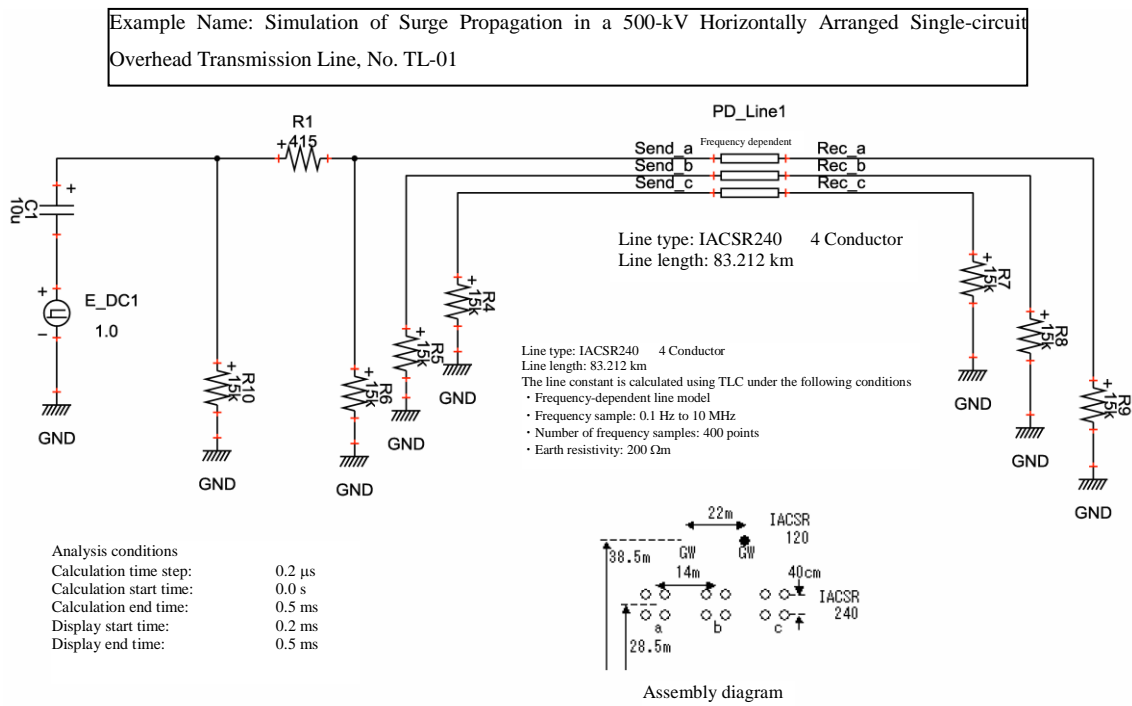


Figure 5 Example of XTAP input

Analysis Results

The results (far-end voltage waveform) of executing this example in XTAP are shown in Figure 6.

Further, the corresponding measured waveforms are shown in Figure 7. It can be seen that the calculation results agree well with the measurement results.

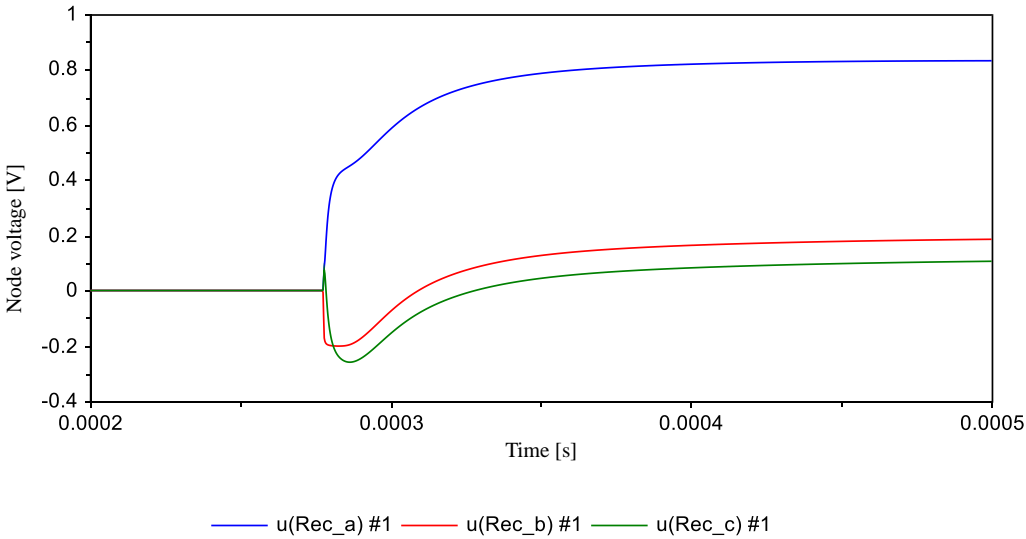


Figure 6 Results of analysis using XTAP

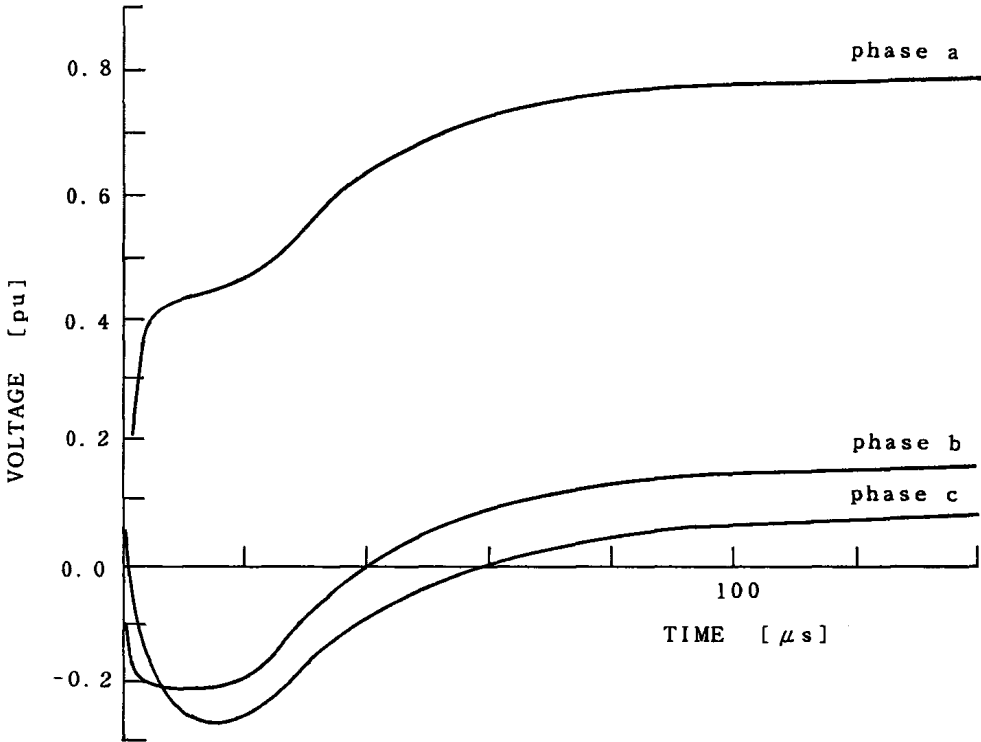


Figure 7 Measurement results

END

Change Log		
Date	Example file version	Content changes
2014/11/19	2.0	Update for XTAP Ver. 2.00 Recalculation of line constants owing to change in XTLC
2012/07/19	1.2	Update for XTAP Version 1.20
2011/10/18	1.1	Update for XTAP Version 1.11 Change in the line constant file owing to changes in number of valid digits in XTLC
2010/07/16	1.0	Creation of first edition (for XTAP Version 1.10)

<b>XTAP Example Collection</b>		<b>No.</b>	STL-02
<b>Name of the Example</b>	Simulation of Surge Propagation in a 500-kV Vertically Arranged Double-circuit Transmission Line		
<b>Field</b>	Surge analysis (overvoltage analysis), line model		
<b>Reference</b>	Central Research Institute for Electric Power Industry, Research Report H07005, "A Transmission Line Model for Electromagnetic Transient Analysis Based on the Frequency Region Partitioning Algorithm"		
<b>Outline</b>	<p>In various surge analyses (overvoltage analyses), an accurate simulation of the surge (high-voltage traveling wave) propagating through the transmission lines and underground cables is important.</p> <p>In this example, we conduct the simulation of a surge propagation in a 500-kV vertically arranged double circuit line commonly used in Japan. A frequency-dependent line model that takes into consideration the skin effect of the electric wire and earth, as well as its frequency characteristics, is used.</p>		

## Analysis Circuit and Conditions

Figure 1 shows the pillar assembly of the analyzed 500-kV vertically arranged double circuit transmission line, and Figure 2 shows the surge propagation simulation circuit.

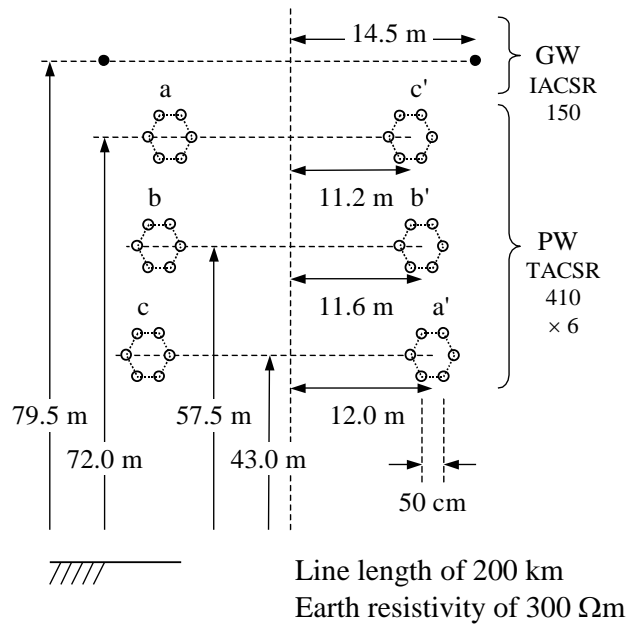


Figure 1 Pillar assembly of 500-kV vertically arranged double circuit transmission line

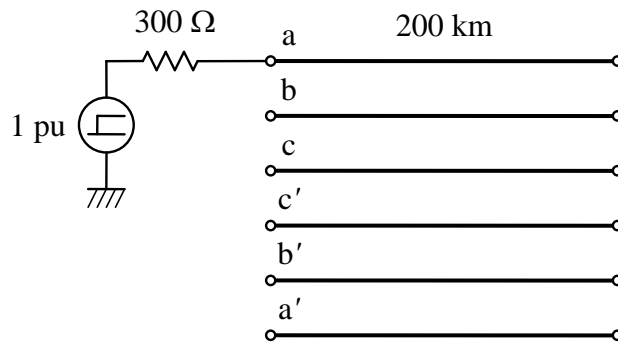


Figure 2 Surge propagation simulation circuit

[Analysis Phenomenon]

When a surge propagates on a  $n$ -phase transmission line, its waveform can be decomposed into  $n$  propagation modes. Such a six-phase line can be decomposed into five line-wave modes and one ground return mode. In line wave mode, because the forward and return paths are power lines and the current flows through a conductor, the attenuation is less, and the propagation speed is almost the speed of light. In contrast, in ground return mode, because the six power lines form the forward path and the ground forms the return path, the current flows through the ground. Hence, the attenuation is large, and the propagation speed is less than the speed of light. A detailed explanation of the current distribution in each of the five line modes is given in the following study.

Ametani, “Distribution Parameter Circuit Theory,” Corona Publishing Co., Ltd.

As shown in Fig. 2, when a rectangular voltage wave is applied to a phase of the starting edge, the voltage waveform branches into the above six modes (branching phenomenon) as it propagates along the transmission line, and at the far-end, it is possible to observe the five line-modes arriving first, followed by the arrival of the ground return mode.

[Creation of the Line Model]

Using the line constant calculation program XTLC included in XTAP, and inputting the pillar assembly shown in Figure 1, we create a frequency-dependent line model (for a classification of the line models, refer to “Modeling of Transmission/Distribution Lines and Underground Cables”). Using the frequency-dependent line model, the skin effect of the transmission lines and the ground, along with its frequency characteristics (which cause the branching phenomenon), can be reproduced.

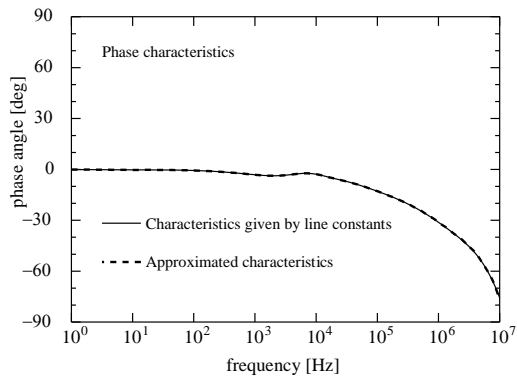
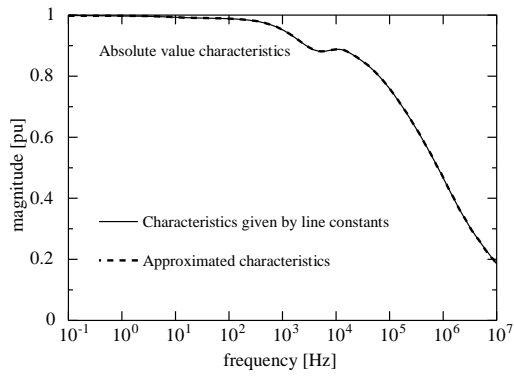
The conditions for creating a frequency-dependent line model are as follows. We input the pillar assembly in Figure 1 and the parameters below to create the model file of the frequency-dependent line model (.xmf). At this time, from the graph displayed on the screen, we confirm whether the frequency characteristics of the line calculated using XTLC from the pillar assembly (frequency characteristics of the propagation function and the characteristic admittance) match the frequency characteristics of the line model (Figures 3 and 4).

- Frequency range: 0.1 Hz to 10 MHz
- Number of frequency samples: 400 points

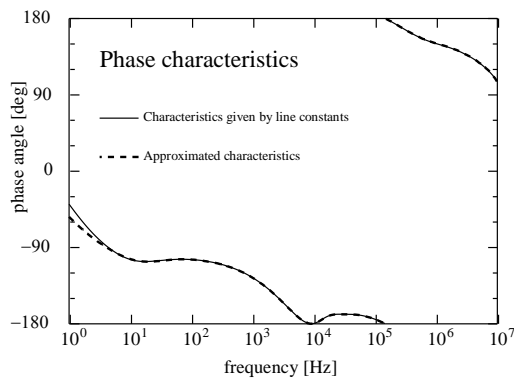
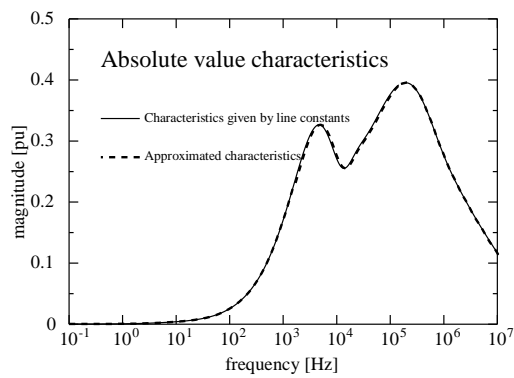
· Earth resistivity:

300  $\Omega\text{m}$

components (1, 1) and (2, 3)

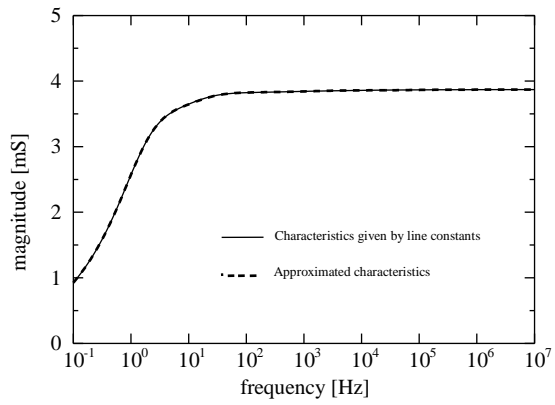


(1, 1) Elements

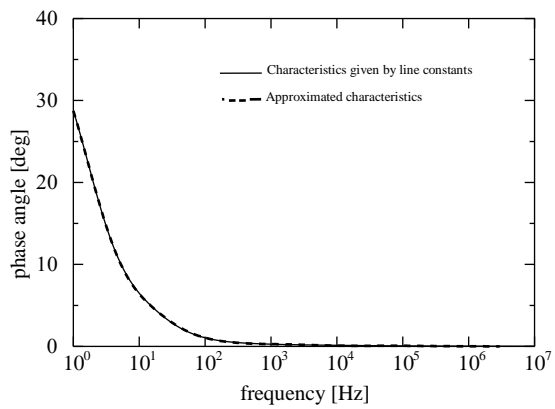


(2, 3) Elements

Figure 3 Results of frequency characteristic approximation of the propagation function matrix



(a) Absolute value characteristics



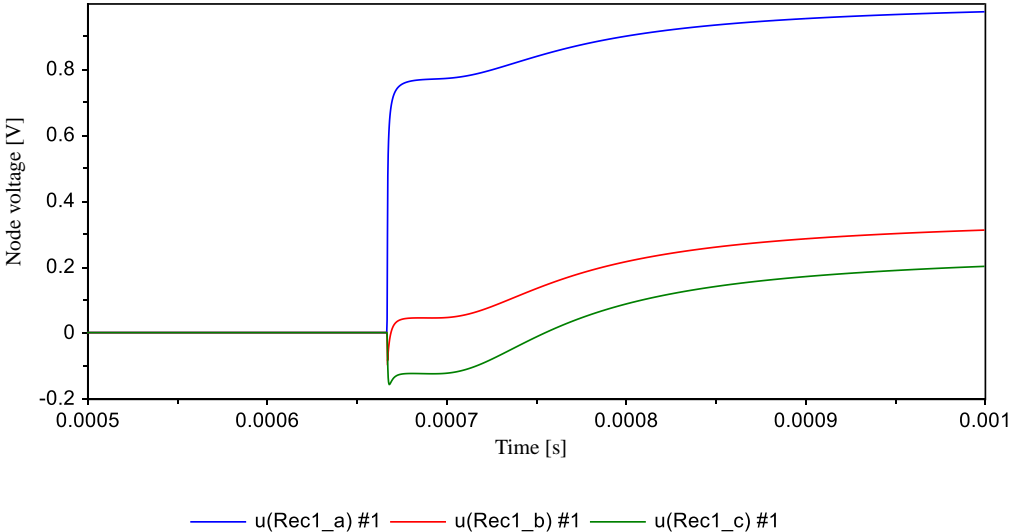
(b) Phase characteristics

Figure 4 Results of frequency characteristic approximation of the characteristic admittance matrix component (1, 1)

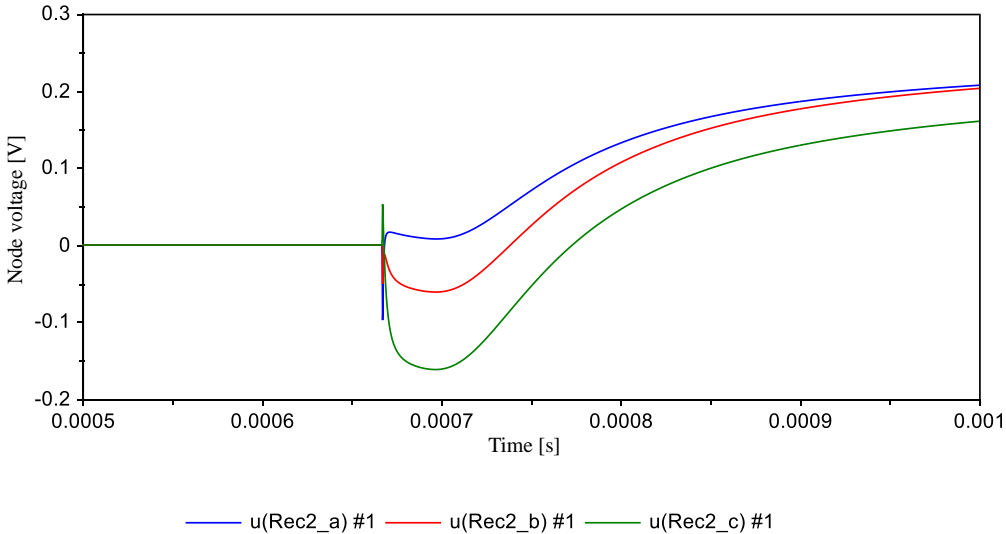


# Analysis Results

Figure 6 shows the results (far-end voltage waveform) of executing this example using XTAP.



(a) Far-end voltage waveform of the first circuit



(b) Far-end voltage waveform of the second circuit

Figure 6 Results of analysis using XTAP

END

Change Log		
Date	Example file version	Content changes
2014/11/19	2.0	Update for XTAP Ver. 2.00 Recalculation of line constants owing to changes in XTLC
2012/07/19	1.2	Update for XTAP Version 1.20
2011/10/18	1.1	Update for XTAP Version 1.11 Change in line constant file owing to changes in the number of valid digits of XTLC
2010/07/16	1.0	Creation of first edition (for XTAP Version 1.10)

<b>XTAP Example Collection</b>		<b>No.</b>	<b>STL-03</b>
<b>Example Name</b>	Flashover Calculation using Arcing Horn Flashover Model for Short-tail Waves (Detailed Model, AC Superimposition not Possible)		
<b>Field</b>	Lightning surge analysis and overvoltage analysis of substations		
<b>References</b>	Motoyama, “Development of a New Flashover Model for Lightning Surge Analysis,” Journal of IEEJ, B, Vol. 115, No. 7, pp. 839-846, 1995.		
<b>Outline</b>	<p>In a lightning surge analysis of the substations, the calculation is conducted under the assumption that the lightning surge enters the substation through a flashover of the upper phase arcing horn of the first steel tower. Further, in a lightning surge analysis of the transmission lines, a ground fault is estimated based on the presence or absence of a flashover in each arcing horn. Therefore, an accurate modeling of the flashover phenomenon of an arcing horn is extremely important for an accurate lightning surge analysis of the substations and transmission lines.</p> <p>Conventionally, the leader model proposed by Shindo et al. or its simplified version represented by an inductor and a switch are being used as the flashover model of an arcing horn. However, in these models, it is necessary to conduct preliminary calculations beforehand assuming a condition in which the arcing horn does not flashover. Further, although the actual voltage applied to the arcing horn is a short-tail wave, the model constants were derived from experiments using standard waves. Hence, improvements are necessary. Therefore, Motoyama developed a new arcing horn flashover model, where, by calculating the progress of the leader (discharge) at the same time as the lightning surge calculation, the need for a preliminary calculation is eliminated, and the model constants are derived experimentally using a short-tail wave.</p> <p>In this example, we conduct a flashover calculation using the above-mentioned arcing horn flashover model with a short-tail wave (Motoyama model) and compare it with the measured results.</p> <p>* The leader model introduced in this example may not be able to conduct proper calculations in cases in which an impulse voltage is superimposed over a steady AC voltage, such as the case of a lightning strike when a system voltage is applied. When applying to cases in which a steady AC voltage is present, the simplified model introduced in example no. STL-04 is used.</p>		

## Analysis Circuit and Conditions

The analysis circuit is shown in Figure 1. The left side of the analysis circuit is equivalent to an impulse generator (IG) that generates a short-tail voltage wave, and the voltage generated is applied to the arcing horn, which is the specimen used.

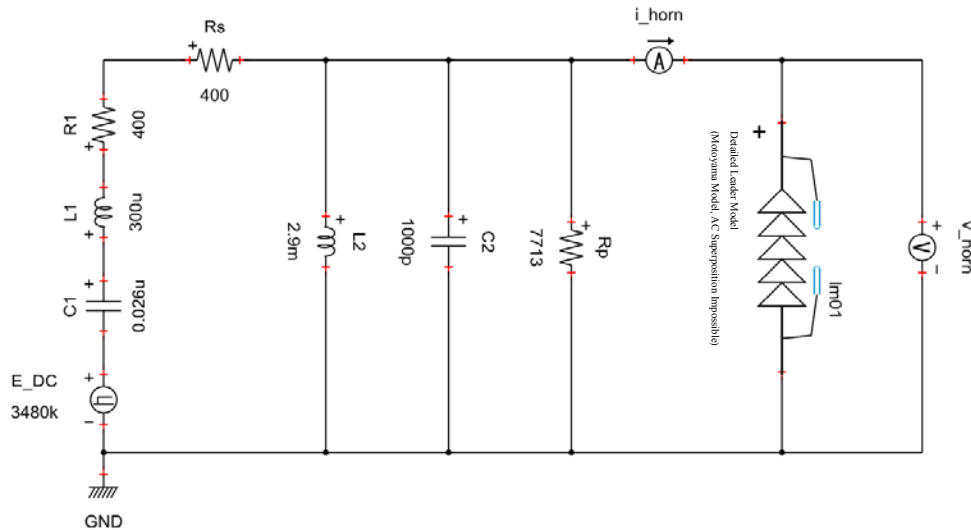


Figure 1 Analysis circuit

### [Arcing Horn Flashover Phenomenon]

Here, idealizing an arcing horn and considering it as a rod-rod electrode, we explain the outline of the arcing horn flashover phenomenon. When a high voltage is applied between the rod-rod electrodes, the electron avalanche first switches over to a streamer discharge between electrodes, where an ionizing wave then propagates. However, in the phenomenon described thus far, because the current is extremely small, there is no strong light-emission. Subsequently, a leader accompanied by a strong light-emission is generated from the tip of both electrodes and progresses toward the direction in which the electrodes can be short-circuited. Finally, both leaders join near the center of the space between electrodes to create a short circuit, thereby completing the flashover. The short-circuited leader then shifts to an arc discharge through the heating of ionized gas.

In an arcing horn flashover model, we model the above phenomenon and reproduce the presence of a flashover at the time of a lightning strike and the current flowing during the leader progression. From here, we will outline the arcing horn flashover model for a short-tail wave using Motoyama and its modeling in XTAP. For details, refer to the references shown on the cover page of this example.

[Calculation of Leader Progress Start Condition]

As mentioned earlier, in the phenomenon that occurs until the start of the leader progression, because the current is extremely small, it only has a slight effect on the lightning surge analysis. Therefore, in Motoyama’s arcing horn flashover model for a short-tail wave (hereinafter abbreviated as “Motoyama model”), it is assumed that no current flows until the leader starts to progress. In the Motoyama model, regarding the voltage between the arcing horns  $V$ , the time  $T_s$  at which the following equation is satisfied is taken as the leader progression start time, and the simulation of leader progression is started from that time.

$$\text{For a positive polarity, } \frac{1}{T_s} \int_0^{T_s} V(t) dt > 400D + 50 \text{ [kV]} \quad (1)$$

$$\text{For a negative polarity, } \frac{1}{T_s} \int_0^{T_s} V(t) dt > 460D + 150 \text{ [kV]} \quad (2)$$

where  $D$  [m] is the distance between the electrodes of the arcing horn. The left side of the above equations is the average voltage applied to the electrodes, and it is assumed that when it exceeds the fixed value defined by  $D$ , shown on the right side, the leader starts to progress. In equations (1) and (2), by adopting the average voltage value calculated through an integration instead of the instantaneous voltage value, the physical requirement in which “for the streamer discharge to short-circuit between the electrodes and transform into a leader, it is necessary to supply a certain value of energy or more between the electrodes,” is approximately reproduced.

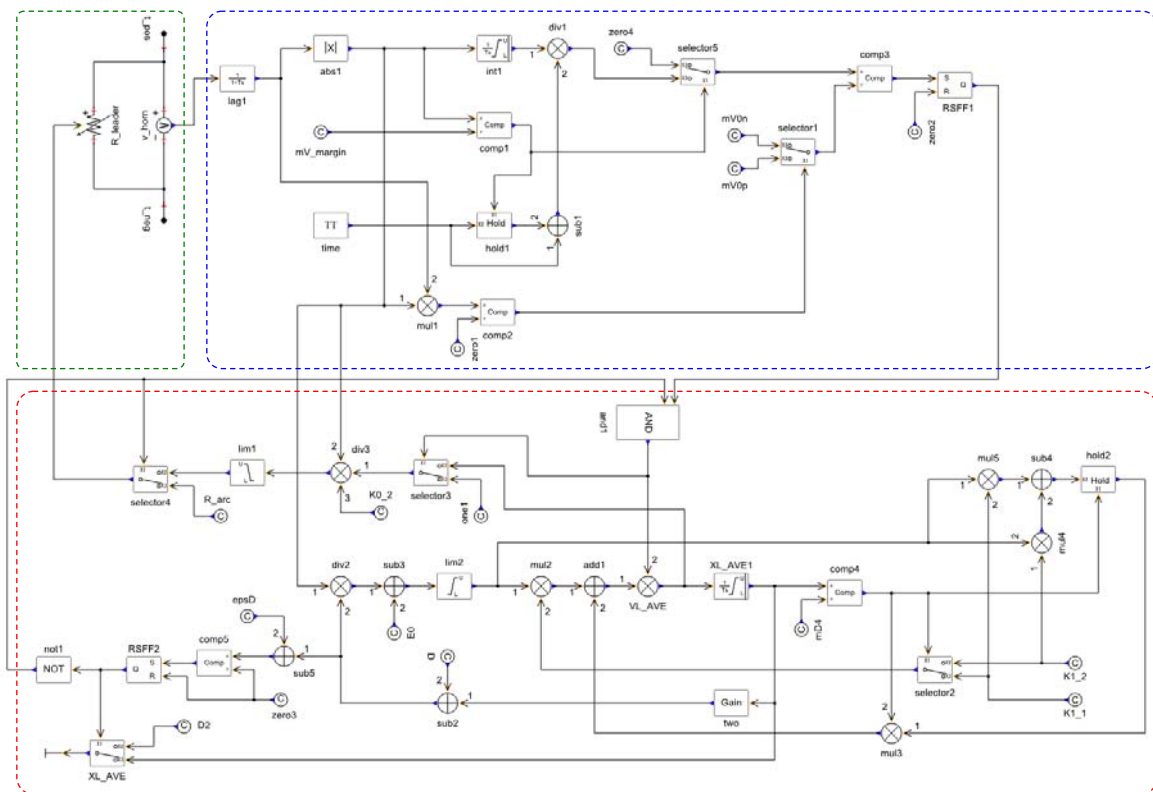


Figure 2 Implementation of Motoyama model (detailed model)

Figure 2 shows the implementation of the Motoyama model on XTAP (this model can be referred by right-clicking on the “Detailed Leader Model” in the circuit diagram of Figure 1 and selecting the “Component Diagram Edit”). In the figure, the part surrounded by the blue dotted line is the part where the leader progress starting condition is calculated. In the implementation, even if there is a time at the beginning of the analysis in which no voltage is applied between the arcing horns, to integrate correctly, the integration is started only after reaching a voltage equal to or higher than a certain level.

Note that, with the above method, a proper calculation may not be possible when an impulse voltage is superimposed during a state in which a steady voltage is applied, such as when assuming a lightning strike when a system voltage is used. When applying to cases in which a steady voltage is present, the model in example number STL-04 is used.

#### [Calculation of Leader Progression Process]

When the leader progress starting condition is satisfied, a simulation of the leader progress process is started. In this simulation, the leader progression speed  $v_{LAVE}$  [m/s] is first calculated through the following equation.

$$v_{LAVE} = K_1 \left( \frac{V}{D - 2X_{LAVE}} - E_0 \right) \quad (3)$$

where  $K_1$  [m<sup>2</sup>/V/s] is the velocity proportional coefficient,  $X_{LAVE}$  [m] is the leader length, and  $E_0$  [V/m] is the lowest leader progression electric field. Because the leader length  $X_{LAVE}$  is the integral of the leader progression speed  $v_{LAVE}$ , it can be calculated through the following equation.

$$X_{LAVE} = \int v_{LAVE} dt \quad (4)$$

At this time, because the current  $I_L$  flowing between the arcing horns is the electric charge per unit time supplied to the leader progressing at a velocity  $v_{LAVE}$ , it can be calculated from the following equation.

$$I_L = 2K_0 v_{LAVE} \quad (5)$$

where  $K_0$  [C/m] is the charge proportional coefficient.

Because  $E_0$  in equation (3) and  $K_0$  in equation (5) are constants, the following values are used.

$$E_0 = 750 \times 10^3 \text{ [V/m]}, \quad K_0 = 410 \times 10^{-6} \text{ [C/m]}$$

Because  $K_1$  in equation (3) is a value that varies depending on the leader length, we take

$$K_1 = 2.5 \text{ [m}^2\text{/V/s]}, \quad \text{when } 0 < X_{LAVE} < D/4 \text{ and}$$

$$K_1 = 0.42 \text{ [m}^2\text{/V/s]}, \quad \text{when } D/4 < X_{LAVE} < D/2.$$

Equation (3) is an expression that conveniently shows that the slope of the leader progression velocity with respect to electric field is  $K_1$ . However, when the leader length exceeds  $D/4$ , even if  $K_1 = 0.42$  is substituted in equation (3) as is, the correct leader progression velocity cannot be obtained. It is necessary to retain the value of the leader progression velocity at the instant in which the leader length exceeds  $D/4$  and calculate equation (3) in a form in which the leader progression velocity increases with a slope of  $K_1 = 0.42$ .

The calculation is continued, and when the leader length satisfies the condition of the following equation, the arcing horns are short-circuited by the leader and the flashover is complete. Subsequently, the leader shifts to an arc discharge.

$$X_{LAVE} \geq \frac{D}{2} \quad (6)$$

Further, if the voltage  $V$  between the arcing horns decreases and the condition in the following equation is satisfied, the value inside the parenthesis of equation (3) becomes negative, and the leader stops its progress.

$$V < (D - 2X_{LAVE})E_0 \quad (7)$$

In the implementation of the Motoyama model shown in Figure 2, the part surrounded by the red dotted line applies the calculation of the above-mentioned leader progress process.

[Equivalent Resistance for Simulation]

In this implementation, assuming that no current flows during the time until the condition in which the start of the leader progression in equations (1) or (2) is satisfied, the equivalent resistance value of the arcing horn is set to a very large  $R_{init}$  value. When the leader starts progressing, the leader current  $I_L$  is calculated from the voltage  $V$  between the arcing horns using equations (3) through (5), and its equivalent resistance is set to

$$R_{eq} = \frac{V}{I_L} \quad (6)$$

When equation (6) is established and the arcing horns are short-circuited by the leader, the equivalent resistance value of the arcing horn is set to a small  $R_{arc}$  value corresponding to the arc resistance.

In the Motoyama model shown in Figure 2, the portion surrounded by the green dotted line is the portion corresponding to the above-mentioned equivalent resistance.

[Setting of Parameters]

Although various parameters can be set by double-clicking the leader model of Figure 1, the parameters to be set by the user for each analysis are the inter-electrode distance  $D$  of the arcing horn and the arc resistance  $R_{arc}$ . Other configurable parameters and their default values are shown below (in most cases, there is no need to change the values of these parameters).

Leader constants

Charge proportionality constant  $K_0$  [C/m]

$$K_0 = 410e-6$$

Velocity proportionality constant  $K_1$  [ $m^2/V/s$ ] ( $0 < X_{LAVE} < D/4$ )

$$K_{1\_1} = 2.5$$

Velocity proportionality constant  $K_1$  [ $m^2/V/s$ ] ( $D/4 < X_{LAVE} < D/2$ )

$$K_{1\_2} = 0.42$$

Minimum leader progression electric field  $E_0$  [V/m]

$$E_0 = 750e3$$

Voltage dead band [V] for calculating leader progression start time

$$V_{margin} = 10e3$$

Electrical tolerance of leader bridging determination

$$\mathbf{eps} = 0.05$$

Equivalent resistance before leader progression [ $\Omega$ ]

$$\mathbf{R\_init} = 1e6$$

Time constant of first-order lag filter for internal processing [s]

$$\mathbf{tau} = 10e-9$$

[Analysis Conditions]

The analysis conditions are as follows.

- Calculation time step            1 ns
- Calculation start time            0  $\mu$ s
- Calculation end time            5  $\mu$ s
- Display start time            0  $\mu$ s
- Display end time            5  $\mu$ s

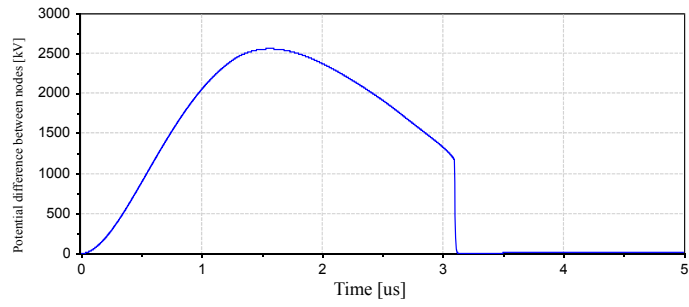
## Analysis Results

Figure 3 shows the calculation results of the analysis circuit of Figure 1, where the distance between the electrodes of the arcing horn D was set to 3 m and the arc resistance  $R_{arc}$  was set to 5  $\Omega$  (and the other parameters were set to the default values). In addition to the voltage between the arcing horns and the leader current, the leader length and leader progression velocity are shown (the leader length and leader progression velocity are output with the variable names XLAVE and VLAVE, respectively). The results of the calculation agree well with the measurement results shown in Figure 4 (reprinted from the references shown on the cover page of this example).

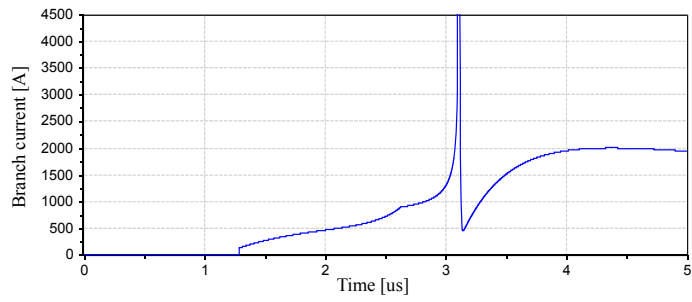
Figure 5 shows the calculation results of the  $V - t$  curve for the cases of positive and negative polarities by changing the inter-electrode distance of the arcing horn D to 1, 2, and 3 m, respectively.

The calculation results are in good agreement with the measured results shown in the following study.

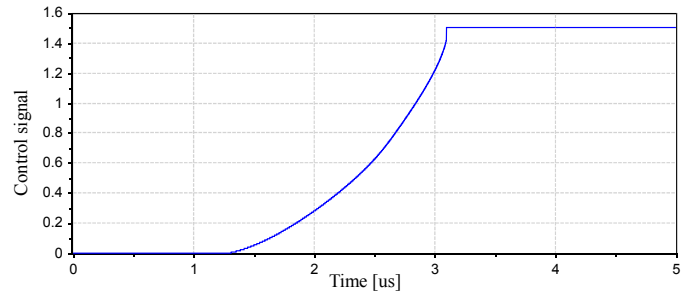
M. Aoshima, "Flashover Characteristics of Air Gaps by Lighting Impulse Voltages with Short Tail," Research Report T87041, Central Research Institute of Electric Power Industry, April 1988.



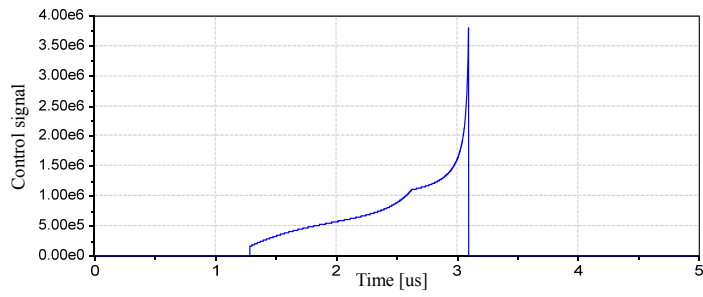
(a) Voltage between arcing horns



(b) Leader current

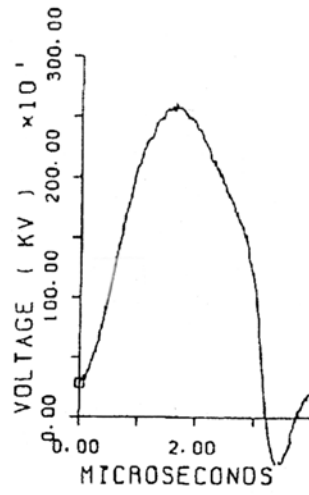


(c) Leader length

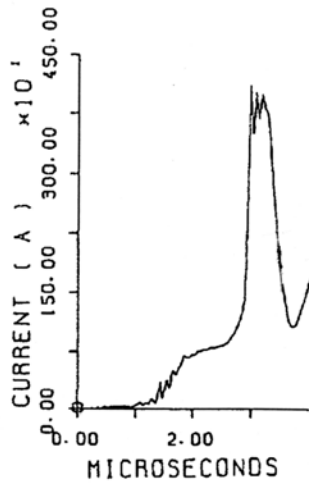


(d) Leader progression velocity

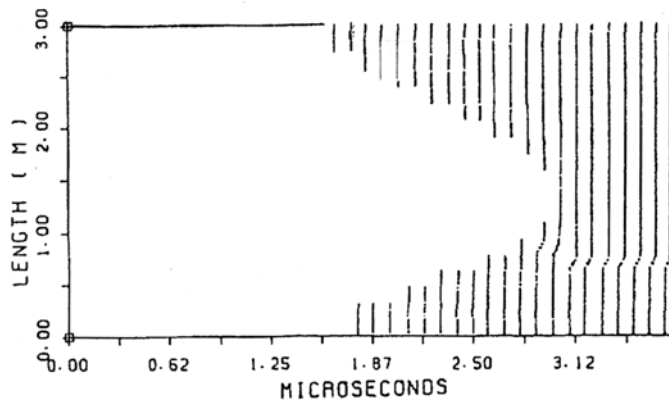
Figure 3 Analysis results



(a) Voltage between arcing horns

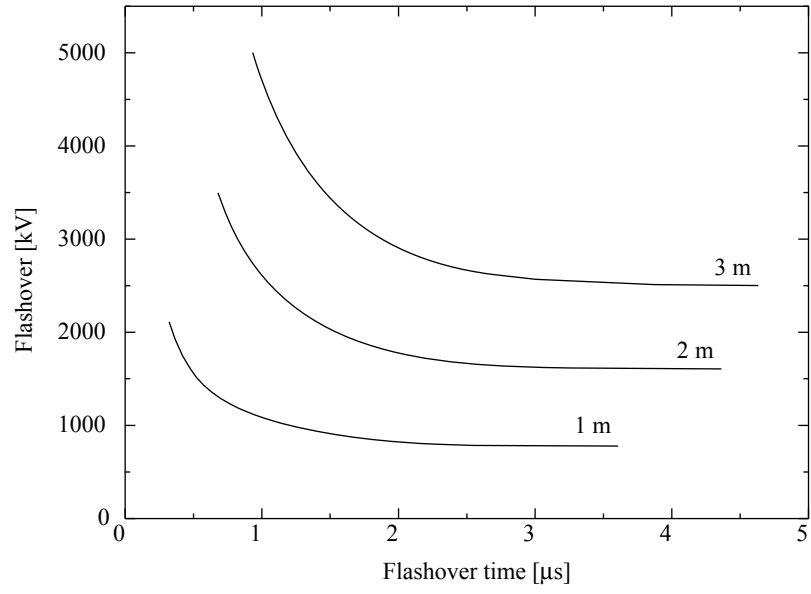


(b) Leader current

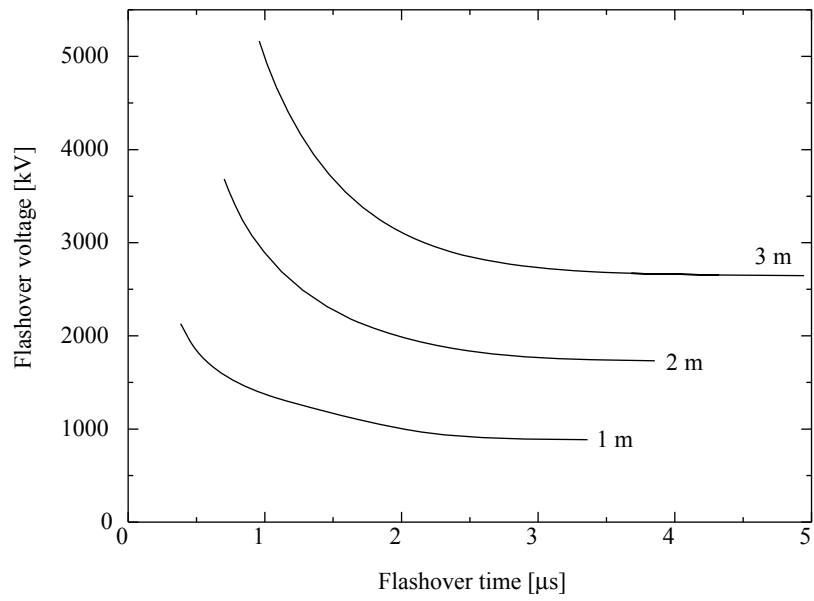


(c) Leader length

Figure 4 Measurement results



(a) Positive polarity



(b) Negative polarity

Figure 5  $V - t$  curve calculation result

Revision History		
Date	Example File Version	Content changes
2022/10/18	2.1	Name changed from SLS-02 to STL-03
2014/11/19	2.0	Update for XTAP Version 2.00
2012/07/19	1.2	Update for XTAP Version 1.20
2011/12/06	1.1	Consistency with SLS-03 was obtained for an explanation of the example title
2011/11/11	1.1	Clearly specified in the icon of the model that an AC superimposition is not possible
2011/11/04	1.0	Creation of the first edition (for XTAP Version 1.11)

XTAP – Example collection		No.	STL-04
Example Name	Flashover Calculation Using Arcing Horn Flashover Model (Simplified Model, AC Superimposition Possible) for Short Tail Waves.		
Field	Lightning surge and overvoltage analyses of power stations and sub-stations.		
References	H. Motoyama, K. Shinjo, Y. Matsumoto, and N. Itamoto, N., “Observation and analysis of multiphase back flashover on the Okushishiku Test Transmission Line caused by winter lightning,” IEEE Transactions on Power Delivery, Vol. 13, No. 4, pp. 1391-1398, 1998.		
Outline	<p>In this example, we simplify the leader progress start condition of the “arcing horn flashover model (detailed model, AC superimposition not possible) for short tail waves,” introduced in example STL-03, and introduce a model that allows a superimposition of the steady AC voltage. For the arcing horn flashover model for short tail waves, refer to the explanation of example STL-03.</p> <p>In the detailed model of example STL-03, the average voltage is obtained by integrating the instantaneous values of the voltages, and the start of the leader progression is determined based on whether this value exceeds the fixed value based on the gap length. This simulates the physical requirement that states, “energy exceeding a certain value must be supplied between electrodes in order to convert a streamer discharge into a leader by short-circuiting the electrodes.” However, when the impulse voltage is superimposed over a steady AC voltage, such as the case of a lightning strike when the system voltage is applied, the integral value of the impulse voltage rises owing to the previous steady AC voltage, and the calculation of an accurate average voltage may not be possible. To solve this problem, a simplified leader progress start condition is adopted, which states that “the leader starts to progress when the absolute value of the average electric field between the arcing horns exceeds 500 kV/m,” and with the simplified model introduced in this example, an analysis is possible even in cases in which the impulse voltage is superimposed over a steady AC voltage.</p>		

## **Analysis Circuit And Conditions**

Figure 1 shows the analysis circuit. The left side of the analysis circuit is an equivalent circuit of an impulse generator (IG), which generates a short-tail voltage wave, and the voltage generated by this is applied to the arcing horn, which is the test specimen.

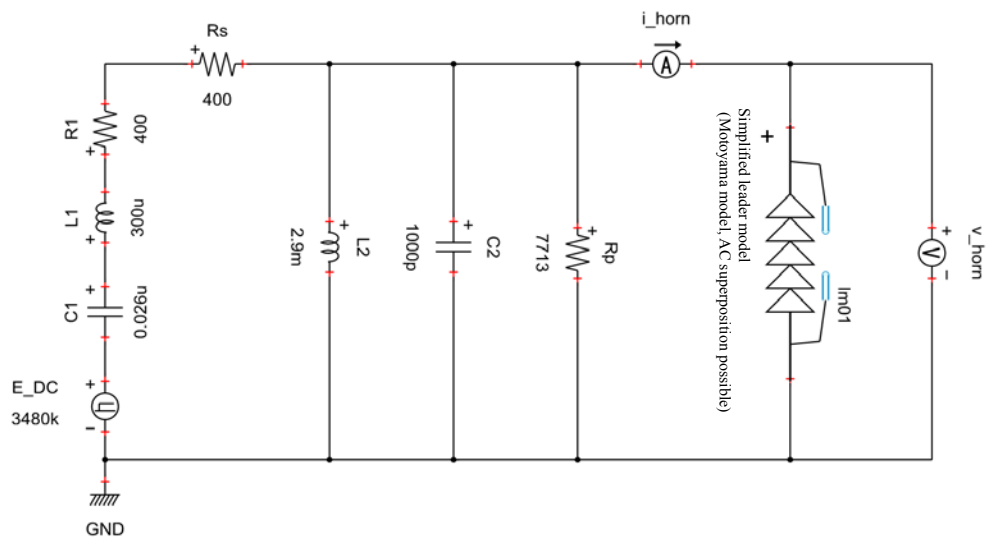


Figure 1 Analysis circuit

[Calculation of the Leader Progress Start Condition]

In the detailed model of example STL-03, the instantaneous value of the voltage is integrated to obtain the average voltage value, and the start of the leader progression is determined based on whether this value exceeds the fixed value based on the gap length. However, in cases in which the impulse voltage is superimposed over a steady AC voltage, such as the case of an assumed lightning strike when the system voltage is applied, the integral value of the impulse voltage rises owing to the previous steady AC voltage, and the calculation of an accurate average voltage may not be possible.

To solve the above problem, in the simplified model of this example, a simplified leader progress start condition is adopted that states, “if the absolute value of the average electric field between the arcing horns exceeds  $E_s = 500$  [kV/m], the leader begins to progress.” Specifically, if  $D$  [m] is the distance between the electrodes of the arcing horn, and the voltage  $V(t)$  [KV] between the arcing horn satisfies

$$\frac{V(t)}{D} > E_s = 500 \text{ [kV]},$$

the leader will start progressing.

Figure 2 shows an implementation of Motoyama’s arcing horn flashover model for a short-tail wave, which adopts the above-mentioned simplified leader progress start condition on XTAP (this model can be referred to by right-clicking on the “simplified leader model” in the circuit diagram of Figure 1, and selecting “component diagram editing”).

Inside the figure, the section enclosed by the blue dotted line is the part that calculates the start condition of the leader progress, and is much simpler compared to the corresponding part of the detailed model in example STL-03.



green dotted line in Figure 2.

#### [Parameter Settings]

Various parameters can be set by double clicking the leader model shown in Figure 1. However, the parameters to be set by the user for each analysis are the inter-electrode distance  $D$  of the arcing horn and the arc-resistance  $R_{arc}$ . Other configurable parameters and their default values are indicated below (in most cases, a modification of these parameters is not required).

#### Leader constants

Leader progress starting electric field  $E_s$  [V/m]

$$E_s = 500e3$$

Charge proportionality constant  $K_0$  [C/m]

$$K_0 = 410e-6$$

Velocity proportionality constant  $K_1$  [ $m^2/V/s$ ] ( $0 < X_{LAVE} < D/4, D < 1$  m)

$$K_{1\_1a} = 1.0$$

Velocity proportionality constant  $K_1$  [ $m^2/V/s$ ] ( $0 < X_{LAVE} < D/4, D \geq 1$  m)

$$K_{1\_1b} = 2.5$$

Velocity proportionality constant  $K_1$  [ $m^2/V/s$ ] ( $D/4 < X_{LAVE} < D/2$ )

$$K_{1\_2} = 0.42$$

Minimum leader progress electric field  $E_0$  [V/m]

$$E_0 = 750e3$$

Tolerance of the leader bridging evaluation

$$\epsilon = 0.05$$

Equivalent resistance value before leader progression [ $\Omega$ ]

$$R_{init} = 1e6$$

Time constant of first-order lag filter for internal processing [s]

$$\tau = 10e-9$$

#### [Analysis Conditions]

The analysis conditions are as follows:

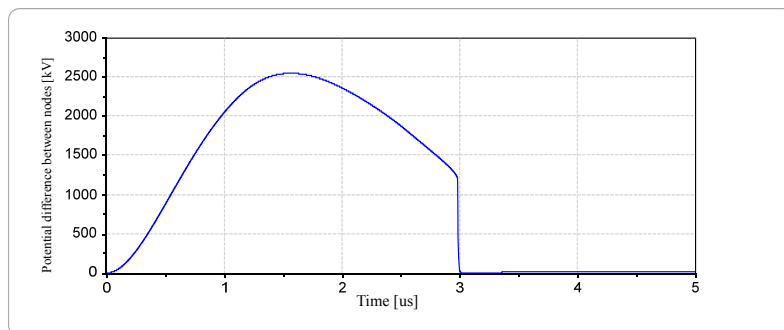
- Calculation time step                      1 ns
- Calculation start time                      0  $\mu$ s
- Calculation end time                        5  $\mu$ s
- Display start time                            0  $\mu$ s
- Display end time                              5  $\mu$ s

### Analysis Results

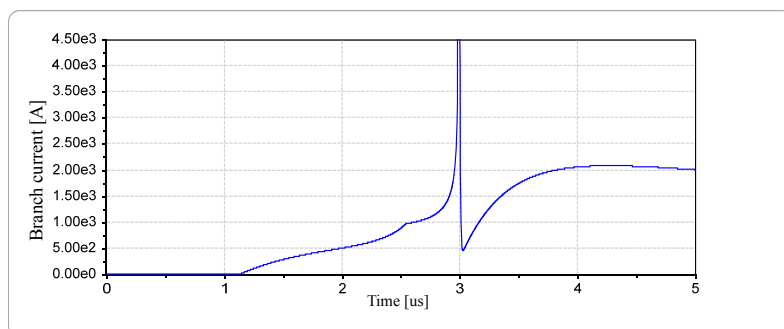
The inter-electrode distance  $D$  of the arcing horn was set to 3 m, and the arc resistance  $R_{arc}$  was set to  $5 \Omega$  (the other parameters were set to their default values). The results of the calculation conducted on the analysis circuit of Figure 1 are shown in Figure 3. In addition to the voltage between arcing horns and the leader current, the leader length and leader propagation velocity are shown (the leader length and leader propagation velocity are outputs with the variable names XLAVE and VLAVE, respectively). The calculation results are consistent with the calculation results of the detailed model described in example STL-03 and with the actual measured results within the range in which no problem occurs in terms of practical use.

Figure 4 shows the calculation results of the  $V-t$  curve for the cases of positive and negative polarities by changing the inter-electrode distance of the arcing horn  $D$  to 1, 2, and 3 m. In the simplified model of this example, because there is no distinction between the positive and negative polarities, the same results can be obtained in both cases. The calculation results agree well with the calculation results of the detailed model and the actual measured results shown in the following reference document within the range in which no problems occur in terms of practical use.

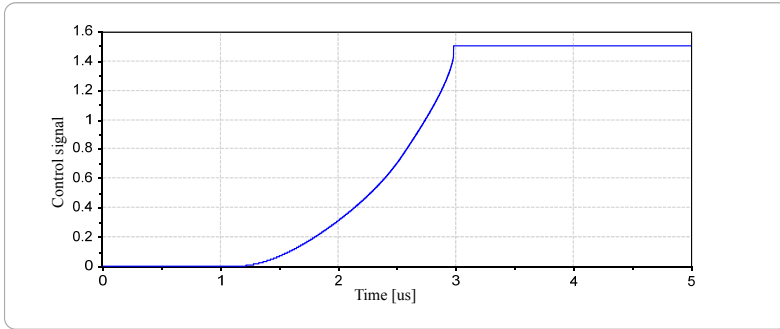
M. Aoshima, “Flashover Characteristics of Air Gaps by Lighting Impulse Voltages with Short Tail,” Research report T87041, Central Research Institute of Electric Power Industry, April 1988.



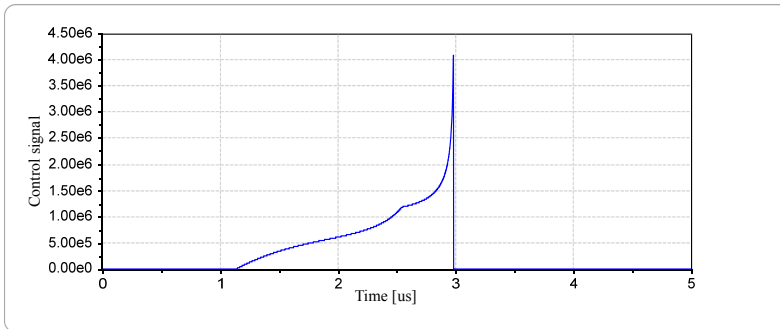
(a) Voltage between arcing horns



(b) Leader current

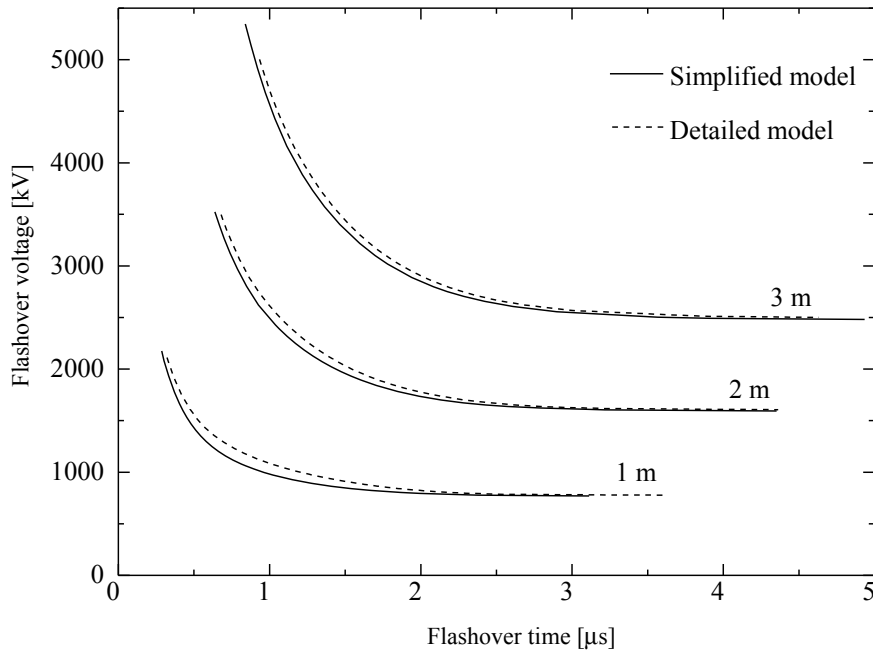


(c) Leader length

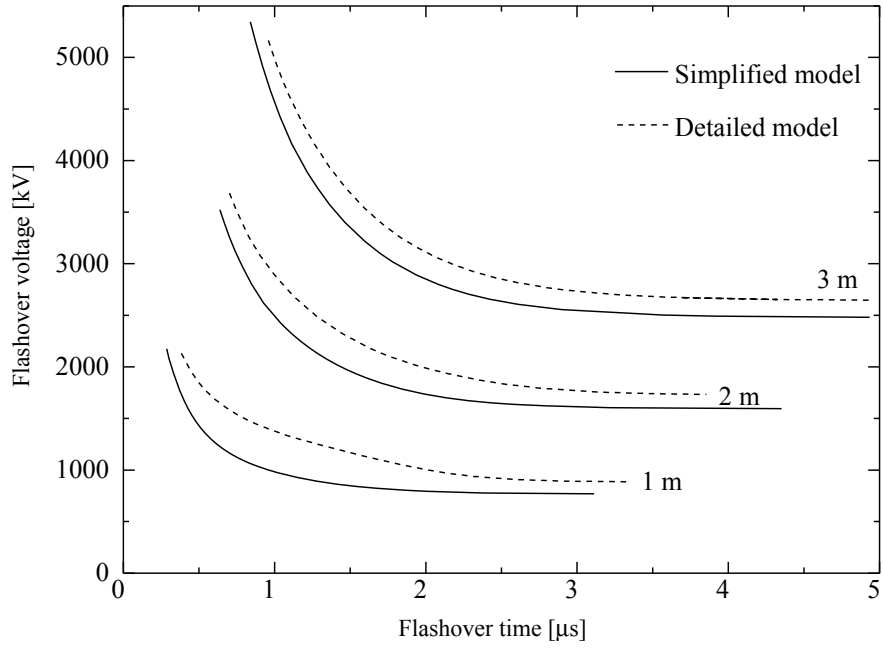


(d) Leader progression velocity

Figure 3 Analysis results



(a) Positive polarity



(b) Negative polarity

Figure 4  $V-t$  curve of calculation results

Revision History		
Date	Example file Version	Content changes
2022/10/18	2.1	Name changed from SLS-03 to STL-04
2014/11/19	2.0	Update for XTAP Version 2.0
2012/07/19	1.1	Update for XTAP Version 1.20
2011/12/06	1.0	Initial version created (for XTAP Version 1.11)

<b>XTAP Example Collection</b>		<b>No.</b>	PV-01
<b>Example Name</b>	Simulation of Single-phase Inverter Circuit for Solar Power Generation		
<b>Field</b>	Power Electronics		
<b>References</b>	“Development of Inverter Simulation Program (Part 2): Verification of Analysis Accuracy by Comparison of Actual Measurements,” Research Report R07016 (June 2008), Central Research Institute of Electric Power Industry		
<b>Outline</b>	<p>With an increase in the amount of power electronic equipment and complexity, the importance of a simulation analysis of the power electronic equipment is increasing.</p> <p>In this example, we simulate an inverter for a recently introduced solar power generation. We simulate the solar power generation panels with a DC power supply, boost it with a boost chopper and connect it to a single-phase 200-V AC system through an inverter. The switches and diodes in the circuit are simulated using the simplified characteristics of ON- and OFF-resistors.</p>		

## Analysis Circuit and Conditions

Figure 1 shows the analysis circuit.

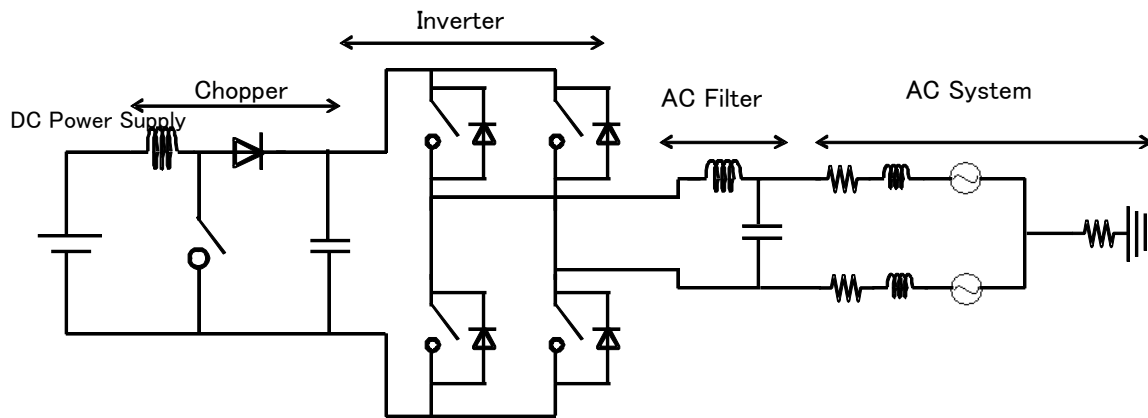


Figure 1 Analysis circuit

### [Circuit Operation]

The DC voltage generated by the DC voltage source on the left side of Figure 1 is boosted to 380 V using a boost chopper. Subsequently, an AC voltage is output using a single-phase inverter and linked to the 200-V system. In this example, because the chopper applies the current control, the ON/OFF timing of the switch is adjusted such that the current flowing through the chopper smoothing reactor follows the command value. The inverter applies a constant DC voltage control and adjusts the output power to the AC system such that the average value of the DC voltage also follows the command value. Further, to remove the higher harmonics superimposed on the voltage and power waveforms output from the inverter, it is connected to the system using an AC filter.

The main circuit parameters of the analysis circuit are as follows:

Chopper smoothing reactor: 1 mH

DC capacitor for energy storage: 5 mF

Reactor for AC filter: 3 mH

Capacitor for AC filter: 30  $\mu$ F

### [Analysis Conditions]

The analysis conditions are as follows:

- Calculation time step            0.2  $\mu$ s
- Calculation start time            0 ms
- Calculation end time            40 ms
- Display start time                20 ms
- Display end time                 40 ms

### [Example of XTAP Input]

An instance of creating this example using XTAP is shown in Figure 2.

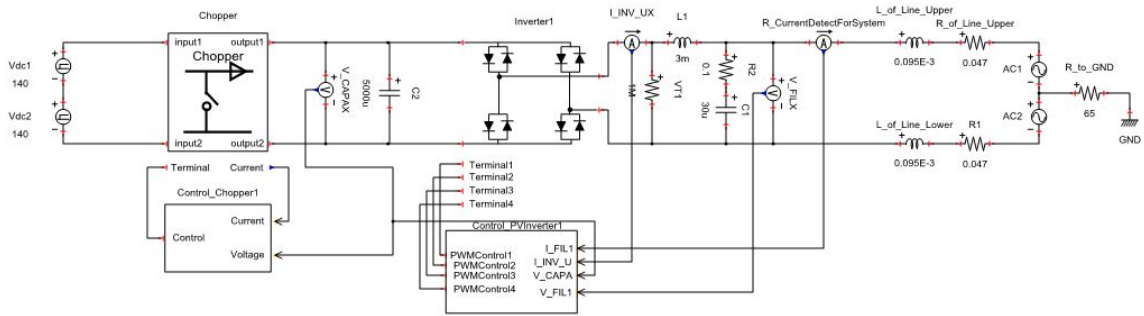
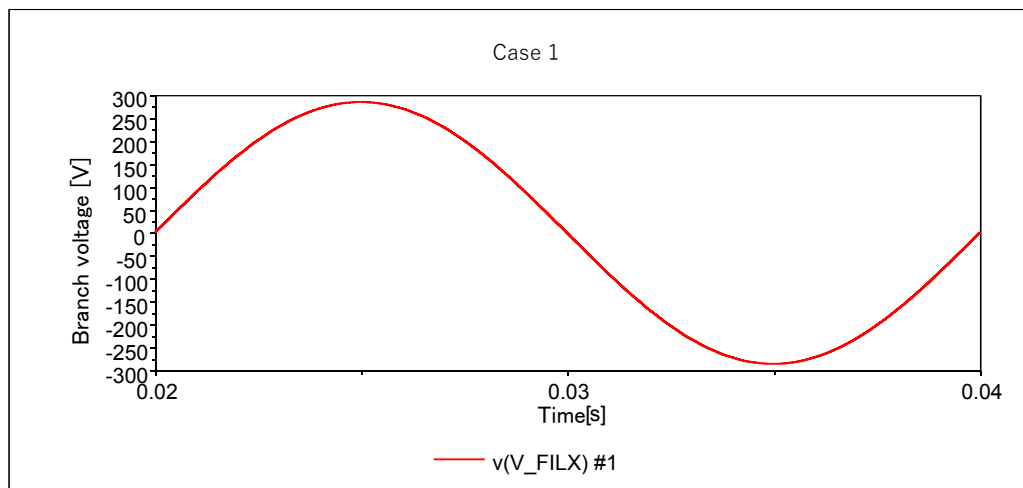


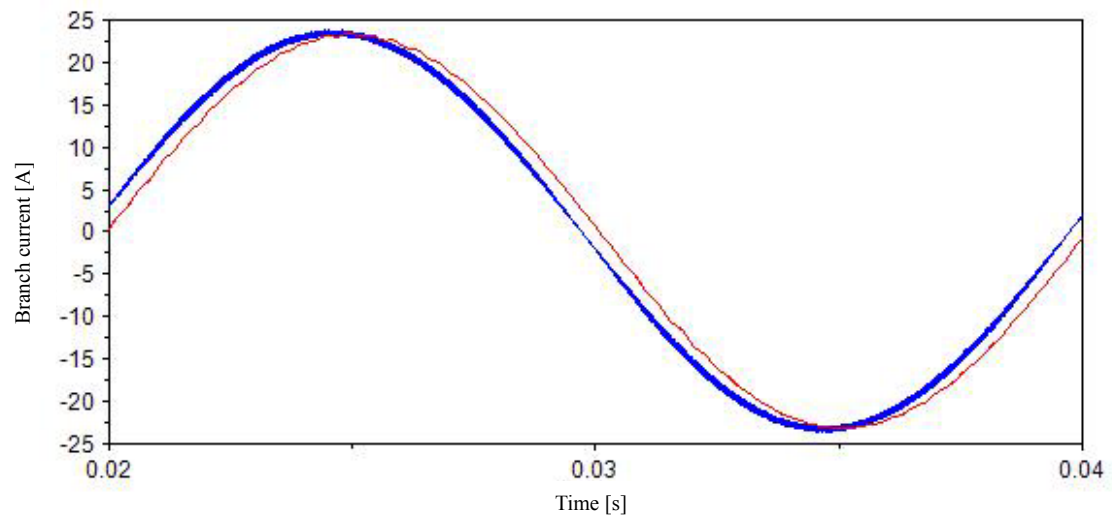
Figure 2 Example of XTAP input

## Analysis Results

The results of executing this example using XTAP are shown in Figure 4. Based on the results of the simulation, it can be confirmed that a single-phase AC current flows through the inverter to the system side, and that the current after passing through the AC filter is cleaner than the current waveform before passing through the AC filter over which the higher harmonic wave was superimposed.



(a) AC voltage waveform at outlet of AC filter



Blue line, AC current before passing through the filter; red line, AC current after passing through the filter

(b) Inverter current waveform

Figure 3 Analysis results

END

Revision History		
Date	Example File Version	Content changes
2021/06/23	2.1	Name changed to PV-01 (contents unchanged)
2014/11/19	2.0	Update for XTAP Version 2.00
2012/07/19	1.2	Update for XTAP Version 1.20
2011/10/18	1.1	Update for XTAP Version 1.11
2010/07/16	1.0	Creation of the first edition (for XTAP Version 1.10)

XTAP Exercises		Number	PV-02-A
<b>Exercise name</b>	Simulation of a system fault using a basic transient analysis model of PCS for utility-scale solar power station (Switching model)		
<b>Fields</b>	Power system analysis, System interconnection, Power electronics		
<b>Reference documents</b>	<p>The main references include:</p> <p>[1] Technical Committee on Massively Interconnected Analysis Model for Distributed Generation, "Massively Interconnected Analysis Model for Decentralized Generating Plants", I.E.E. Japan Technical Report No. 1487, 2020.</p> <p>[2] Yonezawa, Fukushima, Noda, Sekiba, Ito, Misawa, Chida, Yamaguchi, Nakajima, Utsunomiya, and Takeuchi, "Development of a large-scale PV power generation system model for electromagnetic transient simulations under grid faults", I.E.E. Japan Joint Workshop on Electric Power Technology/Power System Technology, PE-15-151, PSE-15-173, pp. 99-104. 2015-09.</p> <p>Other reference documents are listed at the end of this document.</p>		
<b>Outlines</b>	<p>This exercise simulates the transient response in a utility-scale solar power station when a system accident occurs in a high-voltage distribution system where the power station is interconnected. The model for the utility-scale solar uses a basic instantaneous value analysis model of PCS for utility-scale solars, and generates a disturbance assuming 3LGO in the upper level system and 3LS in the high voltage distribution line as the system accident. The model operates normally by outputting a constant active power during a normal condition in the system voltage, but once the voltage drops due to a system accident, depending on the degree and time of the drop, the model continues to operate, or performs operations such as gate block function to stop the operation of the switching device or performing parallel-off from the system. Also, when the voltage drops, the control to limit the output current will work.</p> <p>Distributed power sources such as utility-scale solars normally have various requirements stipulated by the system interconnection regulations, but the purpose of this exercise is to simulate the transient response characteristics when an accident occurs. Therefore, the PCS model uses the basic model as it is and does not include various system protection functions. The FRT requirement also considers only the simple LVRT (voltage drop tolerance).</p>		

## Circuit to be analyzed and analysis conditions

Fig. 1 shows the circuit diagram of the high-voltage distribution system simulated on the XTAP and the utility-scale solar connected to it. The system frequency is 50 Hz.

A Distribution substation is simulated as a series connection of  $0.0001 + j0.08$  p.u. impedance and voltage sources with its transformer for distribution and back system together, and the neutral point is grounded with a resistance of  $30 \text{ k}\Omega$ , which is the value of the limiting resistance of the GPT from the primary side [1]. There are two feeders from the distribution substation and a 500 kW utility-scale solar is interconnected at the end of one of the feeders (4 km away). A 3 MW resistive load is connected at the end of the other feeder.

Exercise name: Basic transient analysis model of PCS for utility-scale solar system (Switching model)

PV-02-A

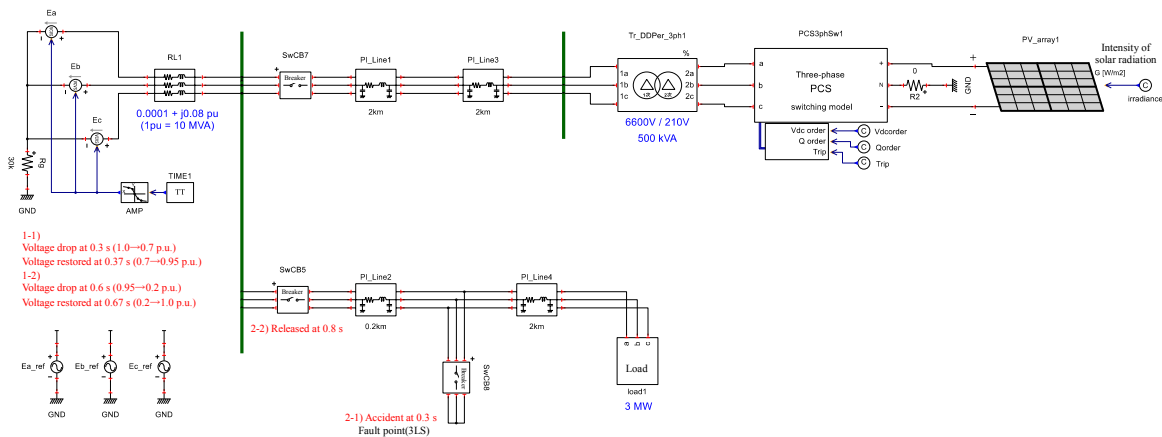


Fig. 1 Circuit diagram of the high-voltage distribution system simulated on the XTAP and the utility-scale solar system connected to it.

The utility-scale solar consists of PV panels with a DC output voltage of about 350 V and an output of about 500 kW, a PCS model for basic transient analysis, and a 500 VA step-up transformer to boost the voltage to high voltage. A three-level NPC bridge is used as a inverter inside the PCS, and the switching frequency of the PWM control is set to 4.5 kHz. The PCS employs DCAVR for d-axis current control and AQR for q-axis current control, and specifies 1.0 for the DC voltage command value and 0.0 for the reactive power command value. Since the PCS does not include the MPPT control, the DC voltage command value does not change even if the maximum power output point of the PV panel changes due to changes in solar irradiation, etc. (To simulate changes in solar irradiation, the MPPT control must be added to the PCS). For the LVRT, which controls implementation of continuous operation and gate blocking, etc., when the system voltage drops, gate blocking starts at 0.3 p.u. (gate block time: 0.1 s), and the PCS is disconnected from the system when gate blocking continues for 0.3 s. The current limit will operate when the system voltage drops less than 0.9 p.u.

The following two types are assumed as the system faults.

- (1) Assuming 3LG-O in the upper system, the amplitude value of the supply voltage at the distribution substation will vary as follows.
  - <1> 0.3 to 0.37 s ... drops to 0.7 p.u.
  - <2> 0.6 to 0.67 s ... drops to 0.2 p.u.
- (2) Assuming 3LS in the high voltage distribution line, three-phase short circuit occurs at 0.3 s at a point 0.2 km from the distribution substation of a feeder where utility-scale solar is not interconnected, and then the feeder is shut down 0.5 s later (0.8 s).

The PCS model used in this exercise is a model that actually performs switching, and the calculation time step is set to 2  $\mu$ s to ensure sufficient simulation of the switching in semiconductor devices.

## Analysis results

### I. Instantaneous voltage drop assuming 3LG-O in the upper system

Fig. 2 shows the system voltage and output current of each phase on the AC side of the PCS, voltage on the DC side, the active and reactive power output by the PCS, the d-axis current command value (DCAVR output), the effective value of voltage to determine the voltage drop, and the gate block signal. Each time zone will be discussed below.

#### (1) 0 to 0.3 s: Operation start to steady state

The PCS will be initialized since it is not initialized at  $t = 0$  (except for the DC capacitor). The DC voltage rises as power is supplied from the PV panels, but when the active power is output to the AC side, the DC voltage gradually decreases and converges to the commanded value of 1.0 p.u. (350 V).

#### (2) 0.3 to 0.6 s: Time from which the fault occurs (system voltage drops down to 0.7 p.u.) through recovery

Due to the occurrence of a fault (drop in the system voltage amplitude value simulating the fault), the voltage on the AC side of the PCS drops. This lowers the active power that can be transmitted to the AC side, and the DC power rises. Due to the voltage falling below 0.9 p.u., the current limit is activated to prevent overcurrent, limiting the d-axis current command. Furthermore, since the voltage is above 0.3 p.u., the PCS will continue to operate.

The voltage recovers at 0.07 s after the fault, but since the gate block time is set to 0.1 s, the gate block continues for 0.1 s after the fault and then recovers. After recovery, the active power output is restored and it returns to the steady state. However, the system voltage of 0.95 p.u. after the recovery means the d-axis current command value is controlled to a larger value than before the fault.

#### (3) 0.6 to 1.0 s: Time from which the fault occurs (system voltage drops down to 0.2 p.u.) through recovery

Due to the occurrence of an fault (drop in the system voltage amplitude value simulating the accident), the voltage on the AC side of the PCS drops. In the output current, a whisker-shaped overcurrent flows into the system momentarily, but is quickly suppressed by the fast ACR. Since the system voltage has dropped below 0.3 p.u., the gate block signal is output, and then the active power output to the AC side becomes zero. During the gate block, the breaker remains turned on, generating transient voltages and currents due to the interaction between the system interconnection reactor and filter capacitor. Since no active power is output to the system, the DC voltage rises due to the power supply from the PV panels and reaches about 427 V, which is the maximum open circuit voltage of the PV panels.

Since the voltage recovers from the accident in 0.07 s, it recovers after the gate block time elapsed similar to 2) and returns to the steady state.

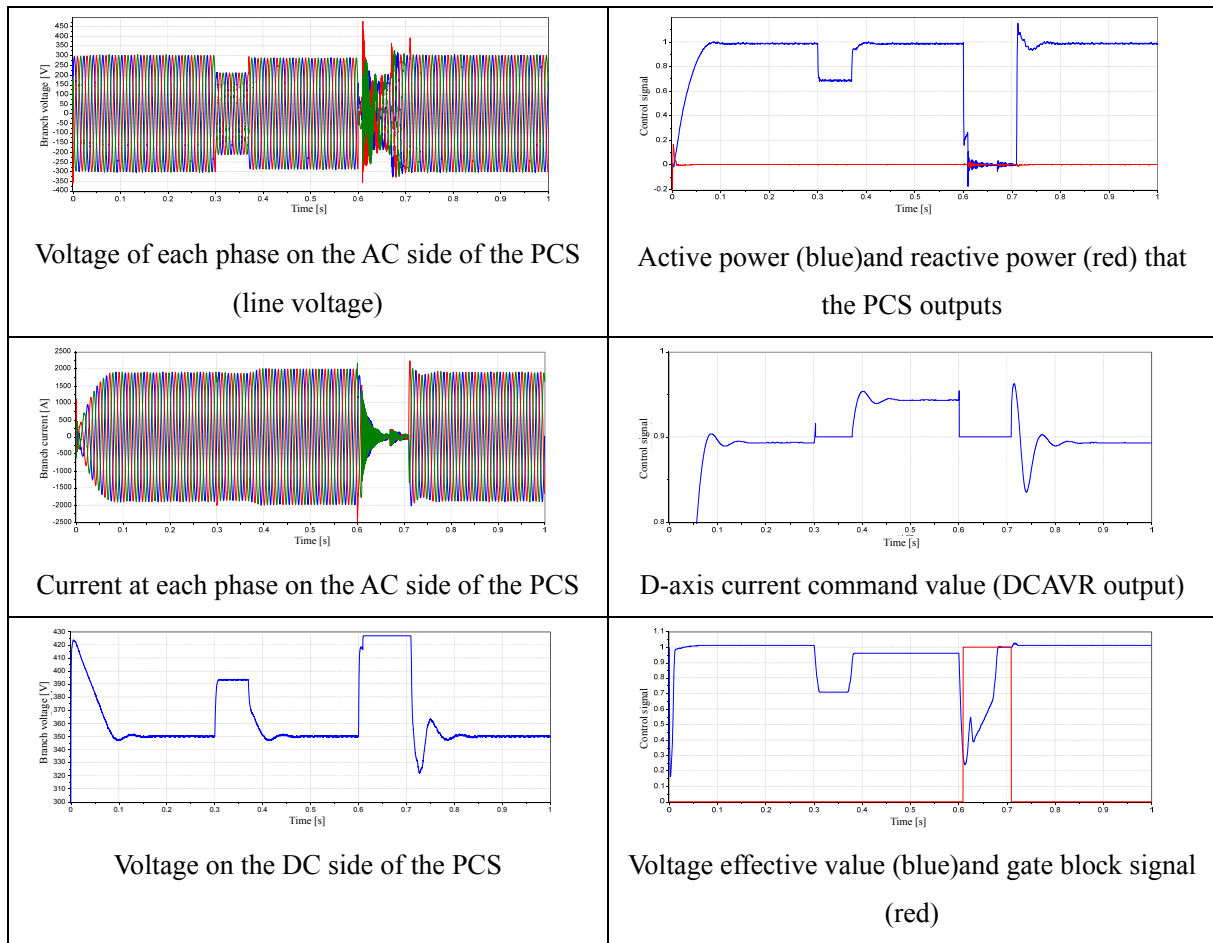


Fig.2. PCS response when an instantaneous voltage drop occurs, assuming 3LG-O in the upper system

## II. Instantaneous voltage drop assuming 3LS in the high voltage distribution line

Fig. 3 shows the system voltage and output current of each phase on the AC side of the PCS, voltage on the DC side, the active and reactive power output by the PCS, the d-axis current command value (DCAVR output), the effective value of voltage to determine the voltage drop, and the gate block signal. Each time period will be discussed below (0 to 0.3 s is omitted because it is the same as I.).

(1) 0.3 to 0.8 s: Time from which the fault occurs (system voltage drops down to 0.3 p.u.) through recovery

Due to occurrence of the 3LS fault at a feeder coming out of the transformer for distribution, the voltage on the AC side of the PCS connected to another feeder in the same bank drops. In this case, since the voltage drops below 0.3 p.u., the PCS will be gate-blocked.

Since the lowered voltage persists even at about 0.61 s, which is 0.3 s after the gate block, the PCS parallels off the breaker on the AC side. As a result of this, the PCS will be disconnected from the system.

(2) 0.8 to 1.0 s: After accidental feeder shutdown

The feeder where the fault occurred is disconnected and the voltage of the feeder to which the utility-scale solar is connected will be restored. However, this model does not incorporate the PCS into the recovery operation once it has been paralleled off, so it remains stopped. To simulate the recovery operation after it has been paralleled off, this control system needs to be added.

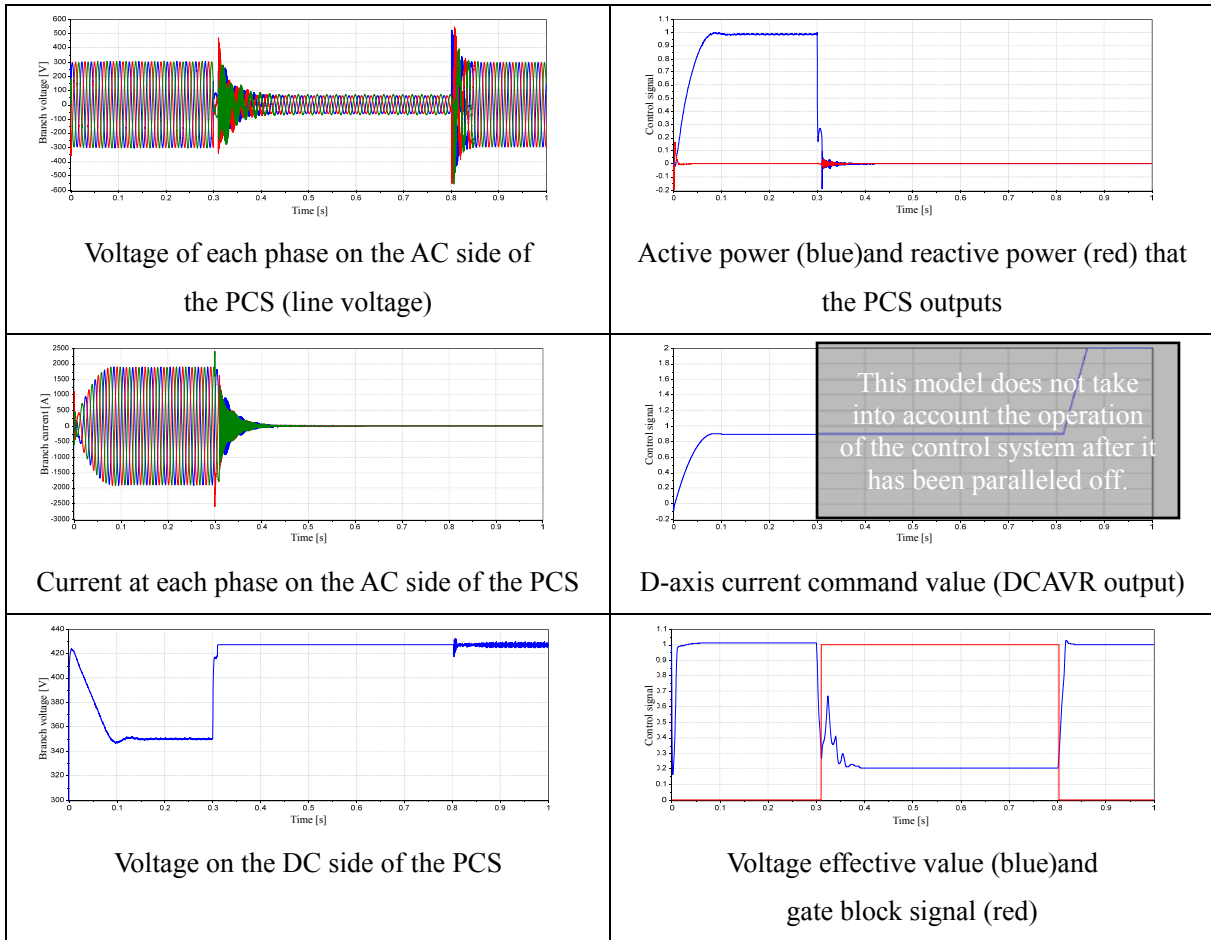


Fig.3. PCS response when an instantaneous voltage drop assuming an 3LS fault in the high voltage distribution line.

## Reference Document

- [1] Investigating R&D Committee on Models for Power System Analysis with Integration of Distributed Generators, "Models for Power System Analysis with Integration of Distributed Generators", I.E.E. Japan Technical Report No. 1487, 2020.
- [2] Yonezawa, Fukushima, Noda, Sekiba, Ito, Misawa, Chida, Yamaguchi, Nakajima, Utsunomiya, and Takeuchi, "Development of a large-scale PV power generation system model for electromagnetic transient simulations under grid faults", I.E.E. Japan Joint Workshop on Electric Power Technology/Power System Technology, PE-15-151, PSE-15-173, pp. 99-104. 2015-09.
- [3] Nagashima and Noda, "A Dynamic Voltage Simulation Method for Power Distribution Systems by Using Electromagnetic Transient Analysis (Part 1): Modeling of Distribution Substation and SVR", Central Research Institute of Electric Power Industry Research Report H13007, 2013.
- [4] Investigating R&D Committee on Control Technology for Power Electronics Equipment, "Control Technology for Power Electronics Equipment," IEEJ Technical Report No. 1084, 2007.

Revision History		
Date	Exercise file version	Details of changes
2021/06/22	1.0	First version created (for XTAP Version 3.3)

XTAP Exercises		Number	PV-02-B
<b>Exercise name</b>	Simulation of a system fault using a basic transient analysis model of PCS for utility-scale solar power station (average value model)		
<b>Fields</b>	Power system analysis, System interconnection, Power electronics		
<b>Reference documents</b>	<p>The main reference documents include:</p> <p>[1] Investigating R&amp;D Committee on Models for Power System Analysis with Integration of Distributed Generators, "Models for Power System Analysis with Integration of Distributed Generators", I.E.E. Japan Technical Report No. 1487, 2020.</p> <p>[2] Yonezawa, Fukushima, Noda, Sekiba, Ito, Misawa, Chida, Yamaguchi, Nakajima, Utsunomiya, and Takeuchi, "Development of a large-scale PV power generation system model for electromagnetic transient simulations under grid faults", I.E.E. Japan Joint Workshop on Electric Power Technology/Power System Technology, PE-15-151, PSE-15-173, pp. 99-104. 2015-09.</p> <p>Other reference documents are listed at the end of this document.</p>		
<b>Outlines</b>	<p>In Exercise PV-02-A "Simulation of a system fault using a basic transient analysis model of PCS for utility-scale solar power station (Switching model)", the analysis was performed using a model that takes into account the switching behavior of the semiconductor devices inside the PCS similar to the actual PCS. In this model, however, it is necessary to take a smaller analysis time step to simulate the switching, resulting in too long calculation time. An average value model that averages the on-off switching of semiconductor devices and simulates the voltage of each arm as a voltage source to accelerate the calculation is known. The average value model does not simulate the harmonics associated with switching, but it takes a longer time step, enabling faster operation. Therefore, this exercise simulates the case where the PCS model used in Exercise PV-02-A is replaced by the average value model, and compares its operation with the switching model.</p> <p>Please refer to the exercise slip for Exercise PV-02-A for the circuit conditions, etc.</p>		

## Circuit to be analyzed and analysis conditions

Fig. 1 shows the circuit diagram of the high-voltage distribution system simulated on the XTAP and the utility-scale connected to it. The system frequency is 50 Hz. Except for the PCS model being the average value model, it is identical to Exercise PV-02-A.

Exercise name: Basic transient analysis model of PCS for utility-scale solar system (average value model)

PV-02-B

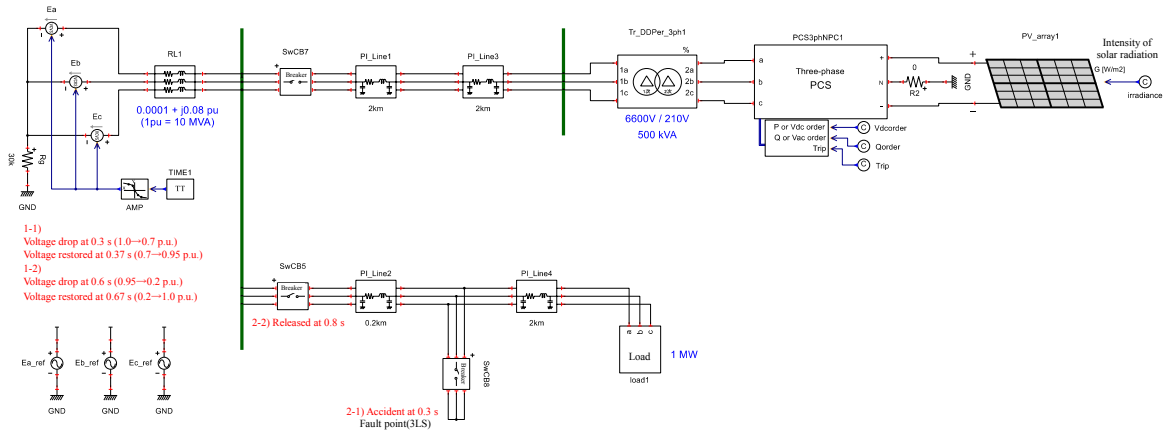


Fig. 1 Circuit diagram of the high-voltage distribution system simulated on the XTAP and the utility-scale solar system connected to it.

Fig. 2 shows the internal configuration of the three-phase PCS (average value model). Except for the part in the frame with the red dashed line in the figure, it is identical to the switching model. In the average-value model, the voltage output of each arm is simulated by a voltage source as described later, PWM is not necessary, and the command value of the output voltage of each phase is input to the bridges as it is.

Three-level NPC bridge PCS model for mega-solar

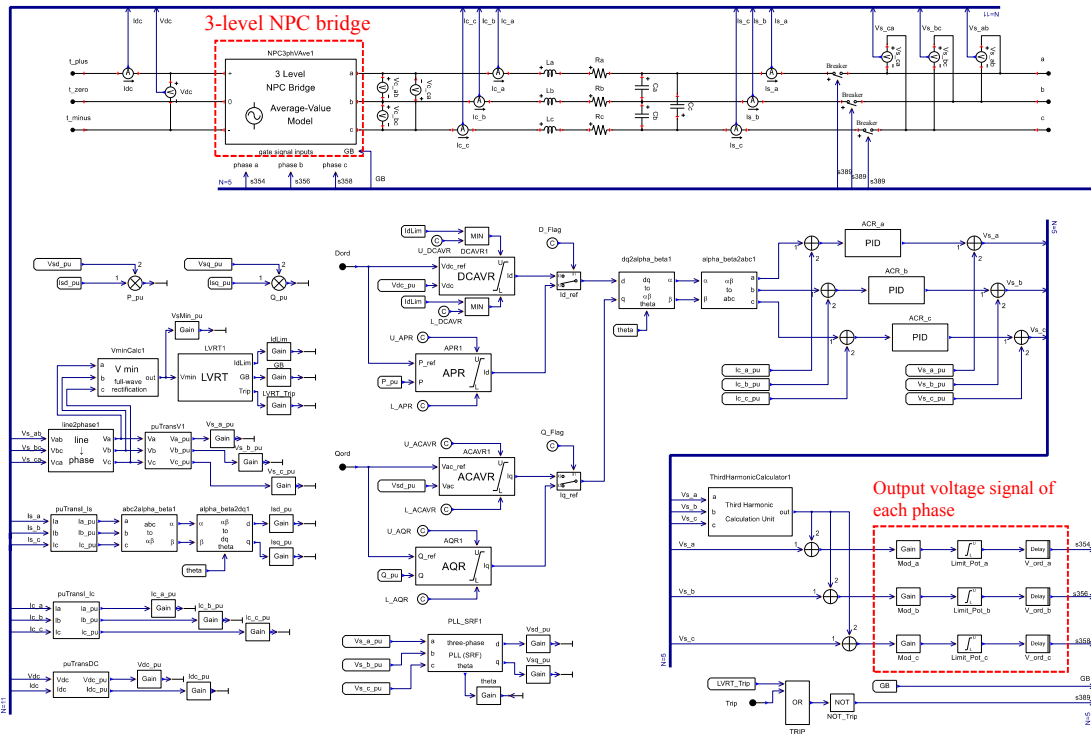


Fig. 2 Internal configuration of the three-phase PCS (average value model)

Fig. 3 shows the average value model for the three-level NPC bridge. A current source is placed on the DC side and a voltage source is placed on the AC side. The current source on the DC side flows current with a value of the current flowing in the voltage source on the AC side multiplied by a signal  $k$  equivalent to the ratio of PWM on/off (equal to the output voltage signal), and the voltage source on the AC side applies a voltage of the DC voltage (voltage of the DC capacitor) multiplied by  $k$ . This makes the power on the DC side equal to the power on the AC side. Various methods have been proposed to implement the averaging model for [3] to [5]. In this exercise, in order to simulate the transient characteristics of the three-level NPC bridge, six current sources are placed in parallel with two capacitors, and six voltage sources are placed on the AC side, as shown in Fig. 3, where the upper and lower sources correspond to the positive and negative sides of the output voltage signal respectively. By configuring the circuit in this way, as described later, transient characteristics equivalent to those of the switching model can be simulated.

When the gate is blocked, the output of each current source and voltage source is set to zero, and the switch located on the AC side is opened to simulate the gate block operation in a simplified manner. If it is necessary to correctly simulate the transient behavior of diodes (rectifier circuits) connected in parallel to semiconductor devices when the gate is blocked, a model that can take this into account should be used (e.g., [6] and [7]).

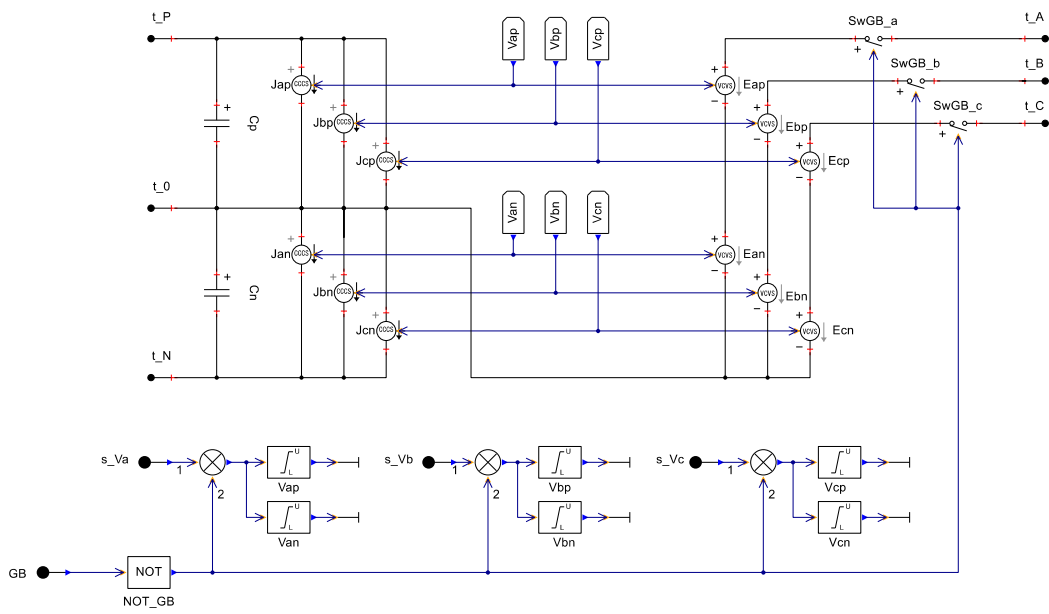


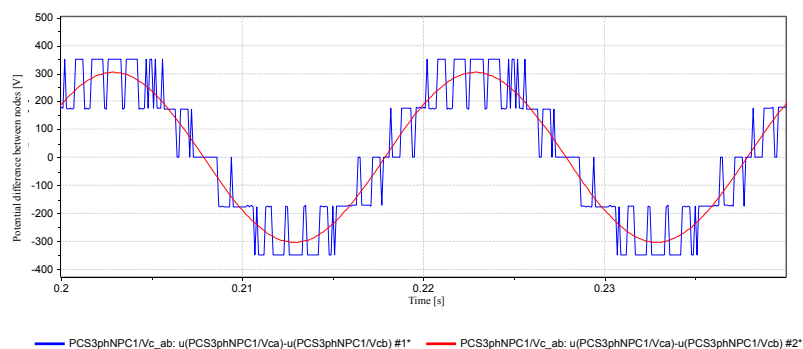
Fig. 3 Average value model for the three-level NPC bridge.

Since this exercise uses the average value model, the calculation time step is set to  $40 \mu\text{s}$ .

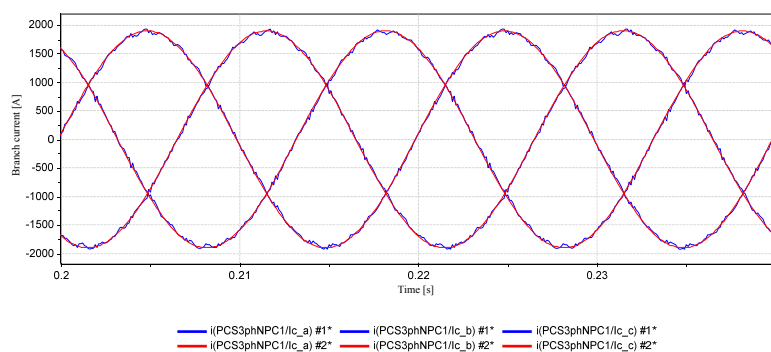
## Analysis results

Here, it is explained that only the operation of the on-delay voltage drop assuming 3LG-O in the upper system.

Fig. 4 shows the results of the switching model (PS-02-A results) cascaded with the results of the average value model in this exercise for the line voltage  $V_{c,ab}$  between ab-phases closer to the inverter side rather than the system interconnection reactor of the PCS and the line current  $I_c$  of each phase during steady state operation (0.2 to 0.24 s). As can be seen clearly from the figure, the voltage waveform in the switching model is square-wave-like (due to three levels, three levels of square waves appear in the phase voltage and five levels in the line voltage), while the voltage waveform in the average value model is a clean sinusoidal waveform with no noise. Regarding the current, it can be confirmed that the harmonics originated from switching are superimposed in the switching model, while the average value model exhibits a clean waveform without these harmonics.



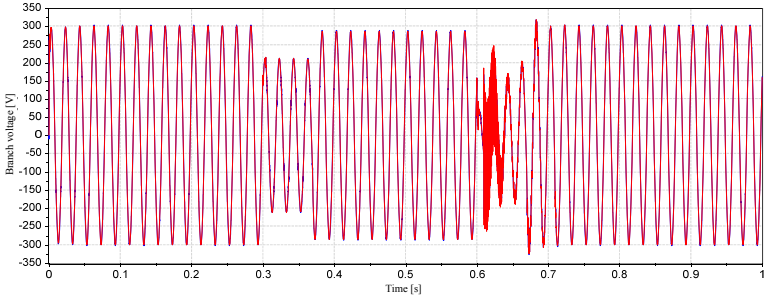
a) Line voltage between ab-phases



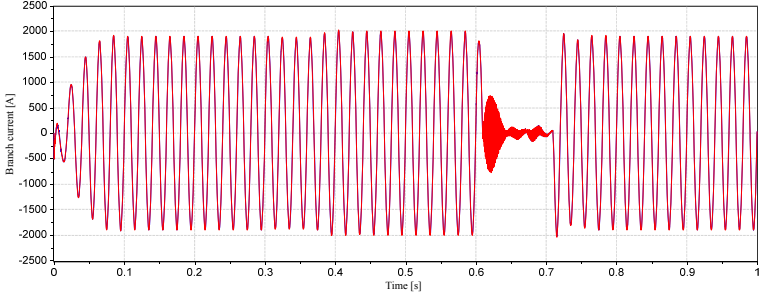
b) Line current of each phase

Fig. 4 Comparison 1 of the switching model and average value model  
(Blue: switching model, Red: average value model)

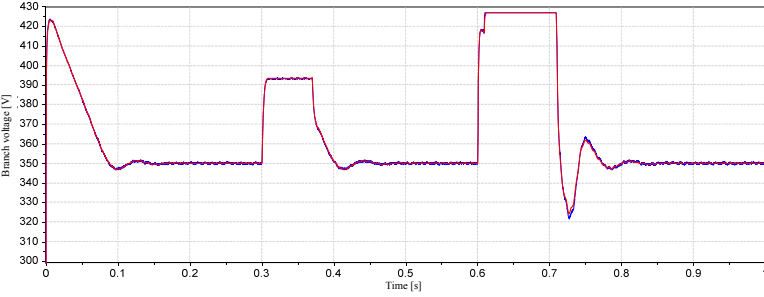
Fig. 5 shows the results of the switching model (results for PS-02-A) cascaded with the results of the average value model in this exercise for the system voltage between the ab-phases on the PCS AC side, the output current of the phase a, the voltage on the DC side, and the active and reactive power output by the PCS. As can be seen clearly from the figure, the switching model and the average value model of this exercise coincide well for all voltage waveforms, current waveforms, and control signals (output power). (The waveforms almost overlap. Please calculate each exercise to verify it by yourself.)



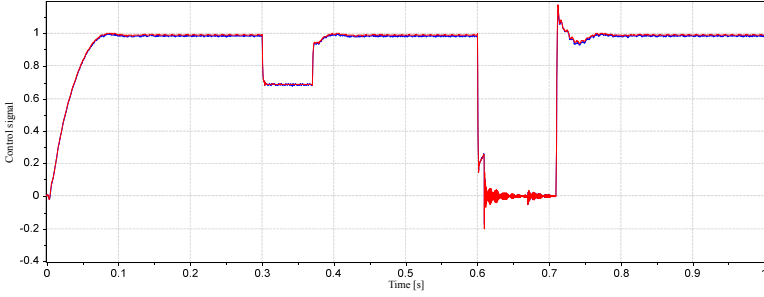
a) AC voltage (between ab phases)



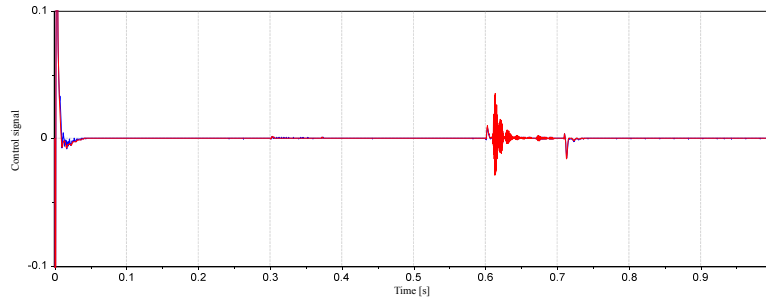
b) AC current (phase a)



c) DC voltage



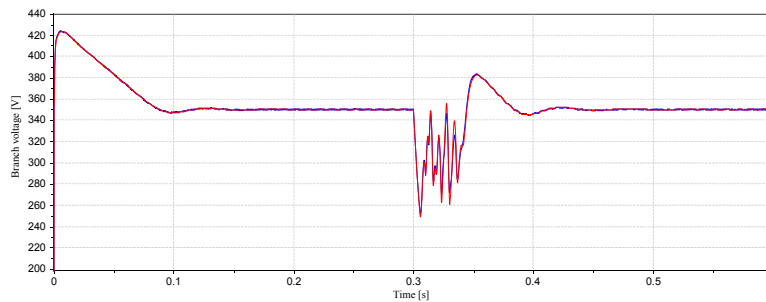
d) Active power



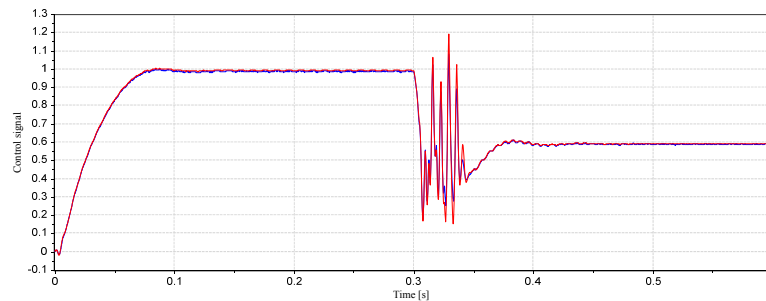
e) Reactive power

Fig. 5 Comparison 2 of the switching model and average value model  
(Blue: switching model, Red: average value model)

Fig. 6 shows the results of calculation of the DC voltage and active power by each model when the input signal (solar irradiation) to the PV panels is changed in a stepwise manner from 1000 to 600 at 0.3 s instead of causing a fault using the same circuit (in an actual PCS, the commanded value of the DC voltage changes by MPPT control when such change in solar radiation occurs; however, this analytical example does not take MPPT control into account, resulting in the commanded value of the DC voltage being constant.). As can be seen clearly from the figure, the transient changes in each waveform are generally reproduced by the average value model even for steep changes in input.



a) DC voltage



b) Active power output by PCS

Fig. 6 Comparison 3 of the switching model and average value model  
(Blue: switching model, Red: average value model)

## Reference Document

- [1] Investigating R&D Committee on Models for Power System Analysis with Integration of Distributed Generators, "Models for Power System Analysis with Integration of Distributed Generators", I.E.E. Japan Technical Report No. 1487, 2020.
- [2] Yonezawa, Fukushima, Noda, Sekiba, Ito, Misawa, Chida, Yamaguchi, Nakajima, Utsunomiya, and Takeuchi, "Development of a large-scale PV power generation system model for electromagnetic transient simulations under grid faults", I.E.E. Japan Joint Workshop on Electric Power Technology/Power System Technology, PE-15-151, PSE-15-173, pp. 99-104. 2015-09.
- [3] Task force on modeling and analysis of electronically-coupled distributed resources, "Modeling guidelines and a benchmark for power system simulation studies of three-phase single-stage photovoltaic systems", IEEE Trans. on power delivery, vol. 26, no. 2, April 2011.
- [4] A. Yazdani, "Electromagnetic transients of grid-tied photovoltaic systems based on detailed and averaged models of the voltage-sourced converter," IEEE PES General Meeting, San Diego, CA, 2011.
- [5] R. Yonezawa, T. Noda, K. Fukushima, T. Nakajima, Y. Sekiba, K. Utsunomiya, E. Ito, K. Misawa, T. Chida, N. Yamaguchi, and Y. Takeuchi, "Development of detailed and averaged models of large-scale PV power generation systems for electromagnetic transient simulations under grid faults," Proc. of IEEE PES Innovative Smart Grid Technologies Asia (ISGT-Asia), pp. 98-104, 2016.
- [6] Kikuma, Okada, "Development of Converter Model for High-speed Transient Analysis - Averaged Model with Rectifier Circuit -," Central Research Institute of Electric Power Industry Research Report R15022, 2015.
- [7] Sano, Yonezawa, Noda: "Instantaneous value analysis model of grid-connected inverters for dynamic voltage analysis of power distribution systems," Transactions of the I.E.E. Japan, vol. 138, no. 8, pp. 685-694, 2018.

Revision History		
Date	Exercise file version	Details of changes
2021/06/22	1.0	First version created (for XTAP Version 3.3)